NUCLEATE POOL BOILING OF NANOPARTICLE BASED FLUIDS

Ph.D. Thesis

by

SOMESH BHAMBI

DEPARTMENT OF CHEMICAL ENGINEERING
INDIAN INSTITUTE OF TECHNOLOGY ROORKEE
ROORKEE – 247667 (INDIA)
JUNE, 2018

NUCLEATE POOL BOILING OF NANOPARTICLE BASED FLUIDS

A THESIS

Submitted in partial fulfilment of the requirements for the award of the degree

of

DOCTOR OF PHILOSOPHY

in

CHEMICAL ENGINEERING

by

SOMESH BHAMBI

DEPARTMENT OF CHEMICAL ENGINEERING
INDIAN INSTITUTE OF TECHNOLOGY ROORKEE
ROORKEE – 247667 (INDIA)
JUNE, 2018

INDIAN INSTITUTE OF TECHNOLOGY ROORKEE

ROORKEE

CANDIDATE'S DECLARATION

I hereby certify that the work which is being presented in this thesis entitled **" NUCLEATE POOL BOILING OF NANOPARTICLE BASED FLUIDS**" in partial fulfilment of the requirements for the award of the of Doctor of Philosophy and submitted in the Department of Chemical Engineering of the Indian Institute of Technology Roorkee, Roorkee is an authentic record of my own work carried out during a period from January, 2013 to June, 2018 under the supervision of Dr. V.K. Agarwal, Professor, Department of Chemical Engineering, Indian Institute of Technology Roorkee, Roorkee.

The matter presented in this thesis has not been submitted by me for the award of any other degree of this or any other Institution.

(SOMESH BHAMBI)

This is to certify that the above statement made by the candidate is correct to the best of my knowledge.

(Vijay Kumar Agarwal)
Supervisor

The Ph. D. Viva-Voce Examination of Mr. Somesh Bhambi, Research Scholar, has been held on September 7, 2018.

Chairman, SRC **Signature of External Examiner**

This is to certify that the student has made all the corrections in the thesis.

Signature of Supervisor **Head of the Department**

Date: September 7, 2018

ABSTRACT

This thesis pertains an experimental investigation on nucleate pool boiling of distilled water and nanofluids namely, alumina – distilled water and copper oxide – distilled water on stainless steel heating tube surface at atmospheric and sub atmospheric pressures. Basically, it deals with the synthesizing of alumina – distilled water and copper oxide – distilled water nanofluids and their characterization. It also deals with the effect of operating variables namely, heat flux, pressure and concentration of nanoparticles on the heat transfer coefficient for the pool boiling of nanofluids. Further, it also includes the comparison of heat transfer coefficient of nanofluids with that of distilled water. Finally, an empirical dimensionless correlation for calculation of heat transfer coefficient of nanofluids has been developed.

Experiments have been carried out for synthesizing of the nanofluids as per the standard procedure as mentioned in section 3.2. The thermophysical characteristics namely density, viscosity and thermal conductivity of alumina-distilled water and copper oxide-distilled water nanofluids have been studied. The experimental data of density of these two nanofluids have been generated for various concentrations of nanoparticles at atmospheric pressure and an empirical correlation is developed as given below:

$\rho_{eff} = C_1+C_2\varphi_p+C_3T$

The value of these constant depends upon the type of nanofluids. The predicted values of density matches excellently well within an error of $\pm$ 2.5%.

The experimental data of thermal conductivity of both the nanofluids have been generated for various concentration of nanoparticles at various temperatures. The value of thermal conductivity has been found to vary with temperature and concentration of nanoparticles according to power law relationship as given below:

$$\frac{k_{eff}}{k_{bf}} \propto \varphi^a T^b$$

The prediction of thermal conductivity matches with the experimental values within an error of $\pm$ 6%.

The experimental data on viscosity have been generated for various concentration of nanoparticles in nanofluids for different temperature and a logarithmic relationship has been developed by regression analysis which is given below:

$$\ln(\mu_{nf}) = \frac{A}{T} - B$$

The predicted values for viscosity using correlation matches excellently within an error of $\pm$ 7%.

Experiments have been carried out for the pool boiling of distilled water, alumina – distilled water and copper oxide – distilled water nanofluids on an electrically heated stainless steel heating tube surface. The heating tube is a stainless steel cylinder having 18 mm inner diameter, 32 mm outer diameter and 150 mm effective length. It is heated by placing a laboratory made electric heater inside it. The wall temperature and liquid pool temperature are measured by using well calibrated polytetrafluoroethylene (PTFE) coated copper – constantan thermocouples. The thermocouples are placed inside four coaxially drilled holes at a pitch circle diameter of 25 mm for the measurement of surface temperature. Similarly thermocouple probes are placed in liquid pool corresponding to wall thermocouple positions in heating tube to measure the liquid pool temperature. A digital multimeter measures emf of thermocouples. Power input to the heater is increased gradually from 240 W to 440 W in six equal steps and pressure from 45.47 kN/m^2 to 97.71 kN/m^2 in five steps. The maximum uncertainity associated with the measured value of average heat transfer coefficient is of the order of $\pm$ 1.69%.

Experimental data for saturated pool boiling of distilled water on stainless steel heating tube at atmospheric and sub atmospheric pressures have been processed to obtain local as well as average heat transfer coefficient. Analysis of the data has shown that surface temperature, for a given value of heat flux, increases from bottom to side, to top positions of heating tube at atmospheric and sub atmospheric pressures. However, liquid temperature remains almost constant. Further, the local heat transfer coefficient increases from top to side to bottom positions irrespective of heat flux and the heat transfer coefficient has been found to vary with heat flux according to power law relationship, $h_\psi \propto q^{0.7}$ for all the values of pressures. Furthermore, average heat transfer coefficient of distilled water boiling on stainless steel heating tube has been found to vary according to the relationship $h \propto q^{0.7}$ for atmospheric and sub atmospheric pressures. This corroborates with the findings of various researchers such as [A10, A11, B3, C10, L7, M1, T4, Y4].A dimensional equation for heat transfer coefficient has been developed as $h = C_1 q^{0.7} p^{0.32}$ using

regression analysis for the pool boiling of distilled water on stainless steel heating tube surface, where C_1 is a constant whose value depends on the type of liquid and the surface characteristics of heating tube.

Experimental data for the boiling of alumina distilled water and copper oxide – distilled water nanofluids at atmospheric and sub atmospheric pressures on stainless steel heating tube surface resulted in analogous behavior as that of distilled water. The functional relationship of heat transfer coefficient with heat flux and pressure is same as observed for distilled water and therefore a dimensional equation, $h = C_2 q^{0.7} p^{0.32}$ for the boiling of nanofluids at atmospheric and sub atmospheric pressures has been developed by regression analysis within an error of $\pm$ 9% ; where C_2 is a constant whose value depends upon the concentration of nanoparticles in the base fluid and heating surface characteristics of heating tube. These observations also corrobates with the findings of various researchers such as Park & Jung [P2]; Kole and Dey [K14]; Kim et. al. [K11]; Johnathan and Kim [J4]; Sarfaraz and Peyghambarzadeh[S2] and Wen and Ding [W5,W6] over boiling of different compositions of nanofluids.

Comparison of boiling characteristics of distilled water and the two nanofluids has been carried out. The pool boiling heat transfer coefficient enhances with increase in concentration of both alumina and copper oxide nanoparticles in distilled water. This behavior continues upto a certain optimum value of concentration of nanoparticles in distilled water. The maximum enhancement of 52.76% and 30.71% is obtained in heat transfer coefficient in case of alumina – distilled water and Copper Oxide – Distilled Water respectively, at 0.05% by concentration of both the nanoparticles in the distilled water. However, on further increasing the concentration of nanoparticles in base fluid i.e. distilled water yields deterioration in the boiling heat transfer coefficient. These facts were also corroborated by various researchers such as Das et. al. [D1,D2] , Kwark et.al. [K17] for the boiling of nanofluids beyond critical concentration and White et. al. [W10] in their work.

A dimensionless correlation has been developed to estimate the heat transfer coefficient for pool boiling of nanofluids $Nu = 3.709x10^{-4} Pr^{1.32} QP^{0.017} Ja^{-0.97}$. This equation has been compared with the data of present investigation as well as other investigators namely Ceislinski [C7, C8]; Kole and Dey [K14]; Bang & Chang [B2]; Wen & Ding [W5,W6]; Ding & Chen [C2] and Yang & Liu [Y2]. The comparison between the experimental values and predicted values due to correlation match excellently well within an error of $\pm$10%.

Acknowledgement

I would like to express my sincere gratitude to my supervisor Dr. V.K. Agarwal, Professor Department of Chemical Engineering, Indian Institute of Technology Roorkee for the continuous support of my Ph.D study and related research, for his patience, motivation, and immense knowledge. His guidance helped me in all the time of research and writing of this thesis. I could not have imagined having a better advisor and mentor for my Ph.D study.

Besides my supervisor, I would like to thank the rest of my thesis committee: Dr. Akhilesh Gupta, Dr. Shishir Sinha (Head Chemical Department), Dr. B. Parsad and Dr. Amit Dhiman for their insightful comments and encouragement which incented me to widen my research from various perspectives.

I extend my grateful thanks to technical as well as administrative staff of the Chemical Engineering Department for their help provided from time to time during the entire period of this study. Mr. Raj Kumar , Vijay Singh, Vipin Ekka, R. Bhatnagar and Akhilesh Sharma deserve special mention for their kind help, continuous support and cooperation provided during the completion of experimental work and thesis writing.

I thank all my fellow labmates Dr. Umesh Kumar, Dr. Chandra Kishore, Surya Prakash, Gajendra, Vikrant, Hemant , Baljinder, Brijesh, Anirudha, Bhupendra Suryawanshi and friends Daksh, Vishal , Mayank, Bir and Balpreet for the stimulating discussions and continuous help and moral support during this work.

I express my sincere gratitude to Mrs. Alka Agarwal for their affection and encouragement during entire period of the work.

I sincerely thank IIT Roorkee and Ministry of Human Resource and Development, Government of India, for providing financial support to undertake the work. The facilities and the environment at the institute are great and are highly conducive for the research work.

Last but not the least, I would like to thank my family: my parents, my wife and daughter and to my brother and sisters for supporting me spiritually throughout writing this thesis. I feel extremely grateful to my wife and daughter Akshita for bearing all the difficulties and pain smilingly during this doctoral programme and always stood along me whenever required. Her patience, loving and

caring nature gave me strength enough to complete this work. The care, support and encouragement provided by them during this work means a lot to me.

I fully understand that the research experience and knowledge that I have gained during the course of my doctoral program would be highly useful in my carrier profession. This work was possible due to contribution of many. I am thankful to all of them and extremely sorry if anyone is left out to acknowledge. I thank God for helping me in one or the other way and providing me strength, knowledge and support enough in doing this work.

(Somesh Bhambi)

Contents

List of Figures

List of Tables

Nomenclature

CHF	Critical Heat Flux
HTC	Heat Transfer Coefficient
DW	Distilled Water
EG	Ethylene Glycol
CNT	Carbon Nano Tube
MWNT	Multi Wall Nano Tube
SWNT	Single Wall Nano Tube
SS	Stainless Steel
VEROS	Vacuum Evaporation onto a Running Oil Substrate
VSANSS	Vacuum Submerged Arc Nanoparticle Synthesis System
SEM	Scanning Electron Microscope
EDAX	Energy Dispersive X-ray Analyzer
XRD	X ray Diffraction
SSA	Specific Surface Area, m^2/gm
Ra	Surface particle interaction parameter
Al_2O_3	Alumina
CuO	Copper Oxide
T	Temperature, °C or K

T_w	Wall Temperature, °C or K
T_l	Liquid Pool Temperature, °C or K
ΔT_w	Wall Superheat, °C or K
L	Effective Length, m
d_h	Pitch Circle diameter, m
A	Heat Transfer Surface Area,m^2
d_i	Inside Diameter of Heating Tube
d_o	Outside Diameter of Heating tube, m
d_{np}	Nanoparticle size
g	Gravitational acceleration, m/s^2
P	Pressure, kN/m^2
ΔP	Pressure Drop, kN/m^2
h_ψ	Local heat transfer coefficient, $W/m^2°C$
h	Heat transfer coefficient, $W/m^2°C$
q	Heat Flux, W/m^2
R_a	Surface Roughness, µm
σ	Surface Tension
μ_{nf}	Viscosity of nanofluid
μ_{bf}	Viscosity of basefluid
k_{nf}	Thermal conductivity of nanofluid W/m°C
K_{bf}	Thermal conductivity of basefluid W/m°C

k_{np}	Thermal conductivity of nanoparticle W/m°C
ρ_{np}	Density of nanoparticle, kg/m^3
ρ_{nf}	Density of nanofluid, kg/m^3
ρ_{nf}	Density of base fluid, kg/m^3
P_v	Density of vapor, kg/m^3
c_{np}	Specific Heat of nanofluid
c_{bf}	Specific Heat of base fluid
c_{nf}	Specific Heat of nanofluid
φ_v	Volume fraction
φ_m	Mass fraction
ζ	Zeta Potential
U	Electrophoretic Mobility
φ	Fluidity
ε	Liquid dielectric constant
n	Empirical shape factor
ψ	Sphericity
r_c	Minimum radius of nucleation site
p	Operating Pressure
C_{sf}	Surface liquid combination factor
h_{fg}	Latent Heat of Vaporization
ν	Kinematic viscosity

Subscripts

bf	base fluid
exp	experimental
i	inner
nf	nanofluid
np	nanoparticle
o	outer
pred	predicted
sf	surface liquid combination factor
s	saturation
v	vapor
w	wall

Dimensionless Group

Nu	Nusselt number	$\frac{hD}{k_{nf}}$
Pr	Prandtl number	$\frac{c_{pnf}\mu_{nf}}{k_{nf}}$
Ja	Jakob number	$\frac{c_{pnf\Delta T}}{\lambda}$
Re	Reynolds number	$\frac{Dv\rho}{\mu}$

Chapter – 1

INTRODUCTION

1.1 Background and Motivation

Energy has been considered as one of the vital issue facing mankind and touching all the fields of science and technology since last fifty years. Basically, energy conversion takes place at molecular level so it is expected that nanotechnology can play an important role in simulating the emerging energy oriented industries. Among all the modes of energy that is being in use today more than 80% is generated in the form of heat. Heat transfer intensification and reducing the heat loss by increasing the efficiency of the system has become a challenging task these days considering the worldwide energy demand. Efficient methods of heat transfer enhancement and control of heat loss are the challenges that are being faced in most of the high heat flux operations such as nuclear fission, pharmaceuticals, refrigeration, nano electronics, micro chemical reactions and process intensification.

Boiling is a complex phenomenon that involves nucleation, bubble formation and intricate dynamics of vapor bubbles. Thermal transport in pool boiling is governed by two major physical mechanisms that are: 1) latent heat of vaporization, and 2) dryout of the surface of the heating medium. Both parameters work in contradiction to each other in order to carry the heat away from the surface and thus preventing the heater element from break down in the pool boiling scenario. With the increase in wall superheat the nucleation site density increases that results in an increase in the bubble formation frequency. Some of the approaches or techniques adopted for increasing the pool boiling heat transfer are: 1) by increasing surface wettability of the liquid on the heater surface by oxidation of the heating surface or by selective fouling of heater surface, 2) by coating the heat transfer which increases the nucleation sites on the heating surface, 3) by the application of electrophoretic effect i.e. application of electric field to increase the bubble departure frequency, 4) vibration of heaters and fluid vibration that promotes the bubble departure from heater surface, and 5) by changing the orientation of heater to facilitate the bubble release from the surface.

Apart from the above-mentioned approaches, with the advent of nanoparticles application of nanofluids has shown great prospects in the chemical and automotive industries in the recent years. The term nanofluids was first proposed by Choi [C3, C4] which refers to suspensions made up of

nanometer sized particles dispersed in base fluid. Particles used to prepare nanofluids could be metal, metallic oxide or ceramic material with size less than 100 nm. Most commonly employed nanoparticles for the synthesis of nanofluids are metallic oxides such as aluminium oxide, copper oxide, titanium dioxide and silicon oxide. The base fluids generally used for dispersing the nanoparticles are water, ethylene glycol, lube oil etc. The prime advantage of the nanofluids is their ability to enhance the thermal conductivity in comparison to that of base fluid and hence found applications in various single phase heat transfer systems. The enhancement in thermal conductivity is set to be the basis for carrying out extensive research and exploring the potential application of nanofluids in phase change heat transfer intensification. The pioneering work carried out by Das et. al. [D1, D2, D3] in the field of pool boiling heat transfer in nanofluids and the results given by them exhibits either an increase or deterioration or sometimes negligible impact on heat transfer characteristics depending upon the level of stability and various other parameters such as heater surface characteristics, wettability, contact angle etc. Although level of enhancement depends on several factors viz. concentration, size and shape of nanoparticles, presence of additives and surfactants and stability of suspension as reported by Vassalo et. al. [V2]; Bang and Chang [B2]; Kathiravan et. al. [K4]. Wen and Ding [W5, W7, W8] observed an enhancement in heat transfer when boiling of alumina Al_2O_3 nanofluid was carried over a 150 mm stainless steel disc. The results were in contradiction to the Bang and Chang [B2] work and the possible reason given for this contradiction was low concentration of nanoparticles used.

The high thermal conductivity of the metallic oxides and the various physical characteristics such as size, shape and large specific surface area of the nanoparticles stimulated to carry out the potential investigation of the role of metallic oxide nanoparticles in heat transfer intensification. Specifically the high thermal conductivity possessed by alumina and copper oxide nanoparticles make them promising material for synthesizing the nanofluids with base fluid as distilled water. No consolidated theory defines the mechanism and the behavior of the nanoparticles in the base fluid clearly and the reasons responsible for enhancement in thermal conductivity of the nanofluids. This research focusses on investigating the impact of temperature on various thermophysical characteristics of nanofluids such as density, viscosity and thermal conductivity.

Research work focusing on the application of nanofluids in augmenting the heat transfer coefficient is still in the stage of infancy. A detailed review of nanofluids indicate that conflicting results were reported by different researchers on the impact of nanoparticles on the boiling heat

transfer coefficient of nanofluids. Many researchers observed deterioration in the boiling heat transfer coefficient [D2,D4,D5, B2, K3] while others reported either no change or fairly large increase in the heat transfer coefficient of nanofluids [B7,K3,K4,K7,K14,M3,M10,P2,R3]. This anomalous behavior of nanofluid indicated the need of further investigation. Also, most of the researchers carried out the work at high concentrations of nanoparticles in the base fluid .Generally the concentration of nanoparticles lie in between 1% to 6% by mass. Various researchers carried out the boiling experiments over nanofluids at atmospheric pressure. Thus, a comparative study of the impact of nanofluids containing well dispersed metallic oxide nanoparticles on the heat transfer coefficient of the base fluid with various compositions of nanoparticles in distilled water to be investigated.

1.2 Objectives of this Research

Keeping the above in view, an experimental investigation on nucleate pool boiling of nanoparticle based fluids on an electrically heated stainless steel heating tube surface with distilled water and nanofluids namely Alumina – Distilled Water and Copper Oxide – Distilled Water at atmospheric and sub-atmospheric pressure has been planned with the following objectives:

1. To synthesize the stable nanofluids namely Alumina – Distilled Water and Copper Oxide – Distilled Water with various concentration of nanoparticles.
2. To characterize the synthesized nanofluids by estimating the various properties namely thermal conductivity, viscosity and density at various temperatures.
3. To conduct experiments on nucleate pool boiling of saturated distilled water on a horizontal stainless steel heating tube surface at atmospheric and sub atmospheric pressures to investigate the effects of operating parameters on local heat transfer coefficient as well as average boiling heat transfer coefficient. Further, an attempt has been made to generate a correlation that could compute the average heat transfer coefficient as a function of heat flux and pressure.
4. To conduct the experiments for saturated boiling of nanofluids namely Alumina – Distilled Water and Copper Oxide – Distilled Water on a horizontal stainless steel heating tube surface at atmospheric and sub-atmospheric pressures and thereby to obtain the effect of operating parameters viz. heat flux, pressure and different concentrations of nanoparticles in distilled water on heat transfer coefficients and to develop the correlations.

5. To compare the heat transfer coefficient of nanofluids with that of distilled water in order to determine the percent enhancement of heat transfer coefficient.
6. To develop a dimensionless correlation for predicting the heat transfer coefficient during pool boiling of nanofluids on stainless steel heating tube surface.

1.3 Structure of Thesis

This thesis has been organized in seven chapters summarized as follows:

Chapter 1: This chapter provides the background and motivation for Nucleate Pool Boiling of Nanoparticle Based Fluids, its motivation and gaps. Further, it describes the objectives of the present research.

Chapter 2: In this chapter an attempt is made to present the relevant literature covering the techniques employed in synthesis of nanofluids, stability and thermophysical characterization of the nanofluids and nucleate pool boiling characteristics of nanofluids.

Chapter 3: In this chapter synthesis of stable nanofluids namely Alumina – Distilled Water and Copper Oxide – Distilled Water have been carried out. Further, the characterization of nanoparticles as well as nanofluids has been performed using Scannning Electron Microscopy, X ray Diffraction Method and Energy Dispersive X-Ray Analyser (EDX). Also, this chapter presents the effect of various parameters like nanoparticle concentration in the base fluids and temperature on the various thermophysical characteristics of nanofluids such as density, viscosity and thermal conductivity.

Chapter 4: This chapter describes the detailed description of experimental set up employed to investigate the heat transfer behavior of distilled water and nanofluids.

Chapter 5: This chapter discusses the experimental procedure to conduct the nucleate pool boiling of various liquids on stainless steel heating tube surface. This chapter also discusses the various integrity tests performed such as deaeration of vessel, leakage testing and calibration of thermocouples and various operating parameters taken during this work in order to attain accuracy and consistence in the experimental data.

Chapter 6: This chapter presents the results of experiments conducted for saturated boiling of Distilled Water and nanofluids namely Alumina – Distilled Water and Copper Oxide – Distilled

Water on a horizontal SS heating tube surface and there interpretations. It also includes a comparison between the boiling heat transfer coefficient with respect to heat flux for Alumina based nanofluids and copper oxide based nanofluids with base fluid as distilled water. Also, comparison between the thermal effectiveness of the base fluid and the two nanofluids namely Alumina – Distilled Water and Copper Oxide – Distilled Water has been investigated in order to bring out the scope of application of nanoparticle based fluids during nucleate pool boiling. Furthermore, a dimensionless correlation is proposed for the prediction of heat transfer characteristics of nanofluids during pool boiling on stainless steel heating tube surface at atmospheric and sub-atmospheric pressures.

Chapter 7: This chapter presents the conclusions drawn from the present research work along with the scope of future work.

Chapter – 2

LITERATURE REVIEW

Boiling has been found to be one of the most adequate mode for the heat transfer that founds application in transfer of energy in the form of heat in large number of industrial applications such as automotive industries, nuclear reactors, heat exchanger systems, power plants, refrigeration systems, heating, ventilation and air conditioning (HVAC),electronic cooling etc.

Large number of research work has been carried out since the 1930's for the analysis of the process of boiling& its characteristics. The pioneering work on boiling was done in 1934 by Nukiyama [N4]. Rohsenow [R2] proposed correlations for heat flux & heat transfer coefficient for various liquids. Although a lot of research is being carried out on the mechanism of pool boiling, it is still not accurately understood.

Various boiling regimes classified on the basis of excess temperature are nucleate boiling, transition boiling &film boiling. Nucleate boiling is considered to be an efficient heat-transfer mechanism; however, in order to incorporate nucleate boiling in practical operations, it is important to maintain the heat flux value below the critical heat flux and it should not be more than the critical heat flux (CHF). CHF phenomenon is the threshold limit for the boiling phase change phenomenon. When the critical point is attained a film of vapor bubble covers the surface of heating medium and acts as a barrier in heat flow from the surface to fluid. Thereby the surface temperature of heater rises exceptionally which results in burnout of the material of the heater surface. In addition to this, there is a transition from efficient nucleate boiling region to lesser efficient film boiling phenomenon at the CHF point thereby decreasing heat transfer rate. So, there is a huge demand to increase the CHF for safety as well as effective execution of thermal setups.

For decades, research has been carried out in order to establish more effective heat-transfer fluids, and also to raise the CHF of the thermal system that could improve the process efficiency as well as scale down the operational costs. This is where engineered colloidal fluids called nanofluids could play an important role; they could possibly revolutionize heat transfer area.

This chapter presents a detailed review of the work of prominent researchers related to nanofluids and their potential impact on the heat transfer performance. Numerous studies have been reported on boiling phenomenon and boiling curves by various researchers. First the techniques employed

by various researches to synthesize stable nanofluids have been reviewed. Preparation of stable dispersed nanofluids was the pre-requirement in order to ensure that reliable experimental data is collected. Next, observed impacts on the boiling heat transfer, surface modification of the heating medium and critical heat flux are discussed based on the results of the existing pool boiling studies of various researchers.

2.1 Nanofluids: Synthesis

In last two decades nanofluids have gained more attention due to their property of large relative surface area and wider applications in heat transfer performance. Nanofluids refer to fluids synthesized by dispersing the particles with size less than 100 nm (metallic nanoparticles, metallic oxides, nanofibers, nanosheets etc) in base fluid such as ethylene glycol, distilled water etc. Nanofluid synthesis with negligible agglomeration and less settling is the basic step in carrying out experimental work with nanofluids. Formulation of nanofluid is not a simple two phase mixture of solid- liquid but require some special physical and chemical treatments in order to obtain stable and well dispersed suspensions of nanoparticles in base fluid with minimal agglomeration and not altering the chemical properties of the fluid as well as surface properties of the nanoparticles. The preparation techniques of nanofluids are broadly classified into two categories:

a) Single step method
b) Two step method

One step technique involves simultaneous synthesis and dispersion of nanoparticles to the base fluid while in two step method nanoparticle synthesis and preparation of dispersions are carried out separately. Some of the prominent physical one step method are discussed here. In such methods nanoparticles are directly vaporized in vacuum. Nanoparticles are also prepared using submerged arc technique in which electric arc is used to heat the metal electrode while the vaporization of base fluid and its condensation in the vacuum chamber takes place simultaneously.

Zhu et. al. [Z4] employed the one step technique for the synthesis of CuO- Ethylene Glycol nanofluids. They prepared the nanofluid by reduction of copper sulfate under microwave irradiation. In this method $CuSO_4.5H_2O$ was reduced with $NaH_2PO_2.H_2O$ under microwave irradiation. The nanofluids thus synthesized were well dispersed and nanoparticles were stably

suspended in the base fluid. Nanofluids results exhibit strong influence of microwave radiation and addition of $NaH_2PO_2.H_2O$ on the rate of reaction and influences the thermal and rheological characteristics of Copper nanofluids. The major advantages of one step method are synthesis of more stable nanofluids with less agglomeration , negligible oxidation of metallic nanoparticles in synthesis of metallic nanofluids. The nanofluids prepared by using one step method contain uniform nanoparticle size. On the other had basic drawback of one step technique is to scale up the synthesis of nanofluid and not to restrict the production of nanofluid upto lab scale and it is difficult to synthesize high volumetric concentration of nanofluids. Another important drawback of one step method is the removal of the unwanted reactants present along with the desired nanoparticles in the base fluid due to incomplete reaction remains a challenge for the researcher. These unwanted reactants in nanofluid leads to the impurity effect which in turn impacts other thermal characteristics as well as heat transfer performance of nanofluid.

Akoh et. al.[A8] synthesized a new approach termed VEROS (vacuum evaporation onto a running oil substrate) technique in Japan few years ago. With the help of this technique nanoparticles are synthesized with less agglomeration in the form of condensed powders from the vapor phase directly into a flowing low-vapor-pressure fluid. This method has not been employed largely by the researchers in their work as it has a drawback of separating the nanoparticles from the fluids in order to make dry powders or bulk materials.

Wagener et al. [W1] and Eastman et al. [E2, E4] developed another technique based on direct evaporation based on the modifications in the VEROS. This technique overcomes the challenges of the VEROS and prepare stable and well dispersed nanofluids. The nanofluids thus synthesized from direct evaporation–condensation process have a uniform distribution of nanoparticles in base fluid. With the help of this technique researchers prepared well dispersed copper nanofluids with negligible agglomeration and excellent dispersion characteristics. The thermal conductivity of base fluid i.e. ethylene glycol enhances by 40% on addition of 0.3% by volume concentration of Cu nanoparticles. However, there were certain disadvantages of the technology used by Eastman et al.[E3] like with the help of this technique large scale formulation of nanofluids was not possible and another disadvantage is that this method founds application for the base fluids which have low vapor pressure.

Choi et. al. [C3, C4]; Hong [H7] and Yang [Y1] widely employed two step dispersion methods for the synthesis of nanofluids due to the commercial availability of dry nanoparticles by various

companies. In two step technique nanoparticles are first synthesized or procured from the commercial suppliers and then dispersed in the base fluids. Dry Nanoparticles can be synthesized by employing several techniques like mechanical milling, inert gas condensation and chemical vapor deposition. It is found difficult to prepare stable dispersion of nanofluid as nanoparticles tend to agglomerate due to vander walls forces acting among the particles which tend to form agglomerates. For preparation of stable dispersion with no agglomeration of particles ultrasonicators are used. Two step method is more suitable and widely adopted by different researchers for synthesis of nanofluids with metal and their oxides as nanoparticles. During the synthesis of metallic nanoparticles, oxidation of the nanoparticles may cause further difficulties in formulation of metallic nanofluids. There are certain other techniques apart from use of ultrasonication to attain the stability of nanofluids and avoid the sedimentation of nanoparticles such as addition of dispersants or changing the pH of the fluid and keeping the pH away from the isoelectric potential. The addition of surfactants or altering the pH results in modification of the surface characteristics of the nanoparticles thereby suppressing the tendency of the particles to form agglomerates. Thus, selection of surfactants or dispersants depends on how it affects the surface properties of the nanoparticles as well as the properties of the base fluid. However, deterioration in heat transfer performance of the nanofluids has been reported by various researchers on the addition of foreign agents such as surfactants. Such effects are undesirable during experimental studies and must be considered. Choi et. al. [C3, C4] reported that experimental work at high temperature may result in the breakdown of the surfactants and altering the pH in order to attain stability may lead to corrosion concerns. The major advantage of two step technique over single step technique lies in large scale production of nanoparticles, low cost and increased usability of the nanofluids in real time applications.

As the time advances researchers have focused on developing other methods of nanofluid formulation apart from these one step and two step methods. Some of the novel nanofluid synthesis techniques are discussed here.

Yu et. al. [Y6, Y7] in their efforts developed a continuous flow micro fluidic reactor for the synthesis of Copper nanofluids. With the help of this reactor Copper nanofluids were synthesized continuously by controlling the various parameters such as reactant concentration, additive and flow rate . They synthesized 10% by volume CuO nanofluid using a novel precursor transformation technique by the use of ultrasonic and microwave irradiation. In this method the

precursor $Cu(OH)_2$ is transformed using microwave irradiation to CuO in H_2O. The ammonium citrate is also added to the suspension to avoid the formation of aggregates thereby increasing the stability of CuO-H_2O nanofluid with high thermal conductivity in comparison to CuO nanofluids prepared using other methods. Various other novel formulation methods have been adopted for the synthesis of nanofluid where the microstructure of nanoparticle can be controlled or varied by adjusting various synthesis parameters such as temperature, acidity, flow rate of reactants, ultrasonic and microwave radiation frequency and concentration of the additives used to avoid the settling of nanoparticles.

2.2 Stability of Nanofluids

The major challenge in practical usability of nanofluids is to attain excellent stability of the order of several days. Thus,, there are several methods to attan stability by incorporating surfactant or additives to the nanofluid, by maintainin pH of the nanofluid and controlling the ultrasonication time. Following paragraph discusses the pertinent literature of stability of nanofluids.

On further investigation and from the work of prominent researchers Kim et. al.[K10], Lee et. al. [L4, L5], Wang et. al. [W3] it was observed that stability of nanofluids is influenced by multiple variables. The smaller the size of the nanoparticles more is the probability for the nanoparticles to escape the gravity and thereby avoiding the settling of nanoparticles. Although surface to volume ratio of the system increases dramatically with decrease in the particle size. Thus the energy barrier must exists in between the particles that restricts or controls the particles from crossing from unstable to stable energy state is termed as metastable or colloidaly stable state. This energy barrier should be strong enough in order to prevent the impingement of the nanoparticles on each other due to their Brownian motion. The interaction among the nanoparticles is thus governed by the Vander walls forces and electrostatic and steric repulsions. The repulsive barrier is created due to the changes on the surface of the nanoparticles. The nanoparticles having like charges on their surface tend to repel each other thereby avoiding the clustering of nanoparticles. Surface charge of the nanoparticles is created or modified by the addition of the acid or base or chemical surfactants leads to the ionization of the particle surface. However settling of nanoparticles in so formed nanofluids do take place at a slower rate leading to higher stability of nanofluids for longer period of time.

Eastman et. al. [E3] employed one step method i.e. physical vapor condensation technique for the synthesis of copper-ethylene glycol nanofluids to avoid the formation of agglomerates in nanofluids. This reduces the probability of agglomerate formation hereby increasing the stability of nanofluids. The stability of nanofluid increases as in this method there is no requirement of drying of nanoparticles also problems of storage and transportation of nanoparticle is not there. They employed vacuum submerged arc nanoparticle synthesis system [V-SANSS] to formulate the nanometer sized particle suspensions. The suspensions prepared using this technique also exhibits fairly good stability as it prevents the nanoparticles to form agglomerates in the suspension. The different shapes of the nanoparticles such as polygonal , cylindrical , spherical etc. highly influence the dispersion parameters as well as thermal and rheological characteristics of nanofluids such as thermal conductivity , viscosity etc.

Hong et. al. [H7] in 2005 investigated various methods to improve stability of nanofluids by incorporating following techniques such as addition of surfactants or additives to the nanofluids; controlling the pH of the nanofluids and carrying out ultrasonication for a specific time period at which minimum agglomeration is there. Their work reflected that stability gained by the nanofluids using surfactant tends to break down at high temperature after certain time period say few days. In order to attain stability of the order of several months ultrasonication of nanofluids is required to be done frequently or more accurate and fine methods of synthesis of nanofluids is required as discussed in the work done by various researchers such as Yang & Liu [Y2]. The strong repulsive forces in between the particles and the good wettability with the base fluid are the reasons responsible for the stability of nanoparticles in the suspension. These repulsive forces avoid the agglomeration and settling of the nanoparticles particles in base fluid. Zeta Potential is the parameter used to quantify the extent of stability attained. Hemholtz - Smoluchowski equation (Cosgrove, 2010) is used for determining the zeta potential of nanofluid.

$$\zeta = \frac{U}{\varphi\epsilon}$$

Where U represents electrophoretic mobility

φ is fluidity i.e. reciprocal of viscosity,

and ε is the liquid dielectric constant

Thus, zeta potential is defined as the ratio of electrophoretic mobility to fluidity normalized by dielectric field i.e. the ratio of the relative motion of the particles under an electric field to the relative motion of the fluid under stress. The nanofluid is termed as stable only when it is far away from the isoelectric point which can be obtained by moderating the pH to slightly acidic or basic nature. The isoelectric point refers to the pH level where the particles does not carry any electric charge, thus particles tend to repel each other at isoelectric point. This behavior of the particles hinders the particles to agglomerate and thus improves the stability of the nanofluid. Nanofluids having very high or very low pH possess large zeta potential generally greater than 30 m eV and are considered to be stable in nature. Thus one can employ any one of the method or both i.e. addition of surfactant or moderating the pH of the nanofluid to improve the stability of the order of several days or months.

2.3 Effect on Thermophysical Characteristics:

Initially researchers focused and restricted their work to explore the methods for synthesizing stable nanofluids and to investigate the thermal behavior of nanofluids. Till 2008, most of the research work was carried out to explore the effect of nanoparticle concentration, size and shape on thermal conductivity of the base fluids. The thermal conductivity of base fluid and nanofluid is determined using transient hot wire technique by most of the researchers as this method produces results with high accuracy as reported by Lee et. al. [L5]. Other methods that have been used to determine the thermal conductivity values by different researchers. Other prominent methods to determine thermal conductivity of nanofluids are steady state method and oscillating temperature method. Most of the researchers used transient hot wire method for determining the thermal conductivity of the nanofluids as this method is considered to reproduce more consistent and accurate results for thermal conductivity. A teflon coated 99.9% pure platinum wire was used in the determination, this wire worked as both heater and probe to measure the thermal conductivity. Thermal conductivity of nanofluids is determined as a function of the concentration of nanoparticle after sonification. Lee et. al. [L5] initiated the work on investigating the thermal conductivity of nanofluids but could not gain much attention until Eastman[E3] carried out work on thermal characteristics of copper oxide ethylene glycol nanofluids.

Eastman et. al.[E3] in 2001 found a dramatic rise in thermal conductivity of nanofluids with Cu nanoparticles. They employed single step evaporation technique to prepare the Cu nanofluids.

Interestingly, an enhancement of 40 % in thermal conductivity for 0.3% particle concentration was observed when copper nanoparticles coated with thioglycol acid were used. This work has exhibited an increase in stability of the dispersions as the surface properties of the metallic nanoparticles were modified by coating with surfactant. Furthermore, the work by Lee et.al.[89] shows a large difference in the values of thermal conductivity of copper nanofluids determined experimentally and those determined using macroscopic theories. Thus a new horizon to research was opened to investigate impact of low concentration nanofluids on volume fraction.

Choi et. al. [C3] employed the two step technique to disperse the multi wall nanotubes to the base fluid synthetic poly – alpha olefin and found almost 150% enhancement in the thermal conductivity values of oil with 1% concentration by volume of nanotubes in the oil. No existing theory given by Maxwell J.C. [M10] in 1873; Hamilton and Crosser [H1] in 1962 could justify such change in thermal conductivity of nanofluids. The results or thermal conductivity values of the nanofluids given on the basis of above theories were almost linear while the experimental values of Choi et. al. [C3] gave a non-linear relationship in between the thermal conductivity and the concentration of the nanotubes in base fluid. However, conventional heat transfer fluids with micro meter sized particles does not exhibit such non-linear relationship in between the volumetric concentration of particles and the thermal conductivity.

In 2004, Xue et. al. [X7] performed experimental investigation of the impact of carbon nanotubes on the various thermophysical properties. The major driving force behind this work were the fascinating characteristics of the nanotubes such as large aspect ratio, better thermal conductivity and low density. But the experimental work did not yield the expected results and the reasons behind such results were investigated. They observed the orientation and geometry of the carbon nanotubes as well as the concentration by volume loading of the nanotubes and adhesion between the fibers and particle were the prominent intervening factors responsible for the unexpected behavior. Further, the work by Eastman et. al. [E3,E4] also showed that particle coating deteriorates the performance of nanoparticles toward increasing the thermal conductivity of the base fluid at only 3 % weight loading of the carbon nanotubes.

Chandrasekhar et. al.[C1] performed experimental investigation with alumina nanoparticles dispersed in distilled water as base fluid to explore the thermal conductivity and viscous behavior of nanofluids. The microwave assisted chemical precipitation technique was used to synthesize the

alumina nanoparticles and nanofluids of desired concentration were engineered by dispersing the nanoparticles in the base fluid by using sonicator. The work be Chandrashekhar et. al. reveals an enhancement in thermal conductivity with increase in the volumetric concentration of alumina nanoparticles in the base fluid. Also an increase in viscosity of the nanofluids was observed with the increase in nanoparticle concentration. The experimental values obtained by Chandrashekhar et. al. were in good agreement with the experimental data.

As another example Yu et. al. [Y6] in 2003 reported an increase of 300% in thermal conductivity when compared to that of base fluid. The prominent reason behind such large increase in thermal conductivity was the alignment of the carbon nanotubes in the direction of the fluid movement. Further in 2003, Choi et. al. observed an 10% additional enhancement in thermal conductivity of the carbon nanotubes when aligned in the direction of the fluid movement. From the work Choi et. al. concluded that various parameters such as aspect ratio, interfacial layer resistance and interaction between the matrix and tubes to be the major reason behind such large enhancement.

Hussein et. al.[H8] in 2013 performed experimental and numerical simulation work to investigate the effect of volumetric concentration on the heat transfer, friction factor, thermal conductivity and viscosity inside a horizontal tube. Their findings depict an enhancement of 19 % in thermal conductivity and a deviation of 6 % in viscosity with increase in concentration of nanoparticles in the base fluid. Both the thermophysical properties exhibits enhancement with increase in the concentration. Also, an increase in the nusselt number and the friction factor is observed from the simulation work for the concentration change. The researchers performed the heating of nanofluid over flat tube and found an increase of 6% in the heat transfer values and a 4% decrease in the pressure drop for a particular concentration when compared with the boiling data carried over a circular heating tube.

Layth et. al.[L3] in his work made a comparative investigation of the thermal conductivity of micro fluids and nanofluids. Nanofluids were synthesized using silver and zirconium oxide nanoparticles. The experimental results of Ismael et. al. exhibits an enhancement in the thermal conductivity values of the nanofluids due to the stronger presence of nanoparticles than the microfluids. Thus from their work it is concluded that thermal conductivity enhancement is due to the presence of highly conductive nanoparticles. Particles in the nano size range have fascinated the researchers due to their better stability characteristics in comparison to microfluids.

Furthermore the results depict that the thermal conductivity values for nanoparticle based fluids doubtlessly reveal that the size and nature of nanoparticle plays a vital role affective conductive transport in the nano-suspensions.

Hwang et. al. [H9] performed the experiments to compare the thermal conductivity values of alumina – distilled water nanofluids with that of Fe- Distilled Water nanofluids. They carried out the experimental work believing that the theory behind enhancement in the thermal conductivity values cannot be explained only by the conventional theory of two component mixtures but other factors such as use of surfactants, stability of nanofluids, Brownian motion of nanoparticles also play an important role. Yu et. al. [Y6] investigated the effect of pH and carried out experiments to determine the thermal conductivity of alumina-distilled water dispersions at different pH values such as 7, 9.65 and 10.94. The thermal conductivity values for alumina- distilled water nanofluid was found to be closer to the values determined using Hamilton – Crosser model. Also the effect of pH on the thermal conductivity of nanofluids was studied and the results reported indicates that thermal conductivity of nanofluids is improved by controlling the pH values of the nanofluid.

Madhesh et. al. [M1] in their work took a combination of nanoparticles Cu and Titania and illustrated the dependence of thermal conductivity on particle volume concentration of nanofluid. Results of their work revealed an enhancement of 52% and 49% in convective heat transfer coefficient and Nusselt nuber for 1% volumetric concentration of nanofluid.Also they observed a decrease in heat transfer coefficient at higher volumetric concentration. For 1.6% volume concentration of nanofluid they observed an enhancement of 27% in convective heat transfer coefficient.

Keblinski et. al.[K6] in their work focused on exploring the probable causes behind the rise in thermal conductivity of nanofluid with increase in particle concentration. They reported four prominent causes responsible for such behavior which are listed here:

1) Brownian motion of the nanoparticles.
2) Molecular layer formation of liquid in between the liquid-particle interface
3) Impact of the clustering of the nanoparticles.
4) The nature of heat transport in the nanoparticles.

Pantzali et. al. [P3] in their work prepared a 4% CuO suspension in water and performed a set of experiments to study the application of nanofluid as a coolant. The work by the researchers indicated that thermophysical properties were considerably improved on addition of nanoparticle to the base fluid. They also studied the performance of the nanofluid on plate heat exchanger. These studies also exhibit that the flow in the heat exchanger also effects the efficacy of the coolant. Thus the viscosity of nanofluid accounts to be a crucial factor. From the work of M.N. Pantzali it was concluded that large volume fraction of nanofluids were not found to be suitable for coolant replacement in plate heat exchanger. Table 2.1 below summarizes the work presented on thermal conductivity by prominent researchers and the observations made by them for various combinations of nanoparticle-base fluid.

Table 2.1: Brief Summary of experimental work on thermal conductivity of nanofluids

Researcher	**Nanoparticles**	**Size(nm)**	**Base Fluids**	**Observations(Thermal conductivity)**
Eastman et. al.(1997)	Al_2O_3, CuO, Cu	33;36; 18	Water, HE-200 oil	60% enhancement for 5 % concentration of CuO nanoparticles in water
Lee et. al. (1999)	Al_2O_3; CuO	24.4/38.4;18.6/23.6	Water, EG	20% increase for 4% of CuO-EG mixture
Wang et. al. (1999)	Al_2O_3, CuO	28/23	Water, EG, PO, EO	12 % increase for 3% by volume of Al_2O_3-H_2O nanofluids
Das et. al. (2003 c)	Al_2O_3, CuO	38.4,28.6	Water	2 - 4 times increase over range of 21 °C – 52 °C
Li and Peterson(2006)	Al_2O_3,CuO	36,29	Water	Thermal conductivity increases with concentration and temperature
Xuan and Li (2000)	Cu	100	Water, Oil	Stable suspension of Cu nanoparticles reported 43 % enhancement in thermal conductivity.

Eastman et. al. (2001)	Cu	<10	EG	40% increase for 0.3 volume % Cu- based nanofluids
Hong et. al.(2005)	Fe	10	EG	18% increase for 0.55 volume% Fe/EG nanofluids
Murshed et. al. (2005)	TiO_2	ϕ10 × 40, ϕ 15	DW	For 5 volume % 33% increase and 30 % increase for 10 volume %
Xie et. al. (2001, 2002 b)	SiC	ϕ26, 600	Water, EG	15.8% increase at 4.2 volume% forϕ26 SiC - H_2O and 22.9% for 4 vol % for ϕ600 SiC-H_2O
Choi et. al. (2001)	MWNTs	ϕ25 × 50 μm	Oil	Exceeds 250% at 1.0 vol%
Biercuk et. al. (2002)	SWNTs	ϕ3 – 30	Epoxy	125% enhancement at 1.0 wt%
Xie et. al. (2003)	TCNTs	ϕ15 × 30 μm	DW,EG,DE	19.6%, 12.7% and 7.0% increase respectively at 1 vol % for TCNT-DE/EG/DW, respectively

2.4 Pool Boiling of Nanofluids

Although, thermal conductivity enhancement plays a significant role and stands as a basis to investigate the impact of nanoparticles on the heat transfer characteristics of nanofluids. Apart from thermal conductivity there are several other parameters that also influence the heat transfer properties of nanofluids such as density, viscosity, shape and geometry of nanoparticles , heating tube geometry, orientation etc. For example, the heat transfer coefficient for forced convection in tubes depends on many properties such as fluid viscosity, fluid pressure, velocity , physical geometry of the cross section through which the fluid is flowing. Therefore, it is essential to measure the heat transfer performance of nanofluids directly under flow conditions. Various

researchers reported different results based on their observations for heat transfer coefficient. The work of different investigators show that introduction of nanoparticles to the base fluid not only influences the thermophysical characteristics but also have a significant impact on the heat transfer coefficient value when compared to that of base fluids. Experimental work of several researchers reveal that the heat transfer coefficient values for nanofluids are much better than expected from enhanced thermal conductivity alone when investigated for pool boiling and flow boiling with laminar and turbulent flow. However, for natural convection, nanofluids have lower heat transfer than that of base fluids. Anomalous results have been reported by various researchers in their work on pool boiling of nanofluids. Several researchers in their investigation found an increase in the pool boiling heat transfer while others reported a reduction or negligible change at all in the pool boiling heat transfer. Based on heat transfer modes research work so far carried out by various researchers to investigate the thermal transport behavior of nanofluids has been broadly classified into three types:

1. Thermal Conductivity
2. Convective Heat Transfer
3. Pool Boiling Heat Transfer

From the research work carried by different researchers anomalous results of heat transfer yields considerable disagreement over the effective application of nanofluids in heat transfer. Since, the prime focus of work is pool boiling heat transfer investigation of the nanofluids the following paragraph will cover a detail review of the work done so far by various researchers in the field of nanofluid pool boiling.

Yang & Maa [Y3] performed boiling experiments with different size Alumina nanoparticles and water as base fluid. The size of the nanoparticles taken were 50 nm , 300 nm and 1 μm. They took different compositions of alumina distilled water nanofluids with varying concentration of alumina nanoparticles ranging from 0.1% to 0.5% in the nucleate pool boiling regime. They observed significant improvement in the pool boiling performance at low volumetric concentration of alumina nanoparticles. However for 1 μm sized alumina particle synthesis of stable suspension and the problem of faster settling of particles onto the heater surface was reported by Yang & Maa which in turn results in the erosion of the surface.

Faulkner et al. [F1] in their work reported significant enhancement in the overall heat transfer value for the CNT's (Carbon nanotubes) dispersed in base fluid water. They carried out fully

developed convection heat transfer experiments with the CNT – Distilled Water base nanofluids and observed considerable enhancements in the overall heat transfer coefficient. They observed a rise in heat transfer coefficient of the nanofluids on increasing the Reynolds number. From their work they reported that nanofluids with lower concentration of nanotubes (upto 1.1% by volume) depict better enhancement in terms of heat transfer than those of higher concentration of the order of 2.2% to 4.4%. Also the heat transfer coefficient values were twice in comparison to the base fluid i.e. water on the upper range of the Reynolds number. This behavior is unexpected and, indeed, counterintuitive result. The primary reason behind such negative concentration dependence of the heat transfer enhancement could the interaction among the particles. Faulkner et al.[F1] proposed microscale mixing and pseudo turbulence induced in fluid due to the mixing of the nanotubes and the rolling and tumbling of the nanotube agglomerates to be the reason responsible for enhancement in the laminar heat transfer coefficient. Since industrial operations are carried over a wide range of heat flux values and Reynolds number thus further research is required in the field of nanofluids to develop new generation nanofluids . In contrast to the work of Faulkner et al.[F1], Yang et al. [Y2] also performed experiments in the field of laminar flow of nanofluids and experimentally determined the convective heat transfer coefficients for various nanofluids in a horizontal tube heat exchanger. They employed graphite nanoparticles having disk shaped geometry in their work. The average size of the graphite nanoparticles used by them is about 1 to 2 μm, with a thickness of around 20 to 40 nm. The experimental results of Yang et. al. depicts an enhancement in the heat transfer coefficient values although when experimental results are compared with the predicted values using experimental shows that the enhancement is much less than that predicted from a conventional correlation. They gave explanation of near-wall particle depletion during laminar shear flow as one possible reason behind the difference in the experimental and values from correlation for heat transfer coefficient. However, as the particle size of the graphite particles is of the order of micron thus there is a doubt that if this work falls in the category of nanofluids at all .

Das et. al. [D2] in their work performed the pool boiling experiments in order to compare the heat transfer coefficient and other boiling parameters for alumina based DW nanofluids and pure water. The boiling of the nanofluid and distilled water was done using a cylindrical cartridge heater and the various limitations and applications of nanofluids were investigated during the phase change. The experiments were performed using the SS Heating tubes with 20 mm diameter and the

concentration of the nanoparticles in the distilled water varied from 4 % to 16 % by weight. Nanofluid synthesis is done without using any of the stability agent such as surfactant or electrostatic stabilization techniques. As such, at higher concentration nanofluids reported faster settling of nanoparticles over the surface of the heating tube which in turn results in deterioration of the boiling performance and poor heat transfer coefficient values were recorded. The surface of the heating tube becomes smooth due to the settling of nanoparticles and this is considered to be the probable reason behind the deterioration of the boiling performance characteristics. Later on in 2003 , Das et. al [D3] in their work exhibited that qualitatively the heat transfer performance differs when the boiling performance takes place with narrow heating tubes. This time they took the heating tubes with diameter 4mm and 6.5 mm for performing the pool boiling experiments and investigated the heat transfer characteristics of alumina – distilled water nanofluids. This time the results reported by Das et. al [D3] were quite different from their previous work where they employed heating tubes of larger diameter. Although deterioration in Boiling heat transfer was reported but it was less in comparison to that found during the boiling experiments carried over large diameter heating tubes. This difference in heat transfer deterioration was attributed to the change in the bubble sliding mechanism. The smaller diameter of the heating tube results in large curvature of surface that results in direct departure of bubbles with large diameter instead of sliding over the heating tube surface. The interpretations of Das et. al.[D3] were in contradiction to the work of Bang and Chang [B2] who investigated the boiling performance of the same nanofluid i.e. Alumina – Distilled Water which has been discussed in the paragraph below.

Bang and Chang [B2] further in their work performed pool boiling experiments with Alumina – Distilled Water nanofluids over the heating tube with highly smoothened surface. The surface roughness value of the heating tube is measured to be = 370 nm. They performed the pool boiling experiments with the same concentration of alumina – distilled water nanofluids as taken by Das et. al. [D2,D3] i.e. 4 to 16 weight percentage. The experiments are performed at higher heat fluxes and deterioration in the heat transfer coefficient and pool boiling was observed similar to Das et. al. The rate of heat transfer observed differ from the work of Das et. al. [D3] which they attributed to the surface properties such as roughness, shape of heater as well as the orientation of the heating tube. Their work further reveals that pool boiling data does not conforms to the Rohsenow correlation just by altering the nanofluid properties. Bang and Chang [B2] tried various correlations by making changes in the effective conductivity or altering the values of surface

interaction parameter C_{sf} in Rohsenow correlation and reported that on varying the thermal properties of the nanofluid and bringing the changes in the surface fluid combination factor leads to better proximity to the experimental boiling data. The work by Bang & Chang and their findings indicate that the change in the surface characteristics of the heating tube can lead to change in the value of surface – fluid combination factor (C_{sf}) which might give better explanation for the enhancement or deterioration of the pool boiling heat transfer as reported in the work of Yang et. al [Y1] and Das et. al [D3]. The observations made by Bang and Chang were in contradiction to the work of Das et. al [D3] as they reported deterioration of the heater surface i.e. roughness value increases with the increase in the concentration of nanofluid. They supported their observations by giving explanation that the deterioration in the heat transfer value may occur due to the closeness in the values of roughness surface and the particle size which results in the overriding of the fouling effect i.e. the particle layer does not form over the surface of the heating tube. Thus from the work of Bang & Chang [B2] it was concluded that for roughness value smaller than the particle size, formation of porous layer of particles over the heating tube was expected.

Wen and Ding [W5*] performed experiments with γ-Al_2O_3 nanoparticles* with distilled water as base fluid. They were among the initial investigators who explored the effect of nanoparticles on the laminar entry flow of nanofluids. In their work they reported an enhancement in the heat transfer coefficient of γ-Al_2O_3 and distilled water nanofluids in comparison to base fluid alone at the entrance region and a longer entry length for the nanofluids. Wen and Ding et al. [W6] in 2004 also investigated the heat transfer characteristics for carbon nanotube dispersions laminar entry flow. With 0.5% by weight of carbon nanotubes in water they observed 350% enhancement in the heat transfer coefficient for the laminar flow having Reynolds number 800 . From such enhancements Wen and Ding concluded that increase in thermal conductivity due to presence of nanoparticles could not be the only reason responsible for such large increase in the heat transfer coefficient and explored several other possible reasons behind such a high level of enhancement. They proposed various mechanisms responsible for such behavior like high aspect ratio of carbon nanotubes, particle orientation, flow characteristics.

Wen and Ding [W7, W8,W9] in their work observed an enhancement in the boiling heat transfer coefficient during the pool boiling of nanofluids. Completely different results are reported by Wen and Ding in their work during the boiling of same nanofluids as taken by Das et. al. [D3] in their work. Wen and Ding acquired the alumina nanoparticles from the Nanophase Technologies;

U.S.A. with particle size ranging in between 10 to 50 nm. The nanofluids thus synthesized using two step technique were kept stable by keeping pH value near to 7 which is far away from the iso-electric potential of alumina i.e. 9.1. Even after using high speed homogenization, agglomeration of nanoparticles was observed and the average diameter was found to be 167.54 nm but the nanofluids at this size were reported to exhibit fair stability by the researchers. The results reported by Wen and Ding are in contradiction to the earlier workers as they found an enhancement in heat transfer coefficient as high as 40 % for 1.25 weight % of nanoparticles in Distilled water. As the enhancement in heat transfer coefficient values is reported to be larger than the enhancement in thermal conductivity values therefore Wen and Ding concluded that thermal conductivity enhancement alone cannot be expected to be the sufficient reason to support the enhancement in heat transfer coefficient values. They also observed that the values of heat transfer coefficient increases with the rise in heat flux for a particular concentration, thus heat transfer coefficient was found to be strongly dependent on particle volumetric concentration as well as heat flux. Along with nanoparticle concentration and heat flux Wen & Ding also reported several other reasons such as surface properties other than roughness like wettability; influence of surfactant and stabilizing agent and characteristic size of the system to be the most possible reasons that could also influence the pool boiling process and can change the heat transfer characteristics. Wen and Ding in their work took gamma phase Al_2O_3 nanoparticles and observed no deposition of the nanoparticles during the boiling of nanofluids on a stainless steel disc having roughness of the order of microns. In another study by Wen & Ding over the same set-up for TiO_2 nanoparticles an enhancement of approximately 50 % was observed in the boiling heat transfer values. No particle deposition on heater surface was observed by the researchers for titania based nanofluids also. Truong et. al. in their work found 68% increase in boiling heat transfer coefficient of alumina- DW and silica- DW nanofluids during pool boiling experiments.

Xuan and Li [X5, X6] in their work also depict a significant enhancement in the turbulent heat transfer coefficient. They performed experiments to determine convective heat transfer coefficient for nanofluids containing copper nanoparticles in well dispersed state. From the experimental work and their results they reported an enhancement of 40% in heat transfer coefficient on addition of 2% by concentration of copper nanoparticles in water. Xuan et al also compared their experimental findings with the heat transfer coefficient values predicted using Dittus–Boelter correlation and observed that the predicted values from the equation failed to match with the experimental heat

transfer behavior of nanofluids. Recent studies shows that the effect of various parameters such as particle size, shape and extent of dispersion becomes predominant factors responsible for enhancing heat transfer coefficient in nanofluids. Even formulation method of nanofluids such as one step or two step method significantly influences the heat transfer effects.

Tiwari [T5] in their investigation observed maximum enhancement in heat transfer coefficient at 1% by volume concentration of alumina nanofluids. They prepared alumina nanofluids with various composition ranging from 0.3% to 1% by volume of alumina nanoparticles uniformly dispersed in water. The results reported by Tiwari et al. revealed an enhancement in overall heat transfer coefficient by 27.9 % respectively for the maximum concentration for alumina nanoparticles.

S.S. Chougule and Sahu [C6] in their work took CNT's and Alumina dispersion in water. They observed an increase in the heat transfer with rise in concentration of both the nanoparticles . They prepared various compositions of alumina nanofluids with concentrations 0.15%, 0.45%, 0.6% and 1.0% respectively and the rise in heat transfer observed were found to be 23.0%, 33.12%, 40.38% and 52.03%. For CNT _ water suspensions maximum enhancement was found to be 90.76%as compared to alumina suspensions. Further they also observed an enhancement in nusselt number for increase in CNT concentration and concluded that the enhancement in heat transfer coefficient can result in size reduction of radiators in automobile engines leading to an improvement in the fuel efficiency of the vehicle.

Chopkar et. al. [C5] observed enhancement as well as deterioration in the boiling heat transfer coefficient during their work. They took zirconia nanoparticles suspension and performed boiling experiments on a copper block and observed an enhancement in heat transfer for low concentration of zirconia nanoparticles but as the concentration is increased or for repeated runs a deterioration in heat transfer was seen. The influence of surfactants on HTC was also studied and observed anomalous behavior. The researchers concluded that it is difficult to predict the exact behavior as they observed both enhancement and deterioration in the HTC of nanofluids with particle loading.

Narayan et. al. [N3] performed experimental work on alumina nanofluids. They took vertical cylindrical tubes with different surface roughness values ranging from 48 – 524 nm to perform tests. The researchers gave a surface interaction parameter i.e. simply the ratio of the surface roughness value of the tube to the average particle diameter. The authors concluded in their findings that when the value of interaction parameter is one heat transfer increases as the surface

roughness value is greater than the average particle diameter and vice-versa. They also came to conclusion that if the average particle size of the nanoparticle equals the roughness value of the tube, the nucleation sites will be blocked resulting in the heat transfer of the tube.

Suresh et. al. [S18] carried out experimental work with hybrid nanofluids. They took a combination of alumina and copper nanoparticles dispersed in the base fluid and investigated the heat transfer and pressure drop characteristics across the fully developed laminar flow. They employed a circular heating tube of uniform cross section as heating medium. They prepared nanofluids of hybrid nature by using thermos chemical procedure. To prepare nanofluid of 0.1% composition a hybrid mixture of 90% alumina and 10% copper were taken in the base fluid. The hydrogen reduction technique is used to formulate the suspension of nanocomposite powder in the base fluid i.e. water. The experimental findings reveal an enhancement of 13.56% in Nusselt number when the laminar flow of nanofluid is kept at a Reynolds number value of 1730 when compared to Nusselt number of water. Further the researchers compared the friction factor with that of Alumina – water nanofluids and was found to be slightly more. Also it was clear from the experimental work of Suresh et. al. that there is an increase in thermal conductivity and viscosity of nanofluid with the increase in the nanoparticle volume concentration. There is a 12.11% increase in the thermal conductivity for 2% by volume concentration of nanofluid. Also the experimental results were compared with the classical theoretical models available in the literature. The thermal conductivity and viscosity of nanofluids have been measured and it has been found that the viscosity increase is substantially higher than the increase in thermal conductivity.

Hwang et. al. [H9] carried out experimental investigations to explore the effect of alumina nanoparticles onto the pressure drop and the convective heat transfer coefficient of suspensions. The nanofluids containing alumina nanoparticles dispersed in distilled water were formulated for different concentrations. The pressure drop and heat transfer coefficient of nanofluid flowing in a laminar profile across a uniformly heated circular tube is experimentally determined. The experimental results for the friction factor exists in good agreement with the values from the Darcy's equation for single phase flow. Comparing the heat transfer coefficient value with that of water Hwang et. al reported an enhancement of 8% for 0.3% concentration of alumina nanoparticles in the base fluid and this enhancement cannot be predicted by Shah equation. Furthermore, the experimental results depict a larger enhancement in the convective heat transfer coefficient enhancement in comparison to the change in the thermal conductivity.

Witharana [W11] studied heat transfer phenomenon in 2013 for boiling for nano-fluid with gold & silica particles suspended in base fluid: water & ethylene glycol. The suspensions of low volumetric concentration i.e. 0.001% by weight of Gold nanoparticles in distilled water are synthesized. The heating of the nanofluid suspension was carried over a flat plate heater. They performed their experiment in a cylindrical vessel at atmospheric conditions. Their heater surface was in form of Cu plate whose diameter was 100 mm. Researchers observed that HTC increased by 21 % in case of Au/water of 0.001 wt. % concentration. Witharana also observed that the HTC increased with increase in concentration of gold particle & that the rate of increase of HTC by increasing heat flux is greater in case of nanofluids than in case of pure water. They observed larger temperature differences in case of silica-water & silica-ethylene glycol solutions than that of their respective pure fluids. Thus they concluded that the addition of silica particles to water and ethylene glycol solutions resulted in detrimental effects on the boiling heat transfer coefficients. The results of pool boiling of nanofluids reveal an enhancement of the order of 11 % in heat transfer coefficient which further increases upto 21% with increase in the concentration of nanofluids.

Prakash et. al. [P5] in their work made an attempt to remove the ambiguities of the observations of several researchers and give a better understanding of pool boiling mechanism of the nanofluids. They took alumina- distilled water stable suspensions prepared for different size of alumina nanoparticles. Prakash et. al. investigated the heat transfer coefficient values for different concentration of nanofluids . Also the heaters with different surface roughness values were used for heating of nanofluids and the orientation of the heaters used was vertical. The experimental findings of Prakash et. al. reveals that when the average nanoparticle size is equal to or near the surface roughness value of the heating tube, the number of nucleation sites is greatly reduced whereas when the average particle size is less than the surface roughness value the number of nucleation sites on the heating surface increases. Prakash et. al. defined the ratio of surface roughness value of the heating medium and the average size of the nanoparticle as surface particle interaction parameter (Ra). The significance of this surface interaction parameter is that when its value is less than 1 ; it means average particle size is greater than surface roughness thereby the number of nucleation site decreases and vice – versa.

Kim et. al. [K10] in their work investigated the impact of nanoparticle deposition over the heating surface on the boiling characteristics. They observed formation of a porous layer of nanoparticles

on the heating surface due to settling of nanoparticles after pool boiling because of which the surface wettability characteristics increases. The researchers performed surface wetting experiments over the heating surface already boiled in the pool of nanofluid containing alumina nanoparticles having average size of the order 110 to20 nm, ZrO_2 nanoparticles with size 110 to 250 nm and silica nanoparticles with size 20nm to 40 nm. The work of Kim et. al. exhibits strong dependence between surface wettability and boiling process mechanism. Following observations were made by them such as the surface wettability increases, there is a reduction in the number of active nucleation sites which in turn results in decrease in rate of bubble departure frequency from the heating surface when compared with that of boiling of pure water. These observations could explain the deterioration in heat transfer as observed by other researchers but could not strongly support the observations of enhancement in heat transfer enhancement made by Witharna [W11]; Wen & Ding [W5]; Prakash et. al. [P5].

Kole and Dey [K14] explored the pool boiling behavior of Copper – Distilled water nanofluids over three cylindrical heating tube surfaces made up of copper and brass. The experimental results exhibit an enhancement in heat transfer for all the three heating tubes at increasing concentration of nanoparticles In their work effect of surface roughness, different material surface as well as varying concentration of copper nanoparticles in the nanofluids on the heat transfer coefficient has been investigated. The increase in surface roughness of both Copper and Brass heating tube after each run with Copper – Distilled Water happens due to the scattered deposition of copper nanoparticles onto the heater surface making it rougher which in turn increases the number density of the nucleation sites and results in more active boiling . From the observations of the work carried out by Kole et. al. it has been concluded that surface material of heating tube also has a significant influence on the heat transfer coefficient of nanofluid. Under identical conditions overall 45 % enhancement has been recorded in heat transfer coefficient for copper heating tube in comparison to that of brass surface.

Harish G. et. al. [H2] made an attempt to understand the surface interaction between the heater surface and nanoparticles and the impact of this surface interaction on the boiling phenomenon. Harish performed boiling experiments over electrostabilized alumina- distilled water nanofluids at the heaters with smooth as well as rough surface at different nanoparticle concentration. The surface wettability parameter is determined by measuring the advancing contact angle and various other surface properties were characterized by using non-intrusive optical techniques and atomic

force microscopy. The results reported by Harish et. al. give an insight of the practicability of existing boiling heat transfer mechanisms under various experimental parameters. Harish et. al. [H2] carried out experiments to investigate the boiling characteristics over the nanoparticle coated heaters and gave a fitting solution to counter the disadvantageous transient nature of the pool boiling process. Experimental results show that on varying the values of the surface interaction parameter results in the enclipsing of the surface cavities or nucleation sites thereby enhancing or deteriorating the heat transfer coefficient values. The transient nature of the boiling process can be countered by modifying the heater surface with the application of nanoparticle coating. This coated heater surface alters the surface wettability of the heater that counters the transient behavior of the boiling process. The non – intrusive techniques employed for surface characterization reveals that change in surface properties such as roughness and wettability to be the dominant mechanism behind this transient nature of boiling process.

Kwark. et. al. [K17] performed experiments at low concentration of nanofluids (<1gm/L) to study the nature of pool boiling carried over a flat heater at atmospheric pressure. The results reported by Kwark et. al. exhibits an increase in the CHF value due to the formation of a nanoparticle layer because of settling of nanoparticles over the heater surface. Further the work by Kwark et. al. also indicated nanoparticles deposition over the surface to be to be the probable reason for the deterioration of the heat transfer coefficient during nucleate pool boiling . Micro layer evaporation was held to be responsible for the settling of the nanoparticles onto the heater surface during nanofluid boiling.

Further extending the work of Yu et. al. [Y5], Kwark et. al.[K17] carried out nucleate pool boiling experiments to measure the heat transfer coefficient of water based nanofluids at atmospheric pressure. The experimental results reported a decrease in the heat transfer coefficient with increase in concentration of nanoparticles in the base fluid. Also, they observed an enhancement in critical heat flux with increase in volumetric concentration until a certain critical value of concentration is attained. An increase in surface wettability was given the reason behind the increase in the Critical Heat Flux of nanofluids. Thus 0.025g/L of nanoparticle concentration was found to be the optimum value for maximum enhancement in critical heat flux and minimum degradation in boiling heat transfer was observed. The wettability was increased upto a certain extent as porosity of the layer does not improved on further deposition. However, as the particle deposition onto the surface continues the thermal resistance of the heater surface increases thereby resulting in

deterioration of pool boiling heat transfer. Additionally, Kwark et. al. also observed an increase in the wall superheat that resulted in heat transfer degradation as nucleate boiling continued at constant heat flux. Thus the researchers concluded their work by postulating CHF enhancement of nanofluids with distilled water as base fluid as a function of surface wettability and independent of the duration of the pool boiling tests. They also explored a convincible theory behind the settling and deposition of the nanoparticles onto the heating surface. In this theory they suggested that boiling is the instrumental reason for the nanoparticle covering phenomenon. This was likewise reliable with Kim et. al. who proposed the settling of the nanoparticles onto the surface of the heating medium when boiling is carried out. They expected that the nanoparticle covering was framed by nucleated vapor bubbles developing at the warmer surface and the vanishing fluid that is abandoned inciting a concentrated microlayer of nanparticles at the air pocket base. The measure of settled nanoparticles onto the surface additionally relies upon the nanoparticle fixation. They additionally carried out two tests in order to investigate the impact of nano covered surfaces on pool boiling execution. For this two types of heaters were used by them; one cleaned with alumina nanofluid and second nanocovered heater with water and they reported that both the cases gave an indistinguishable improvement in critical heat flux , thereby concluding that it is the upgraded wettability due to surface covering that resulted in heat flux improvement and not the suspended nanoparticles in the base fluid.

Ramakrishna N. Hegde [R1] performed pool boiling experiments with copper oxide – distilled water nanofluids. The pool boiling experiments were carried out at atmospheric pressure in a cylindrical vessel with a vertical heating tube to investigate the behavior of copper oxide- distilled water nanofluids. The experiments were carried out for five different concentrations of copper oxide nanoparticle varying from 0.1 gm/L to 0.5 gm/L. The base fluid taken is distilled water. Experimental findings by Hegde reveal considerable rise in Critical heat flux and decrease in the heat transfer coefficient value with increase in concentration. For very low concentration of nanofluids (0.1 gm/L) an increase of approximately 33.4% in critical heat flux was observed when compared with pure water. SEM images of the heater surface and determination of the surface roughness values of the heating tube after the experiments confirms the formation of a non-porous layer due to settling of nanoparticles over the heating tube. Due to the settling of nanoparticles onto the surface of heating tube the roughness value of the heater surface reduces from 0.33 μm to 0.23 μm.

Sarfaraz et. al. [S2] performed nucleate pool boiling experiments to study the influence of alumina nanoparticles dispersed in a binary mixture of water and glycol. The heat flux was changed upto 91 KW/m^2 for different volume fractions of glycol ranging from 1% to 5% in distilled water. The alumina nanoparticle concentration in the binary mixture is taken to be 0.5%; 1% and 1.5%. The experimental findings for different alumina nanoparticle concentration reveals that pool boiling heat transfer coefficient increases with the increase in nanoparticle concentration whereas the wall superheat temperature of the surface decreases. Also a simple semi- mathematical model is proposed by Sarfaraz et.al. for making a rough estimate of the enhanced heat transfer values with an uncertainty of about +/-8%. Also as expected the heat transfer coefficient values were strongly dependent on heat flux . It means that for higher heat flux values high enhancement in heat transfer coefficient is reported in presence of nanoparticles when compared with the binary mixture of distilled water and glycol without any nanoparticles.

Layth [L3] carried numerical as well as experimental investigation and the experimental results depict an increase in the heat transfer values with increase in solid concentration at all values of Rayleigh number. He reported that TiO_2 (50 nm)nanoparticle based suspension showed lowest heat transfer values due to the formation of agglomerates and boiling process dominated by conduction whereas higher heat transfer values were found for Ag(20 nm) and Cu (30 nm) dispersions in distilled water respectively. In another work, Dr. Khalid Faisal Sultan performed experimental analysis of heat transfer for Ag and ZrO2 nanoparticles dispersed in oil. The experimental results depict maximum heat transfer enhancement for the Ag(Silver) nanoparticles when compared with the ZrO_2 (Zirconia)– oil nanofluids. The generation of strong nano convection current due to the presence of Ag and ZrO_2 nanoparticles results in better mixing and stability which leads to enhancement in heat transfer and pressure drop when compared with base fluid.

Chougule and Sahu [C6] took Carbon nanotube and (Alumina) Al_2O_3 – DW nanofluids and observed an increase in the values of heat transfer coefficient on increasing the nanoparticle concentration in an automobile radiator. Results given by the researchers recorded 52.02% increase in heat transfer coefficient for 1% Al_2O_3 concentration whereas for CNT-DW nanofluids 69.42% enhancement in heat transfer values was observed.

Alam et al [A10,A11] performed experimental studies for nucleate pool boiling at atmospheric pressure. They have used water as the working fluid. Their experiment involved uncoated and

coated mild steel heating tubes. They coated heating tubes with copper of variable thickness (19, 26, 33, 41 and 60 μm).They also carried out experiment at sub atmospheric pressures.

They also carried out studies to investigate the effect of pressure, heat flux and coating thickness on heat transfer coefficient. Heating tubes were installed along with thermocouples which were placed in the cylindrical heating tube. So the temperature read by the thermocouple was not the same as that of the temperature on the outside of the wall which is in contact with water. So outer temperature was determined by calculating the temperature drop through the thin cylinder:

$$\delta T_w = q \frac{d_o}{2k} ln \frac{d_o}{d_h}$$

And coefficient for heat transfer was calculated as:

$$h = \frac{q}{(T_w - T_l)}$$

The experimental findings of Alam et. al. reported an increase in heat transfer coefficient with pressure increase irrespective of the heat flux.

Yu et. al. [Y5] performed the nucleate pool boiling experiment for alumina – distilled water nanofluids and reported no significant change in the heat transfer coefficient with change in the nanoparticle concentration. The experimental work was performed at low concentration of Alumina nanoparticles in Distilled water lying in between 0.0001% to 0.005%. The boiling of the nanofluid took place over a square shaped heating surface with 10mm side dimensions. The Boiling process was carried out at sub atmospheric pressure.

Vassallo et. al. [V2] explored the pool boiling heat transfer behavior of Silica – Distilled Water suspensions. The concentration of the silica nanoparticles taken in the suspension was as low as 0.5% by weight and the nanoparticle size varied from 15 nm to 300 nm. The atmospheric pool boiling experiments were conducted using 0.4 mm nichrome wire as a heater and no significant change in heat transfer coefficient was observed at low and high heat fluxes but as the heat flux approaches near to critical heat flux, the researchers observed a deterioration in heat transfer coefficient for nanofluids containing 50 nm Silica nanoparticles. Stable film boiling at temperature close to the melting point of nichrome wire was attainable with the nanofluids but not with the micro-particle suspensions. However, surface properties of the heating element specifically surface

roughness alone cannot be the sufficient reason to explain the heat flux behavior due to presence of nanoparticles which indicates the need for further investigation and to explore the mechanisms that could explain the enhancement in the heat transfer coefficient at higher values of heat fluxes. As critical heat flux is an area of research in itself thus the literature in detail is not presented here.

Taylor et. al. [T3] in their review work suggested a deposition of nanoparticles resulting in layer formation onto the heater surface followed by boiling as a contributing factor responsible for increase in Critical Heat Flux and decrease in boiling heat transfer performance during nucleate pool boiling. As the thickness of the layer formed due to settling of nanoparticles increases it behaves as an insulation thus increases the resistance leading to deterioration of the pool boiling heat transfer. Also, the deposited layer exhibits porous behavior that allows micro-fluidic effect within the coating leading to the offset of thermal resistance.

Shi et. al. [S12] employed Al_2O_3 and Fe nanoparticles for the synthesis of nanofluids. The nanofluids thus formed were boiled in a copper block. Fe nanoparticles were found to be more promising than Al_2O_3 nanoparticles as enhancement in heat transfer was recorded more in case of Fe nanoparticles than Al_2O_3 particles. The increase in thermophysical characteristics and surface tension are considered to be the prominent reasons behind the enhancement observed in heat transfer coefficient. Tu et.al. in their work also observed an enhancement in heat transfer coefficient for Al_2O_3 nanofluids due to the four fold rise in the number of nucleation sites which indicates some settling of the nanoparticles onto the heater surface.

Chapter – 3

SYNTHESIS AND CHARACTERIZATION OF NANOFLUIDS

This chapter discusses the experimental procedure followed during this research work for characterizing the nanoparticles as well as investigating the thermophysical properties of nanofluids. The experimental methodology adopted to investigate the nanoparticle properties is discussed in section 3.1 while the nanofluid formulation and stability evaluation methods are discussed in section 3.2. The experimental procedure and the various thermophysical characteristics of nanofluids such as thermal conductivity, viscosity and density are discussed in section 3.3.

3.1 Characterization of Nanoparticles

Al_2O_3 (alumina) and CuO (copper oxide) nanoparticles are procured from Nanolabs India Limited and two step technique was employed for the synthesis of nanofluids. Characteristic analysis of both the nanoparticles procured from nanolabs is listed in the Table 3.1 and Table 3.2.

Table 3.1 Characteristic Analysis of Alumina Nanoparticles (Source Nanolabs)

Alumina Nanoparticles Composition and Characteristics			
Al_2O_3	>= 99%	Purity	99 %
Cao	<= 0.017 %	SSA	130 – 140 m^2/gm
Fe_2O_3	<= 0.001%	Bulk Density	1.5 gm/cm^3
MgO	<= 0.001%	True Density	3.97 gm/cm^3
SiO_2	<= 0.05%	Color	White
		Morphology	Spherical
		Crystallographic Structure	Rhombohedral
		Atomic Weight	101.96 g/mol
		Melting point	2055 °C

Table 3.2 Characteristic Analysis of Copper Oxide Nanoparticles (Source Nanolabs)

Copper Oxide Nanoparticles Composition and Characteristics			
CuO	>= 99%	Purity	99 %
S	<= 0.1 %	SSA	10 m^2/gm
Si	<= 0.35%	Bulk Density	0.79 gm/cm^3
Mg	<= 0.067%	True Density	6.4 gm/cm^3
Al	<= 0.2%	Color	Black
		Morphology	Spherical
		Atomic Weight	79.54 g/mol
		Melting point	1326 °C

3.1.1 Particle Size Analysis

From the zeta sizer particle size distribution and the average particle size of alumina and copper oxide nanoparticles as procured from Nanolabs were measured directly and given in the figures 3.1 (a) and 3.1 (b), respectively.

Figures 3.1 (a) & 3.1 (b) depict the overall size distribution of both the nanoparticles which are scattered throughout the plot. Thus from the graphs it is clear that average particle size of alumina nanoparticles is found to be 122.10 nm without ultrasonication. The distribution of copper oxide nanoparticles as shown in Figure 3.1 (b) depicts the particles size of the order of 167.1 nm without ultrasonication. Hence, from the graphs it is clear that average particle size of the copper oxide nanoparticles are found to be 167.1 nm. The results confirm that both the nanoparticles exist in loosely formed agglomerates which are also confirmed through the SEM images of the nanoparticles in the following sections. These loosely formed agglomerates of nanoparticles are dispersed in distilled water by employing magnetic stirring followed by ultasonication for a specific time period which depends on the nanoparticle behavior. After carrying ultrasonication the size of the nanoparticles are reduced to 60.6nm and 88.1 nm as shown in Figures 3.2(a) and 3.2 (b).

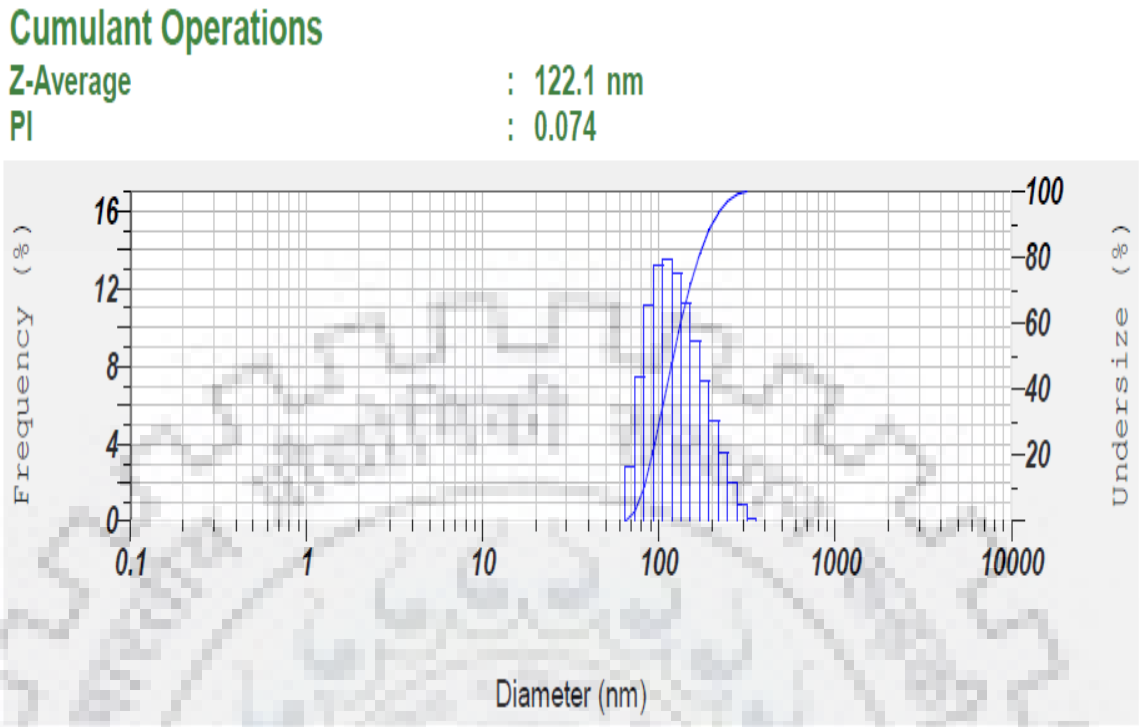

Fig. 3.1 (a): Size Distribution of Alumina nanoparticles (before ultrasonication)

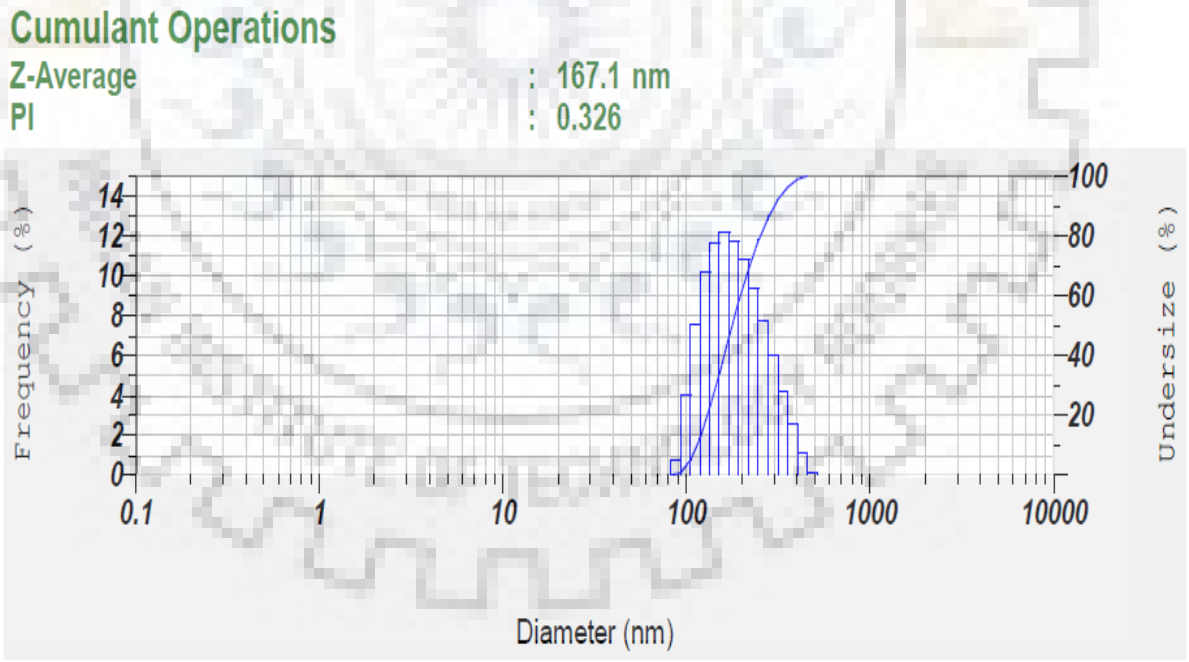

Fig. 3.1 (b): Size Distribution of Copper Oxide nanoparticles (before ultrasonication)

Cumulant Operations

Z-Average	:	60.6 nm
PI	:	0.283

Molecular weight measurement

Molecular weight	:	---
Mark-Houwink-Sakurada parameters	:	---

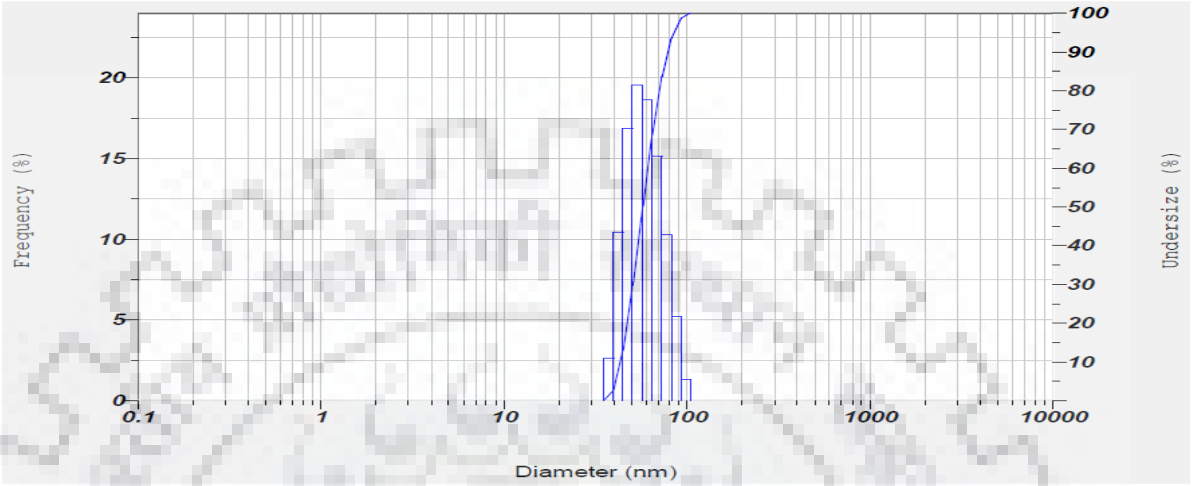

Fig. 3.2 (a): Size Distribution of Alumina nanoparticles (after ultrasonication)

Cumulant Operations

Z-Average	:	88.1 nm
PI	:	0.237

Molecular weight measurement

Molecular weight	:	---
Mark-Houwink-Sakurada parameters	:	---

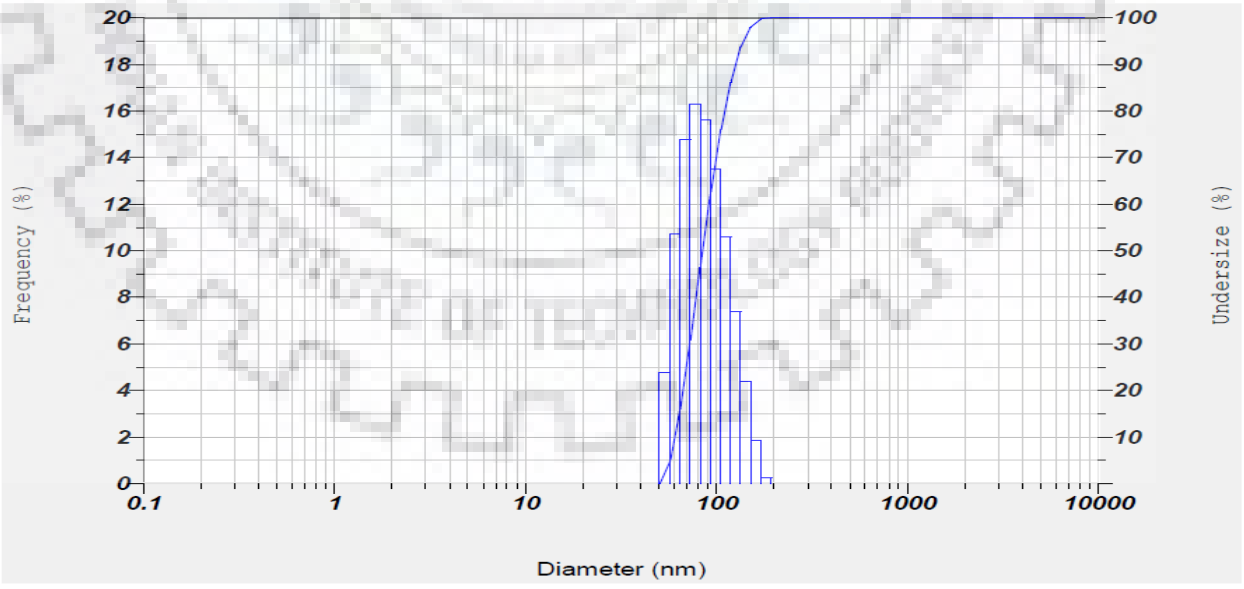

Fig. 3.2 (b): Size Distribution of Copper Oxide nanoparticles (after ultrasonication)

3.1.2 SEM Analysis

SEM analysis of the nanoparticles (Alumina and Copper oxide) is carried out to characterize the particle size, extent of agglomerates, morphology and structure. Micrographs were taken at a suitable accelerating voltage in order to obtain the images with best possible resolution using the SEM device. The SEM images of Alumina and Copper Oxide nanoparticles shown in Figure 3.3 (a) and 3.3 (b) unveil a fine particulate matter where the particles are spherical in shape, it appeared like aggregation structures. The distribution pattern of the Al_2O_3 (alumina) and CuO (copper oxide) nanoparticles as viewed under a Scanning Electron Microscope (SEM) magnifications is shown in Figure 3.3 (a) & 3.3 (b). From the SEM images of nanoparticles it is clear that nanoparticles exist in loosely formed agglomerates which can be easily broken either by high speed homogenization or ultrasonication. Also from the SEM image it is clear that nanoparticles are spherical in shape.

3.1.3 EDX Analysis

An Energy Dispersive X-Ray Analyser (EDX or EDS) is employed to gather elemental identification and quantitative compositional data of the nanoparticles. The information provided by EDX analyser consist of spectra where peaks correspond to the elements involved in the formation of the true composition of the sample under observation. Elemental mapping of a sample and image analysis is also possible. Energy Dispersive X-Ray Spectroscopy (EDS or EDX) is carried out in conjunction with scanning electron microscopy (SEM) to investigate the purity and atomic composition of the alumina and copper oxide nanoparticles. The EDS technique detects x-rays emitted from the sample during bombardment by an electron beam to characterize the elemental composition of the nanoparticles. The results from EDX analysis indicates that Alumina and copper oxide nanomaterial procured are pure to the extent of 99% since in EDX graph are found only specific peaks for alumina and oxygen in case of alumina nanoparticle as shown in Figure 3.4(a) and Copper and oxygen peaks in case of copper oxide nanoparticles is shown in Figure. 3.4 (b).

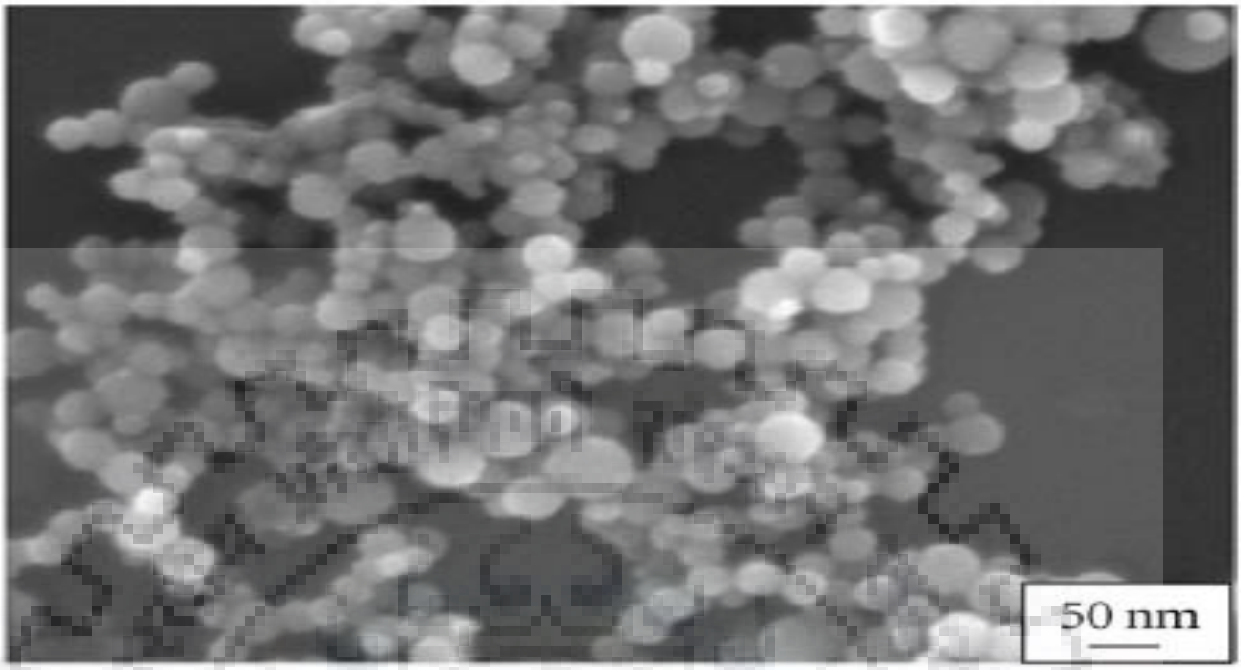

Fig. 3.3 (a): SEM images of Alumina (Al_2O_3) nanoparticles

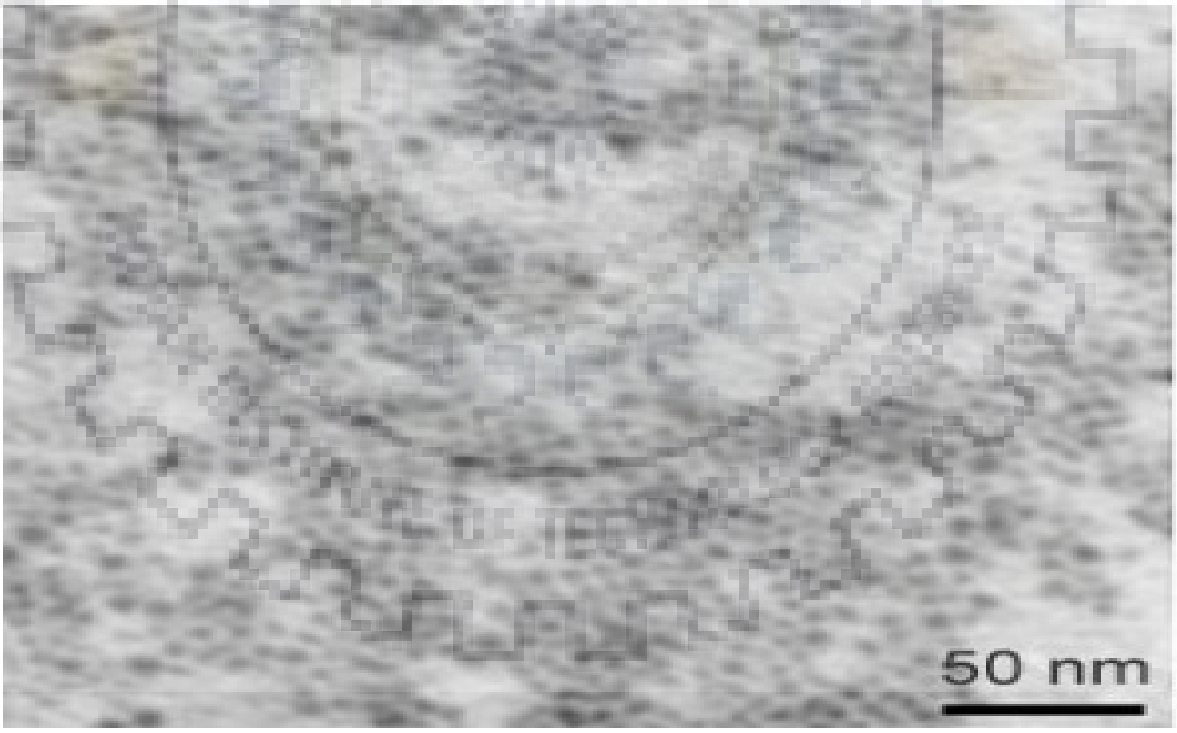

Fig. 3.3 (b): SEM images of Copper Oxide (CuO) nanoparticles

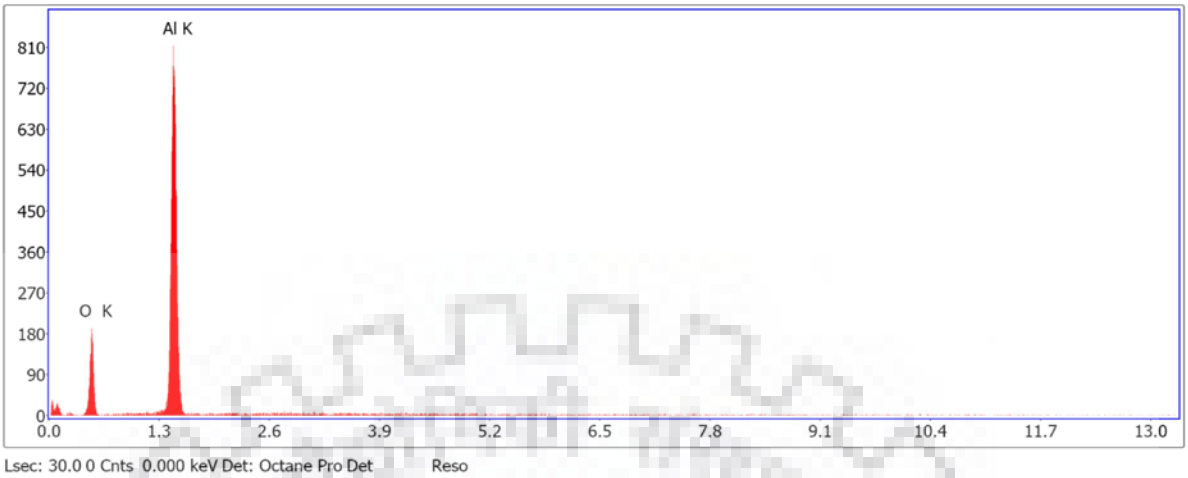

eZAF Smart Quant Results

Weight %	Atomic %	Net Int.	Error %
37.69	50.49	64.1	10.09
62.31	49.51	382.94	4.04

Fig. 3.4 (a) : EDX images of Alumina nanoparticles

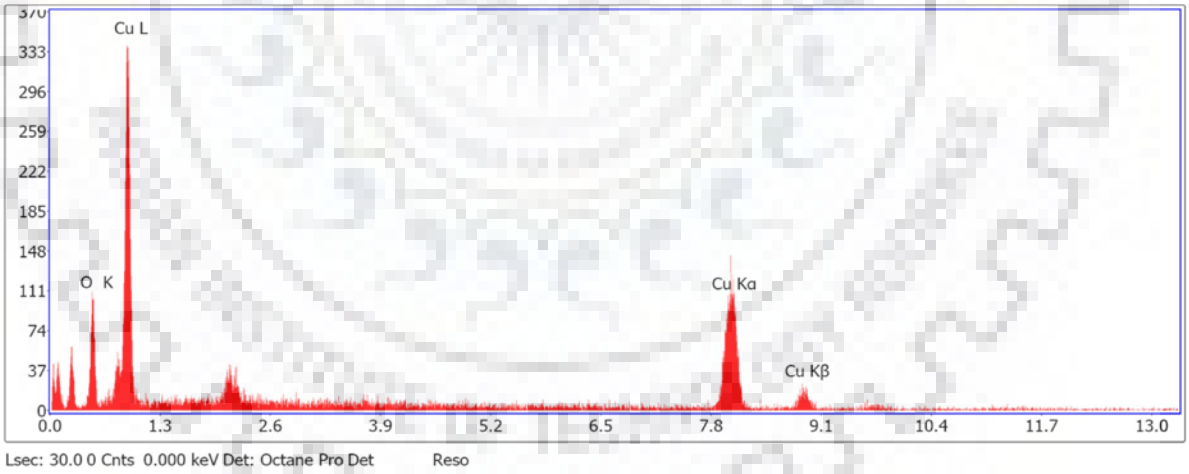

eZAF Smart Quant Results

Weight %	Atomic%.	Net Int.	Error %
15.77	42.65	42.65	9.99
84.23	57.35	128.61	3.08

(b)

Fig. 3.4 (b): EDX images of Copper Oxide nanoparticles

3.1.4 XRD Analysis

XRD analysis of the nanoparticles allows the identification of crystalline structures in samples. In XRD analysis X- ray beam is focused onto the nanoparticle sample and the beam is diffracted on interaction with the plane in the crystalline structure. In order to detect diffracted beams signal of different planes, it is important that the diffracted beam lie in the same phase with respect to one another one, in other case the beams get cancel.

Fig.3.5 (a) & 3.5 (b) show the XRD plots of Alumina and Copper Oxide nanoparticles. Certain distinct maxima which are called peaks corresponding to various values of diffraction angle (2θ) were observed. From the peaks, it is clear that the maximum peak exists at 40° and beyond that the peaks start decreasing with increase in the diffraction angle. Thus, from the plots the intensity distribution with respect to diffraction angle was evaluated throughout the crystal. The corresponding values of 2-θ were used in Debye Scherrer equation which gives the corresponding lattice spacing (d) which was further used in measuring the crystal size for a particular diffraction angle. The average crystallite size was found to be 0.43 nm.

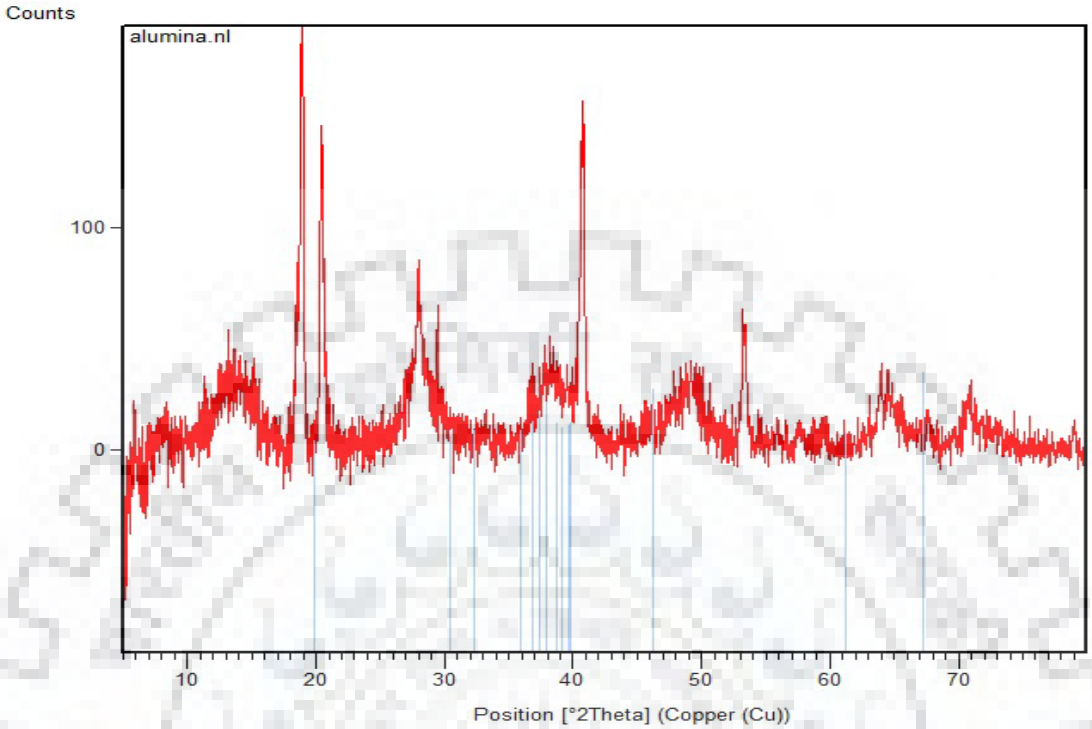

Fig. 3.5 (a): XRD images of Alumina nanoparticles

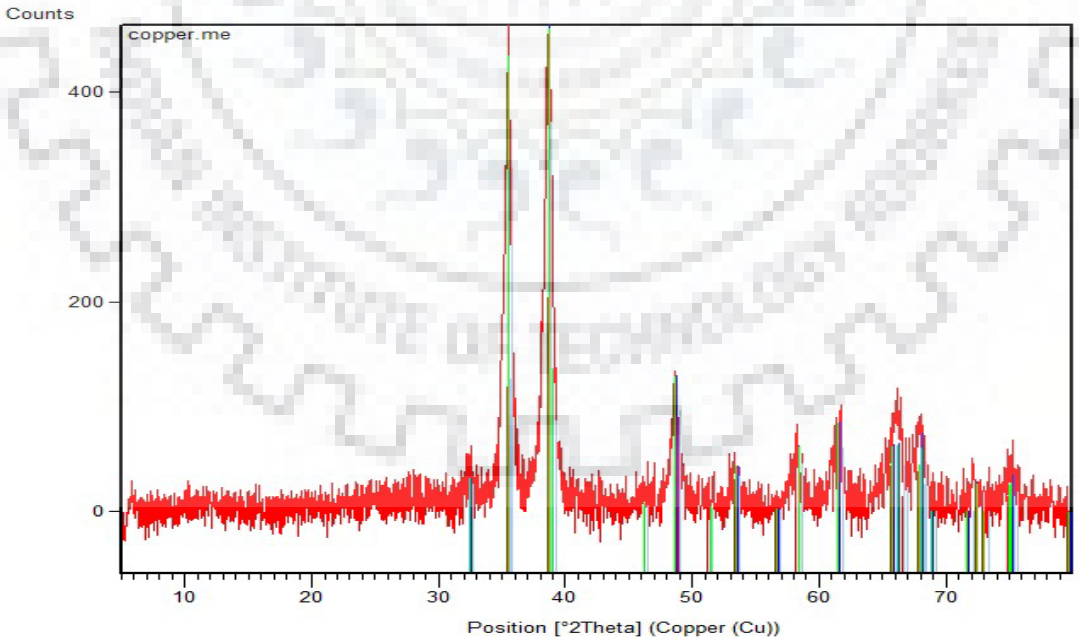

Fig. 3.5 (b): XRD images of Copper Oxide nanoparticles

3.2 Nanofluid Synthesis and Stability

Following paragraphs, discuss the synthesis of nanofluids and common techniques used for evaluating the stability of nanofluids.

3.2.1 Nanofluid Synthesis

Synthesis of stable and even nanofluids is the prerequisite in determining the thermal properties experimentally. In order to formulate nanofluids certain important requirements are to be met, for example no agglomeration of nanoparticles in base fluid should be observed, the chemical behaviour of the base fluid should not change, the suspension formed should be highly stable. In this work two step technique was adopted for synthesis of nanofluids. Alumina and Copper Oxide nanoparticles were procured from Nanolabs India in the size range of 20 to 50 nm. These nanoparticles were dispersed into the distilled water taken as base fluid using magnetic stirrer followed by intensive ultrasonication at high frequency for 10 hours. The nanofluids thus prepared with maximum concentration of 0.1% by volume fraction looked promising and were found to be highly stable and uniform for 72 hours when kept in atmosphere. Although slight settling of the copper oxide nanoparticles and formation of agglomerates were observed with copper oxide-distilled water nanofluids after 48 hours when kept in atmospheric conditions. No stabilizing agent or surfactant was used for preparation of nanofluids for attaining higher stability as they tend to alter the chemical behaviour of the base fluid.

Because of the more dominant nature of hydrodynamic forces acting over the surface of nanoparticle in comparison to gravitational forces, it is considered more stable to take volume fraction instead of mass fraction for preparing nanofluids with varying concentration. Thus, alumina- DW and Copper Oxide nanofluids were prepared with varying concentration of the nanoparticles (0.001% by volume to 0.05% by volume) by dispersing the nanoparticles in distilled water at different volume fractions with the help of conversion formula given by Bang and Chang [13].

$$\varphi_v = \left[\left(\frac{1-\varphi_m}{\varphi_m}\right)\frac{\rho_{np}}{\rho n_f} + 1\right]^{-1} \qquad \text{……(3.1)}$$

3.2.2 Optimum Time of Ultrasonication

In particular the optimum time required for sonication to be done is to be evaluated in order to produce nanofluid of an acceptable quality. As such, there are no specific guidelines given in literature on the sonication time; still the sonication time differ from few minutes to more than 12 hours in most cases. An Al_2O_3-water and CuO- Water nanofluid with a 0.1% nanoparticle volumetric concentration was tested. During the experimental work it was observed that prolonged ultrasonication of the nanofluids lead to the coalescing of the particles leading to agglomerate formation. The optimum duration of ultrasonication is determined by varying the time of ultrasonication from 1 hour to 30 hour and measuring the average particle size at regular intervals. This process was carried out for both alumina and copper oxide nanofluids in order to determine the optimum time of ultrasonication for both nanofluids.

Figures. 3.6 (a) & 3.6 (b) show the particle size v/s time of ultrasonication. These figures reveals that the minimum average particle size of alumina nanoparticles in the suspension was found when ultrasonication is done for 6 to 7 hours whereas for copper oxide – Distilled Water nanofluids the minimum average particle size is observed when the ultrasonication is carried for 10 to 12 hours.

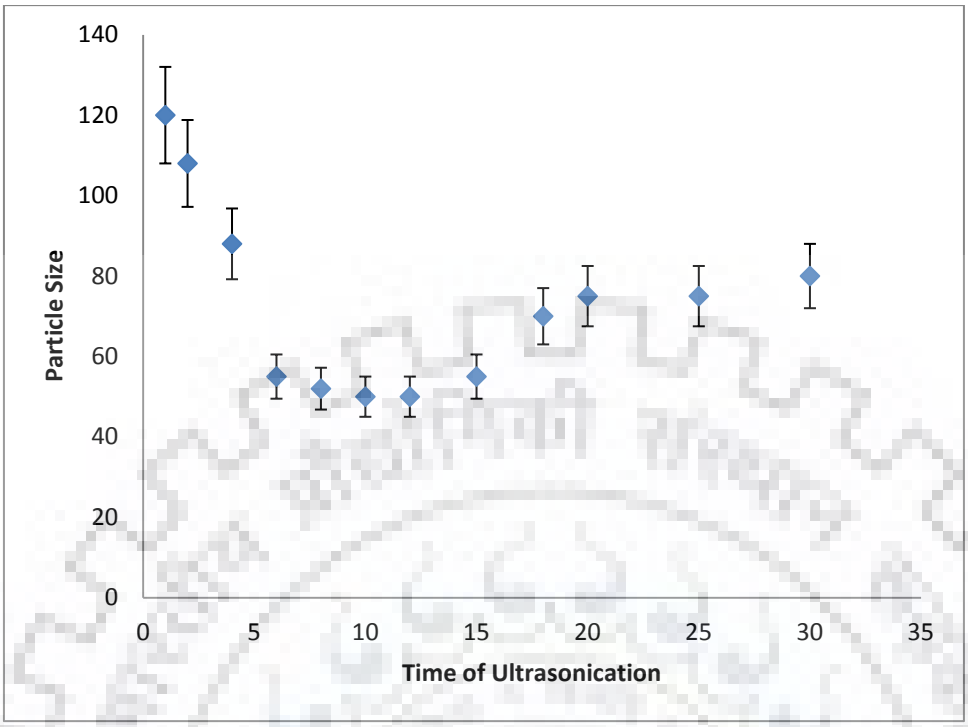

Fig. 3.6 (a): Average particle size of Alumina – DW nanofluids for different ultrasonication time intervals.

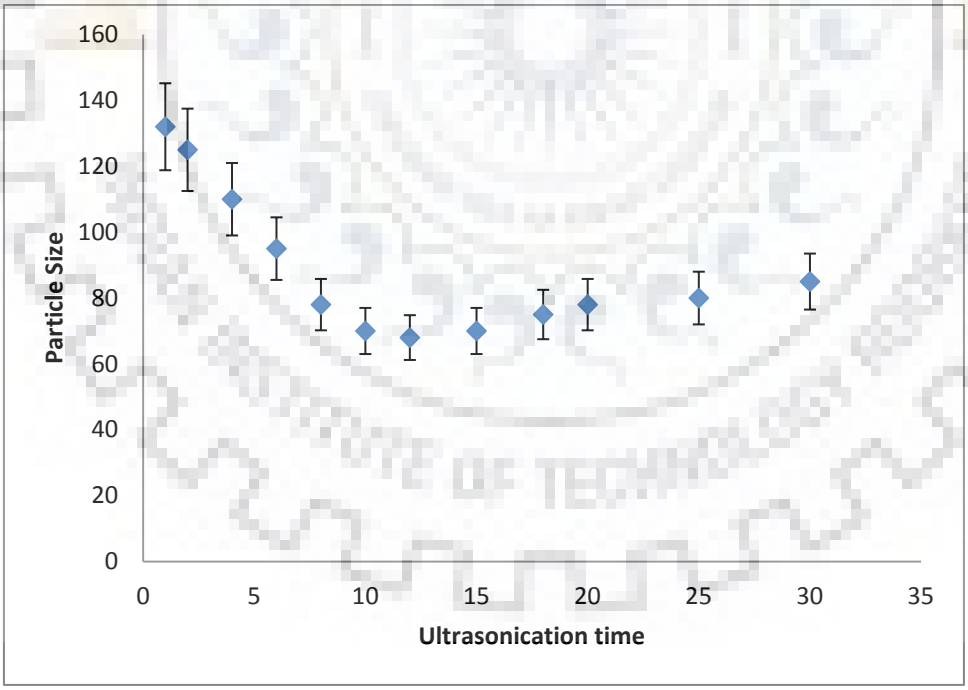

Fig. 3.6 (b) : Average particle size of CuO- DW nanofluids for different ultrasonication time intervals.

3.2.3 Nanofluid Stability

Nanofluid characterization consists of evaluating the stability of the dispersed nanoparticles in the base fluid. Nanoparticles in the base fluids tend to coagulate together resulting in formation of agglomerates that can settle down due to gravity. Stability in general is defined by the rate of agglomeration and settling of the particles which should be kept to the minimum value in order to formulate stable suspensions. The extent of coalescing of particles together is estimated by measuring the frequency of collisions among the particles and the cohesion probability of the particles during collision.

The nanofluids stability assessment is essential to investigate the extent of dispersion The settling of the nanoparticles was observed visually and observing the degree of agglomeration and settling of the agglomerates was the primary focus of this study.

Despite the maximum practical time of sonication allowed, the samples still presented up to some degree agglomeration and sedimentation over extended relaxation times (no agitation) as no surfactant was used to stabilize the two-phase mixture. The common techniques that are used in this work to judge the stability of the Alumina-DW and CuO-DW are shown in the Figure 3.6.

3.2.3.1 Sedimentation

The simplest method used by most of the researchers and used in present work to evaluate the stability of nanofluids is sedimentation method. The sediment volume of the nanoparticle in the base fluid or the weight of the sediment under the influence of any external force such as gravity is an indicative parameter to assess the stability of the nanosuspension formed. The nanofluids are considered to be stable when the nanoparticles remain in the suspended form when kept for settling for a prolonged time. The visual observation technique and the photographs of the nanofluid samples in test tubes taken at regular time intervals is a usual method adopted to analyze the stability of nanofluids. The photographs of the 0.1% by volume of Alumina nanoparticles in distilled water and similar composition of copper oxide nanoparticles in distilled water are observed for time duration ranging from 2 hours to 72 hours. After 72 hours settling of copper oxide nanoparticles were observed whereas alumina nanoparticles remain in stable suspension for 5 days and after that slight settling of the alumina particles was also observed. Figures 3.8 (a) & 3.8 (b) exhibit the settling profile of alumina nanoparticles with respect to time duration for both alumina – distilled water and copper oxide – distilled water nanofluids, respectively.

Excellent stability of the formed nanofluids is due to the negligible growth and agglomeration of the nanoparticles by steric effect results in a stable suspension that depicts no settling of the particles for more than 72 hours that make them suitable for further experimental work. The main reason behind such good stable suspensions formed is due to the existence of electrostatic repulsive forces between the nanoparticles.

3.2.3.2 Zeta Potential Analysis

Zeta potential is defined as the electric potential existing in between the interfacial dual layers at the location of the slipping plane versus a point in the bulk fluid away from the interface and it depicts the potential gradient in between the stagnant layer of the fluid attached to the dispersed particle and the dispersion medium. The main significance of zeta potential lies in predicting the stability of the nanofluids or colloidal suspensions. So, nanofluids having high value of zeta potential are electrically stabilized whereas suspensions having low value of zeta potentials are considered to be less stable as they are prone to coagulate or form agglomerates. In general a value of 25 mV is considered as a datum that separates low charged suspensions from highly charged one. Table 2.3 below lists down the accepted zeta potential values and the extent of stability of the suspensions. The nanofluids having stability in the range of 40 to 60 mV are considered to be excellently stable. Figures 3.9 (a)and 3.9 (b) show the zeta potential values for 0.05% by volume concentration of the alumina and copper oxide nanoparticles in the distilled water. The value lies well within the range of 40 to 60 mV which reflects that the synthesized nanofluids are excellently stable with less settling due to agglomeration of nanoparticles.

Figure 3.10 depicts the stability of the alumina and copper oxide nanofluids with respect to time. The Alumina – DW nanofluids show excellent stability in terms of zeta potential for the 10 days and for 5 days in case of copper oxide – DW nanofluids but as the time passes a reduction in zeta potential of CuO-DW nanofluids was sharp in comparison to Alumina – DW nanofluids. This reveals that floc formation in CuO – DW nanofluids start taking place after 5 days that leads to settling of the particles whereas for Alumina – DW nanofluids the zeta potential remains steady for 10 days and after that it reduces and leads to agglomeration of alumina nanoparticles in the suspension.

Table 3.3 Zeta Potential values and stability criteria

Z – Potential (mV)	Extent of Stability
0	**Little or zero stability**
15	**Slightly stable with sedimentation of particles**
32	**Moderate stability**
45	**Good stability with negligible settling after few hours**
60	**Excellent stability**

3.2.3.3 pH Control:

The stability of nanoparticles in base fluid is directly influenced by the electro-kinetic properties of the base fluid. Strong repulsive forces in between the particles because of high surface charge density can lead to synthesis of well dispersed nanofluids with excellent stability. As shown in the work of Xie et. al. excellent stability was attained for carbon nanotube suspensions by doing slight acid treatment. Here in this work no additional chemicals have been employed to maintain the stability as they could alter the base fluid characteristics. However, pH of the suspension is kept away from the isoelectric potential of both the nanofluids i.e. alumina – distilled water and copper oxide – distilled water by carrying out prolonged ultrasonication and maintaining the zeta potential of the suspension above 32 mV. Isoelectric potential is defined as the concentration of potential charge controlling ions for which the zeta potential value is zero. Thus at the isoelectric potential the surface charge density of the nanoparticles is equal to the charge density hence this point is considered as the initiation point of the diffuse layer. Therefore charge density for the diffuse layer is zero. It is desirable that the repulsive energy among the particle exists and is smaller for small sized particles, so a larger zeta potential is desirable for excellent stability of the suspensions. As the pH of the suspension is kept away from the isoelectric potential of the nanoparticles, the colloidal properties of the suspension get more stable that indirectly influences various thermophysical characteristics of nanofluids. It is noriceable that at higher zeta potential values the potential barrier among the nanoparticles increases which avoids the coalescing of the particles together thereby improving the stability of nanofluids.

Fig. 3.7: Common techniques used for evaluating the stability of Nanofluids

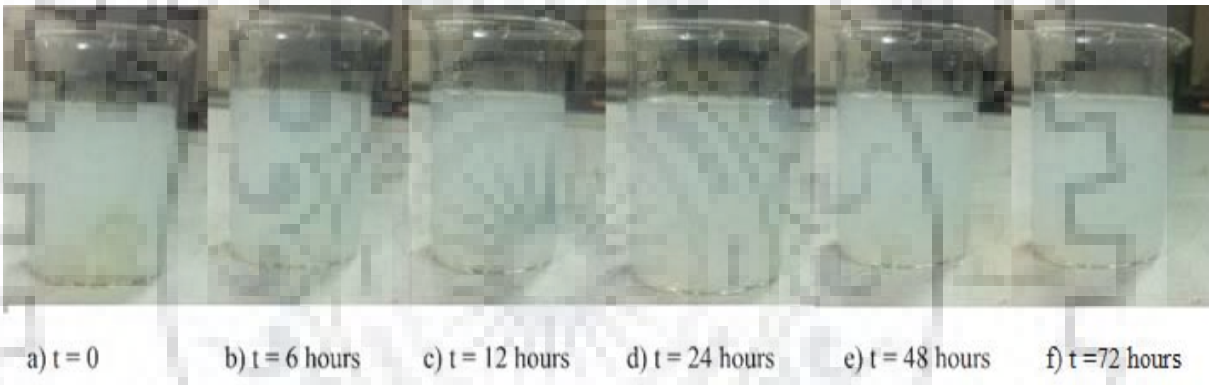

Figure 3.8 (a) : Photographic view of 0.05 % by volume of alumina nanoparticles in distilled water exhibiting settling of nanoparticles at different time intervals

Figure 3.8 (b) : Photographic view of 0.05 % by volume of Copper Oxide nanoparticles in distilled water exhibiting settling of nanoparticles at different time intervals

Calculation Results

Peak No.	Zeta Potential	Electrophoretic Mobility
1	-42.5 mV	-0.000330 cm2/Vs
2	--- mV	--- cm2/Vs
3	--- mV	--- cm2/Vs

Zeta Potential (Mean) : **-42.5 mV**

Electrophoretic Mobility mean : **-0.000330 cm^2/Vs**

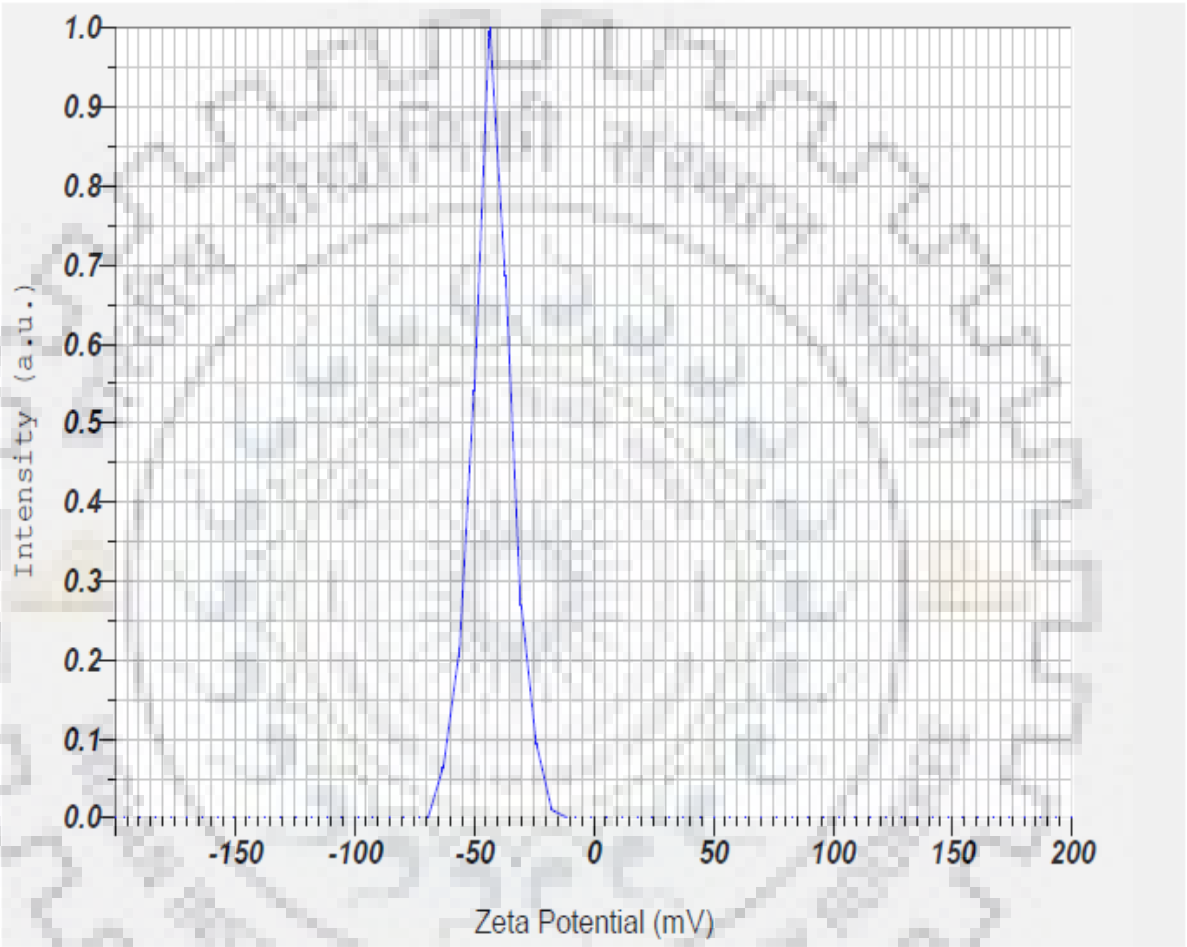

Fig. 3.9(a) Zeta Potential for 0.05% Alumina – DW nanofluid

Calculation Results

Peak No.	Zeta Potential	Electrophoretic Mobility
1	-62.1 mV	-0.000482 cm2/Vs
2	--- mV	--- cm2/Vs
3	--- mV	--- cm2/Vs

Zeta Potential (Mean) : **-62.1 mV**

Electrophoretic Mobility mean : -0.000482 cm^2/Vs

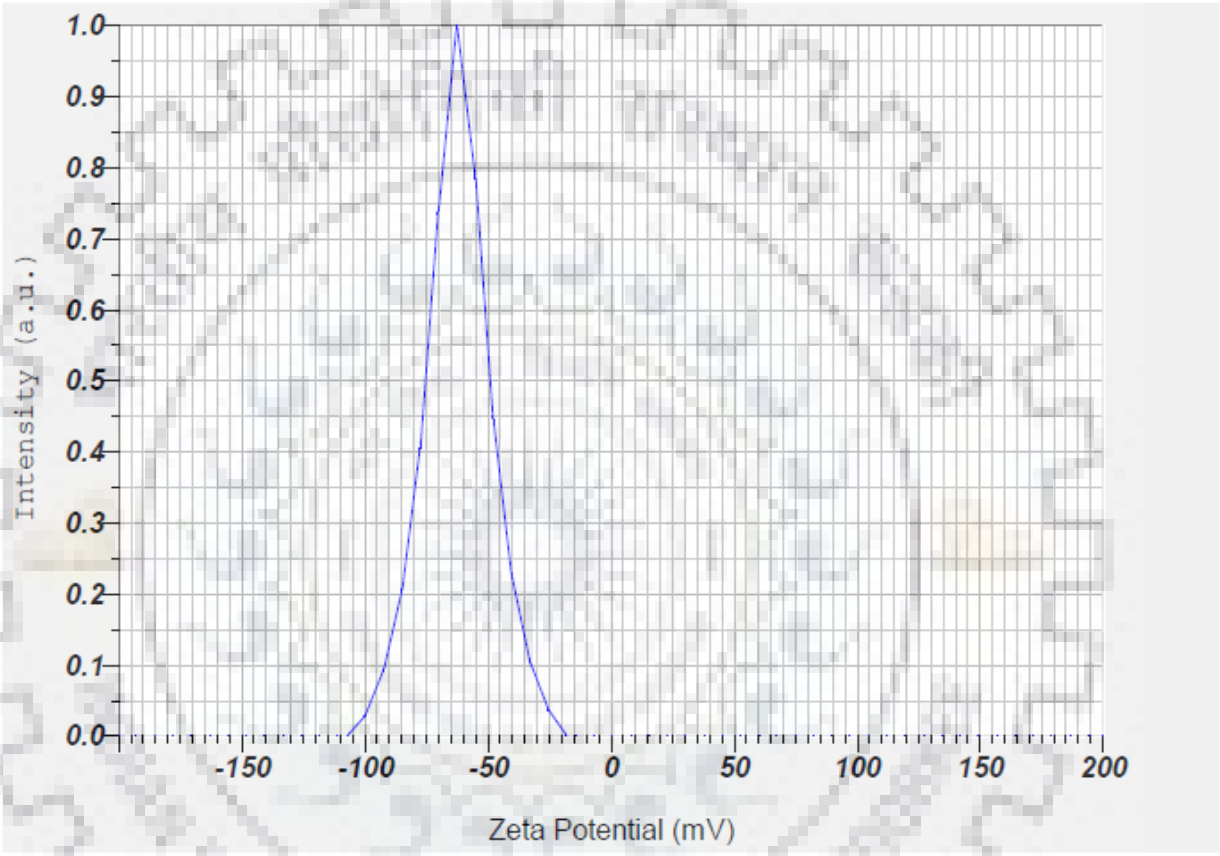

Fig. 3.9 (b) Zeta Potential for 0.05% Copper Oxide - DW nanofluids

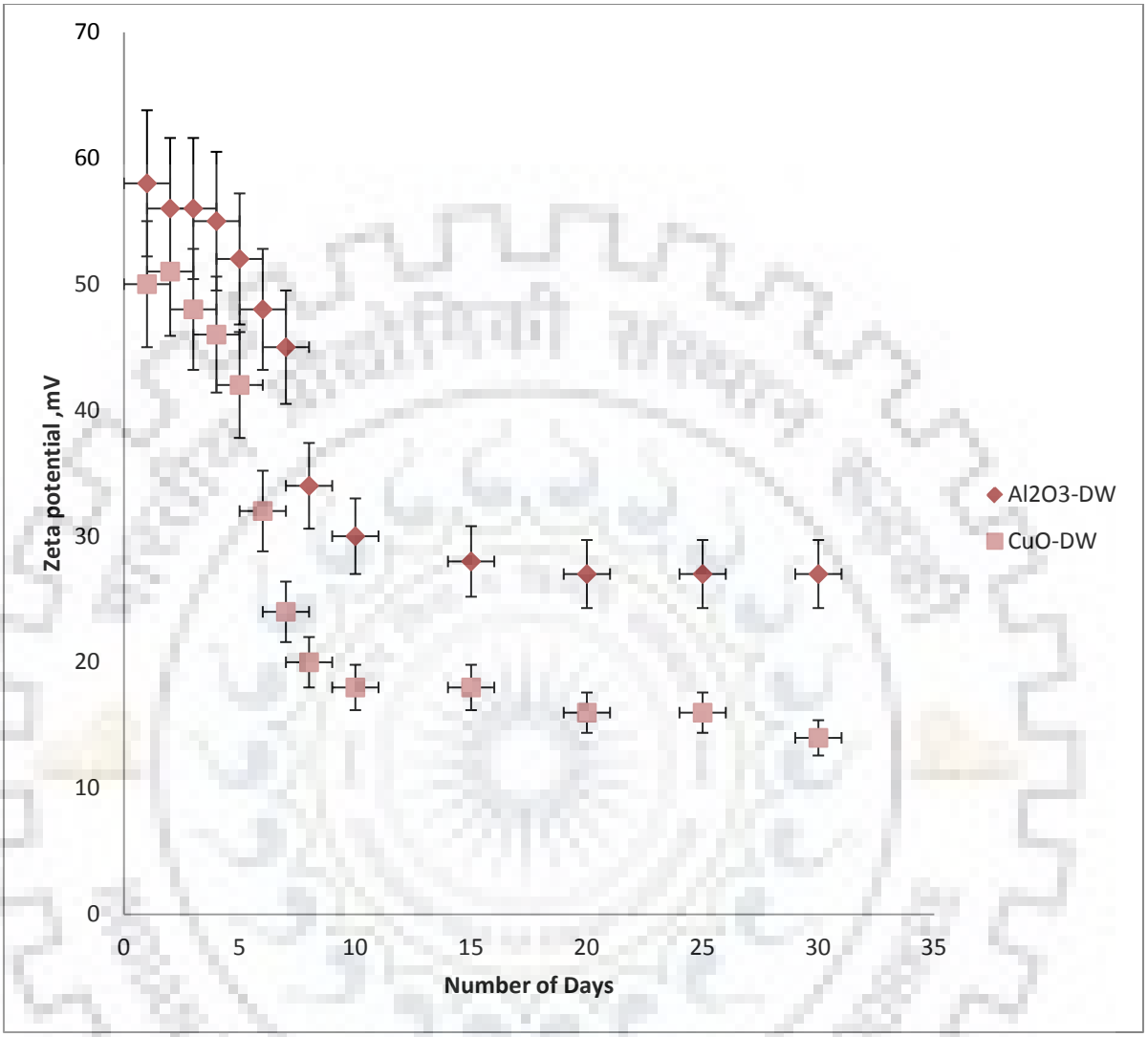

Fig. 3.10 Zeta Potential with respect to time for Alumina and Copper Oxide nanofluids with 0.05% concentration

3.3 Thermophysical Characteristics of Nanofluids

Following sections discuss the thermophysical characteristics viz. density, thermal conductivity and viscosity of Alumina – Distilled Water and Copper Oxide – Distilled Water nanofluids.

3.3.1 Density

Density is one of the characteristic that influences the heat transfer properties of nanofluids. Since nanoparticles are metallic oxide in nature and have density higher than that of base fluid, it led to believing that with increase in the concentration of nanofluids there will be an increase in the density of nanofluid. The theoretical values of density for alumina and copper oxide nanofluids with base fluid as distilled water were obtained using the Pak and Cho correlation or mixing rule, which is given below :

$$\rho_{nf} = \varphi_v \rho_{np} + (1 - \varphi_v)\rho_{bf} \quad (3.2)$$

Where φ_v is volume fraction of nanoparticles in base fluid, ρ_{np} is nanoparticle density and ρ_{bf} is base fluid density.

The experimental values of the density of alumina-DW and Copper Oxide – DW nanofluids at various compositions were determined with the help of specific gravity bottle and theoretically determined using Pak and Cho Correlation. Figure 3.11 (a) & 3.11 (b) represent the comparison of the experimental density values of Alumina – Distilled Water and Copper Oxide Distilled Water nanofluids at room temperature i.e. 25 °C with the calculated values of densities due to Pak and Cho correlation, Eq. 3.2 for various concentration of nanofluids. These figures reveal that the density of both the nanofluids increases with the increase in volumetric concentration of nanoparticles in the base fluid.

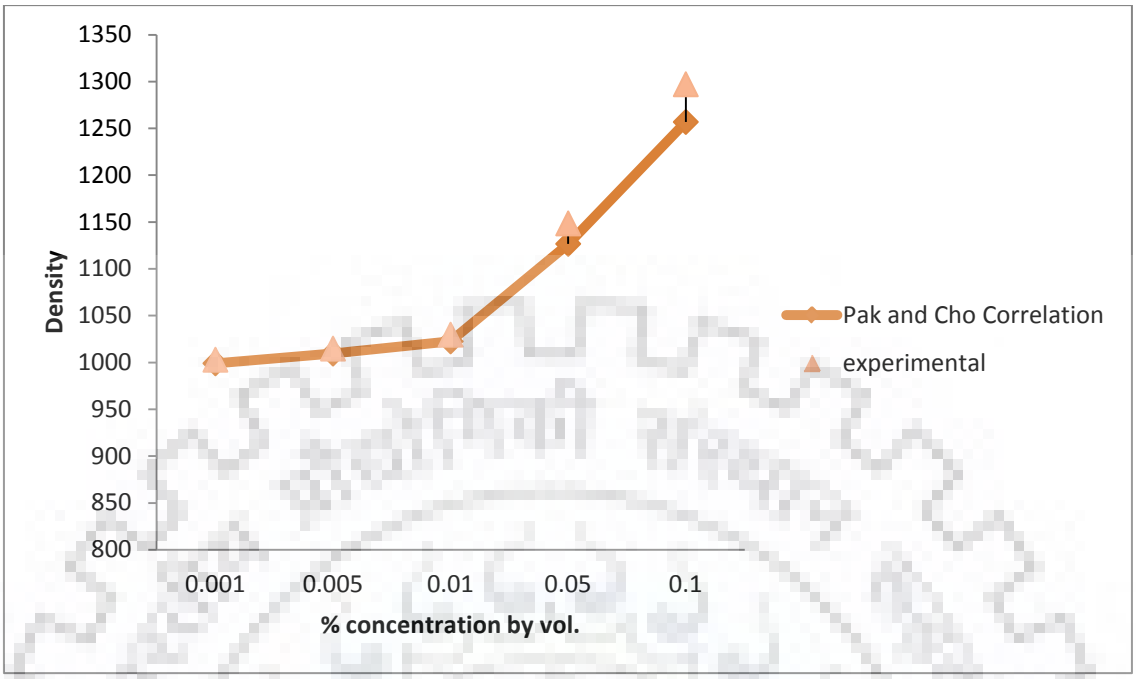

Fig. 3.11 (a) Comparison of Experimental density values for nanofluids with Pak and Cho correlation for various concentration of Al_2O_3 - DW nanofluids at room temperature.

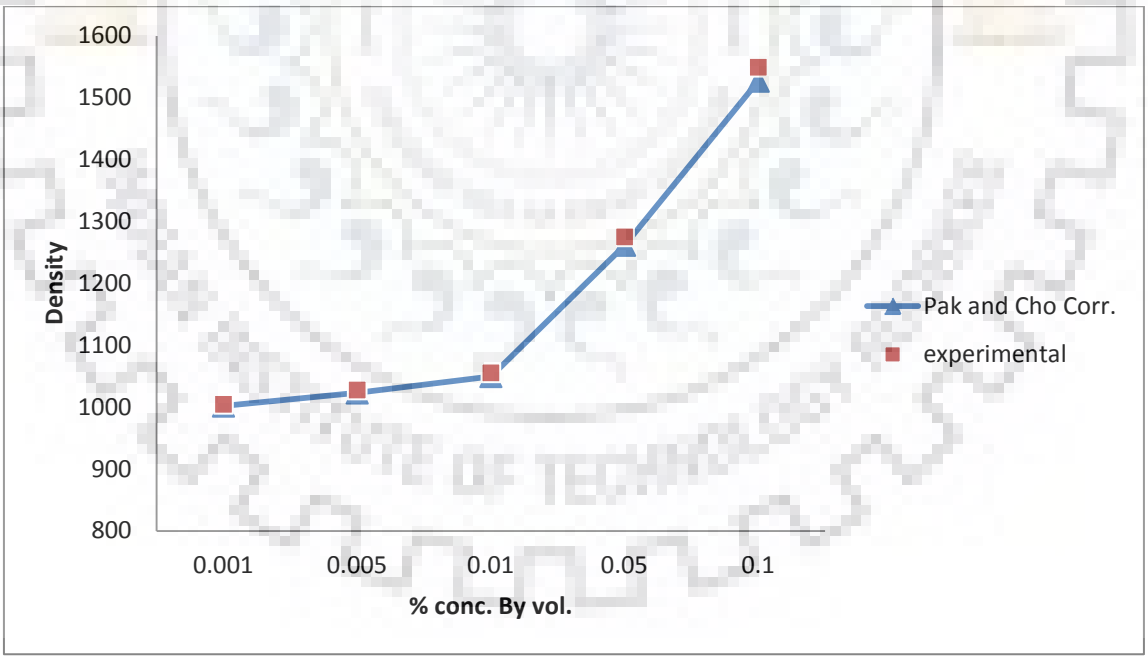

Fig. 3.11 (b) Comparison of Experimental density values for nanofluids with Pak and Cho correlation for various concentration of CuO – DW nanofluids at room temperature.

Figures 3.12 (a) & 3.12 (b) show the variation of density with temperature as concentration of nanoparticles in Distilled water as a parameter for Alumina – Distilled Water and Copper Oxide Distilled Water nanofluids, respectively. These figures show that density of a nanofluid decreases with the rise in temperature irrespective of concentration of nanofluids. Further, at a given temperature the density of the nanofluid increases with the particle concentration of the nanofluids. These observations are obvious and self explanatory.

Furthermore, two correlations of density of Alumina – Distilled Water and Copper Oxide Distilled Water nanofluids are developed using regression analysis. Eq (3.3) shows the empirical correlation of density of Alumina – Distilled Water and Copper Oxide Distilled Water nanofluids.

$$\rho_{eff} = C_1 + C_2\varphi_v + C_3T \qquad (3.3)$$

The values of constants C_1, C_2, C_3 depends upon the nanofluids and their values are given in Table 3.4.

Table 3.4 : Values of constants for density correlation

Nanofluid	C_1	C_2	C_3
Alumina – DW	1001.06	2818.62	-0.32
Copper Oxide - DW	998.8	4278.13	-0.60

Figure 3.13 shows the comparison of the experimental and calculated values of the density from the Eq (3.3). This figure shows that the maximum deviation is $\pm$ 2.5% , respectively.

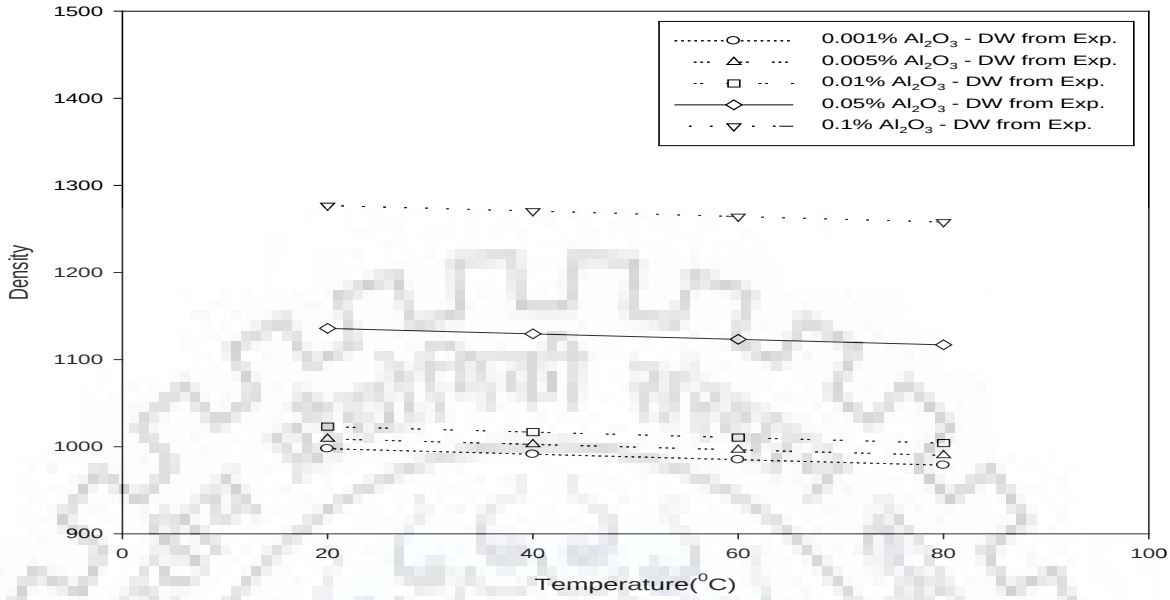

Fig. 3.12 (a) Density v/s temperature curve for alumina-DW nanofluids

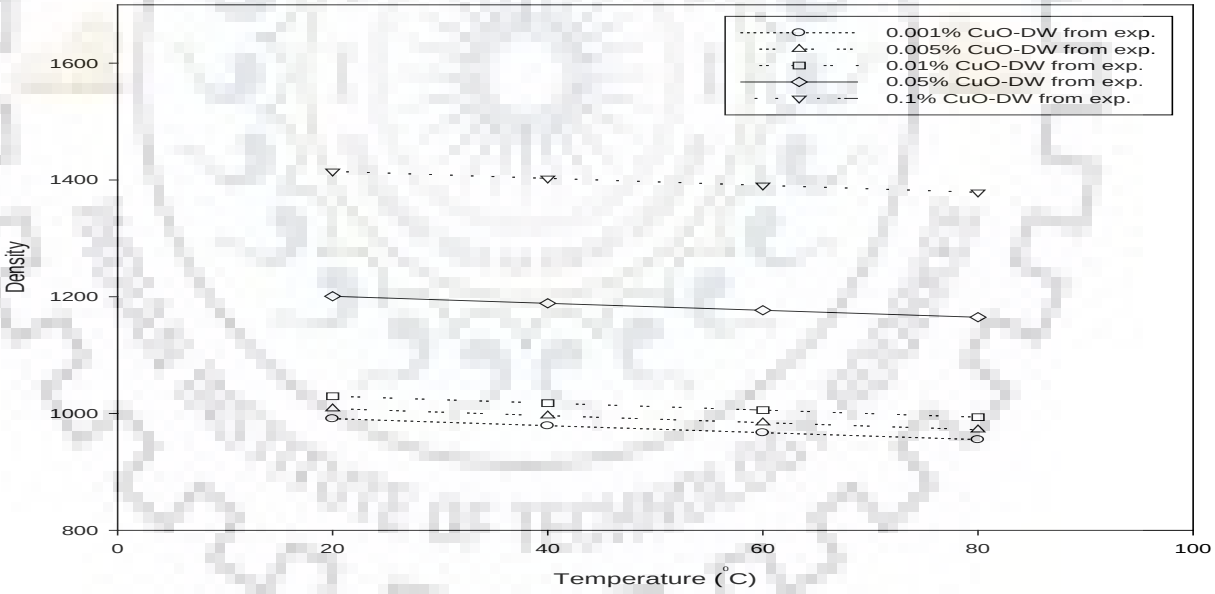

(b)

Fig. 3.12 (b) Density v/s temperature curve for Copper Oxide – DW nanofluids

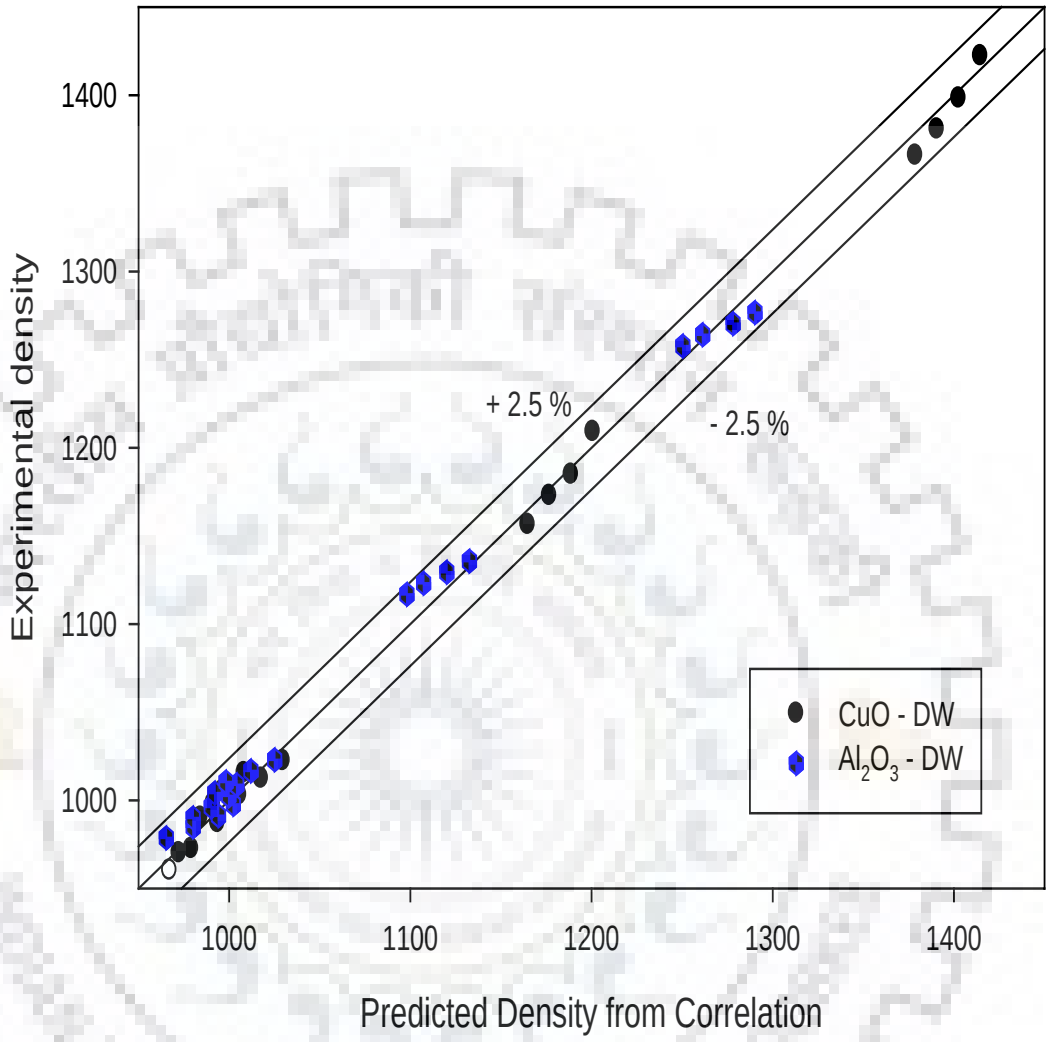

Fig.3.13 Comparison between the experimental and predicted values of density from the proposed correlations for CuO – DW and alumina-DW nanofluids

3.3.2 Thermal Conductivity

In the literature no definitive theory has been given that can predict the thermal conductivity of the nanofluids reliably and explain the behavior. From the work of the previous researchers and their experimental results, following parameters such as shape of the nanoparticle, thermal conductivity values of nanoparticle and base fluid, volume fraction, surface area and temperature are considered to be responsible for the anomalous thermal conductivity of nanofluids. The paragraph below discusses some of the prominent theoretical and empirical models proposed by various researchers to predict the effective thermal conductivity of nanofluids

Maxwell model: Maxwell model is considered to be one of the first model proposed in late 19 th century to determine the thermal conductivity values of solid-liquid mixtures with relatively large particles. Maxwell proposed the model based on the conduction carried out in solution through stationary nanoparticles in suspension.

$$k_{nf} = \frac{k_{np}+2k_{bf}+2\varphi_v(k_{np}-k_{bf})}{k_{np}+2k_{bf}-\varphi_v(k_{np}-k_{bf})}k_{bf} \quad \ldots(3.4)$$

Hamilton and Crosser Model is an extension of the Maxwell model and takes into account the shape of nanoparticles and is applicable for higher volume fraction of nanoparticles. This model stands valid where the ratio $k_{np}/k_{bf} > 100$ and is a two component mixture.

$$k_{nf} = \frac{k_{np}+(n-1)k_{bf}+(n-1)\varphi_v(k_{np}-k_{bf})}{k_{np}+(n-1)k_{bf}-\varphi_v(k_{np}-k_{bf})}k_{bf} \; ; where\ n = \frac{3}{\psi} \quad \ldots(3.5)$$

Where n = empirical shape factor and ψ = particle sphericity defined as the ratio of the surface area of the sphere with volume equal to that of particle to the surface area of the particle.

n= 3 for spherical particles and n= 6 for cylindrical particles

The major limitation of this model is that significant parameters such as nanoparticle size and temperature are not considered.

Wasp model: is a special case of Hamilton and Crossers model with value of n = 3 thus making shape factor unity. This model is based on the effective thermal conductivity of two component mixture

$$k_{nf} = \frac{k_{np}+2k_{bf}+2\varphi_v(k_{np}-k_{bf})}{k_{np}+2k_{bf}-\varphi_v(k_{np}-k_{bf})}k_{bf} \quad \ldots(3.6)$$

Lu and Lin: This model stands in good agreement for spherical as well as non – spherical particles.

$$k_{nf} = (1 + a\varphi_v + b\varphi_v^2)k_{bf} \quad \text{……(3.7)}$$

When shape of the particle is spherical and

For $k_{np} = 10$; a = 2.25 and b = 2.27

For $k_{np} = \infty$; a = 3 and b = 4.51

In this model, the pair interaction of the particles and the effective conduction of composite mixture was modelled. The interaction among the particles was evaluated by solving a boundary value problem involving two aligned spheroids.

Bruggeman model: Bruggeman proposed the model to determine the thermal conductivity of large volume fraction of spherical particles. For small concentration of nanoparticles in the base fluid bruggeman model gave the same thermal conductivity values as given by Maxwell model. For a binary mixture of homogeneous spherical and randomly dispersed nanoparticles.

$$\frac{k_{eff}}{k_{bf}} = \frac{1}{4}\left[(3\varphi_v - 1)\frac{k_{np}}{k_{bf}} + (2 - 3\varphi_v) + \frac{k_{bf}}{4}\sqrt{\Delta}\right] \quad \text{……..(3.8)}$$

1. **Hui, X. Zhang: In this model p**article interaction taken into consideration, and this relation stands in good agreement for all particle volume fraction.

$$\Delta = \left[\left[(3\varphi_v - 1)^2\left(\frac{k_{np}}{k_{bf}}\right)^2 + (2 - 3\varphi_v)^2 + 2(2 + 9\varphi_v - 9\varphi_v^2)\left(\frac{k_{np}}{k_{bf}}\right)\right]\right] \quad \text{……(3.9)}$$

Davis Model

Interaction of spherical nanoparticles is taken. The accuracy of this model is of second order to volume fraction of nanoparticles. The higher order terms of volume fraction represents the interaction among the dispersed nanoparticles.

$$\frac{k_{eff}}{k_f} = 1 + \frac{3(\alpha-1)\varphi_v}{(\alpha+2)-(\alpha-1)\varphi_v}[\varphi + f(\alpha)\varphi_v^2 + 0(\varphi_v^3)] \quad \text{……...(3.10)}$$

KD2Pro thermal property analyzer shown in figure 3.14 was used to determine the experimental values of thermal conductivity for alumina and copper oxide nanofluids (with distilled water as base fluid). The device employs transient heat source approach for evaluating the thermal conductivity of nanofluids and has an accuracy of +/- 5 % for a temperature range upto 90 °C. This device also mets the standards specified by both ASTM D5334 and IEEE 442-1981. The device basically consists of a needle sensor which is placed into the nanofluid and a display unit. For a single reading it takes almost 2 minutes as the first 90 seconds are used by the device to ensure temperature stability, after which the probe gets heated for 30 seconds using a known amount of current. There is a thermistor in the instrument that records the changing temperature whereas microprocessor records the thermal conductivity data. At the end of reading, the thermal conductivity of the fluid is computed using the temperature difference vs. time data.

Before determining the thermal conductivity values of nanofluids it is important to calibrate the sensor needle of the instrument and check the accuracy of the instrument. Thus, the validation of KD2-Pro thermal property analyzer is done as per standard procedure and the results were recorded for Distilled water at room temperature and the experimental values were compared with the available correlations and the data available in the literature. The calculated values of thermal conductivity due to Hagen equation (1999) are compared with experimental values of thermal conductivity of distilled water at room temperature as shown in Figure 3.15. This figure exhibits that good agreement exists in between the thermal conductivity values measured experimentally and those determined from the correlation. The maximum deviation among the thermal conductivity values was found to be $\pm$ 3 %.

The thermal conductivity data for different volume fractions of Alumina – DW and Copper oxide – DW is taken at lab conditions (i.e. temperature of the nanofluid sample is 25 $^{\circ}$C) and the volume fraction of the nanoparticles varies in between 0.1% to as low as 0.001%. The data measured is compared with the thermal conductivity values calculated from the Hamilton-Crosser Model as shown in fig. 3.16(a) & 3.16(b). The comparison is done using the Hamilton - Crosser Model as the particles are spherical in shape and the volumetric concentration of nanoparticles is less than 1 %. The comparison between the two shows that the maximum deviation is + 7%.

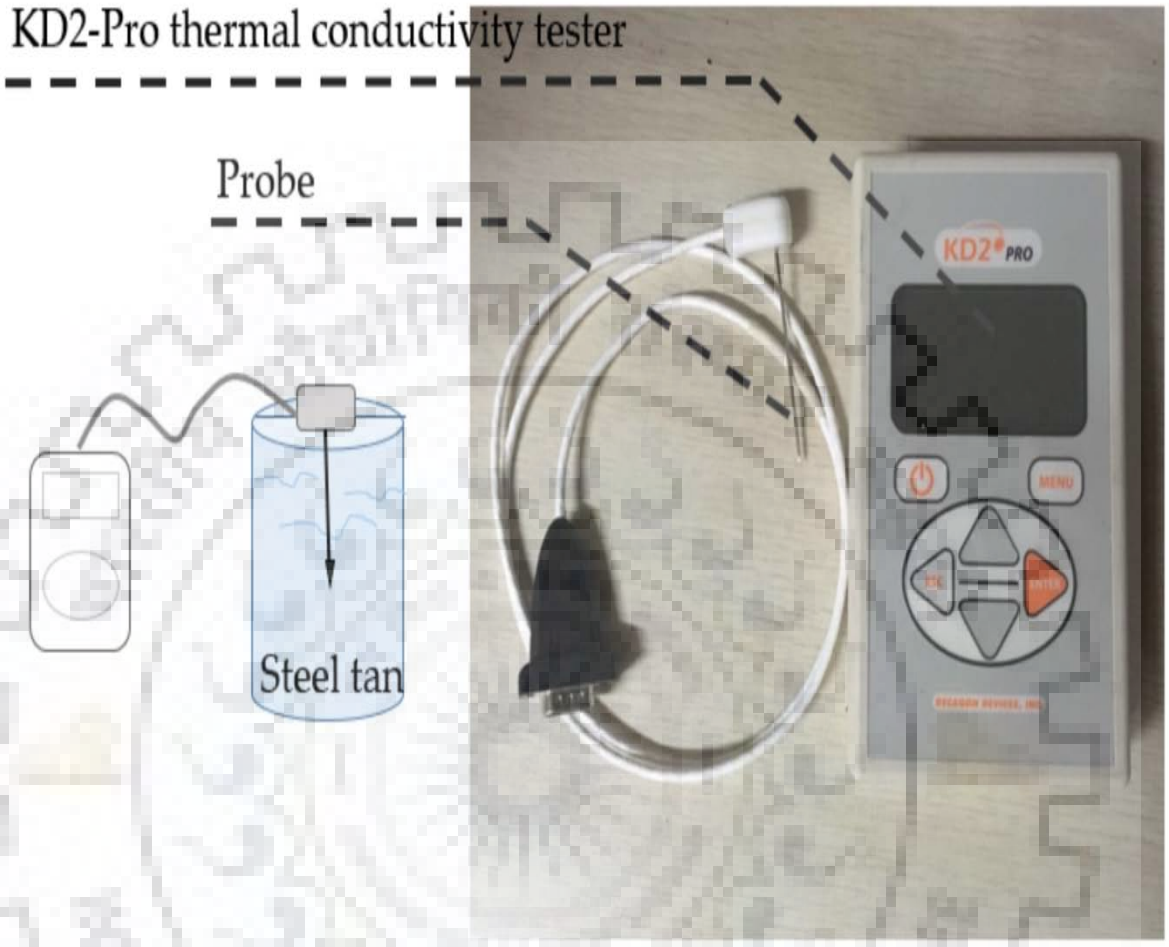

.

Fig.. 3.14: KD2-Pro Thermal conductivity measuring device:

3.3.2.1 Thermal conductivity v/s temperature

Since thermal conductivity measurements for different compositions of Alumina and Copper Oxide nanofluids are to be done at various temperatures i.e. 20 °C, 40 °C, 60°C and 80 °C., the nanofluid sample is placed in an insulated bath where temperature can be controlled. Furthermore, in order to avoid settling of the nanoparticle, a stirrer was also employed in the chamber which periodically stirs the nanofluid thus preventing the nanoparticles to agglomerate and settle down easily. The mixer was activated via a switch placed outside the enclosure. The KD2 probe was placed at a distance 0f 15 mm from the stirring rod to avoid the fluctuations in the readings. For every considered volume fraction of nanoparticles, the data was recorded at different temperature for every 30 minutes.

Figures 3.17 (a) and 3.17 (b) reveal the variation of thermal conductivity as a function of temperature for various values of nanoparticle concentration of Alumina – DW and Copper oxide – DW nanofluids, respectively. The thermal conductivity of the nanofluid increases with the increase in temperature irrespective of concentration of nanoparticles. Further, for a particular temperature the thermal conductivity of nanofluids increases with the increase in concentration of nanoparticles. The reason is obvious because metal ions will have higher thermal conductivity and thereby its oxides will provide higher thermal conductivity than the base fluids. As the temperature increases this results in an increase in the Brownian motion of nanoparticles in the base fluid which result in faster thermal transport thereby resulting higher thermal conductivity.

Experimental data of thermal conductivity of both the fluids have been correlated in the power series correlations as given below:

$$\frac{k_{eff}}{k_{bf}} = C\varphi^{a}T^{b} \qquad \text{……(3.11)}$$

The values of the constant C and exponents a and b for both the nanofluids are given in Table 3.5:

Table 3.5: Values of coefficients and exponents in the correlation for different nanofluid

Nanofluid	Constant 'C'	a	b
Al_2O_3 - DW	0.986	0.041	0.084
CuO – DW	0.876	0.038	0.078

Figure 3.18 depicts the comparison between experimental and predicted values of the ratio of thermal conductivity of nanofluids to the base fluid i.e. K_{nf}/K_{bf} from the equation 3.11. This figure reveals that the data exists well in agreement to a maximum deviation of $\pm$ 6%.

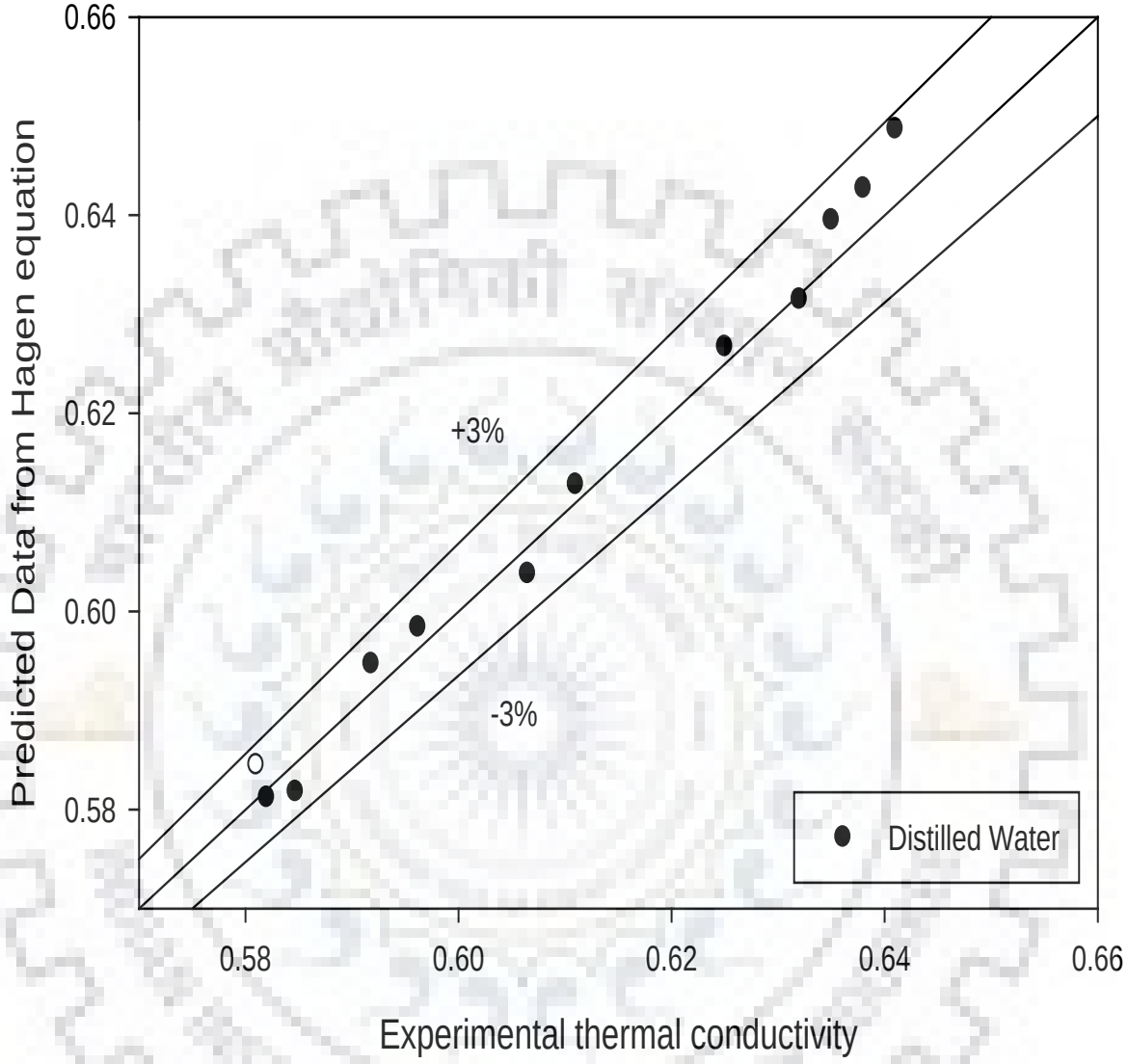

Fig. 3.15 : Thermal conductivity of Distilled water at room temperature in comparison with Hagen correlation

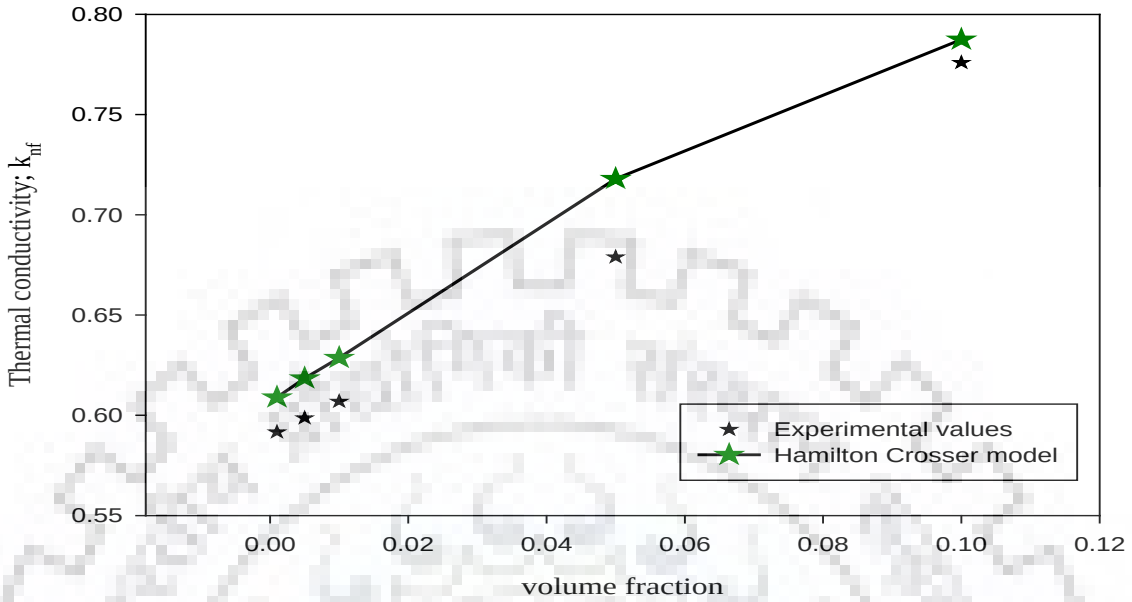

a) Comparison of experimental values of thermal conductivity for alumina – distilled water nanofluids with Hamilton-Crosser Model

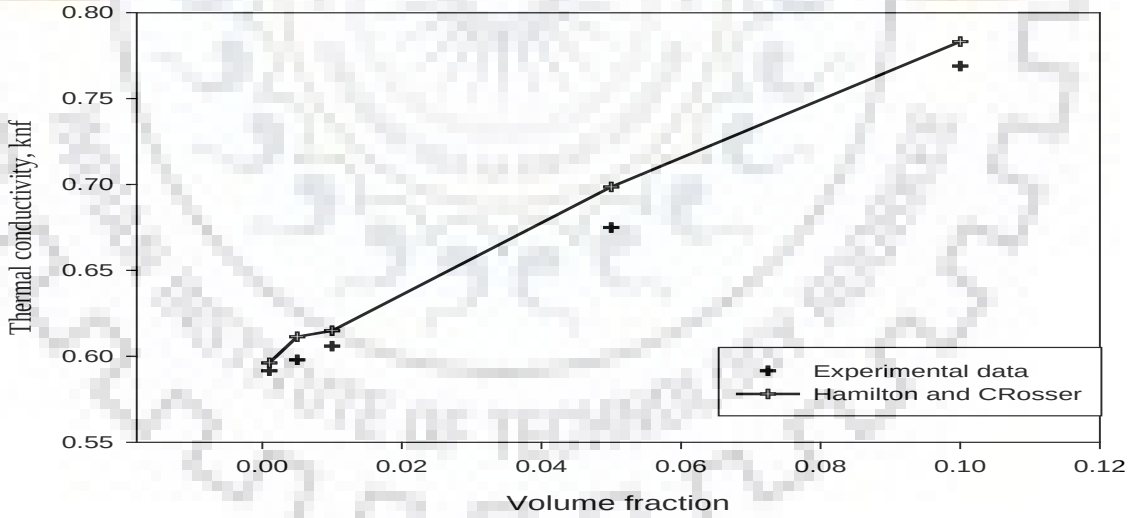

b) CuO - DW

Fig. 3.16 (b) Comparison of experimental values of thermal conductivity for copper oxide – distilled water nanofluids with Hamilton-Crosser Model

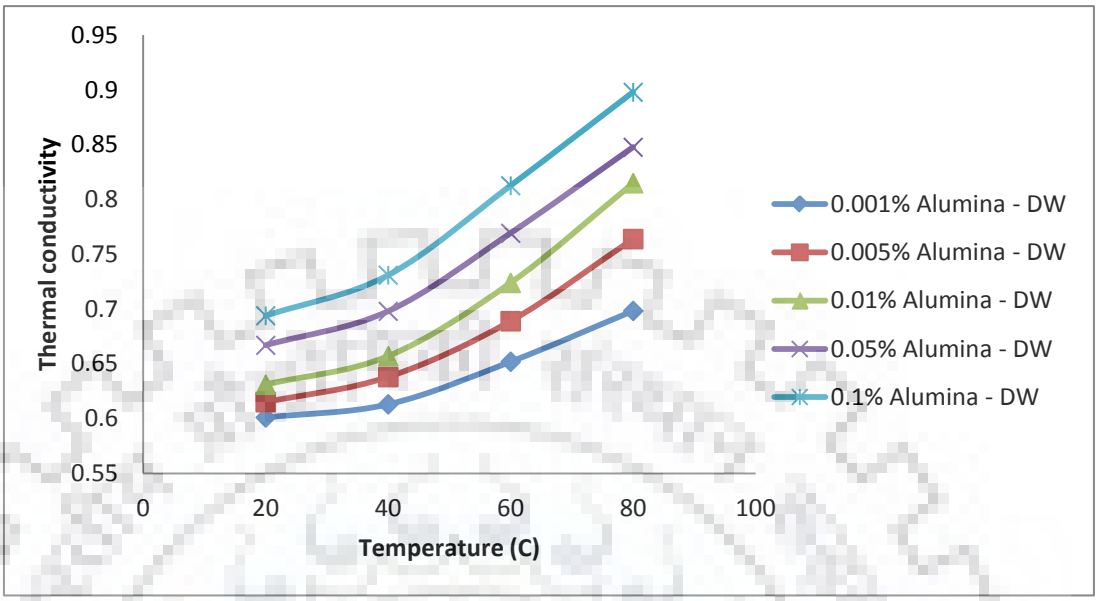

a) $Al2O_3$ –DW

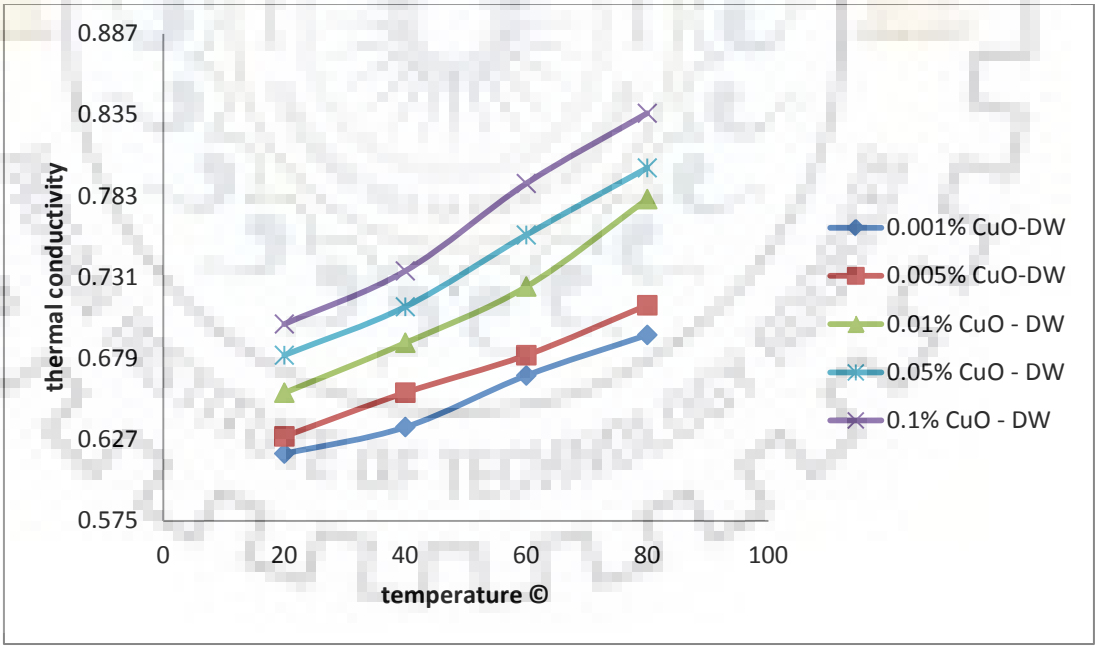

b) CuO – DW

Fig. 3.17 (a) & (b) Thermal Conductivity values of Al_2O_3-DW and CuO-DW nanofluids (for different concentrations) with varying temperature

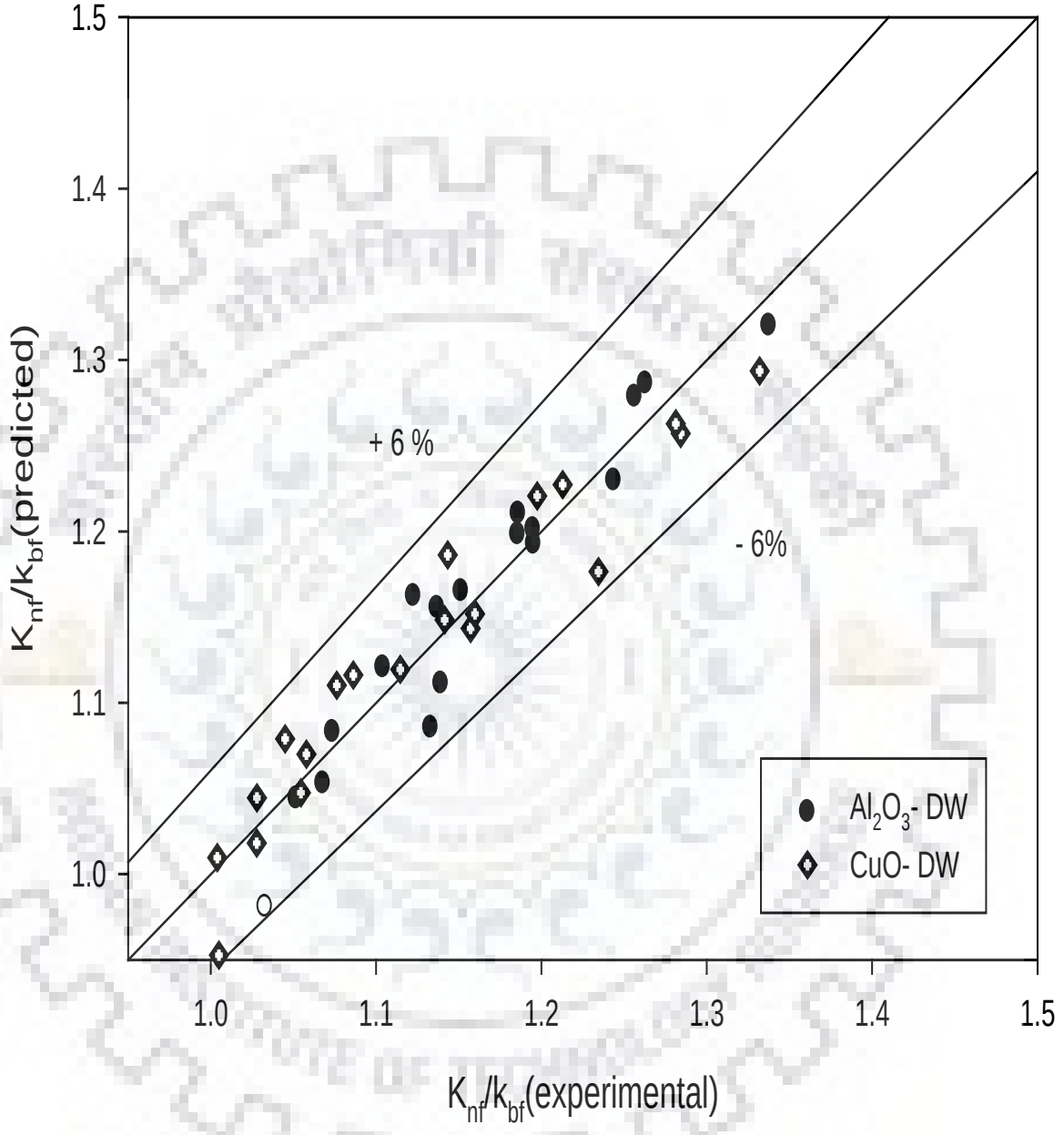

Fig.3.18 : Comparison of the experimental and predicted values of thermal conductivity ratio (k_{nf}/k_{bf}) from the proposed correlations for Al_2O_3 – DW and CuO – DW nanofluids

3.3.3 Viscosity

Compare to the experimental studies on thermal conductivity, limited rheological work has been reported regarding the viscous behavior of the nanofluids. It appears as a challenge to formulate any single theory that can explain the viscous behavior of the nanofluids considering it as a two – phase fluid. Thus, the limitations of classical theory and applications of two phase fluids remains widely open in case of nanofluids. For evaluation of the viscosity of the suspensions certain classical theory and formulas do exist and can be used as it is or are modified by various researchers in their work. Einstien in late 19 th century gave the relation for determining the viscosity of the particulate suspensions having spherical particles. Based on the assumption of the linearly viscous fluid he measured the energy dissipated by the fluid flow around a single particle and then by associating the energy with the work done for moving this particle relatively to the surrounding fluid he obtained the relation:

$$\mu_{nf} = (1 + 2.5\varphi_v)\mu_{bf} \qquad \text{……(3.12)}$$

Where ϕ_v represents the concentration of nanoparticles % by volume and μ_{bf} is viscosity of the base fluid. Einstiens correlation was found to be applicable for the nanoparticle with low volumetric concentration of the nanoparticles (< 2% by volume). For the large volumetric concentration of nanoparticles the deviation between the predicted and experimental value is too large and einstiens formula does not work as it ignores inter particle interaction.

Brinkman extended the work of Einstien and gave the formula for moderate volume fraction of nanofluids, say for concentration less than 5%. His formula is mentioned below:

$$\mu_{nf} = \frac{\mu_{bf}}{(1-\varphi_v)^{2.5}} = (1 + 2.5\varphi_v + 4.375\varphi_v^2 + \cdots)\mu_{bf} \qquad (3.13)$$

Lundgren expressed the Brinkman formula by expanding the brinkman relation using Taylor Series and proposed the following correlation:

$$\mu_{nf} = (1 + 2.5\varphi_v + 6.2\varphi_v^2)\mu_{bf} \qquad (3.14)$$

Batchelor considered the effect of brownian motion of nanoparticles in the suspension and proposed following formula for spherical nanoparticle based suspensions:

$$\frac{\mu_{nf}}{\mu_{bf}} = 1 + 2.5\varphi_v + 4.5\left[\frac{1}{\left(\frac{h}{d_p}\right)\left(2+\frac{h}{d_p}\right)\left(1+\frac{h}{d_p}\right)^2}\right] \quad (3.15)$$

Where, d_p denotes the particle diameter and h represents the inter particle spacing.

Ward Model: This model was proposed by ward to predict the viscosity of spherical nanoparticle based suspensions. This is an exponential model and gave the viscosity values for higher volumetric concentration of nanoparticles .

$$\frac{\mu_{nf}}{\mu_{bf}} = 1 + 2.5\varphi_v + (2.5\varphi_v)^2 + (2.5\varphi_v)^3 + (2.5\varphi_v)^4 + \cdots \quad (3.16)$$

Pak and Cho proposed the equation to measure the viscosity values of nanofluids at room temperature.

$$\frac{\mu_{nf}}{\mu_{bf}} = 1 + 39.11\varphi_v + 533.9\,\varphi_v^2 \quad (3.17)$$

Viscosity Measurement

In this work the viscosity of nanofluid is determined with the help of Brookfield cone and plate viscometer. In this apparatus the spindle drive consists of a cone and the plate is mounted in the specimen cup. Spindle used was CPE -40 and its viscosity range lies in between 0.3 to 128 cP . Using the gap adjustment feature a gap of 0.013 mm is maintained in between the cone and the plate where the sample is placed. As the spindle rotates, the viscous drag force of the fluid against the spindle is measured by the deflection of the calibrated spring. This apparatus requires a small volume of 0.5 to 2 ml of the sample and hence the temperature equilibrium is achieved rapidly within a minute. The speed of the spindle available with this viscometer ranges in between 0 to 100 rpm.

Figure 3.19 presents viscosity data of Al_2O_3- DW and CuO - DW nanofluids as a function of volumetric concentration of nanoparticle at the room temperature . Also, Figure. 3.19 depicts a comparison between the experimental results of viscosity with the theoretical viscosity data obtained from the several classical empirical models. It is clear from the figure that on increasing the concentration of nanoparticles in the base fluid irrespective of nanoparticle the viscosity of nanofluid increases. It is clear from Fig. 3.19 that a recent empirical model proposed by Wang et.

al. [69], the viscosity results of these studies are significantly larger than the predictions by other models.

Most of the prominent theories listed by several researchers describe the viscosity of nanofluids as a function of the concentration of nanoparticles in base fluid and failed to describe viscosity as a function of temperature. However, the value of viscosity also varies with respect to temperature , hence there must exist certain correlation that could predict viscosity as a function of both nanoparticle concentration as well as temperature. In addition to concentration of nanoparticles, effect of temperature on the viscosity of nanofluids is also investigated in present study. Figure 3.20 (a) and 3.20 (b) reveals the variation of viscosity as a function of temperature for various values of nanoparticle concentration of Alumina – DW and Copper oxide – DW nanofluids, respectively. From these Figures it is observed that the viscosity of nanofluids decreases with increase in temperature. This is because at elevated temperatures the shear stress decreases resulting in increased particle- particle interaction and the Brownian motion. The decrease in viscosity with rise in temperature increase is also because of the decrease in intermolecular adhesion forces at elevated temperatures.

Further, from the experimental data collected for the various values of nanoparticle concentration of Alumina – DW and Copper oxide – DW nanofluids two different correlations were developed to predict the viscosity of Alumina – DW and Copper oxide – DW nanofluids, respectively using regression analysis which stands valid for the temperature range in between 10 °C and 90 °C. It is worth noting that for a particular volume fraction of nanofluids at least five readings were taken to ensure consistency as well as the repeatability of the measured data. The equations developed to predict the values of Alumina – DW and Copper oxide – DW nanofluids are given as under.

$$\ln(\mu_{nf}) = \frac{A}{T} - B \quad \text{; where} \tag{3.18}$$

For alumina - DW

$A = 3173 \times \varphi^{2.23} + 17349 \times \varphi + 1167.3$ and

$B = -97.12 \times \varphi^2 + 47.183 + 3.732$ (3.18 a)

For Copper Oxide –DW

$A = 1987 \times \varphi^{1.05} + 13459.49 \times \varphi + 987.14$; and

$B = -71.09 \times \varphi^2 + 51.79 \times \varphi + 3.178$ 3.18(b)

Here A and B are the constants whose value depends on the volume fraction of nanoparticles and dispersion behavior and Brownian motion of nanoparticles in the base fluid.

Figure 3.21 shows the comparison between experimental and predicted values of viscosity of nanofluids from the equations 3.18 for both Al_2O_3 – DW and CuO – DW nanofluids with a maximum deviation of $\pm$ 3%.

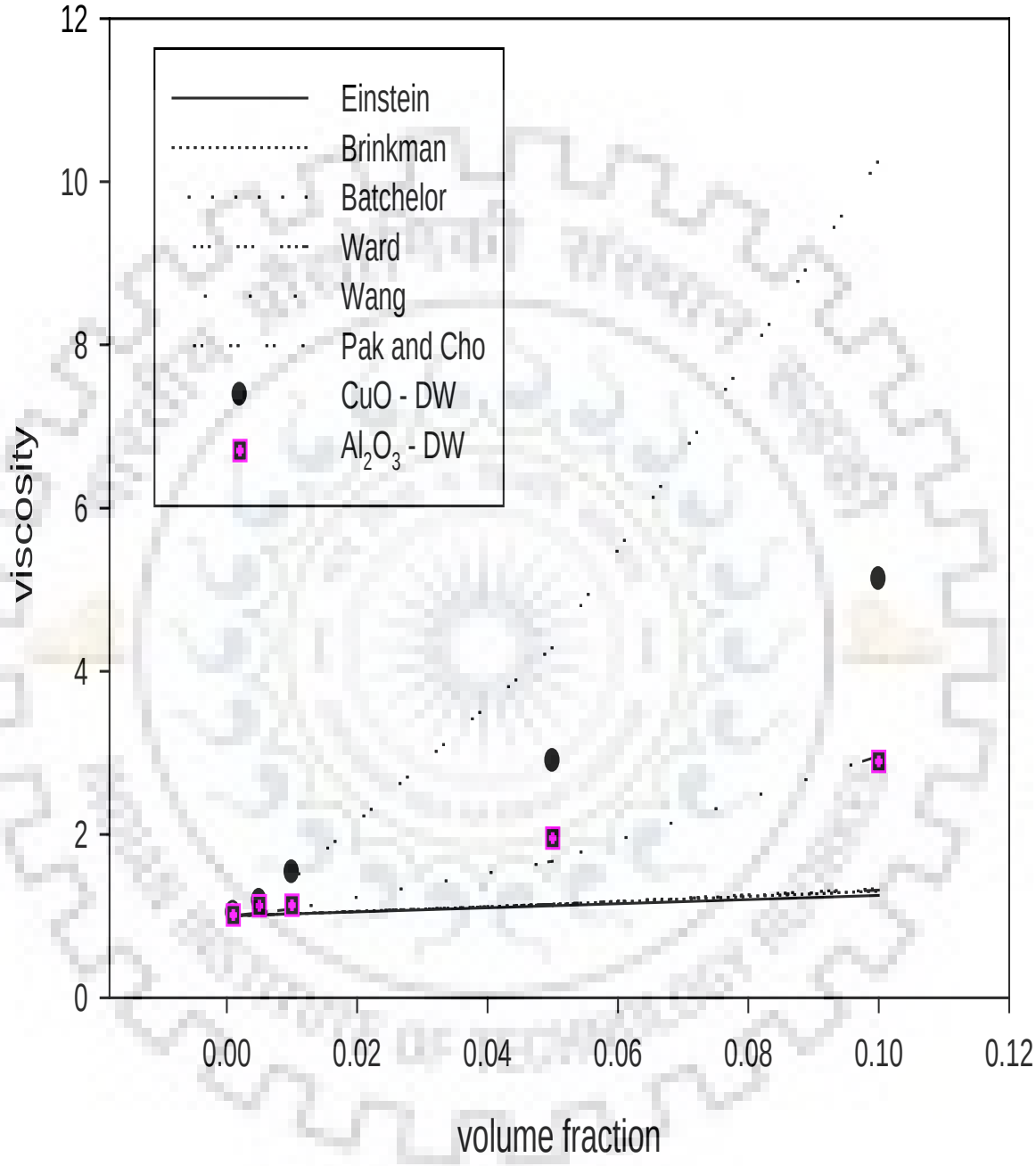

Fig.3.19 Viscosity data of Al_2O_3- DW and CuO - DW nanofluids at room temperature

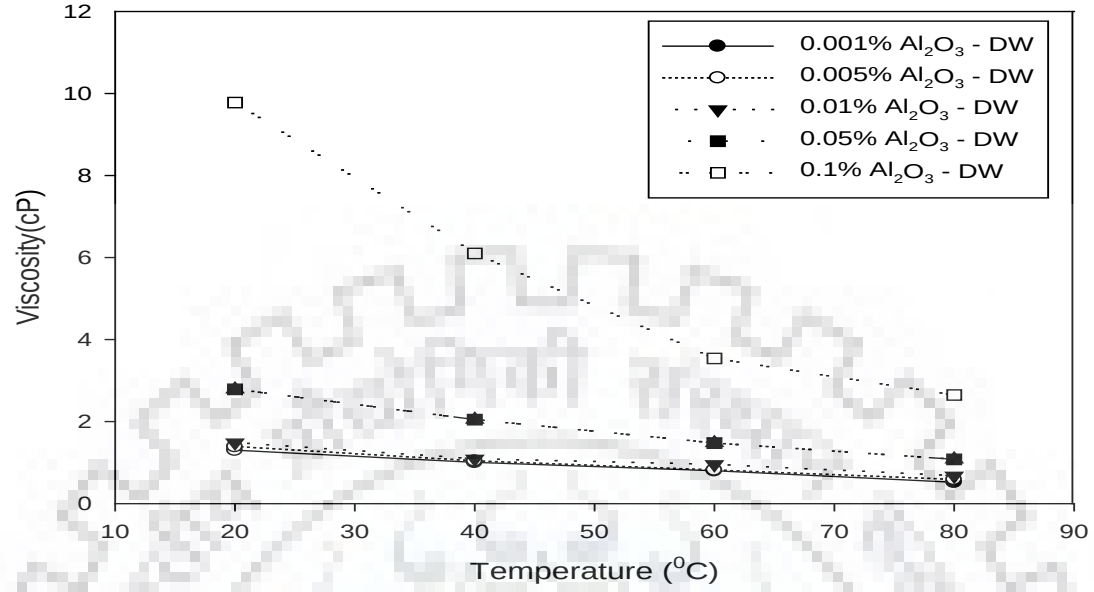

(a) Al_2O_3 - DW

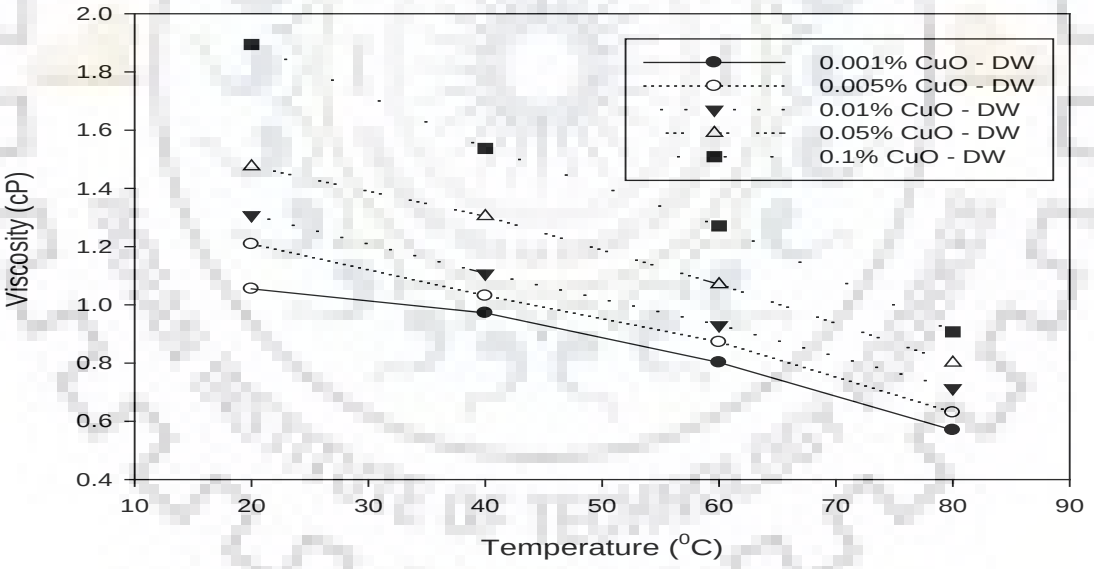

(b) CuO-DW

Fig.3.20(a) & 3.20 (b) Viscosity v/s temperature curve for different compositions of Al_2O_3 - DW and CuO-DW

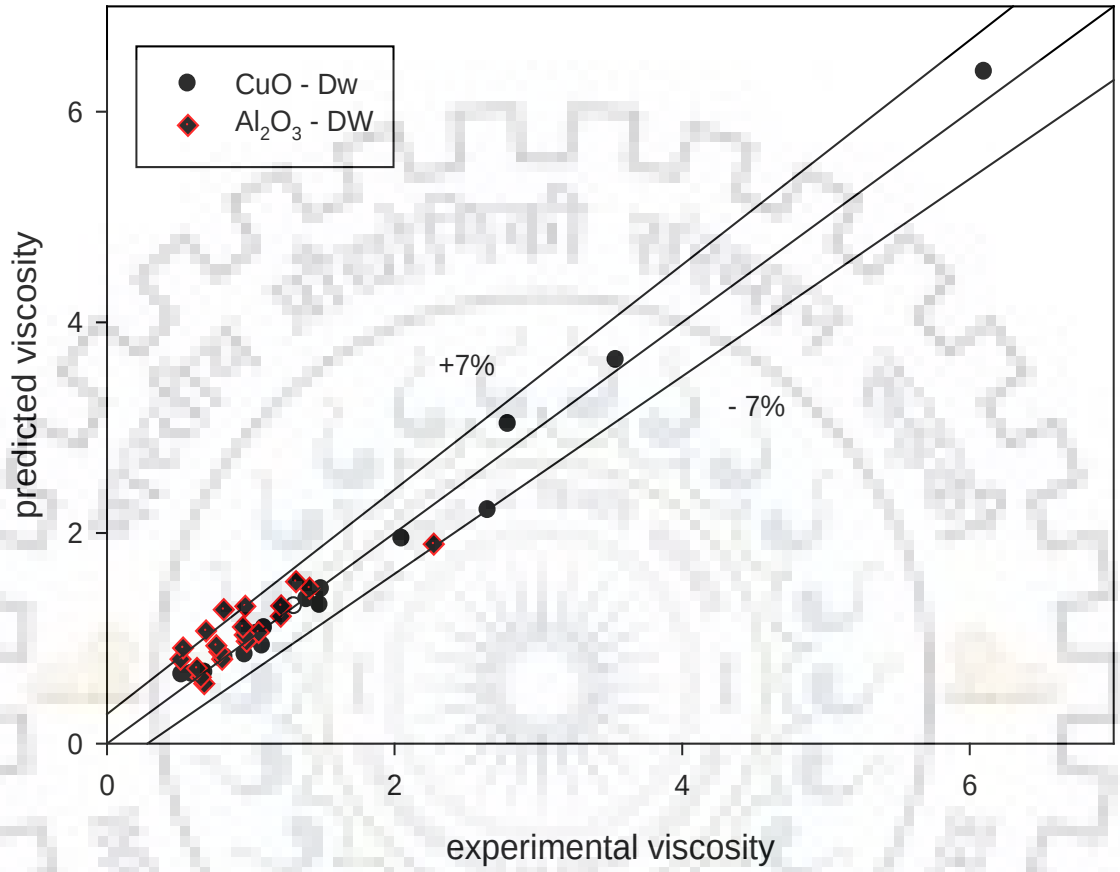

Fig.3.21 Comparison between the experimental and predicted values of viscosity from the Eq. 3.18 for Al_2O_3 – DW and CuO – DW nanofluids

Chapter – 4

EXPERIMENTAL SET-UP

The main objective of this investigation is to obtain the experimental heat transfer data for the pool boiling of nanofluids carried out using submerged cylindrical heating tube. This requires an experimental set up properly designed and fabricated so that consistent, reproducible and precise data can be obtained. The pool boiling experiments are to be performed at atmospheric and sub atmospheric pressures. Therefore following important parameters are considered during the designing , fabrication and commissioning of the different parts of the setup.

4.1 General Design Considerations

- As the experiments are performed at sub atmospheric pressure for various compositions of nanoparticle – base fluid, thus the shape of the vessel is taken to be cylindrical so that the vessel could withstand the operating pressure with minimum development of hoop stresses. The vessel height is taken approximately twice the diameter of vessel to provide sufficient space over the liquid pool so that vapors can disengage their in.
- For viewing the bubble formation and the pool boiling phenomenon over submerged heating tube provision of two visual ports on diametrically opposite ends of the boiling chamber is also there.
- An arrangement in the vessel was such made that the heating tube was placed perfectly in horizontal position and is visible across the view ports provided.
- As the pool boiling process taking place is a cyclic process thus a horizontal condenser above the vessel is incorporated in the test rig for the condensation of the vapors rising due to boiling and proper recycling of the condensate back to the boiling vessel is ensured with the help of piping and valves. Thus, mounting a horizontal condenser over the vessel is considered.
- To reduce the error and increase the accuracy of the experimental data heating tube was properly submerged in the liquid pool. This minimizes the disturbances and the possible error due to the return of the condensed base fluid back to the pool. Also, sufficient free space over the liquid pool was given so that no sub cooling take place due to the return of the condensed vapor back to the liquid pool.

- In the experiments performed transfer of heat occurs radially from the surface of the heating tube to the liquid pool. Thus, one end of the heating tube is left undrilled with sufficient thickness to restrict the longitudinal heat transfer across the surface.
- Adequate arrangements are made to record the temperature across the surface of the heating tube. Four thermocouple probes are placed at top, bottom and two opposite sides of the heating tube. Also the thermocouples are placed in the co-axially drilled holes in the heating tube and not over the surface as they can disturb the bubble formation and vapor bubble dynamics. The mounting of the thermocouple probes is done in such a manner that it does not influence the end effects, thereby thermocouples are to be placed away from the ends of the heating tube..

  Similarly in order to determine the temperature of liquid pool four thermocouples are positioned at top, bottom and two extreme sides across the circumferential surface of the heating tube. Thermocouple probes are placed at a sufficient distance apart from the cylindrical heating tube to get precise temperature of the liquid pool.

4.2 Experimental Set-up Description

Keeping all the design considerations in mind, the experimental set up was fabricated. Utmost care has been taken at each phase of mounting the experimental setup. Each and every component from thermocouple to vessel were properly designed, tested and fabricated before assembling. The schematic line sketch of the experimental set – up with boiling vessel and all the assembly components and instrumentation panel is shown in Fig. 4.1. The photographic view of test rig along with all components of instrumentation panel is depicted in Fig. 4.2. The various components of the experimental set-up are discussed underneath**.**

4.2.1 Vessel

The vessel (1) is considered to be the heart of the experimental set- up. The vessel employed in current investigation is cylindrical in shape and is made from Stainless Steel AISI- 304 grade of 3.2 mm thickness. The dimensions of the vessel are internal diameter 15 cm and height of 37 cm. The two ends of the vessel are closed with the dished cap of same material. The bottom end of the vessel was provided with the fittings to incorporate the thermocouple probe that gives the temperature T_L of the liquid pool beneath the heating tube. Also, at the bottom end of the vessel pipe fittings with valve (V_1) are given for draining the liquid out of the vessel as and when

required. Similarly, on top of the vessel various fittings were provided for mounting the vacuum gauge to record the pressure inside the cylindrical vessel, to fix the condenser and a line with valve (V_2) was also assembled for the release of the dissolved air in the liquid pool to the bubbler (9). Also on the top of vessel a fitting was provided to incorporate the thermocouple (T_L) for recording the temperature of the liquid above the surface of heating tube. To visually observe the pool boiling behavior and the bubble formation over the heating tube inside the vessel two viewports (7) with 75 mm diameter were machined in the vessel at diametrically opposite ends. A socket (5) was fabricated on the vessel to place the heating tube in a perfectly horizontal orientation. This socket was placed at a distance of 10 cm from the bottom of the heating tube. Also, a graduated scale with a liquid level indicator (8) is assembled in the vessel to know the exact level of the liquid within the vessel. Four thermocouple probes are also placed into the vessel to record the liquid pool temperature near the heating tube surface corresponding to the top, bottom and two side positions.

The vessel body as well as all the connection lines are properly insulated using the asbestos rope winding. Also, a thick paste of magnesia powder, asbestos powder and plaster of paris was applied over the asbestos winding to minimize the heat losses to the surroundings.

Figure 4.1: Schematic Representation of Experimental Set

Figure
Photograph
the experin
up

4.2.2 Heating Tube

Stainless Steel heating tube of cylindrical shape is employed in this investigation. Fig 4.3 depicts the pictorial view of the heating tube and fig 4.4 shows the dimensions of the heating tube as well as the heater used in experimental work.

The heating tube is fabricated from a cylindrical stainless steel rod of 215 mm length with 28.94 mm outside diameter and 18 mm inner diameter. This tube was drilled an inner diameter of 18 mm and drilling was done upto a distance of 185 mm from one end of the tube. A portion of 30 mm is left undrilled at the other end of the tube. An inert material possessing very low thermal conductivity such as thick sheet of PTFE is used for covering the undrilled portion of the heating tube to prevent the heat transfer across the longitudinal direction. A portion of SS heating tube is also taken for further SEM (Scanning Electron Microscopy) investigation. Further, a hexagonal nut, a collar and a threaded portion is machined on the open end of the heating tube for which a 35 mm of rod length was left. Thus the effective length of heating tube remained 150 mm. Also, a collar of following dimensions 50 mm diameter and 5mm length are machined on the heating tube which is used to place the heating tube tightly with perfectly horizontal orientation in the socket placed in the vessel. A hexagonal nut of 10 mm length was also machined at the open end of the heating tube surface. The length of the threaded portion is 20 mm and is of 19 TPI. The threads on the heating tube assist in properly placing the tube in the vessel and prevent any sort of leakage. Four holes equi-spaced at 90° are drilled on a 25 mm pitch circle diameter to place the four thermocouples which records the heating tube surface temperature at four circumferential positions respectively top, bottom and two side positions. The holes are drilled across the heating tube with 2 mm diameter and 15 mm length measured from the open end of the heating tube. The positions of the thermocouple holes are clearly shown in Figure 4.3 and Figure 4.4 respectively.

The surface of the cylindrical heating tube is rubbed with the emery paper of different grit sizes such as 800 and 1200 in order to make the surface smooth. Finally polishing of the surface is done with 4/0 grade emery paper. Same procedure is applied across all the heating tubes to obtain uniform roughness of the heating tube for investigation.

Table-4.1: Dimensions of Heating Tube

Tube No.	Heating Tube Nomenclature	Diameter of Tube d, (m)	Inner Diameter d_i, (m)	Pitch Circle Diameter d_h ,(m)	Effective Length L ,(m)
1.	SS-01	0.032	0.01801	0.0250	0.1500
2.	SS-02	0.032	0.01799	0.0250	0.1500

The porcelain tube is cut to the effective length of the heating tube and Nichrome wire with current carrying capacity of 5A is wounded over it. The diameter of the porcelain tube is 16 mm. The heater thus prepared is placed inside the cylindrical tube as shown in Figure 4.4. Both the terminals of the Nichrome wire are covered with porcelain beads are connected to the Autotransformer with the help of a connector. In order to avoid the electric short circuiting the heating rod surface is properly covered with multiple layers of mica sheet and glass tape.

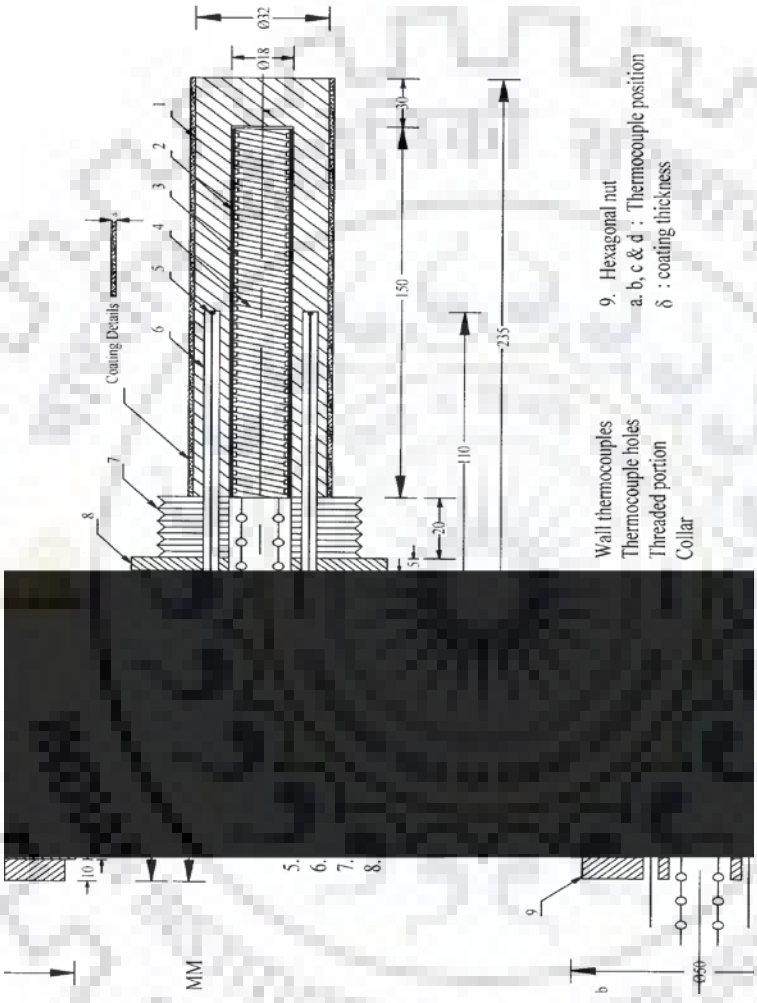

Figure 4.3: Schematic diagram of the heating tube along with heater

Figure. 4.4
Photographic view
the heating tube

4.2.3 Condenser

A knockout condenser (11) of 660 mm length is fabricated u sing AISI 304 stainless steel sheet. The condensor is employed for condensing the vapors coming out of the vessel during the pool boiling of the nanofluid inside the vessel. Basically the condenser works as a double pipe heat exchanger with 25 mm inner pipe diameter and 75 mm outer pipe diameter. The condenser is mounted horizontally with slight inclination over the top of the vessel with one end connected to the vessel and the other end joins the separator. The vapor rising through the boiling vessel flows through the inner pipe whereas water is used as a coolant and runs across the annular space between the two pipes. For ensuring the rapid condensation of the vapors the flow of coolant is kept counter flow. The condenser is kept slightly inclined which keeps the continuous flow of condensate into the separator due to gravity. The condensed vapors are collected in the separator and then returned to the vessel.

4.2.4 Condensate Accumulator

The next important component assembled in the set-up is Condensate Accumulator. This unit (12) lies in between the condenser and the vacuum unit. It is connected to condenser using a universal union. The prime function of incorporating this unit to the set-up, is to remove the non-condensable gases. The air- liquid mixture enters the accumulator tangentially and here the non-condensable gases are released through pipeline at top of accumulator to surge tank and vacuum and the condensate is sent back to the pool.

4.2.5 Vacuum Pump

A two stage oil sealed rotary vacuum pump is also the part of experimental set up in this investigation. The vacuum pump (14) is procured from M/S G.E Motors India Ltd., Faridabad (India). The vacuum pump is run with the help of 0.5 horse power of class B motor having maximum speed of 1500 rotations per minute. The pump has a suction tendency of 7.5 ltr/min and can establish a vacuum of 0.003 mm Hg. The vacuum pump is connected to the vessel through a surge tank (13) and a needle valve (V6). The function of the surge tank is to reduce the pressure fluctuations and also restricts the entrance of liquid condensate to the vacuum pump.

Table 4.2 below describes the various instruments used in the data acquisition system.

Table 4.2 List of Digital Instruments used in the Data Recording Panel

Instrument	Make	Function
Servo Voltage Stabilizer (17)	by M/S Gargy Research Instruments, Delhi (India)	To supply power to the heater.
Constant Voltage Stabilizer (18)	Bhurji Electronics Pvt. Ltd. Gurgaon (India)	Ensures constant power supply to the coil of heater
An Auto-transformer	Agro Transformer Company Ltd., Mumbai (India)	Controls the power input to the heater
Ampere meter	Electronics and Scientific Devices, New Delhi (INDIA)	Measures the current input
Wattmeter	Electronics and Scientific Devices, New Delhi (INDIA)	Measures the power input.
Volmeter	Electronics and Scientific Devices, New Delhi (INDIA)	Measures the voltage

4.2.6 Control Panel Instrumentation

For measuring the nucleate pool boiling heat transfer coefficient of nanofluids, precise determination of following parameters is necessary:

- Determination of accurate power supply to cylindrical heating cartridge;
- Accurate measurement of the temperatures of liquid pool as well as the heating tube surface;
- Determination of set pressure inside the vessel using vacuum gauge

Consequently. the instrumental panel should contain all the instruments with proper calibration and give the respective readings with least error. The details of the various instruments presented in instrumental panel is given in table

below:

Voltmeter, Ampere meter and Watt meter are properly calibrated as per the standards in order to display the readings with least error.

The calibration of vacuum gauge mounted over the vessel is done against the standard Mc leod gauge in order to ensure constant sub- atmospheric pressure readings.

Polytetrafluoroethylene (PTFE) coated 30 gauge copper constantan thermocouple wires are

supplied by M/s Omega Engineering Limited, United Kingdom. Thermocouples are prepared in the laboratory by passing a 12 V DC current across the one end of the wire dipped in the mercury solution and the wires are turned into spherical beads after passing the current. These thermocouples are suitably calibrated by a temperature calibrator with an accuracy of 0.01 °C and a temperature range of -25 °C to +135 °C. Finally after calibration these thermocouples are inserted placed into the vessel and the heating tube at their respective positions. All the thermocouple probes are connected to a 12 point selector switch which is installed in the instrument panel. The selector switch transmits the signals send by thermocouples to the digital multimeter. The Digital Multimeter of Keitheley 177 microvolt made in USA is used to measure the emf generated by thermocouple. The least count of multimeter is 0.1μV in 20 mv range. For the reference junction a bath of ice and water maintained at temperature of 0 °C is used.

Chapter – 5

EXPERIMENTAL PROCEDURE

This chapter discusses the procedure employed in the investigation for attaining precise and reliable experimental results. Also, the steps taken to investigate the reproducibility, accuracy and precision of the results given by each and every component of the set-up individually as well as of complete set-up are discussed here.

5.1 Inspection of Mechanical And Electrical Leakage

Every single component of the experimental setup is tested for any sort of mechanical or electrical flaws individually before getting assembled into a single test rig. Following, paragraphs discuss the various tests performed over the individual components that ensure the proper functioning of the set-up.

Firstly, the leakage detection test is performed over the boiling vessel as well as the valves such as V_1 to V_6 and joints in between different components installed in the set up to ensure the leakage free working of the set-up. The leakage detection test is done by passing the compressed air at a pressure of 210 kN/m^2 through the valve (V_1).

Leakage testing of condenser is performed against the compressed air following the procedure with utmost precautions in order to prevent any sort of leakage.

The condenser is checked against compressed air to avoid the leakage. The procedure adopted is as follows:

The nozzles provided in outer pipe of the condenser are connected to water inlet and fittings and valves of the outlet pipelines are checked to ensure that there is no leakage. Pressure gauge is connected to one end of the inner pipe whereas the other end is connected to a compressor through a valve. Compressed air is forced into the condenser at a pressure of 210 kN/m^2. After this, all the end-valves are closed and soap solution is applied to the welded joints and other portions on outer surface of the condenser. Any leakage is detected by the appearance of air bubble on the surface. If leakage at any joint is detected it should be removed. This process is repeated until no air bubble appears. Further, the pressure drop is not shown in pressure gauge reading. Now the condenser is considered to be leak-proofed.

A pressure gauge is placed on the boiling chamber to have the reading of sub atmospheric pressure. The socket (4) used for fastening the heating tube is closed by a dummy nut and valves are connected to the openings of the vessel. Valve V_2 is kept open for the entry of liquid / compressed air while the remaining valves are kept closed. The pressure in the set-up is maintained at about 210 kN/m^2 pressure by admitting compressed air through the inlet valve V_2. Thereafter valve V_2 is shut-off and the set-up is monitored for a period of 24 hours to identify leakage, if any. The pressure drop indicated by pressure gauge reading verifies the existence of leakage in the set-up. Careful examination of any sort of leakage is done across the experimental test rig out by using the detergent solution at each and every joint and connection present in vessel, piping and at different connectors, elbows and gauges in order to detect any sort of leakage from the joints. If any bubble formation is observed across the joints of the vessel the leakage should be attended immediately. The process is repeated until there is no bubble formation and all the joints are leak - proof. Thereafter, the set-up is again filled with compressed air of pressure of 210 kN/m^2 (g) and kept for a period of 48 hours. If no alteration in the reading of pressure gauge is observed then the set-up is ready for experimental run.

After the set-up is tested successfully against high pressure, it is now tested against vacuum by creating a vacuum. For this purpose, a vacuum gauge is mounted at the vessel. A vacuum of 500kN/m^2 (g) is developed inside the vessel by the use of vacuum pump. No change in the reading of vacuum gauge over a period of 48 hours confirmed that the set-up is completely leak proof.

For operational safety, experimental setup is properly earthed to eliminate any possibility of electrical short-circuiting. For this purpose all wire joint are insulated by tape and screw tightly, heating coil is properly insulated against any electrical leakage. The leaky points are immediately repaired. For safe experimentation run.

5.2 Preliminary Operations

In order to acquire precise, consistent and reproducible data a set of operations are repeated after every experimental run, which includes vessel cleaning, charging the test fluid in the vessel, removal of dissolved air and entrapped gases from liquid pool and stabilizing the cylindrical heating tube. Detailed description of the procedure adopted to carry out these operations is explained in the following paragraph.

- All pipelines and vessel are flushed with compressed air to remove foreign solid particle

adhering to surface of tube, vessel, pipeline etc. This is carried out by forced compressed air in the system through valve V_4 while keeping valve V_1 opened and valve V_2 closed. Thereafter, all valves except V_5 are closed and vacuum is created inside vessel by vacuum pump. The soap –water solution is filled with the help of flexible tube, solution is sucked due to pressure difference created by vacuum pump through valve V_2.

- The vacuum is released during filling of soap solution and compressed air at a pressure of 210 kN/m^2 is admitted to vessel via flexible tube through the valve V_2. Compressed air imparted a whirling motion to soap-water solution in vessel and this helps to loosen the adherence of dust and other foreign particles on inner surface of vessel. Now the solution is drained off from vessel through valve V_2. Consequently, distilled water is admitted into the vessel via flexible tube and after adopting above procedure liquid is drained off. This process is recurring several times till drained-off liquid is found to be completely liberated from dust and other foreign particles. Consequently cleaning of heating tube surface is done using distilled water and acetone and finally with the test liquid before fitting the same in vessel.
- Rinsing of vessel is done by filling liquid under investigation into the vessel, shaking it with compressed air and then draining it off from the vessel. This procedure is repeated several times to ensure rinsing of each component and surface of vessel and heating tube.
- After vessel is cleaned and rinsed properly, liquid is admitted in to it by developing vacuum inside it. The level of the liquid charged in the vessel is kept 75 mm above the heating surface. Now, water (coolant) is passed into the condenser and heater is energized by supplying it a power input of 600 W. Temperature of liquid increases and reaches saturation temperature. The condition of atmospheric pressure is maintained throughout the system by opening valve V_4. At this condition liquid is boiled for several hours. The prolonged submergence of heating tube followed by vigorous boiling of about 72 hours makes the surface aged and thermally stabilized. This operation ensures accurate and reproducible experimental data. Further, this is confirmed by taking data at different intervals of time.

5.3 Data Acquisition

After completing all preliminary operations, series of experimental runs are conducted by following the procedure given below:

The pool boiling heat transfer is highly influenced by the presence of dissolved air in the liquid pool. So before starting the experimental work it is desirable to remove the dissolved gases from

the liquid pool. The removal of dissolved air from the liquid pool is removed by passing the dissolved gases into a bubbler. The bubbler is connected to vessel through valve V_2 with the help of PVC pipe. Also the boiling of liquid pool is carried out for several hours before beginning the experimental work. During deaeration of dissolved gases from liquid pool all the valves in the set-up are kept closed except valve V_2 which is connecting the bubbler to the vessel. Removal of dissolved gases from liquid pool takes place until bubbling in the bubbler ceases which indicates complete removal of dissolved gases from the liquid pool. As all the dissolved gases are removed from the liquid pool, the valve V_2 is closed. This procedure of deaeration is followed every time before beginning the pool boiling experimentation.

After de-aeration process, setup is ready for experimentation. At first the vessel is subjected to atmospheric pressure by opening the valve V_4. Then, heating tube is energized with the lowest heat input of 240 W. As a result, temperature of liquid increases progressively until it reaches saturation temperature corresponding to atmospheric pressure. At saturation condition, the e.m.f readings of all thermocouples as indicated by DMM are kept under continuous observation. When no change in readings of thermocouples is noted, steady state condition is said to exist. As the steady state condition is attained the thermocouple readings are recorded from the digital meter for all the respective positions of the heating tube as well as liquid pool. The power input to the cylindrical heating cartridge is then adjusted to the next predetermined higher value and procedure as mentioned above is repeated. The power supply to the heater is increased uniformly from 240 W to 440 W in six equal steps. After completing experiments at atmospheric pressure, the system is maintained at sub-atmospheric pressure by creating vacuum in it and above mentioned procedure is repeated to obtain boiling heat transfer data. Pressure in the test vessel is increased from 45.47 kN/m^2 to 97.75 kN/m^2. The liquids investigated in present investigation are distilled water, and different concentrations of Alumina – Distilled Water and Copper Oxide – Distilled Water nanofluids.

5.4 Reproducibility And Consistency

Reproducibility and consistency of experimental data is most important for their accurate and reliable analysis. Reproducibility of the experimental data is verified by repeating the experiments multiple times maintaining the same working parameters and conditions. As consistent and similar readings of wall temperature and liquid pool temperature is measured with the help of

thermocouples data is considered to be reproducible.

Also, the confirmation of homogeneity of heating tube surface during preliminary operations validates the consistency of experimental data. Besides, analysis of data for circumferential variation of wall temperature around heating tube shows that surface temperature increases continuously from bottom to side to top position. This behavior is in accordance to the literature available on variation of surface temperature of heating tube during nucleate pool boiling. Thus, above tests proves that data obtained in the present investigation are consistent.

5.5 Operational Constraint

The operating variables in present investigation are heat flux, pressure, and nanofluids. Their ranges are determined by certain operation constraints which are mentioned below:

The maximum power input given heating tube surface is limited by the current carrying capacity of wire used in the construction of electric heater. However, minimum heat input is decided by the value at which sustained nucleate boiling of liquid occurs. In present investigation the 24-gauge nicrome wire having a maximum current carrying capacity of 5 amperes is used to make the heater. Accordingly, the maximum power input to the heater is limited to 440 W, which corresponds to a heat flux of 29255.32 W/m^2. The minimum power input at which sustained boiling of liquid occurs is 240 W, which is equivalent to a heat flux of 15957.45 W/m^2.

As in the pool boiling of nanofluids, formulation of nanofluids is a challenging task. In the present investigation two nanofluids namely Alumina – Distilled Water and Copper Oxide – Distilled Water are prepared as per procedure described in Chapter 3. In the nanofluids it is considered that agglomeration of the nanoparticles to be minimum. Specifically during the experimental run the nanoparticles should remain in suspended form and the formulation of nanofluids should be of specific concentration. The concentration of the nanoparticles namely alumina and copper oxide varies from 0.001% to 0.1% by volume is taken in the base fluid.

The operating parameters of the present investigation are given in Table 5.1:

Table 5.1 Operating variables of present investigation

Sl. No.	Test Fluid	Heating tube	Nanoparticle Concentration	Pressure (kN/m^2)	Heat flux (W/m^2)
1	Distilled Water	H.T. 1	0.001, 0.005, 0.01, 0.05	97.75, 85.17 71.11, 57.12 45.47	15957.45, 18617.02, 21276.6, 23936.17,26595.75, 29255.32
2	Alumina -DW	H.T. 1	0.001, 0.005, 0.01, 0.05	97.75, 85.17 71.11, 57.12 45.47	15957.45, 18617.02, 21276.6, 23936.17,26595.75, 29255.32
3	Copper Oxide - DW	H.T. 2	0.001, 0.005, 0.01, 0.05	97.75, 85.17 71.11, 57.12 45.47	15957.45, 18617.02, 21276.6, 23936.17,26595.75 , 29255.32

Chapter – 6

RESULTS AND DISCUSSION

In this chapter the experimental results of nucleate pool boiling of Distilled Water and nanofluids namely Alumina – Distilled Water and Copper Oxide – Distilled Water on a horizontal Stainless steel heating tube surface and there interpretations are discussed. It also includes a comparison between the boiling heat transfer coefficient with respect to heat flux for Alumina based nanofluids and copper oxide based nanofluids with base fluid as distilled water. Further, the thermal effectiveness of the two nanofluids namely Alumina – Distilled Water and Copper Oxide – Distilled Water is investigated in order to bring out the scope of application of nanoparticle based fluids during nucleate pool boiling.

The pool boiling experimental data of present work for distilled water and nanofluids namely Alumina and copper oxide nanoparticles dispersed in base fluid i.e. distilled water collected at atmospheric and sub atmospheric pressures are listed in tables A.1 to A.11 of Annexure A. The tables listed in Annexure A presents heat flux , pool temperature and the temperature at the surface across four positions viz. two sides, top and bottom positions of the surface of the heating tube and heat transfer coefficient. The heat flux across the heating tube was varied from 15957.45 W/m^2 to 29255.32 W/m^2 in six equal steps. The experimental data for different concentrations of nanoparticles in the base fluids ranging from 0.001 % by volume to 0.1 % by volume were collected at atmospheric pressure and sub atmospheric pressure varied from 85.17 kN/m^2 to 45.47 kN/m^2.

6.1 Limitations of Present Analysis

In current investigation accurate measurement of the temperature of the pool of liquid as well as the surface temperature at different positions namely two side, top and bottom of the heating tube is necessary for the precise measurement of the boiling heat transfer coefficient of the liquid under consideration. For accurate determination of temperature Copper – Constantan thermocouples are installed at the respective four circumferential positions of the heating tube. This gives the variation in the surface temperature across the circumference of the heating tube. The temperature

of the outer surface of the heating tube was not measured directly as the thermocouples are positioned at the pitch circle diameter i.e. [$d_h = (d_i + d_o)/2$] in the wall thickness of the heating tube. Thus, a temperature difference δT_w exists across the thickness of the heating tube between the thermocouple position and the outer surface which can be determined with the help of heat conduction equation for a cylinder using the following equation:

$$\delta T_w = \frac{q d_o}{2k_w} ln\left(\frac{d_o}{d_h}\right) \quad (6.1)$$

Thus, the temperature at the outer surface of the heating tube is determined by subtracting the computed temperature drop δT_w from the recorded temperature of the heating tube which is measured using the wall thermocouple. Further, assumption is made that radial heat transfer takes place from the heating surface to the liquid pool. This assumption is further supported by the fact that no significant change in the thermocouple readings was observed on moving the wall thermocouples longitudinally. The possibility of heat flow from the heating tube across the longitudinal direction was restricted by plugging the end of the heating tube with the help of 25 mm thick sheet of PTFE. This has already been discussed elaborately in Chapter 4. The average temperature of the heating tube is determined by arithmetically averaging the temperatures recorded by the thermocouples placed at their respective positions across the circumferential position of the heating tube. In similar manner liquid pool temperature is measured using thermocouple probes placed at four positions in the liquid pool viz. two sides, top and bottom. These thermocouples are positioned in the pool and are kept a distance a part from the surface of cylindrical heater so as to monitor the liquid pool temperature precisely. The liquid pool temperature is also measured by arithmetically averaging the temperature given by the respective thermocouples positioned at different locations in the pool. Sample calculation as given in Annexure - B reveals the method employed in determining the heat transfer coefficient. The procedure for determining the uncertainty analysis has been outlined in Annexure – C and carried out for each experimental run. The maximum uncertainty associated with heat transfer coefficient was computed for each experimental run and was found to be of the order of $\pm$ 2.49%.

There exists a difference in the temperature of the liquid pool measured with the help of thermocouples and saturation temperature of the liquid corresponding to the pressure prevailing in the unit. The reason behind this difference in the temperature can be the existence of foreign impurities present in the nanoparticles and the liquid under investigation. Further, there exists a insignificant difference in the surface temperature at the two side positions of the heating tube; but

still it has been taken into consideration while determining the values of the local and average heat transfer coefficient. The thermophysical characteristics such as density, viscosity and thermal conductivity of both the nanofluids i.e. Alumina – DW and Copper Oxide – DW are computed at different saturation temperatures which is discussed in Chapter 3.

Also the nanofluids are synthesized by carrying out ultrasonication for optimum time as determined for both the nanoparticles; followed by magnetic stirring in order to obtain excellent stability. The nanoparticles remain uniformly stable in the suspension exhibiting that nanofluids are synthesized with utmost care and are ready for experimental run. The detailed procedure for synthesis of each nanofluid and determination of optimum time of ultrasonication for each nanoparticle viz. Alumina and copper oxide based nanofluids are discussed in Chapter 3.

6.2 Nucleate Boiling of Distilled Water on A Stainless Steel Heating Tube

Table A.1 of Annexure A lists the experimental data for the nucleate pool boiling of Distilled Water. With the help of this data temperature profile, variation of heat transfer coefficient across the circumference of the stainless steel heating tube and average heat transfer coefficient for saturated boiling of Distilled water is computed. It also includes the effect of heat flux, pressure and liquids on local and average heat transfer coefficient and thereby functional relationship between heat transfer coefficient and these variables has been discussed. These are discussed in the following subsections:

6.2.1 Circumferential Variation of Surface Temperature

Figs. 6.1 (a) to 6.1 (e) represent the plots of variation of surface temperature along the circumference of stainless steel heating tube during the saturated pool boiling of Distilled water at atmospheric and sub atmospheric pressure for different heat flux values varying from 15957.45 W/m^2 to 29255.32 W/m^2. Each plot is for a distinct pressure mentioned therein. In the plot the curve for showing the variation in the liquid temperature around the surface is also included. A close examination of these plots reveals the following salient features:

- The surface temperature along the circumferential positions of the heating tube increases from bottom to side to top position for a given heat flux.
- The surface temperature increases with increase in heat flux at a particular circumferential position.
- The variation in the liquid temperature along the circumferential positions is almost negligible.

These features exhibited by the heating tube are consistent and are supported by the following reasoning:

During nucleate pool boiling of the liquids at the specified pressure the formation of vapor bubbles takes place at the active nucleation sites which are randomly distributed across the surface of heating tube. The bubbles thus formed grow in size and finally departs from the heating tube surface on attaining the maximum size, to travel in the pool of liquid. However, when boiling of distilled water takes place at surface of the heating tube the bubble formation and their growth is not uniform throughout the tube surface because of the cylindrical shape of the tube. Thus, due to the cylindrical shape of heating surface bubbles forming at the top position have no hindrance in moving upward whereas for the bubbles forming at the nucleation sites present on two side and bottom positions do not have such freedom. Further, the bubbles that formed at the bottom position tends to move upward to the top position by sliding them along the wall surface and in doing so their movement get continuously accelerated due to rise of buoyancy force. In doing so, the bubbles formed at bottom position push the bubbles formed at adjoining circumferential position upward along with them across the wall surface to reach the top position. Thus, the bubble formation frequency increases as the movement of bubbles from bottom to side and then to top position accelerates. The coalescence of the vapor bubbles thus formed lead to the formation of agglomerates and thereby vapor clouding occurs which engulfs the whole surface of the heating tube in the form of a blanket across the tube circumference. The thickness of this layer increases from bottom to top with maximum at the top position of the surface. This thick layer of vapor bubbles behaves like an insulation and hinders the flow of heat from the heating surface to the liquid pool. Thereby, the heat removal rate decreases across the circumference position i.e. from bottom to side to top position. In other words the bottom position of the tube provides the maximum heat removal rate followed by the two side positions and the minimum heat removal rate is at the top position of the heating tube. As a result the wall temperature of the heating surface exhibits an increasing behavior as we move from bottom position to upward in clockwise direction. The same phenomenon was also noticed by Kang [K3] and Gupta et.al. [G6] in their work. Further, for a given circumferential position, the surface temperature increases with the increase in heat flux, and the reason that supports such behavior is that heat transfer rate

also increases with the heat flux which is accompanied with higher wall superheat and thereby the surface temperature. The temperature of the liquid pool remains constant throughout the experimental run as the pressure has been kept constant.

On the basis of above discussion, it is concluded that significant variation in the wall temperature of the heating tube takes place at different circumferential positions when boiling at atmospheric and sub- atmospheric pressure is carried out. In other words, boiling through a heating tube is a non-uniform phenomenon that seeks further investigation to determine the extent of change in heat transfer coefficient across the heating tube.

6.2.2 Variation of Local Heat transfer Coefficient

Fig. 6.2 shows the variation of local heat transfer coefficient with heat flux as a parameter for boiling of Distilled water on Stainless steel heating tube at atmospheric pressure. Circumferential position in clockwise direction is taken as a parameter in the plot. Following salient features emerge out:

- The value of local heat transfer coefficient increases from top to side to bottom positions on a heating tube for a given heat flux.
- The values of local heat transfer coefficient increases with heat flux at a given circumferential position and the variation between these two variables can be represented by the following relationship:

$$h_{\psi} \propto q^{0.7} \qquad (6.2)$$

The behavior observed is quite obvious and can be explained as follows:

As explained in the section 6.2.1 above the surface temperature of the heating tube increases continuously from bottom to side to top positions at a particular heat flux. Thereby, the wall super heat given by expression $\Delta T_w = T_w - T_s$ also increases in the same order thus the local heat transfer coefficient value is observed to decrease at the respective circumferential positions i.e. from bottom to side to top positions on the surface of the heating tube. This in turn, results in an increase in the value of local wall superheat. Further, the increase in wall temperature results in the decrease in the value of minimum radius of nucleation site at which the vapor bubble can originate decreases. The expression for the minimum radius of nucleation is shown in Eq. (6.3).

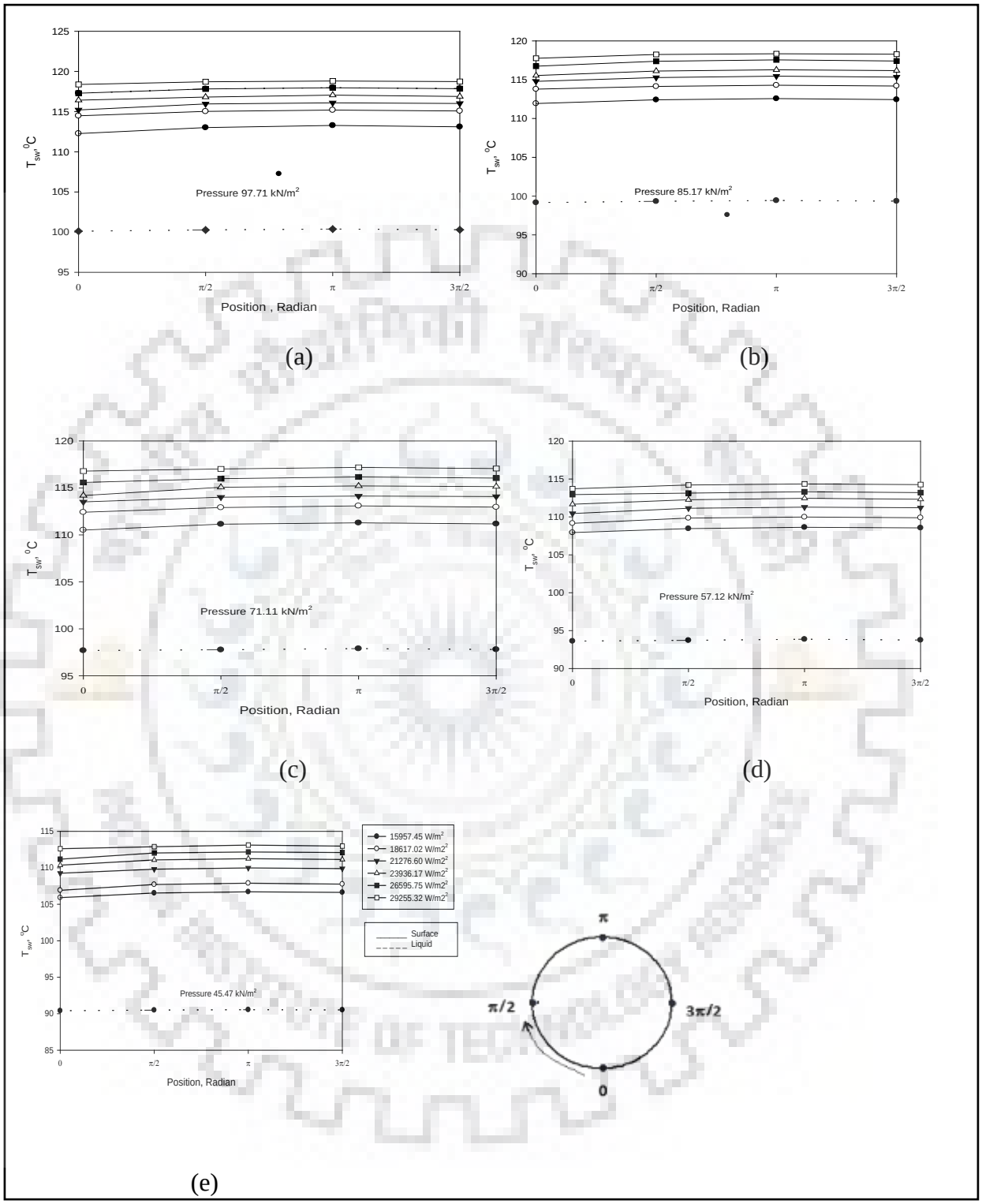

Fig. 6.1 Variation of liquid and surface temperature along circumference at bottom, two sides and top position of Stainless Steel heating tube with heat flux as parameter for boiling of distilled water at atmospheric and sub atmospheric pressures.

$$= \frac{2\sigma}{\left(\frac{dp}{dT}\right)_s \Delta T_w} \quad (6.3)$$

Thus, from Eq. (6.3) the minimum radius of nucleation site is inversely proportional to the local wall superheat. As a result, the intensity of smaller nucleation sites is more than the larger sized sites which results in increase in the frequency of bubble formation, growth and detachment from the surface of the heating tube. Thus, the vapor bubbles formed on the surface detach from the heating surface and travels to the liquid pool at high heat flux conditions. Because of all this behavior of bubble formation the intensity of turbulence in the pool increases which in turn enhances the rate of heat removal. Thereby local heat transfer coefficient is observed to be higher for higher values of heat flux.

Similar features have also been observed by various researchers [A10, A11,B6,G6] during pool boiling of Distilled Water. At this stage from the observations of the plots of local heat transfer coefficient v/s heat flux it may be pointed out that functional relationship between the h_ψ and q remains unaltered irrespective of the fluid under investigation. For a given circumferential position on the heating tube the local heat transfer coefficient value differs from liquid to liquid and the possible reason behind such behavior can be attributed to the variation in the thermo – physical properties of the fluids under investigation. The following investigation also brings out the effect of pressure variation on the local heat transfer coefficient with respect to the circumferential position. Infact, an increase in the local heat transfer coefficient is observed on raising the pressure. The justification given behind such behavior is the change in the thermo-physical properties of the fluid due to increase in pressure. Due to increase in pressure the surface tension of the fluid decreases which results in decrease in the minimum radius of nucleation site. As a result, the minimum radius of nucleation at which bubble formation takes place decreases, as it is clear from Eq. (6.3). Thus, the intensity of bubble formation with smaller diameter from the heating tube surface increases and these bubbles travel from the surface to the pool of liquid and thereby resulting in an increase in intensity of turbulence. Further, due to increase in turbulence the heat removal rate increases which leads to increase in heat transfer coefficient.

From above paragraphs, the dependency of local heat transfer coefficient of fluids under investigation on various parameters such as heat flux, pressure and circumferential position

is explained. Thus, using the method of least square following correlation of local heat transfer coefficient as a function of pressure, heat flux and circumferential position has been developed:

$$h_\psi = C_\psi q^{0.7} p^{0.32} \qquad (6.4)$$

In Eq. (6.4) the constant C_ψ has different values depending upon the circumferential positions of the heating tube.

Table 6.1: Values of constant C_ψ of Eq. 6.3 for various saturated liquids at various circumferential positions.

Liquids	Circumferential Positions			
	Top	Side	Bottom	Side
Distilled Water	0.422	0.472	0.532	0.475

Figure 6.3 depicts a plot between experimentally obtained values of local heat transfer coefficient and those computed from Eq. (6.4) for boiling of distilled water at atmospheric and sub atmospheric pressures. This plot clearly reveals an excellent agreement between the values predicted by Eq. (6.4) within an error of $\pm$ 4% . Hence, Eq. (6.4) can correlate experimental data of local heat transfer coefficient of various boiling liquids. In other words, above equation can be used to calculate the values of local heat transfer coefficient at any circumferential position on heating tube from the knowledge of heat flux and pressure, provided the value of constant C_ψ is known. The value of constant C_ψ depends upon the surface characteristics of the heating tube, circumferential positions and the boiling liquid.

The analytical computation of C_ψ is highly improbable owing to variation in size, shape and number of irregularities present on a tube surface. Eq. (6.4) can be employed for the determination of local heat transfer coefficient of those heating surface combinations whose values of constant C_ψ is not experimentally known. In other words Eq. (6.4) is of limited applicability.

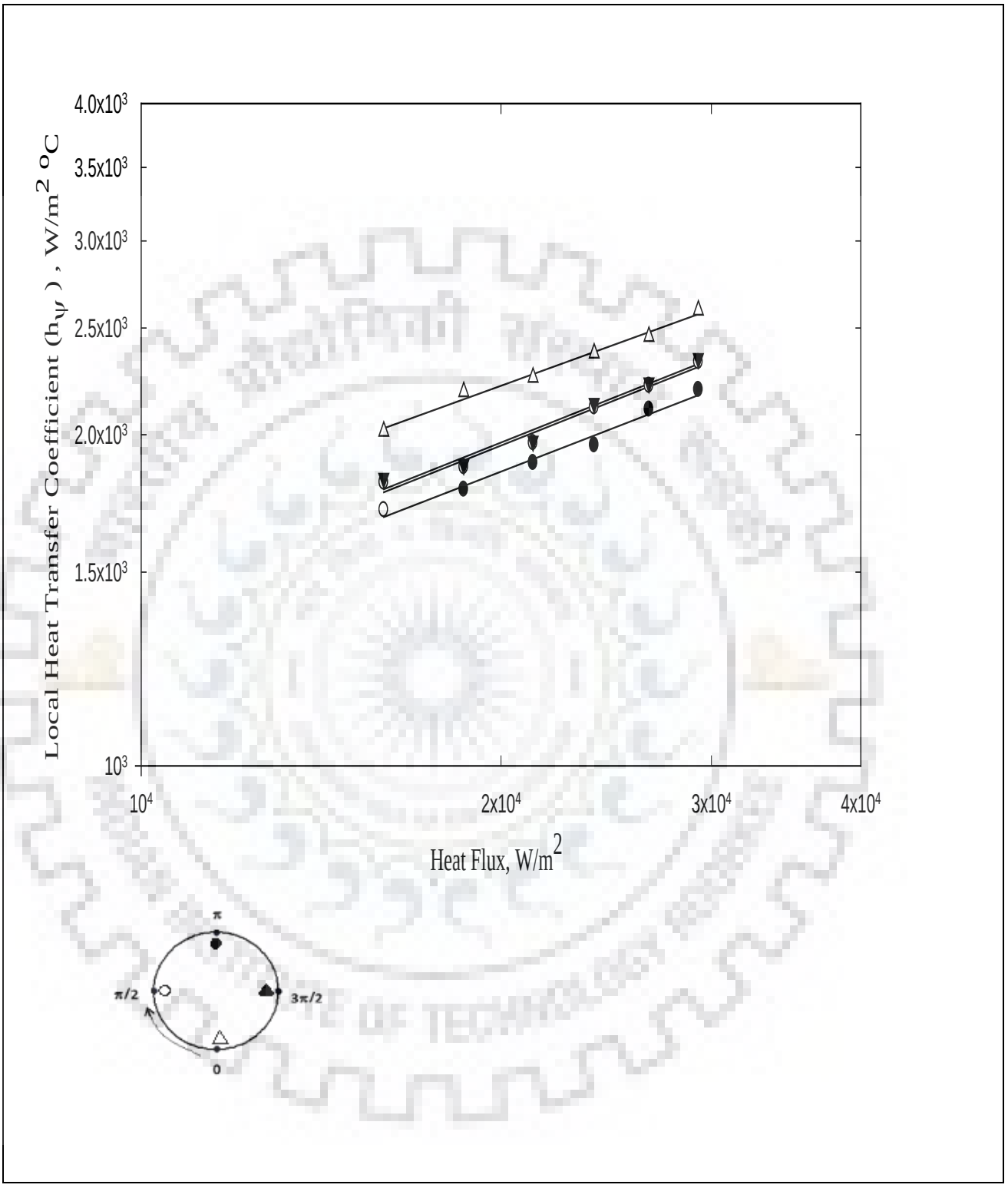

Fig. 6.2 Variation of local heat transfer coefficient with heat flux along circumference of Stainless Steel heating tube for boiling of distilled water at atmospheric pressures.

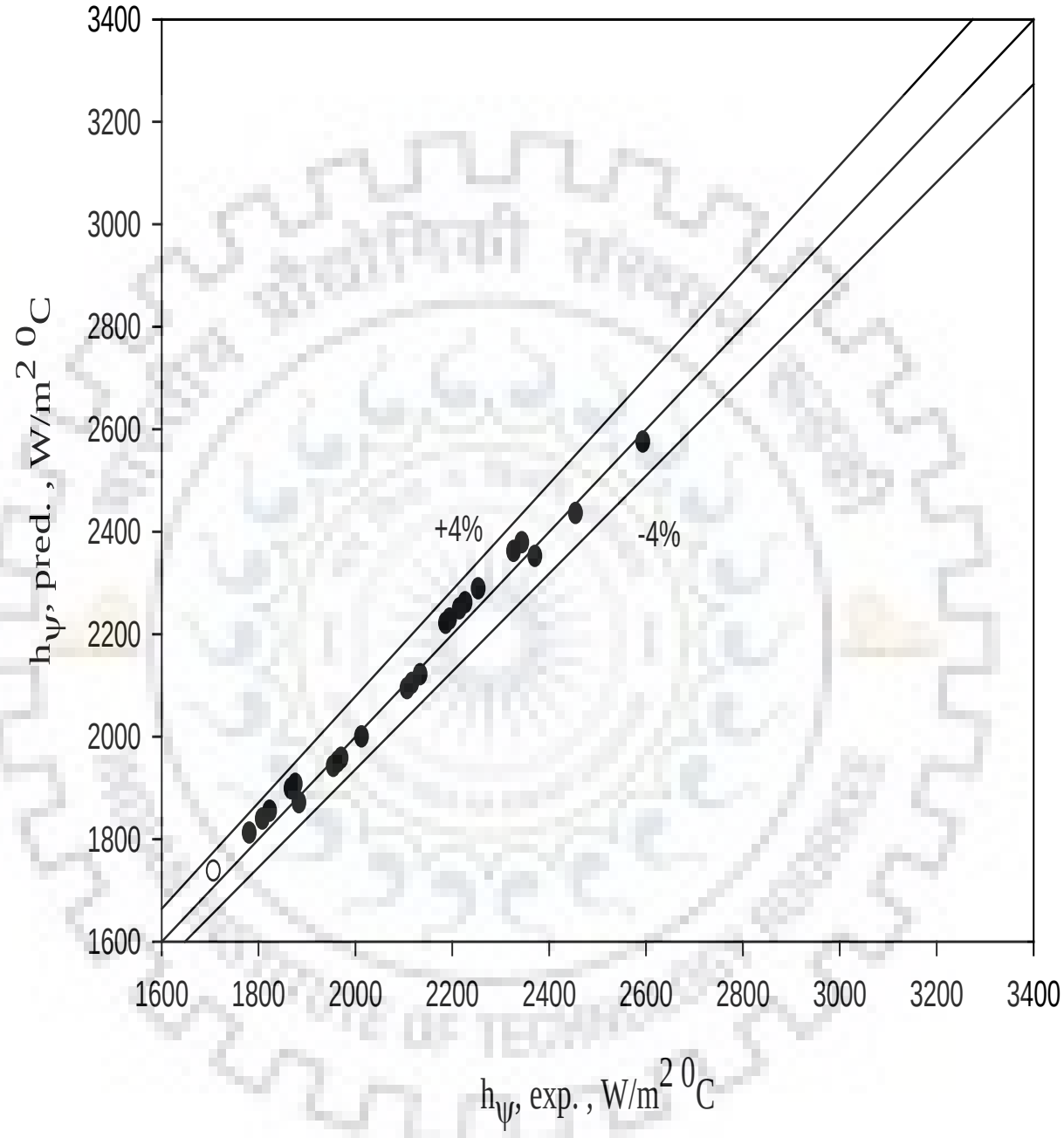

Fig. 6.3 Comparison of experimental local heat transfer coefficient with those predicted from Eq.(6.4) for pool boiling of Distilled Water at atmospheric and sub atmospheric pressures.

6.2.3 Variation of Average Heat Transfer Coefficient for Nucleate Boiling of Distilled Water

As discussed above, a significant variation in surface temperature exists along the circumference of a heating tube. Therefore values of surface temperature measured at top, two sides and bottom position have been averaged arithmetically to obtain true representative surface temperature of the entire tube circumference. Similarly, average temperature of liquid pool has also been calculated. Using them, average heat transfer coefficient (hereafter referred as heat transfer coefficient) has been calculated corresponding to each heat flux subjected to Stainless Steel heating tube for saturated boiling of Distilled Water at atmospheric and sub atmospheric pressure. The procedure used for computation of heat transfer coefficients described in Annexure B – Sample Calculation. The computed values of heat transfer coefficient for each experimental run is given in last column of A.1 to A.11 of Annexure A.

Figure 6.4 depicts a comparison between the experimental data of heat transfer coefficient at different heat flux for distilled water at atmospheric pressure. The plot contains the experimental data of present study along with that of other prominent investigators such as Benjamin & Balakrishnan [B3], Mihir [M1], Cryder and Finalborgo [C10], Liaw & Dhir [L7], T. Hinrichs et. al. [T4], Young & Hummel [Y4], Siraj et. al. [A10, A11] for the purpose of comparison. This plot reveals that the data of this investigation do not agree with those of earlier researchers; infact forms a distinct group. Following salient features are observed on close examination of this plot:

1) Experimental data for present work does not match with the results of other researchers
2) Although there is no match among the data obtained by the earlier investigators and present work, still the data points of this work forms a distinct group and follows the power law relationship, $h \propto q^{0.7}$.

The above observed salient features are quite obvious as boiling is a surface phenomenon therefore disagreement amongst data points of earlier investigators with the present work is bound to occur. The experimental data collected during this work depends on surface characteristics of the heating tube such as surface roughness etc. On the basis of above it can be concluded that it is difficult to compare the boiling heat transfer data of present investigator with those of earlier investigators.

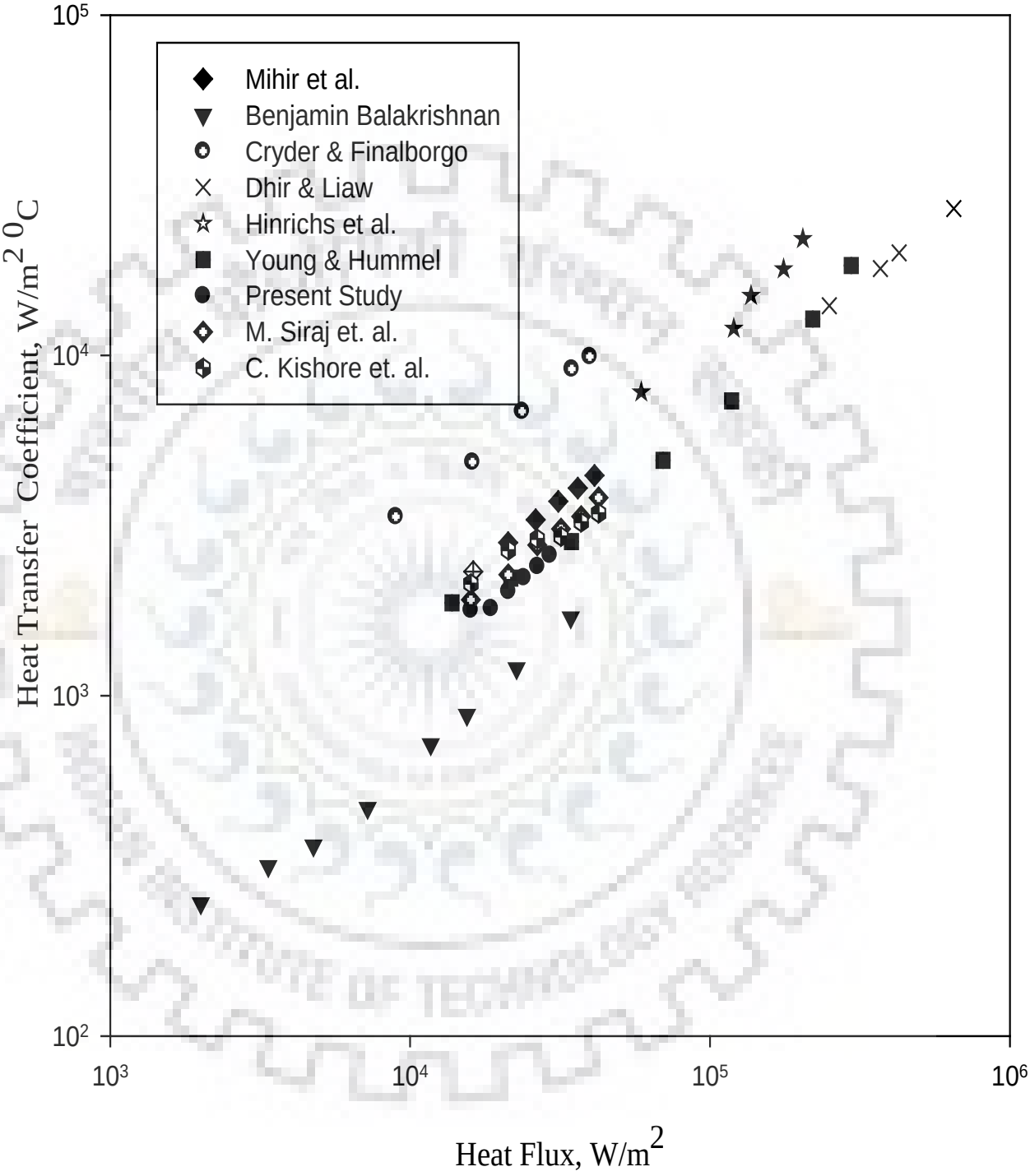

Fig. 6.4 Comparison of heat transfer v/s heat flux data of present investigation with data of earlier investigators for pool boiling of Distilled water at atmospheric pressure

Fig.6.5 represents a plot to exhibit the variation of heat transfer coefficient with heat flux at different pressure for the boiling of distilled water. Pressure is a parameter in this plot. This figure reveals the following salient features:

1) The heat transfer coefficient increases with an increase in heat flux for a given pressure and the variation between the two can be given by a power law,

$$h \alpha q^{0.7}$$

2) An increase in pressure increases the value of heat transfer coefficient for a given heat flux.

Both the above observed features are consistent and follows the boiling phenomenon. The possible explanation for the above features is as follows:

As explained earlier, the local wall superheat increases with rise in heat flux which in turn results in an increase of average wall superheat of the heating tube. The rise in pressure results in change in thermophysical properties but most prominent effect appears in surface tension. This according Eq. (6.3), causes a decrease in the value of minimum radius of nucleation site (r_c) at which the vapor-bubbles tend to originate. Infact, the value of surface tension reduces with increase in the pressure which leads to decrease in the value of minimum radius of curvature of nucleation.

As a result of decrease in radius of curvature of nucleation the bubble formation, growth and bubble departure frequency from the heating surface increases which results in an increase in the intensity of turbulence. Thus, higher heat transfer coefficient are observed at elevated pressure for the given heat flux. Similarly, average wall superheat also rises with increase in heat flux.

The surface deterioration results in high surface particle interaction leading to intensification of turbulence of fluid. Consequently, nucleation sites of smaller sizes present on heating surface get activated and generate vapor bubble. As population of such site is large, more number of small size vapor bubbles forms at enhanced value of heat flux. With increase in pressure, as discussed in subsection 6.2.2 the intensity of turbulence rises due to the vapor bubble dynamics which leads to formation of large population of small sized vapor bubbles which in turn leads to higher rate of heat removal and thereby higher heat transfer coefficient at an elevated pressure.

It may be mentioned here that above features have also been observed by Cryder and Finalborgo [C10] for boiling of water, methanol, carbon tetrachloride and n- butanol on a brass heating

surface, Bonilla and Perry [B7] for boiling of water, ethanol, n – butanol and acetone on copper surfaces and Kurihara and Myers [k18] for boiling of water, carbon tetrachloride, acetone and n – hexane on a copper surface. Thus this investigation has corroborated the findings of earlier investigators for saturated boiling of liquids on stainless steel heating surface at atmospheric and sub atmospheric pressures.

On the basis of above it can be pointed out that heat transfer coefficient of boiling of distilled water on a stainless steel heating tube depends upon heat flux and pressure. A functional relationship amongst them have been developed by the method of least squares using the experimental data of boiling of distilled water. The functional relationship is expressed as follows:

$$h = C_1 q^{0.7} p^{0.32} \qquad \ldots(6.5)$$

Where constant C_1 depends upon the surface characteristics of the heating tube in boiling liquid. The value of constant C_1 for Distilled water is 0.42 for this investigation.

Figure 6.6 describes a plot between the experimentally determined values and those predicted from Eq. (6.5) for boiling of distilled water at atmospheric pressure on a stainless steel heating tube. This plot reveals that the predicted values of heat transfer coefficient match excellently with the experimentally determined values well within the maximum error limits of $\pm$ 7 %. Therefore, Eq. (6.5) which is simple and convenient and can be used for the computation of heat transfer coefficient for distilled water from the knowledge of heat flux and pressure values provided the value of constant C_1 is known.

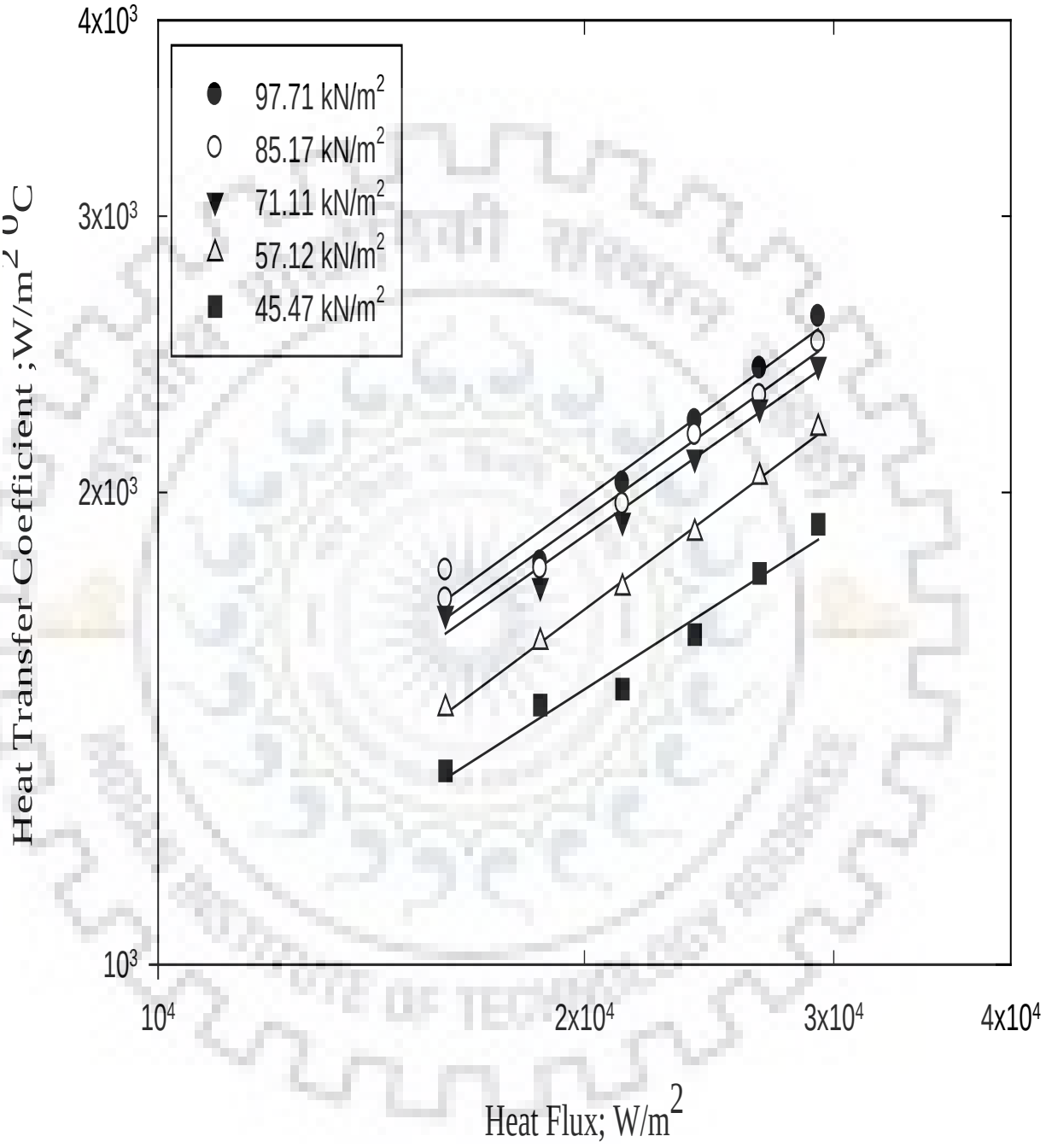

Fig.6.5: Variation of heat transfer coefficient with heat flux for pool boiling of distilled water using heating tube with pressure as a parameter.

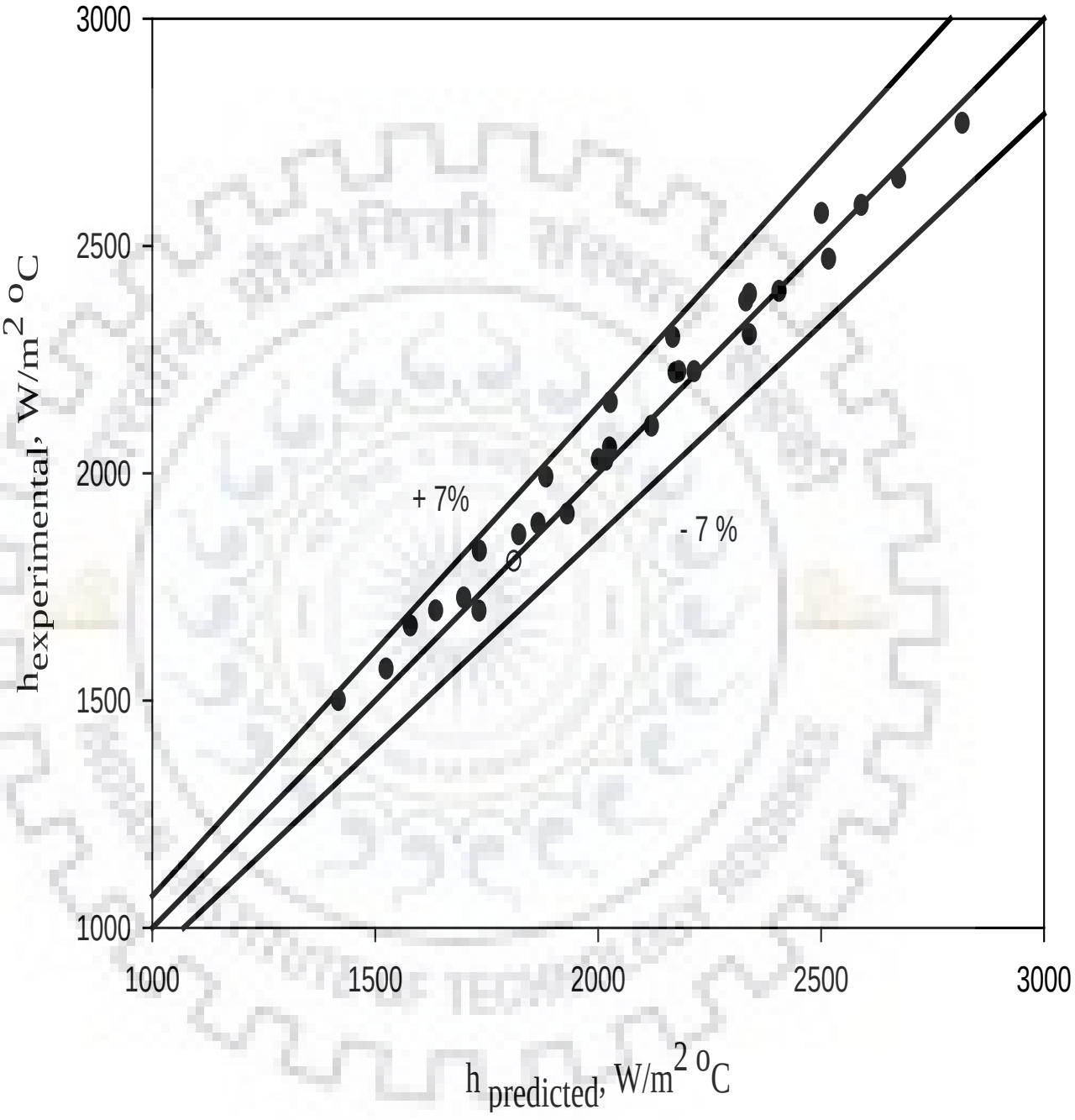

Fig. 6.6 Comparison of experimental heat transfer coefficients with those predicted from equation (6.5) for boiling of distilled water on heating tube at atmospheric pressure and sub atmospheric pressures

6.3 Nucleate Boiling of Nanofluids on Stainless Steel Heating Tube

The experimental data for boiling of various compositions of alumina and copper oxide nanoparticles suspended in distilled water are listed in table A-2 to A-11 of Annexure – A. It includes the measured values of temperature of heating surface, liquid pool (at top, two sides and bottom positions) of heating tube, heat flux as well as the experimentally determined values of heat transfer coefficient for each concentration at atmospheric pressure and sub atmospheric pressure. Based on these data variation of surface temperature and heat transfer coefficient around the circumference of the heating tube and thereby the effect of heat flux, pressure and concentration of alumina and copper oxide nanoparticles in the distilled water on heat transfer coefficient for the boiling of these nanofluids have been presented. Following subsection deals with them.

6.3.1 Circumferential variation of heat transfer coefficient

Figures 6.7 (a) to 6.7(d) and 6.8 (a) to 6.8 (d) represent the plots of surface temperature profile for various concentration of alumina nanoparticles in distilled water and copper oxide nanoparticles in distilled water on a stainless steel heating tube surface at atmospheric pressure, respectively. Heat flux is a parameter in each of these plots. Each plot also contains a curve to show boiling temperature profile of both the nanofluids. An examination of one of these plots reveals the following salient features:

1) Surface temperature is found to increase continuously on moving from bottom to side to top positions of the heating tube for a given heat flux.

2) The surface temperature increases with the increase in heat flux for a given circumferential position.

3) Saturation temperature remains unchanged irrespective of heat flux and circumferential positions around the heating tube.

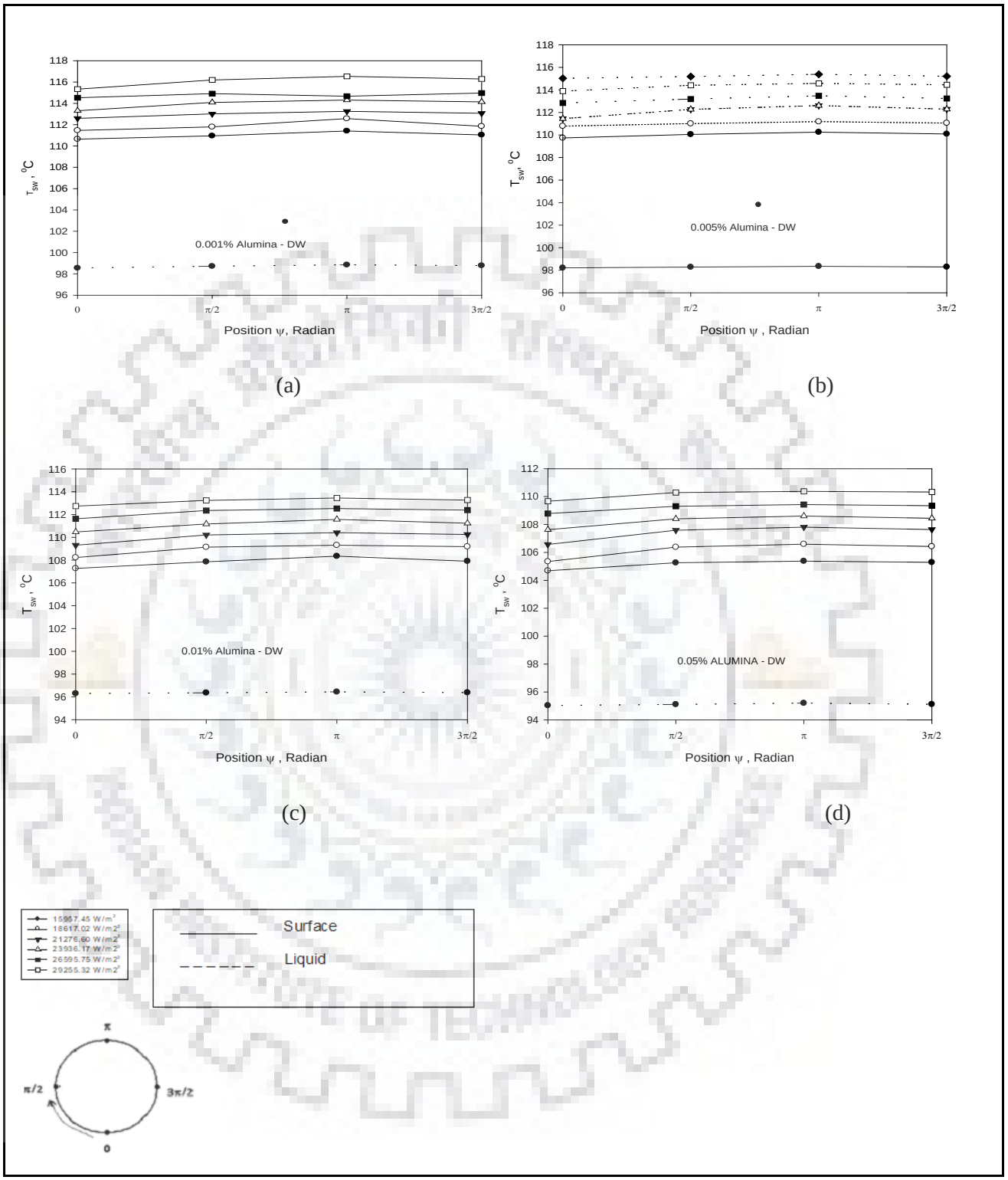

Fig. 6.7 Variation of liquid and surface temperature along circumference at bottom, two sides and top position of Stainless Steel heating tube with heat flux as parameter for boiling of various concentration of Alumina - distilled water mixture at atmospheric pressure.

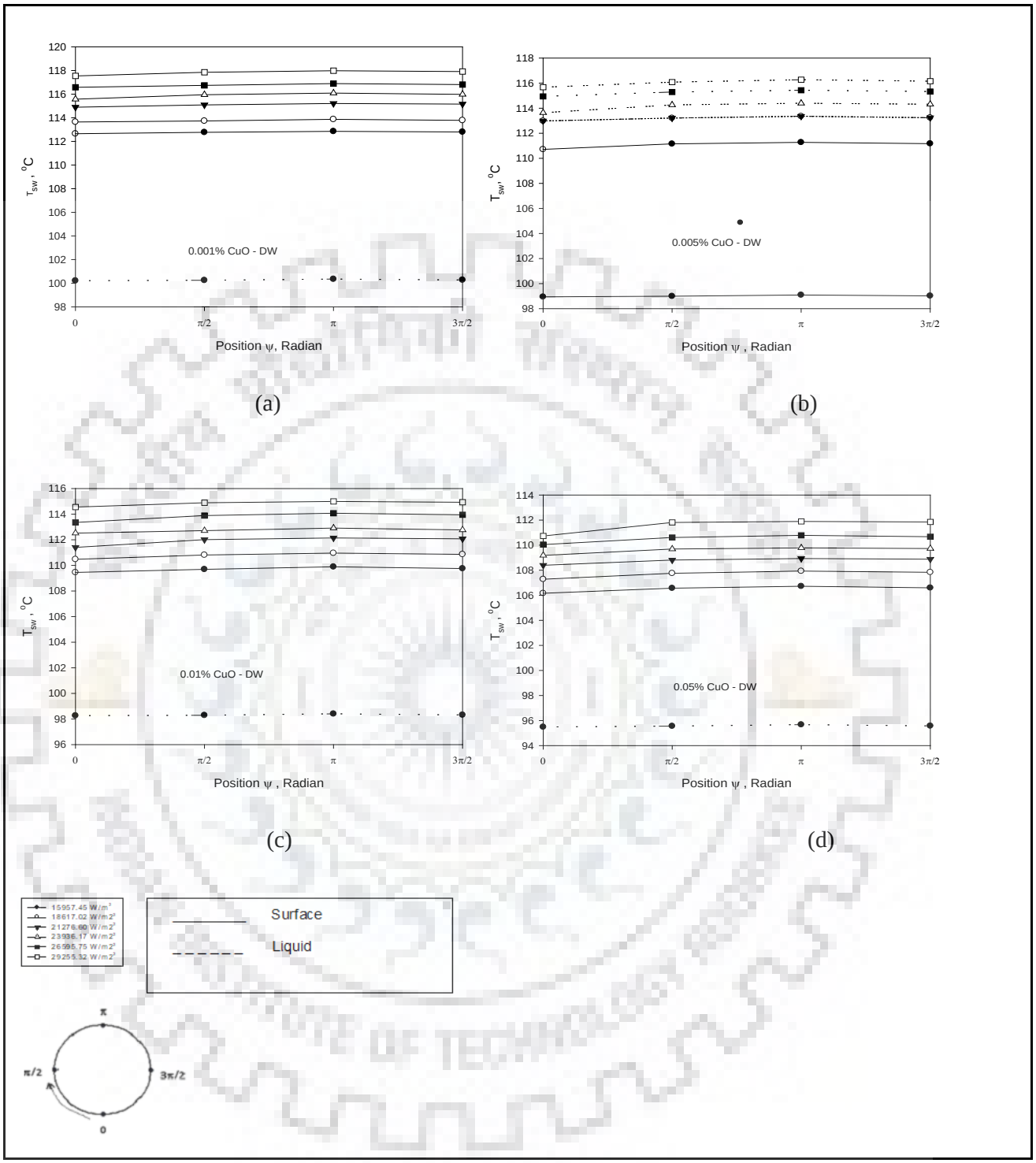

Fig. 6.8 Variation of liquid and surface temperature along circumference at bottom, two sides and top position of Stainless Steel heating tube with heat flux as parameter for boiling of various concentration of Copper Oxide - distilled water mixture at 97.71 kN/m^2 pressure.

The above features have also been found to hold true for boiling of various concentrations of alumina nanoparticles dispersed in distilled water and copper oxide nanoparticles dispersed in distilled water at various sub atmospheric pressure as clearly shown in plots of Figure 6.9, Figure 6.10, Figure 6.11 and Figure 6.12. All the above features are same as observed in case of boiling of distilled water.

Thus, it can be concluded that boiling characteristics for a given concentration of alumina and copper oxide nanoparticles dispersed in distilled water are same in behavior as that of distilled water. Hence, local heat transfer coefficient of the alumina – distilled water and copper oxide – distilled water nanofluids are likely to vary in the similar manner as that of distilled water. Keeping this in view it has not been included here, but a detail analysis of heat transfer coefficient with respect to heat flux, pressure and concentration has been presented here in the following subsection.

6.3.2 Average Heat Transfer Coefficient of Nanofluids

The average value of surface temperature of the stainless steel heating tube has been determined by taking arithmetic mean of local surface temperature. The average saturation temperature of the nanofluid has also been determined by taking arithmetic mean of saturation temperature of the liquid around the liquid pool corresponding to each circumferential position. Using these values, heat transfer coefficient for the boiling of various concentrations of alumina and copper oxide nanoparticles well dispersed in the base fluid i.e. distilled water has been experimentally determined. The method of calculation of heat transfer coefficient values flor the alumina – distilled water and copper oxide – distilled water nanofluids are given in Annexure B – Sample Calculation. Figure 6.13 and Figure 6.14 depict the plot between heat transfer coefficient and heat flux values for boiling of 0.001 % by volume concentration of alumina and copper oxide nanoparticles dispersed in distilled water, respectively, with pressure as a parameter in these plots. A close examination of these plots reveal the following salient features:

1) At a given pressure heat transfer coefficient of a nanofluid increases with the rise in heat flux and the variation between the two can be described by the power law.

$$h \alpha q^{0.7} \qquad \ldots(6.6)$$

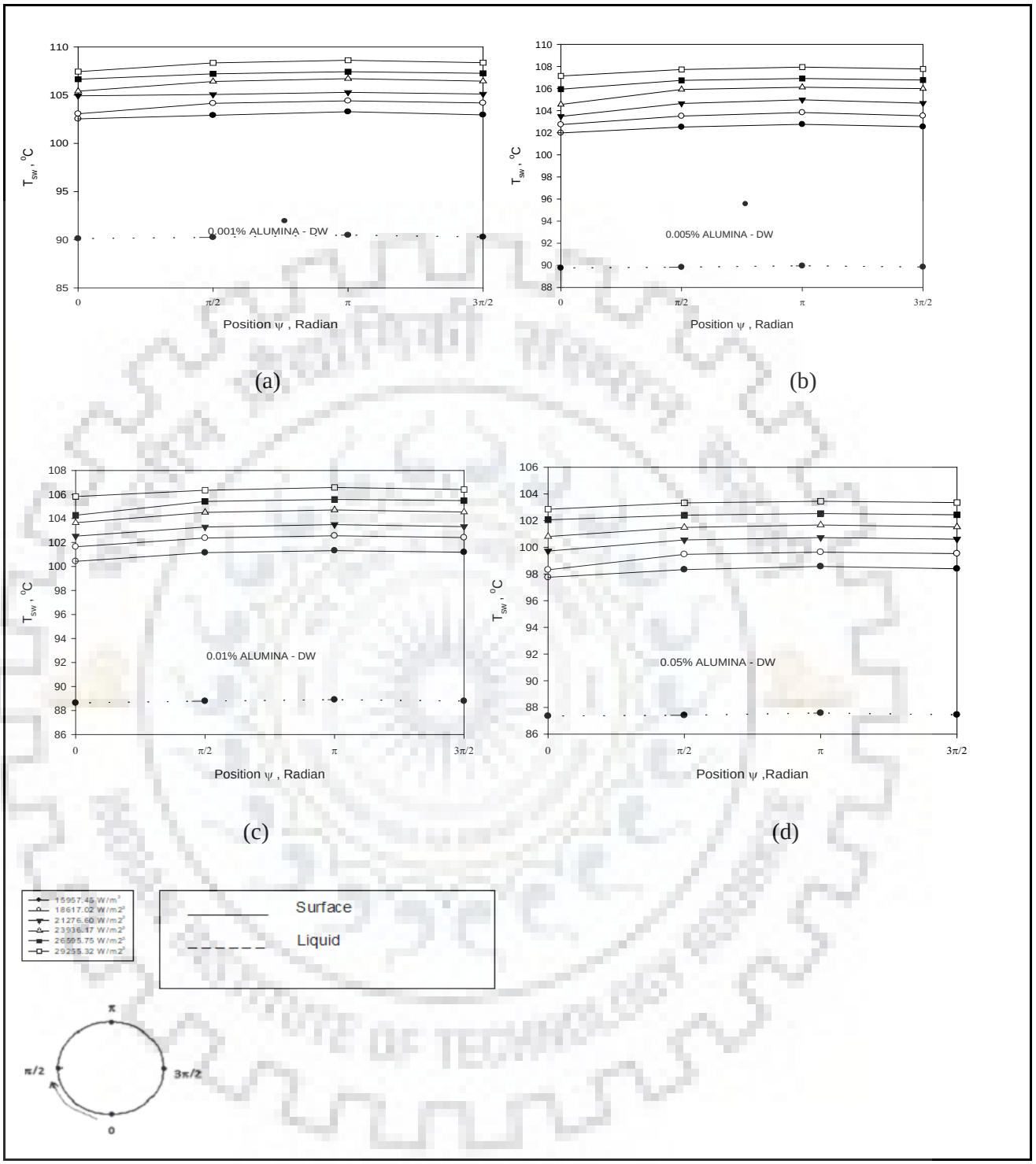

Fig. 6.9 Variation of liquid and surface temperature along circumference at bottom, two sides and top position of Stainless Steel heating tube with heat flux as parameter for boiling of various concentration of Alumina - distilled water mixture at 71.11 kN/m^2 pressure.

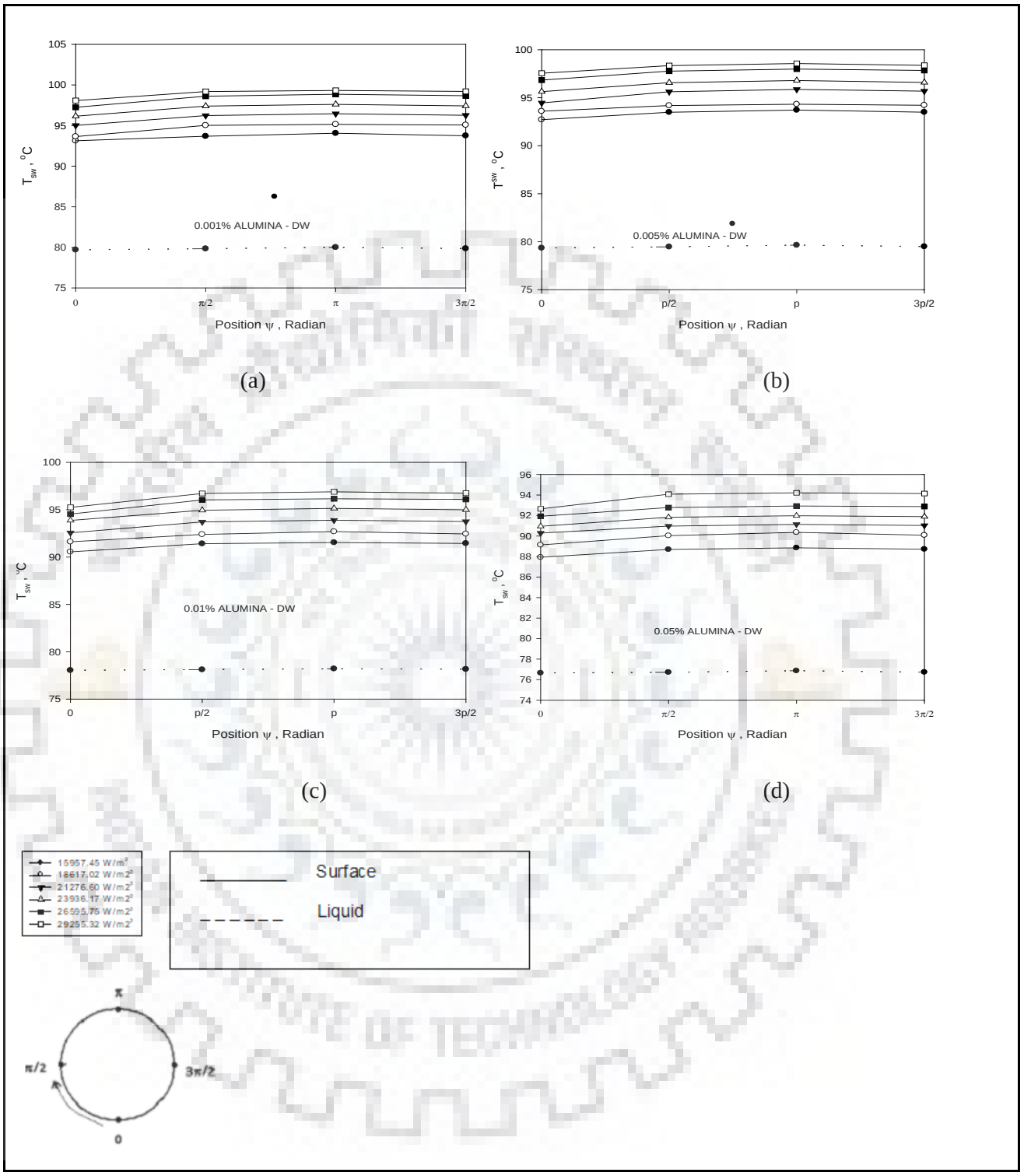

Fig. 6.10 Variation of liquid and surface temperature along circumference at bottom, two sides and top position of Stainless Steel heating tube with heat flux as parameter for boiling of various concentration of Alumina - distilled water mixture at 45.47 kN/m^2 pressure.

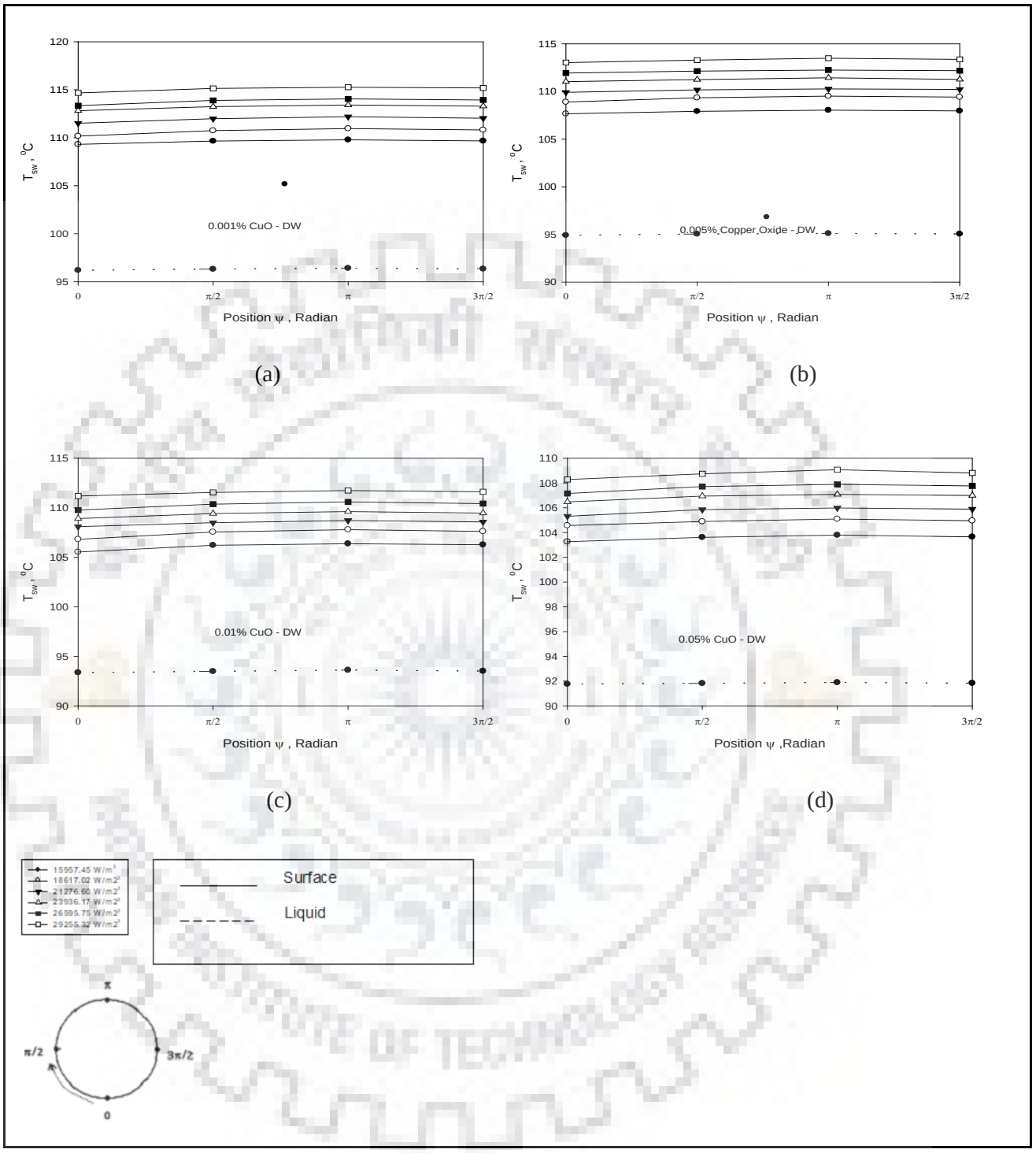

Fig. 6.11 Variation of liquid and surface temperature along circumference at bottom, two sides and top position of Stainless Steel heating tube with heat flux as parameter for boiling of various concentration of Copper Oxide - distilled water mixture at 71.11 kN/m^2 pressure.

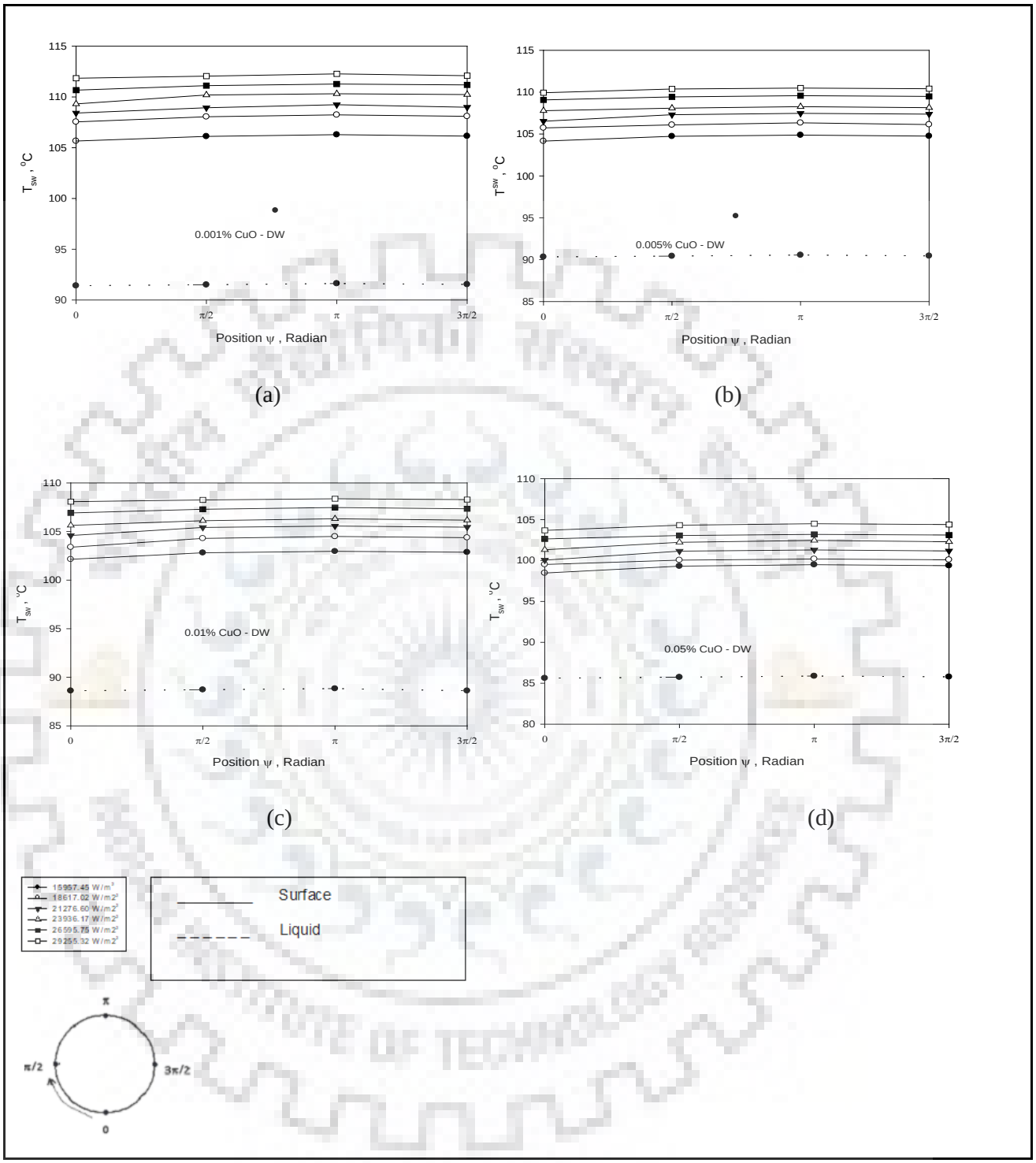

Fig. 6.12 Variation of liquid and surface temperature along circumference at bottom, two sides and top position of Stainless Steel heating tube with heat flux as parameter for boiling of various concentration of Copper Oxide - distilled water mixture at 45.47 kN/m^2 pressure.

2) Increase in pressure increases the value of heat transfer coefficient of nanofluid for a given heat flux.

These features have also been observed for the boiling of other concentrations of alumina and copper oxide nanoparticles dispersed in distilled water at atmospheric and sub atmospheric pressure as can be seen from the plots depicted in Figures 6.15 to Figure 6.18.

Above mentioned features in Figures 6.13 to 6.18 are same as obtained for the boiling of distilled water. Hence, same explanations as given in section 6.2.2 holds true in these cases also. It may be pointed out that these observations also corroborates with the findings of various researchers such as Park & Jung [P2] reported boiling heat transfer enhancement in their work on pool boiling of refrigerants with carbon nano tubes; Kole and Dey [K14] in their work reported boiling heat transfer enhancement for various concentration of Zinc Oxide nanoparticles dispersed in ethylene glycol; Kim et. al. [K10] in their work reported an improvement in nucleate boiling heat transfer with copper nanoparticles suspension; Johnathan and Kim [J4] observed an enhancement in boiling heat transfer for Alumina and Talc nanoparticles suspension; S.M. Peyghambarzadeh [S10] also reported an enhancement in boiling heat transfer for alumina nanoparticles based nanofluids when boiling is carried over Stainless Steel surface and Wen and Ding [W5, W7, W8] in their work on alumina nanofluids observed a significant enhancement in boiling heat transfer during pool boiling of alumina nanofluids. Bang & Chang et. al. [B2] in their work employed the heating surface with roughness of the order of nanometer scale and thus consider the settling of nanoparticles to increase the roughness of the heating surface.

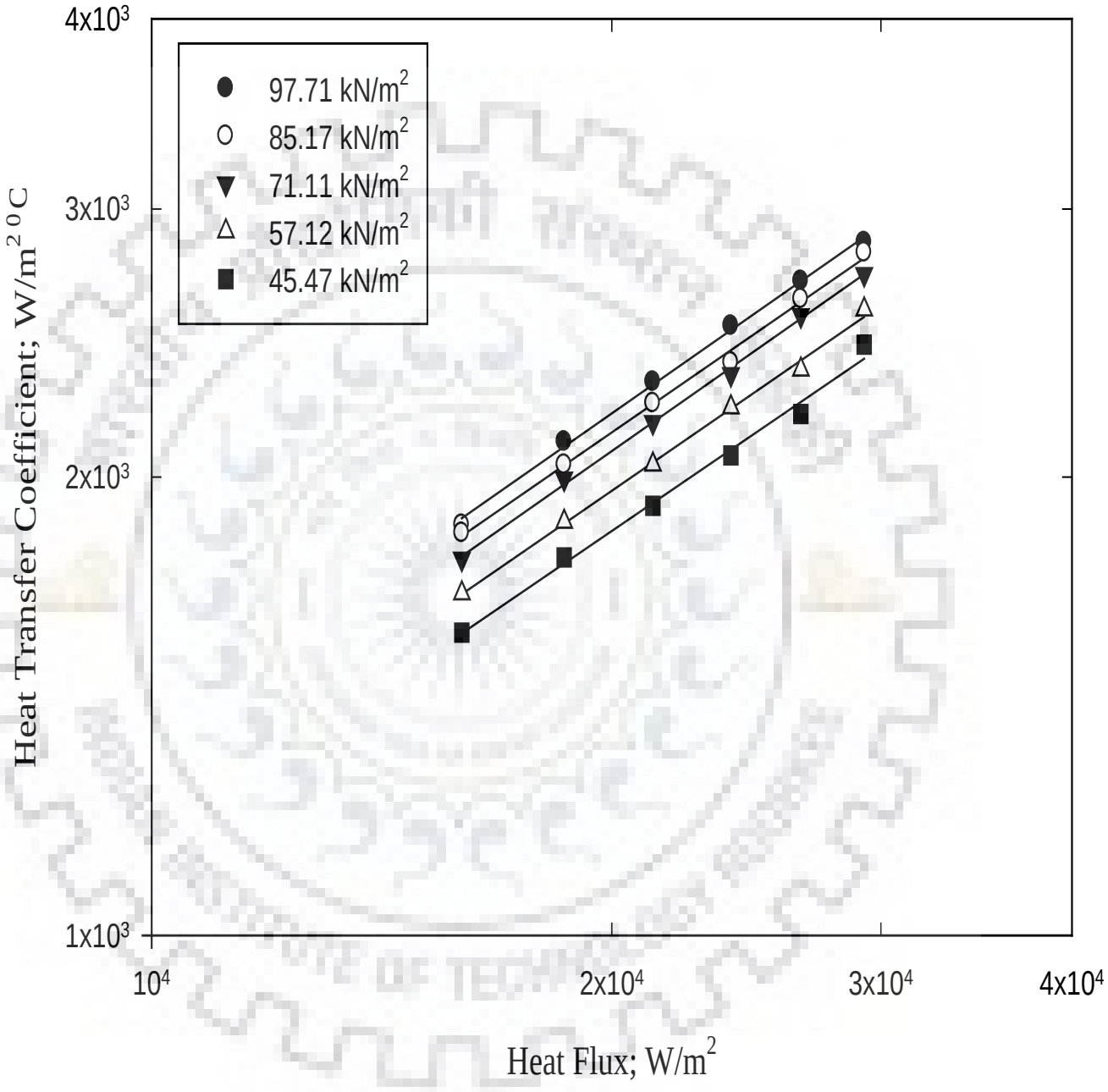

Fig. 6.13: Variation of HTC with heat flux for boiling of 0.001% Alumina – DW nanofluid on a heating tube surface with pressure as a parameter.

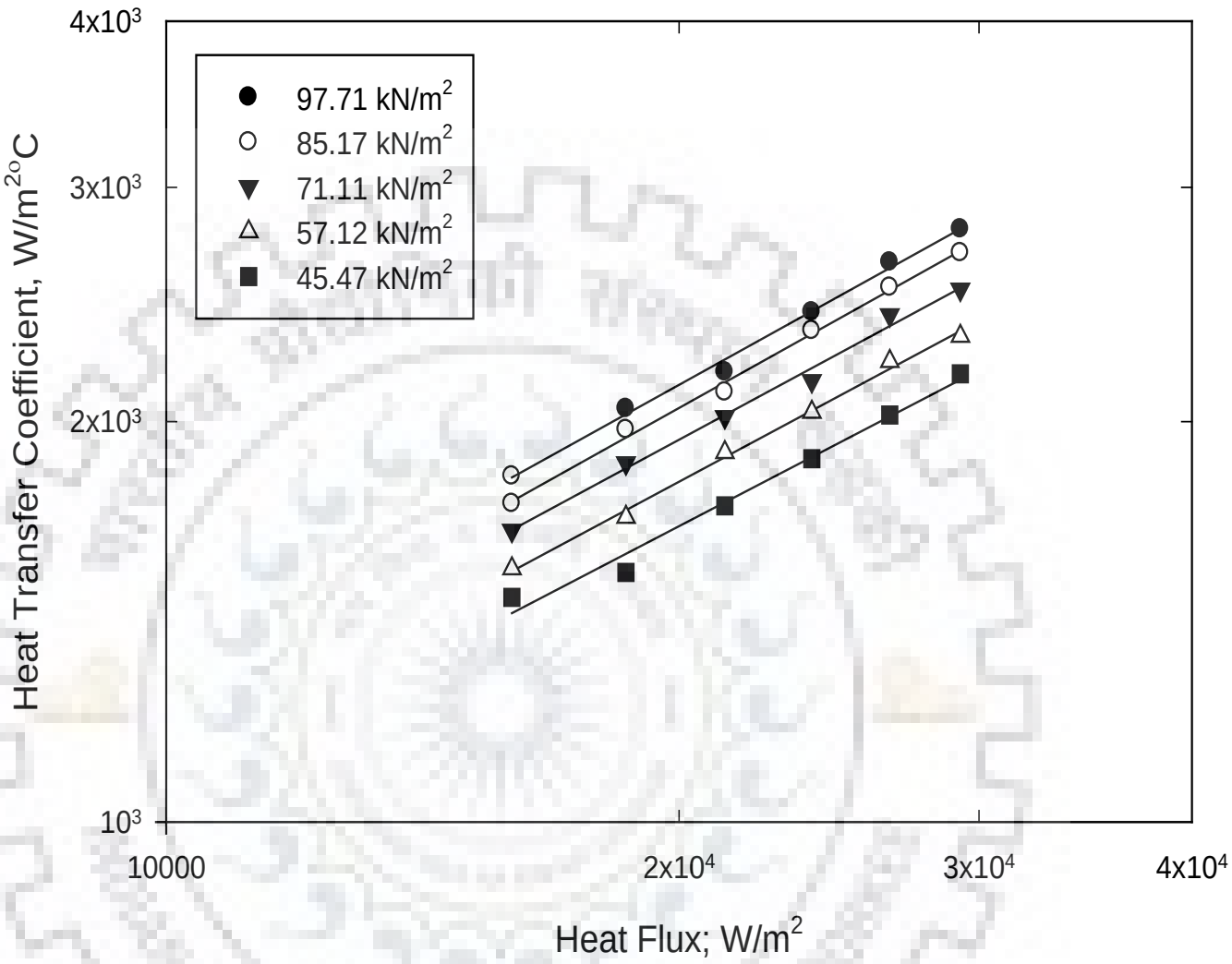

Fig. 6.14: Variation of HTC with heat flux for boiling of 0.001% Copper Oxide – DW nanofluid on a heating tube surface with pressure as a parameter.

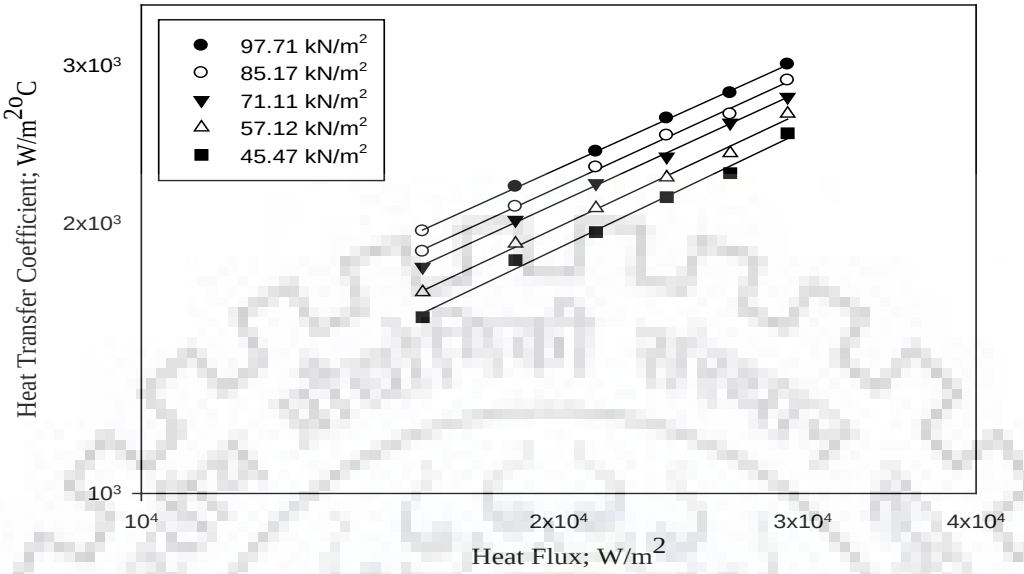

(a)

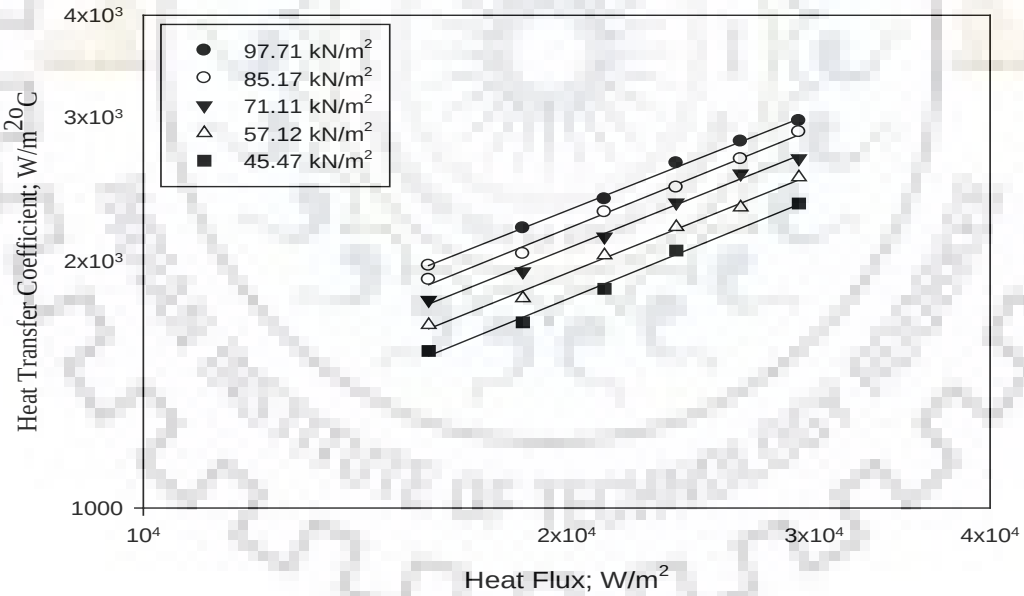

(b)

Fig. 6.15: Variation of HTC with heat flux for boiling of (a) 0.005% Alumina – DW and (b) 0.01% Alumina - DW nanofluid on a heating tube surface with pressure as a parameter.

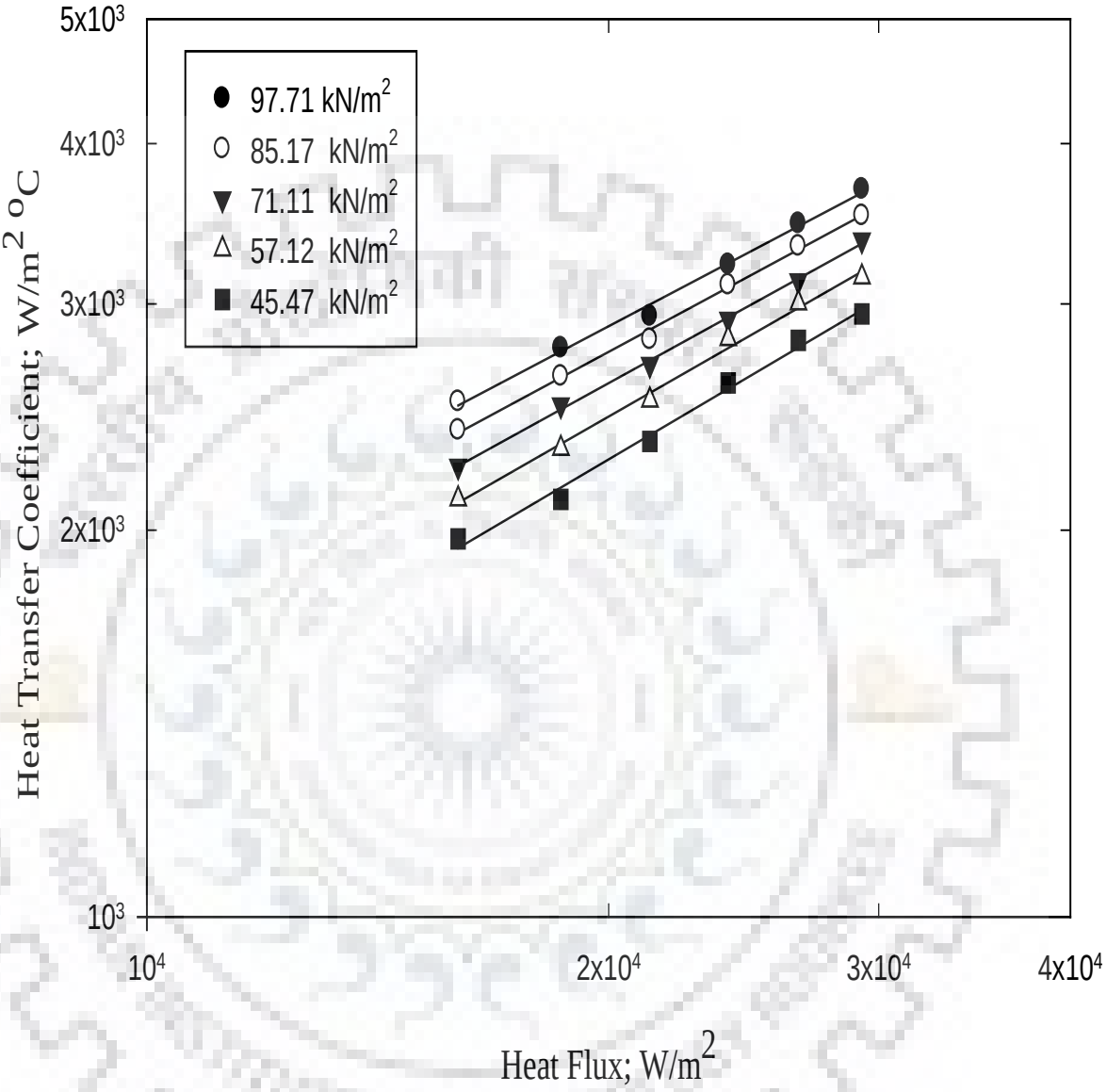

Fig. 6.16: Variation of HTC with heat flux for boiling of 0.05% Alumina – DW nanofluid on a heating tube surface with pressure as a parameter.

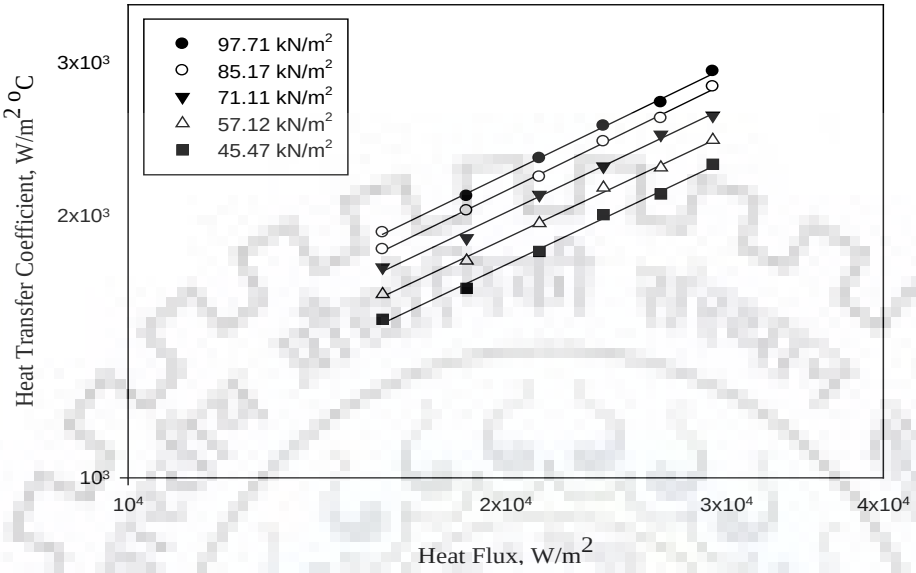

(a)

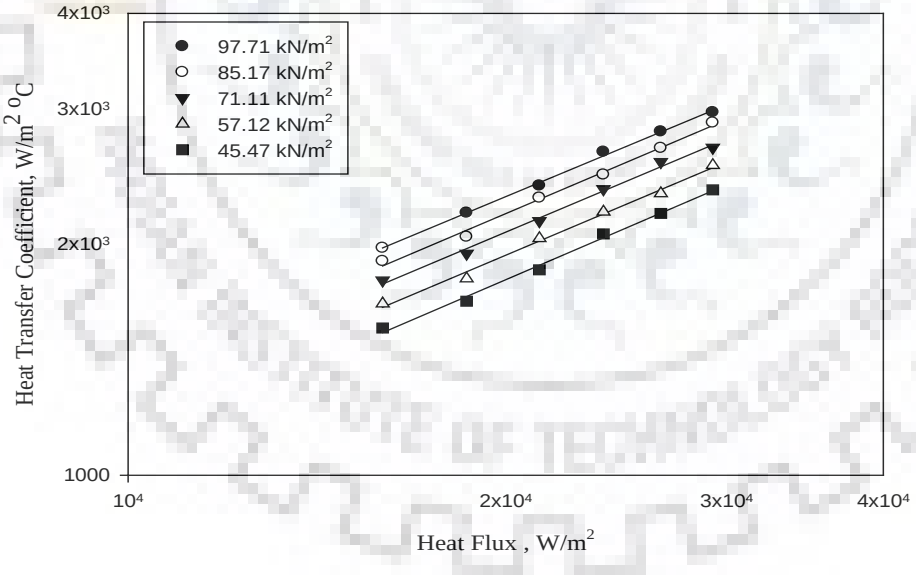

(b)

Fig. 6.17: Variation of HTC with heat flux for boiling of (a) 0.005% Copper Oxide – DW and (b) 0.01% Copper Oxide – DW nanofluid on a heating tube surface with pressure as a parameter.

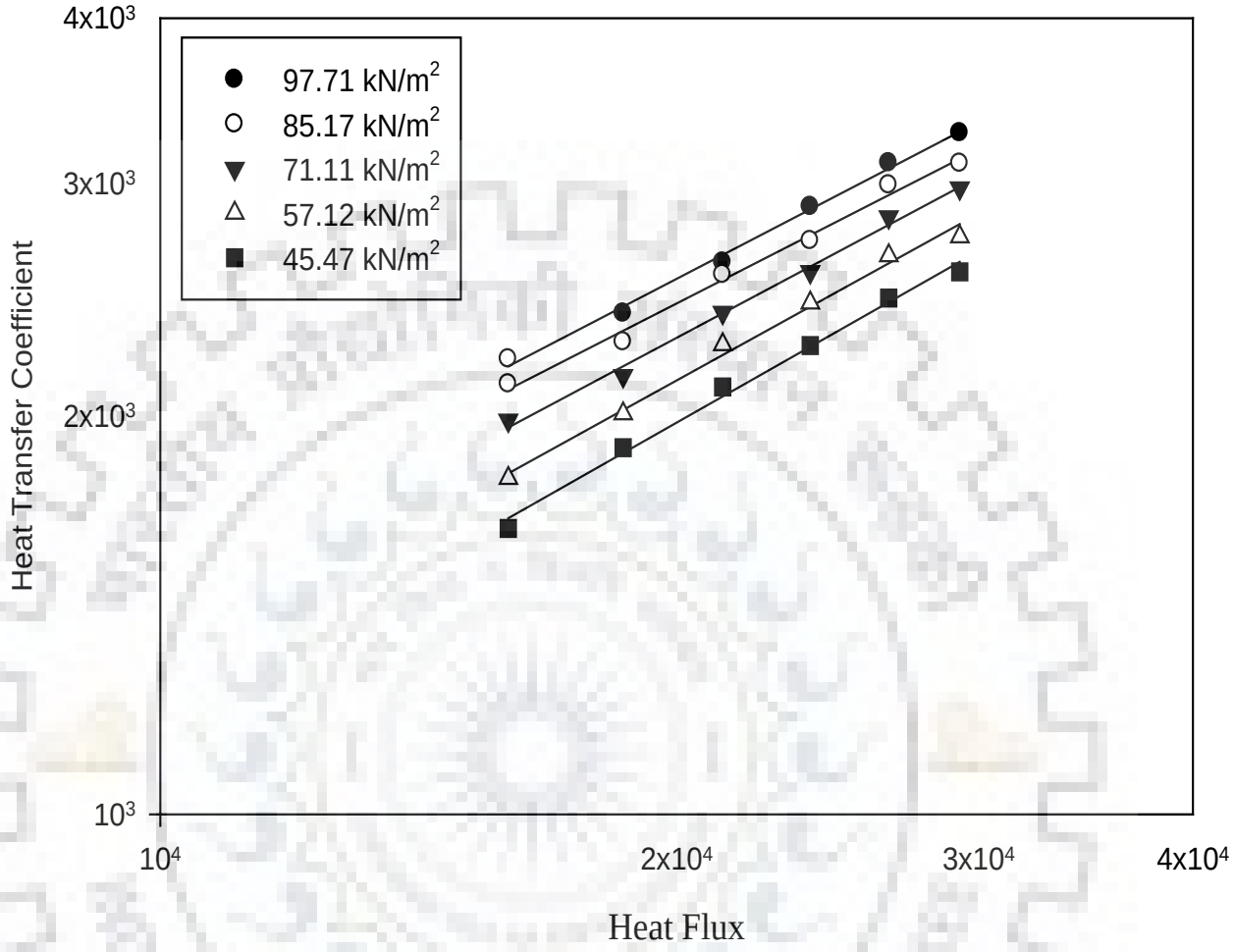

Fig. 6.18: Variation of HTC with heat flux for boiling of (a) 0.05% Copper Oxide –nanofluid on a heating tube surface with pressure as a parameter.

Boiling is a surface phenomenon, it depends on the surface characteristics of the heating tube surface. The variation of heat transfer characteristics of alumina – distilled water and copper oxide – distilled water nanofluids with respect to heat flux and pressure can be described by the following power law equation which has been obtained by regression analysis.

$$h = C_2 q^{0.7} p^{0.32} \quad (6.7)$$

where C_2 is a constant whose values depend upon the percentage concentration of alumina and copper oxide nanoparticles in distilled water and surface characteristics. The values of constant C_2 as determined for various concentrations of alumina and copper oxide nanoparticles in distilled water are given in Table 6.2.

Table 6.2: Values of constant C_2 for various nanofluid compositions

S. No.	Alumina and copper oxide nanoparticles concentration in distilled water (% by volume)	C_2 for Alumina – Distilled water nanofluids	C_2 for Copper Oxide – Distilled water nanofluids
1	0.001	0.501	0.48
2	0.005	0.512	0.503
3	0.01	0.524	0.515
4	0.05	0.65	0.57

An important implication of Eq. (6.7) is that heat transfer coefficient of a given concentration of both the nanoparticles in distilled water can be determined from the knowledge of heat flux and pressure, provided the values of constant C_2 is known.

Fig. 6.19 represents the plot between the experimentally determined values and those determined by using the correlations obtained for boiling of different concentration of Alumina nanoparticles in distilled water at atmospheric and sub-atmospheric pressures. As can be seen from the plot the predicted values matches the experimental values excellently within an error of $\pm$ 9 % only.

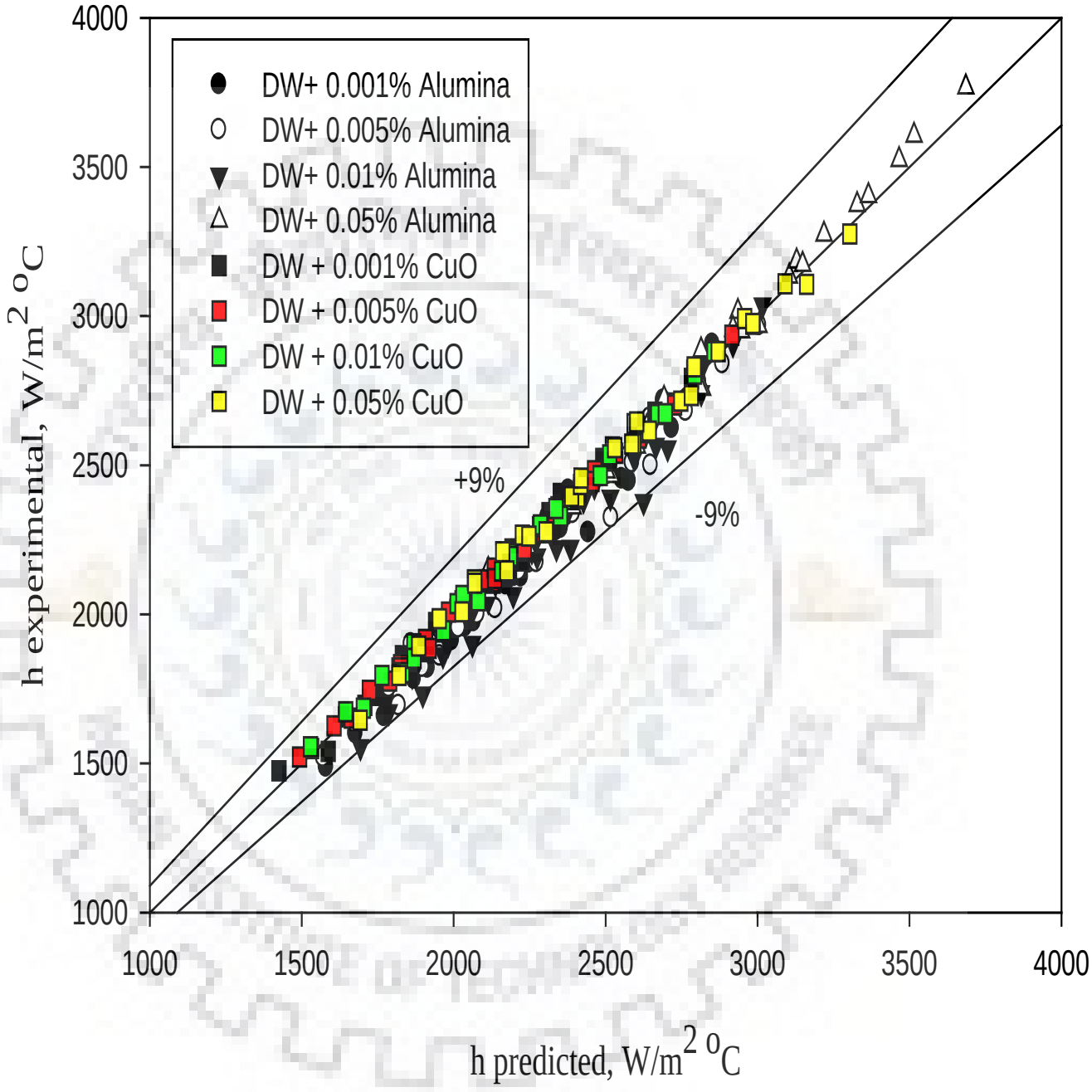

Fig. 6.19: Comparison of experimental heat transfer coefficients with those predicted from the correlations for boiling of various concentrations of Alumina nanoparticles in distilled water at atmospheric and sub atmospheric pressures.

6.4 Comparison of Boiling Heat Transfer Coefficient of Nanofluids v/s Distilled Water on a Stainless Steel Heating Tube

This section have been devoted to make a comparative study of boiling heat transfer characteristics of nanofluids with distilled water on a stainless steel heating tube at atmospheric and sub atmospheric pressures with an objective to obtain the effect of nanoparticle concentration on boiling heat transfer coefficient. Figures 6.20 and 6.21 depict the variation of heat transfer coefficient for various concentrations of Alumina and Copper Oxide nanoparticles dispersed in Distilled Water . These plots also contain the curve for heat transfer coefficient of Distilled water for the sake of comparison. The close examination of these plots reveal that heat transfer coefficient of boiling of nanofluids on stainless steel heating tube is higher than that of distilled water for a given value of heat flux at atmospheric pressure.

The heat transfer coefficient of nanofluids tends to increase upto a concentration of 0.05 % by volume of both the nanoparticles. On further increasing the concentration of nanoparticles in distilled water beyond 0.05%, initially an enhancement in heat transfer coefficient is observed upto a certain optimum heat flux value although this enhancement is less than that observed for 0.05% by volume of nanoparticles in distilled water. On further increasing the heat flux the heat transfer coefficient value steadily deteriorates with further increase in the heat flux. Similar observations have been observed for the alumina and copper oxide based nanofluids at sub atmospheric pressure as depicted in Figures 6.22 to 6.25. The possible reason behind such behavior can be the settling of nanoparticles over the cylindrical stainless steel heating surface and the formation of a nanoparticle layer onto the heating surface. These facts were corroborated by Das et. al. [D2, D3] in their work considered a cartridge heater for heating with roughness of micron scale and thus reported smoothening of the surface on sedimentation of nanoparticles for deterioration of heat transfer coefficient, Kwark et.al. [K17] for the boiling of nanofluids beyond critical concentration, White et. al. [W10] in the boiling of Zinc Oxide – Distilled Water suspensions. White et. Al. [W10] reported that an initial enhancement of 24% in the boiling heat transfer coefficient which steadily deteriorates with the increase in the particle concentration. This behavior is due to the increase in the surface roughness values of the heating tube. The surface characteristics of the stainless steel heating tube were determined in terms of surface roughness after each experimental run with the help of surface profilometer. The results of the surface roughness for each concentration of alumina and copper oxide nanoparticles in distilled water

reflects that the surface roughness increases with the increase in the concentration of the nanoparticles as shown in Figures 6.26 and 6.27, respectively. These figures indicate that as the concentration of nanoparticles increases irrespective of alumina or copper oxide the surface interaction between the nanoparticles and the heating tube surface increases which is another prominent reason responsible for heat transfer enhancement on introducing the nanoparticles to the base fluid. This shows that the nanoparticles settled on a heating surface effectively facilitate bubble nucleation and thus enhance nucleate boiling heat transfer thereby increasing the surface roughness of the heating tube. A thin nanoparticle layer was formed on the heating surface during nucleate boiling of nanofluid which improves the solid – liquid contact. Enhancement in heat transfer can be attributed to the difference in the surface characteristics of heating tube due to presence of this nanoparticle layer. However at higher concentration settling of nanoparticles is fast and thus the settled layer of nanoparticles behave as a thermal insulation layer and also reduces the number of active nucleation sites. Thus , resulting in deterioration in boiling heat transfer coefficient.

Also, the enhancement in heat transfer coefficient of nanofluids has been determined for all the pressures and heat flux at various concentration of nanoparticles. Figures 6.28, 6.29 and 6.30 depicts the percentage enhancement in heat transfer coefficient of nanofluids namely alumina – distilled water and copper oxide – distilled water for different experimental runs as a function of heat flux at atmospheric pressure and sub atmospheric pressure values viz. 71.11 kN/m2 and 45.47 kN/m^2, respectively. These plots reveals that the maximum enhancement of 52.76% and 30.71% is obtained in heat transfer coefficient in case of Alumina – Distilled Water and Copper Oxide – Distilled Water respectively, at 0.05% by concentration of both the nanoparticles in the distilled water at atmospheric pressure.

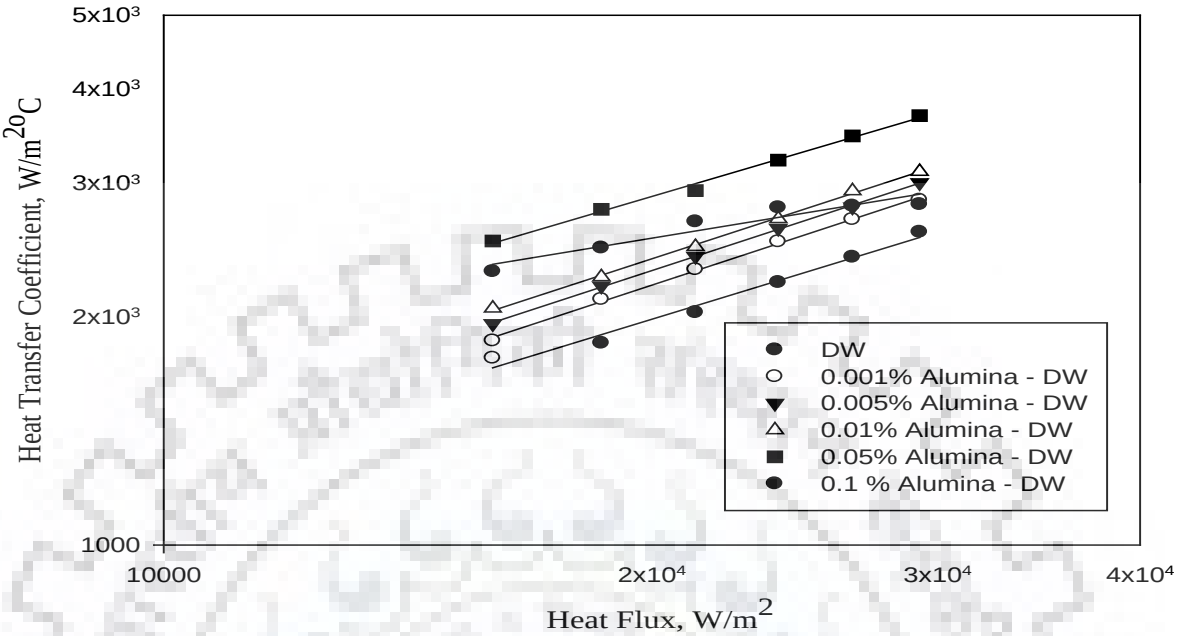

Figure 6.20 Comparison of HTC with heat flux for boiling of varying concentration of Alumina – DW nanofluid and Distilled water at atmospheric pressure

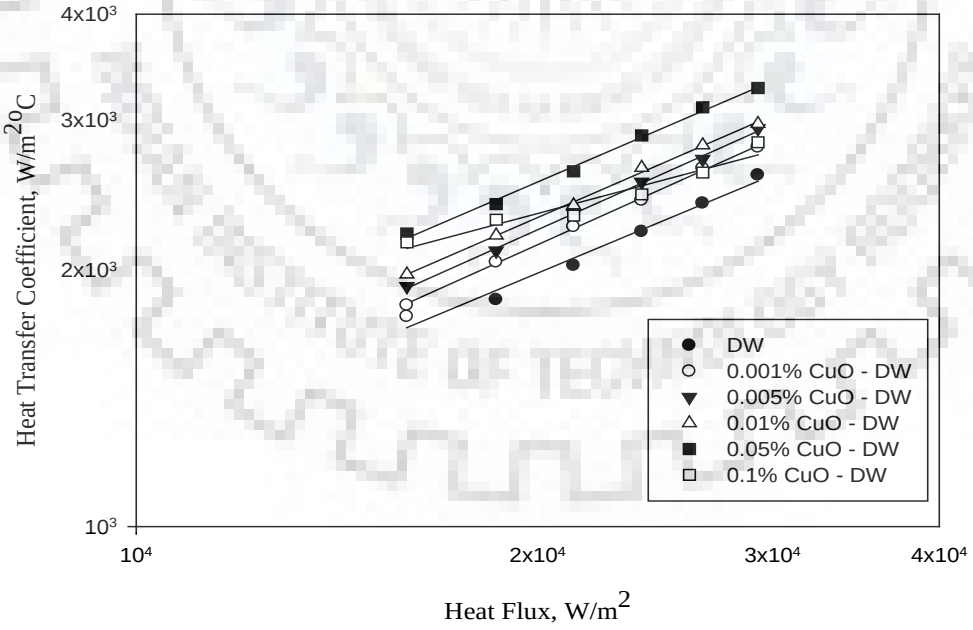

Figure 6.21 Comparison of HTC with heat flux for boiling of varying concentration of Copper Oxide – DW nanofluid and Distilled water at atmospheric pressure

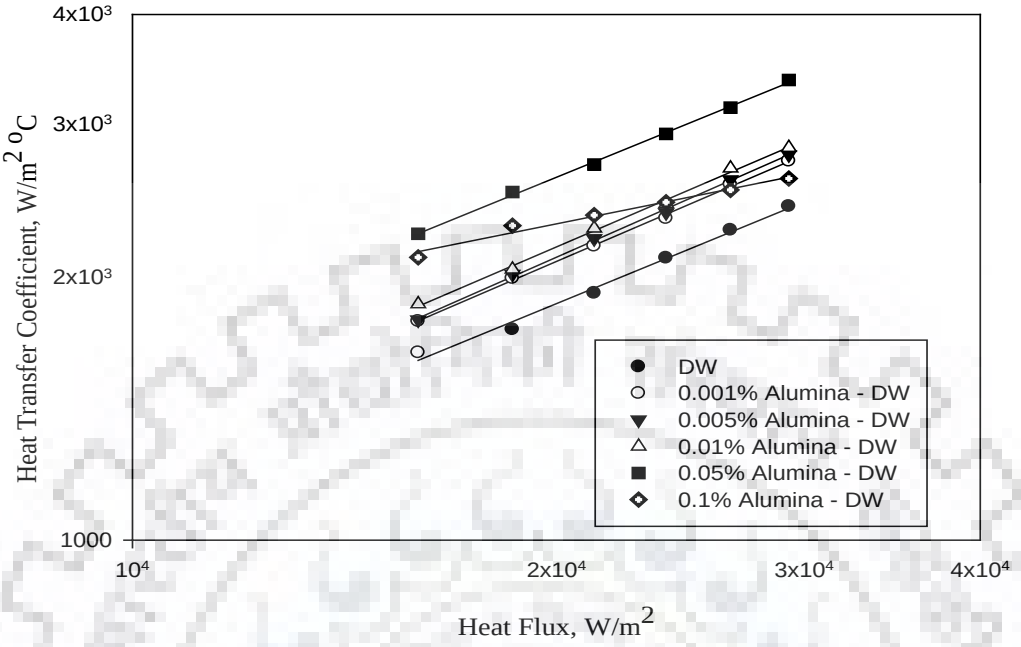

Figure 6.22 Comparison of HTC with heat flux for boiling of varying concentration of Alumina – DW nanofluid at 71.11 kN/m^2

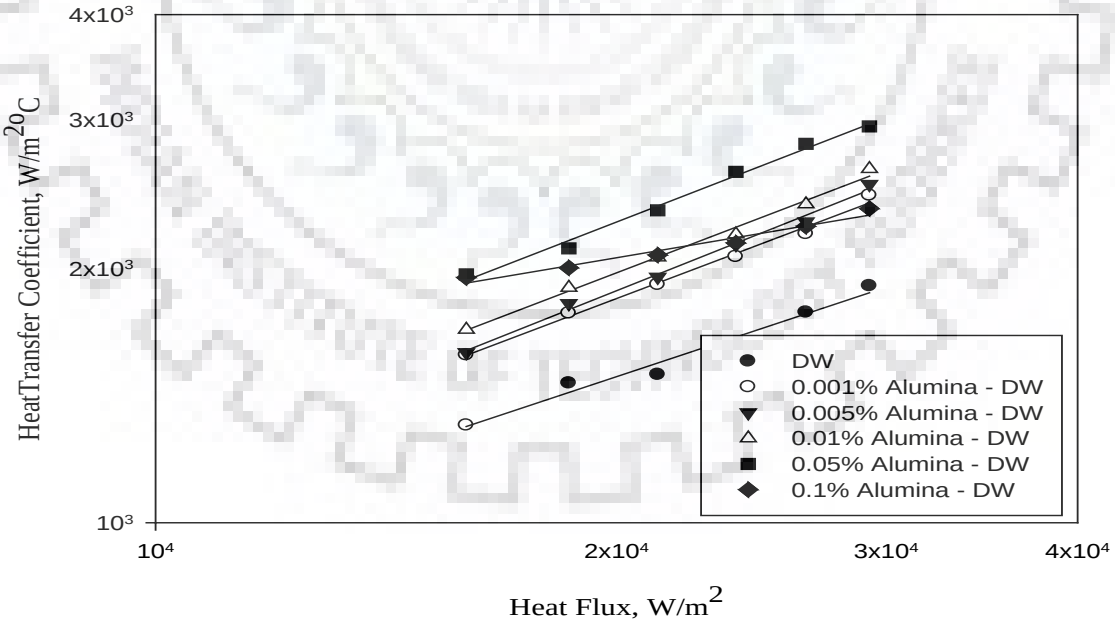

Figure 6.23 Comparison of HTC with heat flux for boiling of varying concentration of Alumina – DW nanofluid at 45.47 kN/m^2

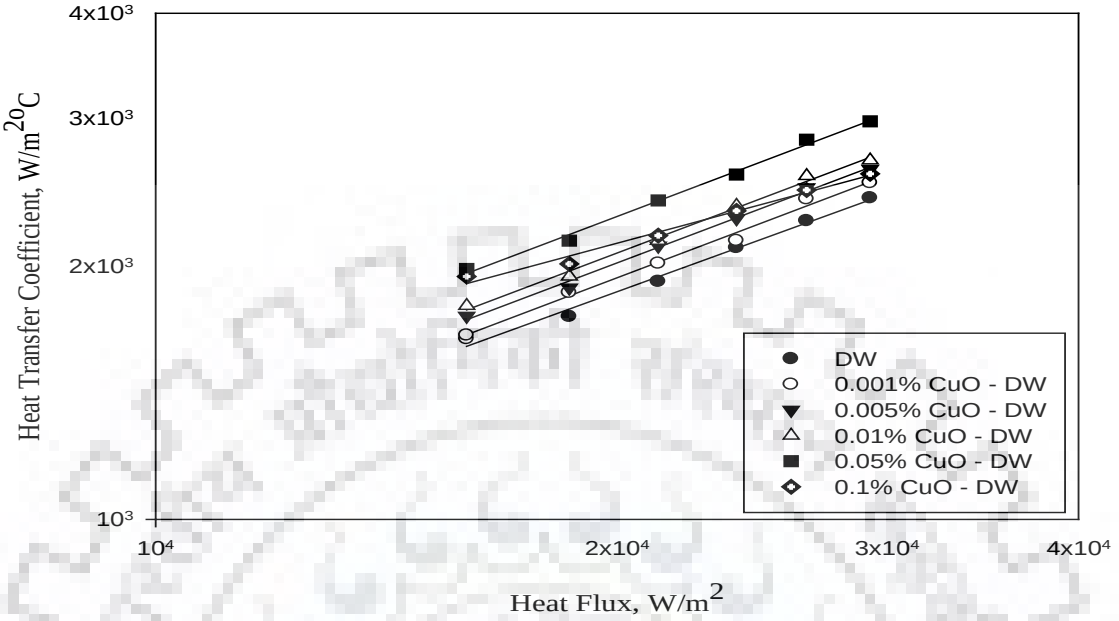

Figure 6.24 Comparison of HTC with heat flux for boiling of varying concentration of Copper Oxide – DW nanofluid and Distilled water 71.11 kN/m^2

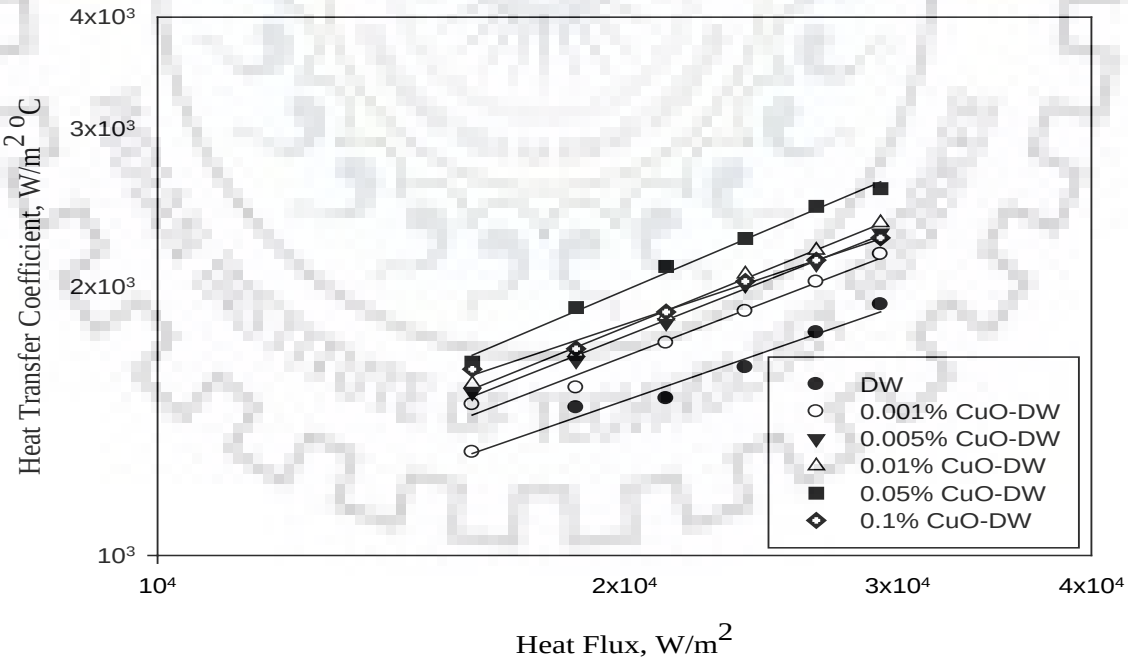

Figure 6.25 Comparison of HTC with heat flux for boiling of varying concentration of Copper Oxide – DW nanofluid and Distilled water at 45.47 kN/m^2

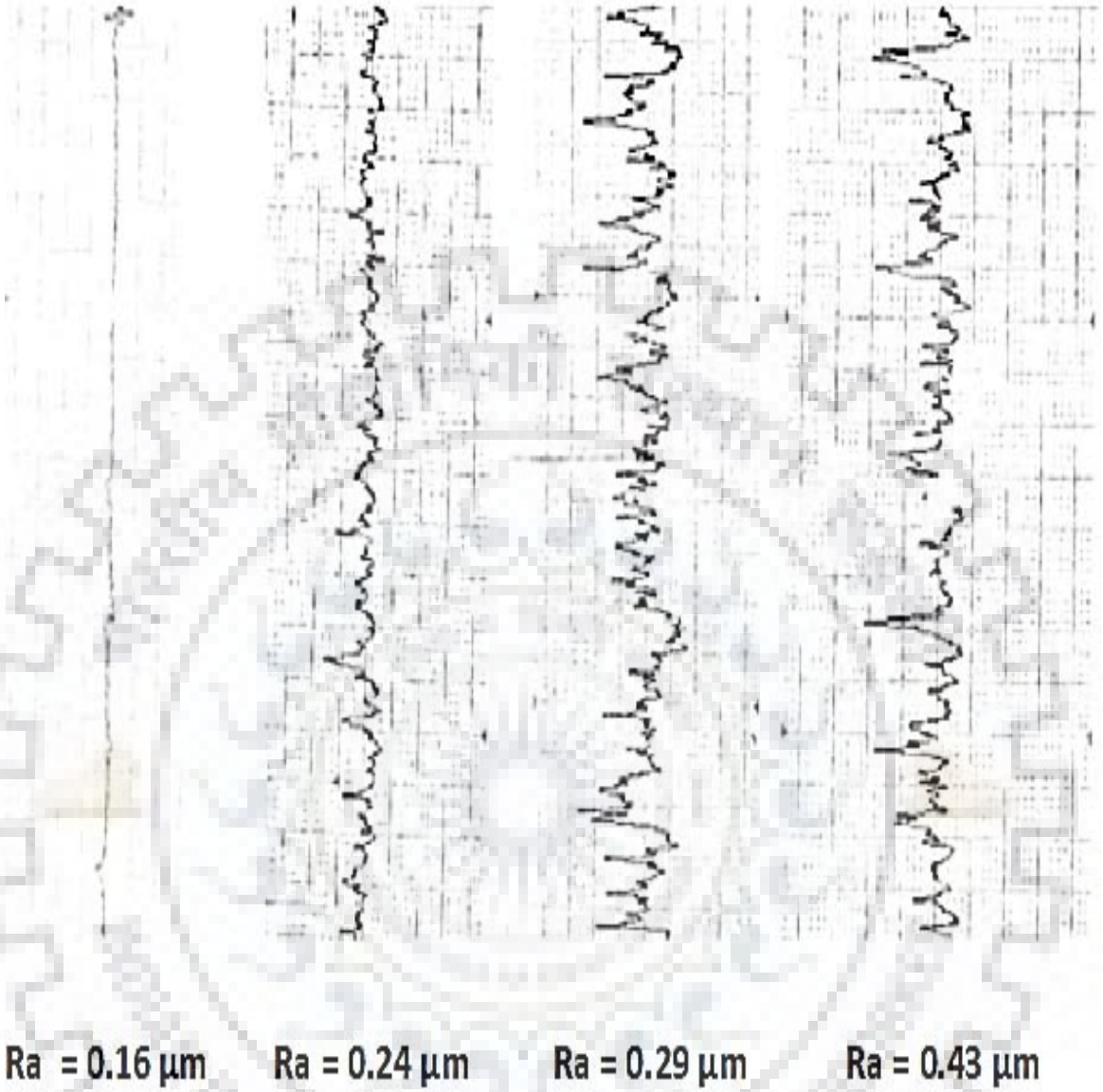

Fig. 6.26 Surface roughness values of the heating tube at different concentration viz. a)0.001%, b) 0.005%, c)0.01%, d)0.05 % by volume of alumina nanoparticles in distilled water.

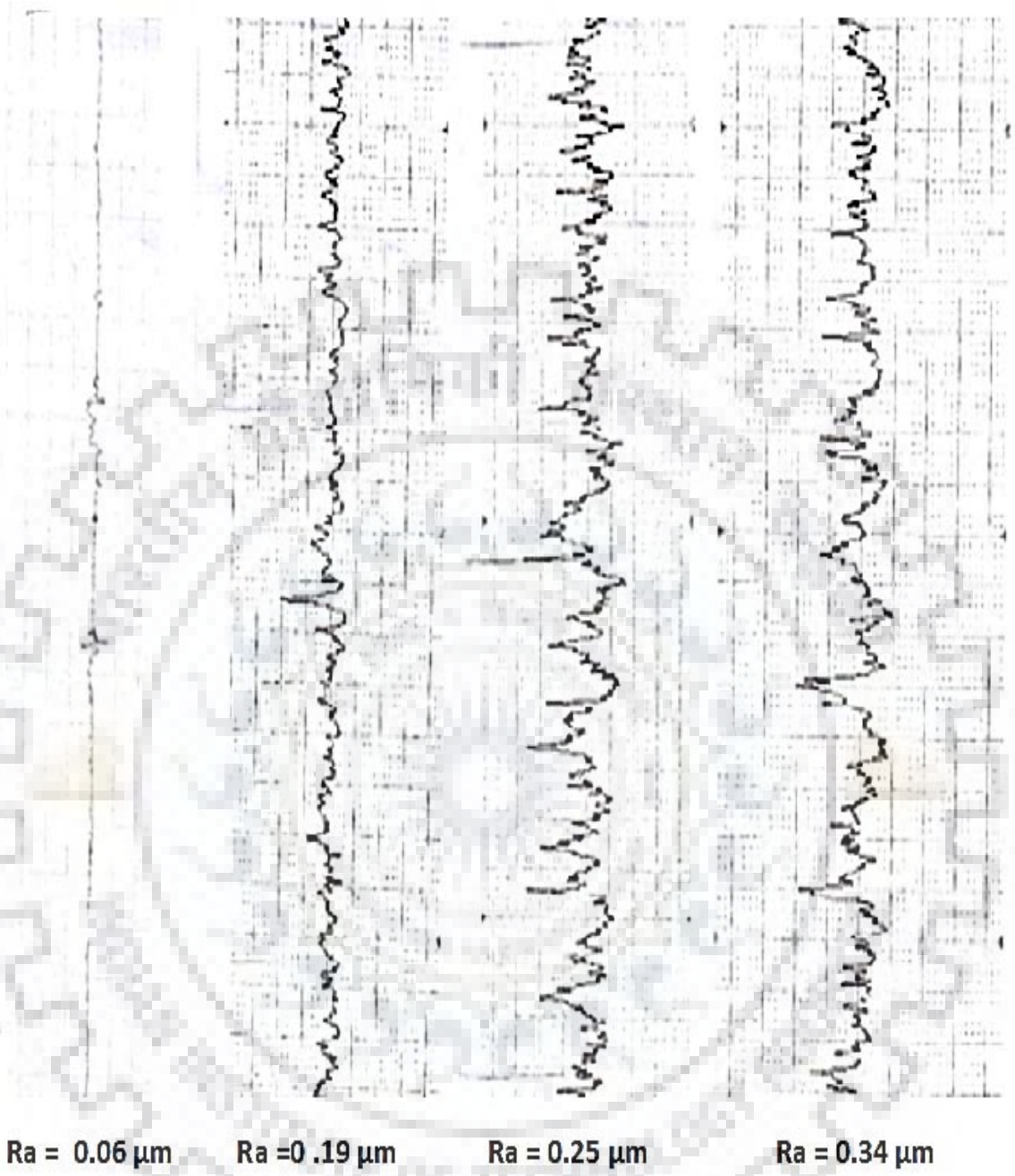

Fig. 6.27 Surface roughness values of the heating tube at different concentration viz. a)0.001%, b) 0.005%, c)0.01%, d)0.05 % by volume of alumina nanoparticles in distilled water.

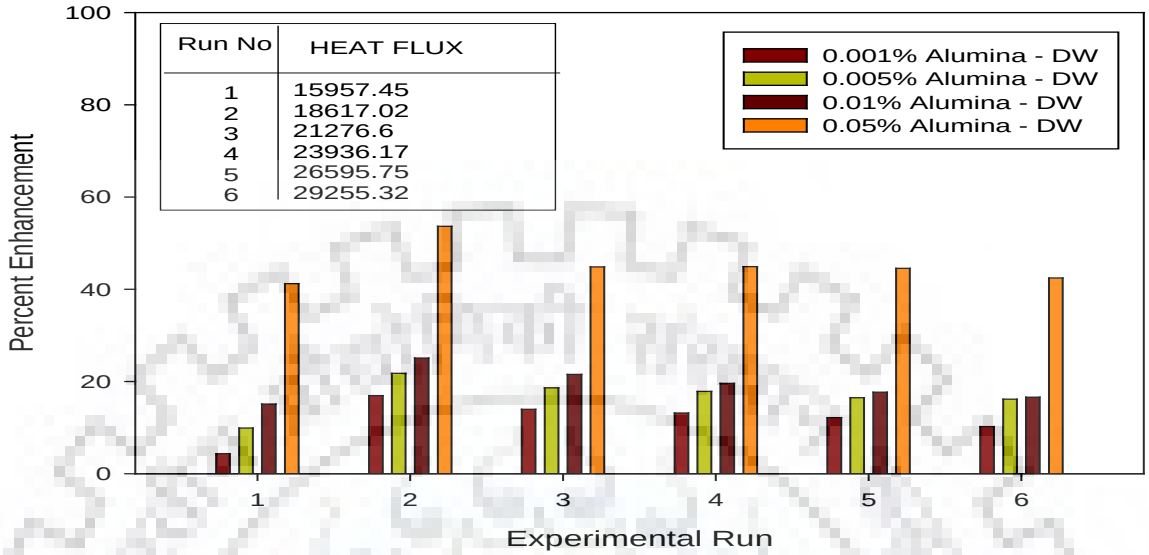

(a)

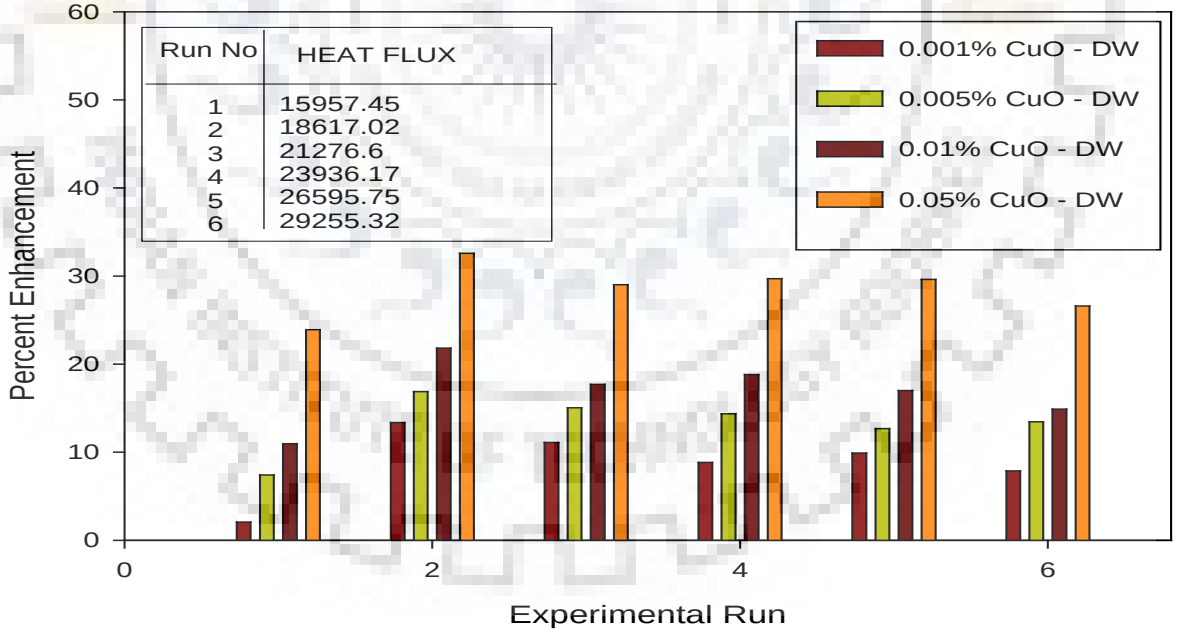

Figure 6.28 (a) and (b) Percentage enhancement in heat transfer coefficient with heat flux for various concentration of Alumina – DW and Copper Oxide – DW nanofluid at 97.71 kN/m^2.

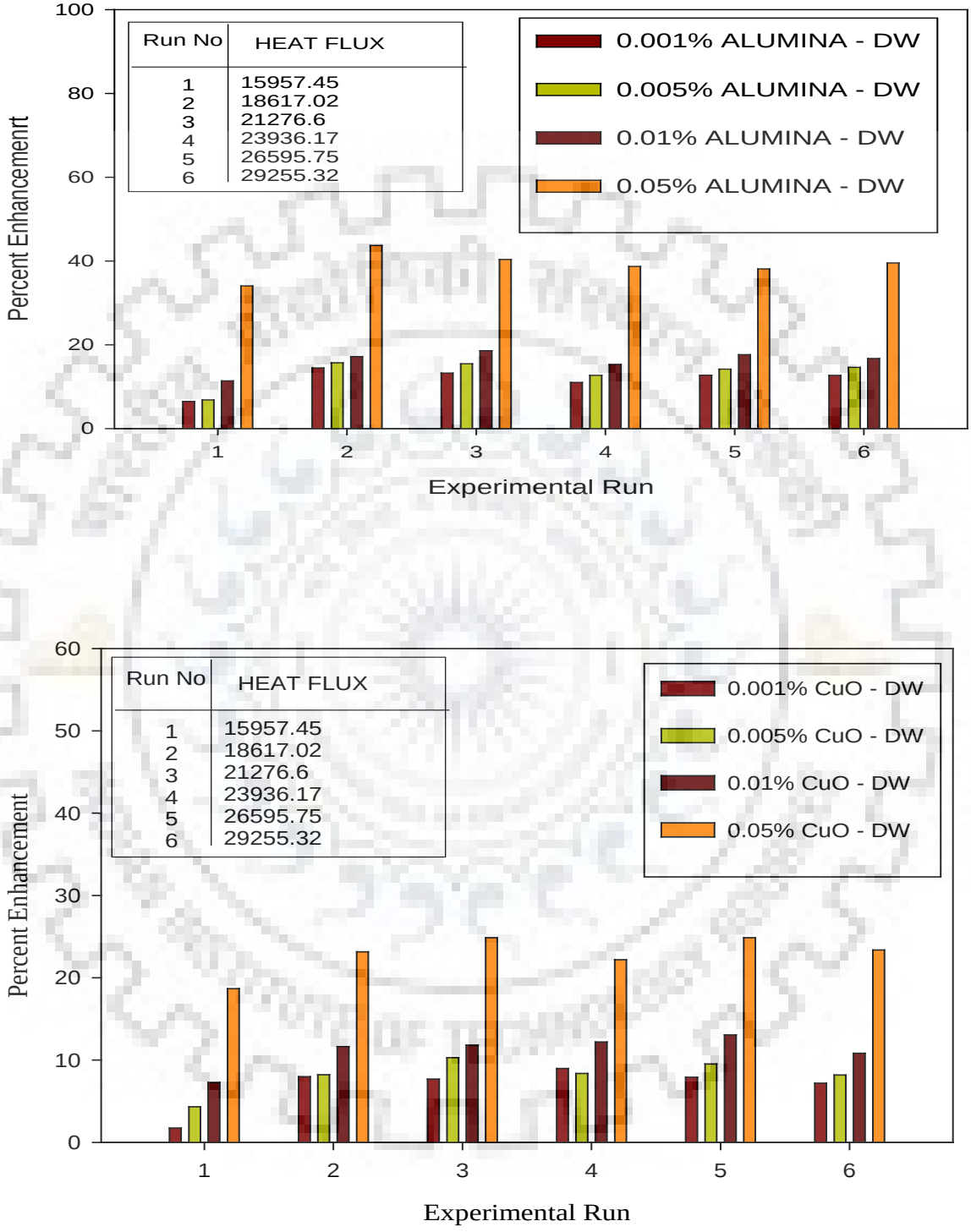

Figure 6.29 (a) & (b) Percentage enhancement in heat transfer coefficient with heat flux for various concentration of Alumina – DW and Copper Oxide – DW nanofluid at 71.11 kN/m^2.

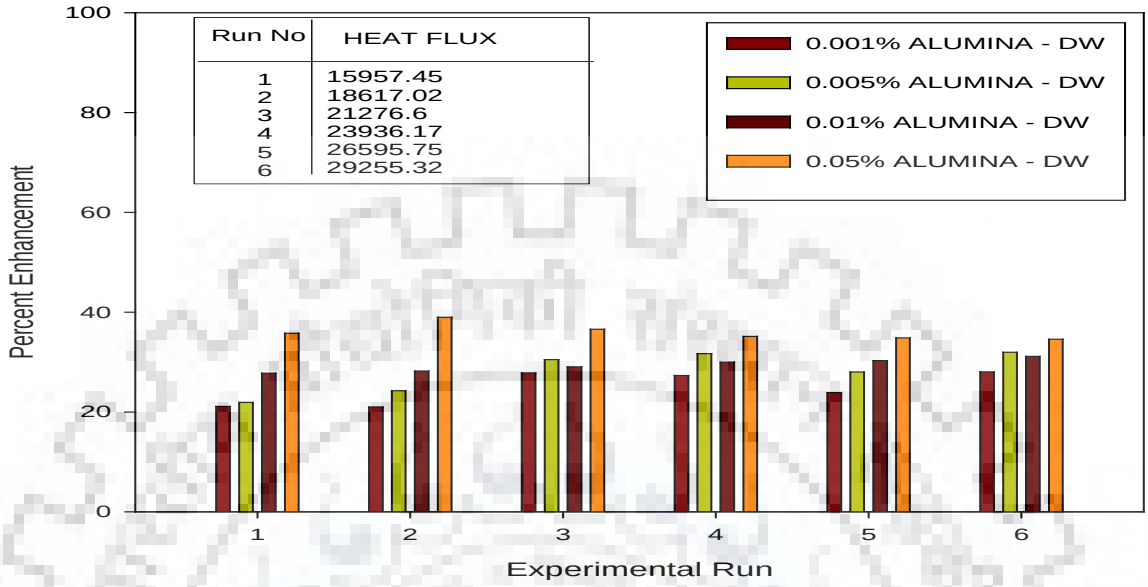

(a)

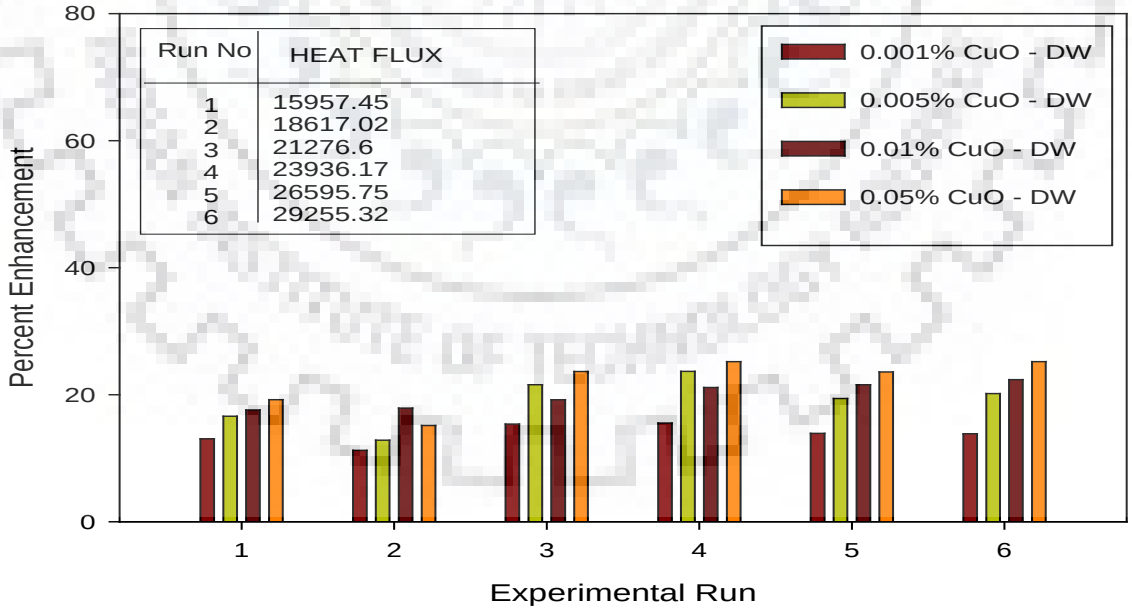

Figure 6.30 (a)&(b) Percentage enhancement in heat transfer coefficient with heat flux for various concentration of Alumina – DW and Copper Oxide – DW nanofluid at 45.47 kN/m^2.

6.5 Development of an Empirical Correlation for Boiling Heat Transfer Coefficient of a Nanofluid

Previous section has demonstrated that heat transfer coefficient for boiling of a nanofluid at atmospheric and sub atmospheric pressure cannot be determined by the use of weighted mean of heat transfer coefficient of individual components. This is due to the fact that nanoparticles deposit on the heat transfer surface alters the surface characteristics of the heating tube. This calls for the development of method which can be applied to predict the boiling heat transfer coefficient of a nanofluid from the knowledge of measurable parameters such as heat flux, pressure, concentration and various thermophysical characteristics of nanofluids. This section has been devoted to it.

For nucleate pool boiling Rohsenow [R2] considered the formation of bubbles from the heater surface and their movement at the point of departure from the surface to be of prime significance and proposed the equation for determining the pool boiling heat transfer coefficient in the region of nucleate pool boiling. The equation is given as under:

$$\frac{C_{sf}(T_s - T_{sat})}{h_{fg}} = C_{sf}\left(\frac{q}{\mu_{nf} h_{fg}}\sqrt{\frac{\sigma g_c}{g(\rho_{nf} - \rho_v)}}\right)^{0.33} Pr^n \qquad (6.8)$$

The value of the constant n is recommended to vary in between 0.8 to 2.0. Determination of constant C_{sf} from the work of previous researchers, accounts not only for the nucleation and number of active nucleation sites present on the heating surface but also accounts for the effect of various thermophysical properties of the fluid. Rohsenow proposed this liquid-surface combination factor that accounts for the surface characteristics of the heating medium during nucleate pool boiling.

Also, Forster and Zuber [F3] in their work proposed a correlation based on their observation. They indicated that during nucleate pool boiling small bubbles grow rapidly in comparison to the larger ones, but the extent of mixing in the surrounding liquid due to bubble formation remains the same. They proposed the below mentioned correlation based on their observation

$$\frac{qC_{sf}\rho_{np}\sqrt{\pi\alpha_{nf}}}{k_{nf} h_{fg} \rho_v}\left(\frac{2\sigma}{\Delta P}\right)^{1/2}\left(\frac{\rho_{nf}}{\Delta P}\right)^{1/4} = 0.0015 Re^{0.62} Pr^{1/3} \qquad (6.9)$$

Yang and Liu [Y2] employed the Kutateladze equation to determine the heat transfer coefficient during pool boiling of functionalized nanofluids prepared using silica nanoparticles on smooth metal surface. The Kutateladze equation is given as under:

$$\frac{h}{\lambda}\sqrt{\frac{\sigma}{g(\rho_{nf}-\rho_v)}} = 7.0\times10^{-4}Pr^{0.35}\times\left[\frac{q}{\rho_v h_{fg} v_1}\sqrt{\frac{\sigma}{g(\rho_l-\rho_v)}}\right]^{0.7}\left[\frac{P}{\sigma}\sqrt{\frac{\sigma}{g(\rho_l-\rho_v)}}\right]^{0.7} \quad (6.10)$$

Based on the above correlations, it was decided that the heat transfer coefficient during pool boiling of nanofluids depends on the concentration of the nanoparticles, characteristic length of heating surface, pressure maintained in the system, heat flux applied to the system and various thermophysical properties of nanofluids. With the help of dimensional analysis following dimensionless correlation for pool boiling of nanofluids has been developed:

$$Nu = 3.709\text{x}10^{-4}\ Pr^{1.32}QP^{0.017}Ja^{-0.97} \quad (6.11)$$

Where;

$$Nu = \frac{hD}{k_{nf}}$$

$$Pr = \frac{c_{pnf}\mu_{nf}}{k_{nf}}$$

$$Ja = \frac{c_{pnf\Delta T}}{\lambda}$$

$$Q = qD/\lambda_v\rho_v$$

$$P = pD/\sigma$$

$$D = \sqrt{\sigma/g(\rho_{nf}-\rho_v)}$$

This equation correlates all the data of this investigation within an error of +10% and – 5% as shown in Figure 6.31.The above equation has also been tested against the predicted data due to experimental data of following investigators: Ceislinski [C7, C8]; Kole and Dey [K14]; Bang & Chang [C7]; Wen & Ding [W8]; Ding et. al. [D8] and Yang & Liu [Y2]. The comparison between the experimentally obtained values of heat transfer coefficient and those predicted by above correlation, Eq. 6.11 is shown in Figure 6.32(a) and Figure 6.32(b). As is clear from these figures that the predictions have matched excellently with the experimental values within an error of $\pm$

10%. Thus, it can be said that correlation given by Equation 6.11 is capable of correlating the experimental data for the nucleate boiling of nanofluids irrespective of the nanoparticles and the base fluids employed for different heating surfaces. It may be pointed out that Equation 6.11 provides a method for the computation of boiling heat transfer coefficient of nanofluids from the knowledge of concentration by volume of nanoparticles in base fluid, heat flux and pressure employed during boiling and various thermophysical characteristics of nanofluids.

Summary

From above observations and present study it can be concluded that the boiling heat transfer characteristics of nanofluid are same as that of base fluid . The functional relationship of heat transfer coefficient with heat flux, liquid pool temperature and pressure is the same as observed for base fluid i.e. distilled water and therefore dimensional equation $h = C_2 q^{0.7} P^{0.32}$ has been developed using regression analysis for nanofluids at atmospheric and sub atmospheric pressure. The value of constant C_2 depends upon the concentration of nanoparticles in the base fluid and the surface particle interaction that results in changes in the surface characteristics of the heating surface during boiling.

A dimensionless correlation has been developed to estimate the heat transfer coefficient for boiling of nanofluids on any surface irrespective of the nanoparticles employed and the surface characteristics of the heating medium. The resultant correlation has been found to correlate the experimental data of the present investigation as well as the work of other researchers very well .

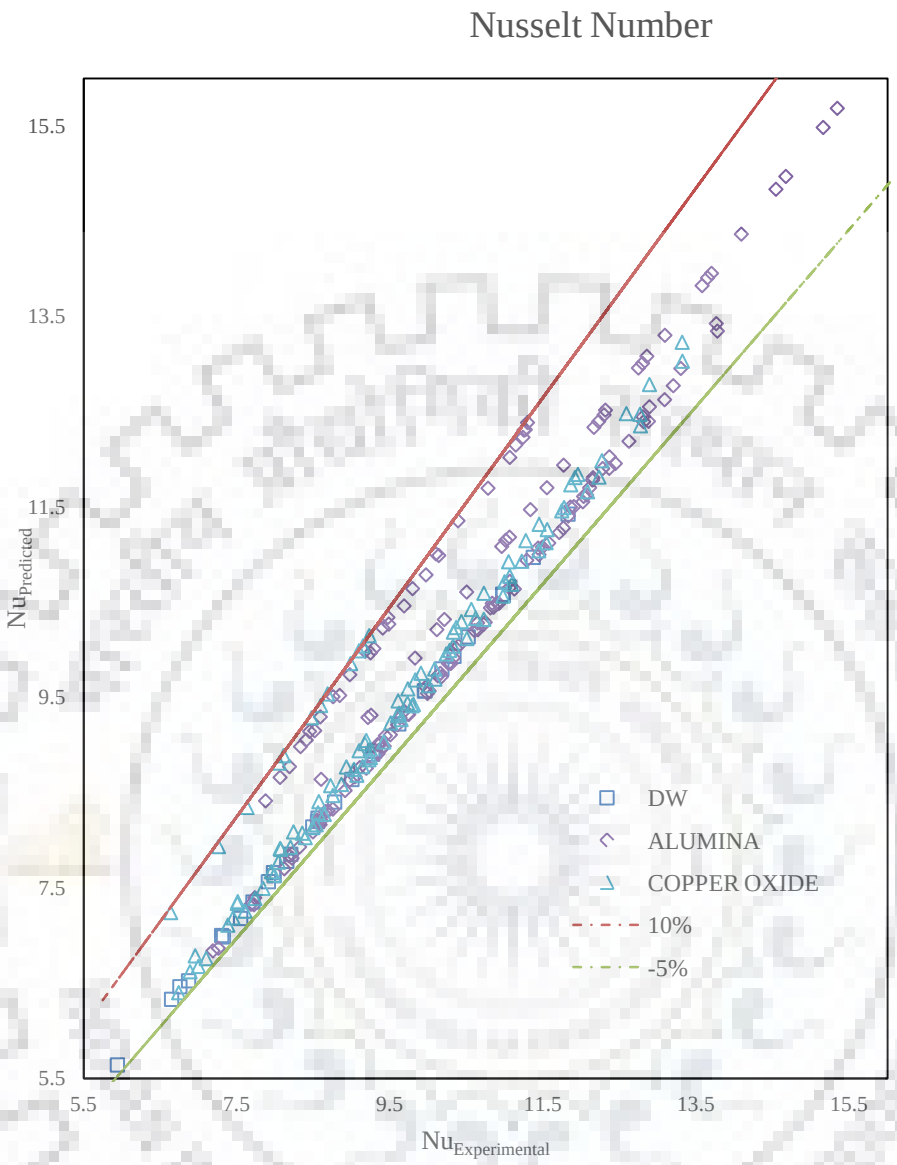

Figure 6.31 Comparison between the Experimental and Predicted values of Nusselt number from Eq.(6.10) for nucleate pool boiling of Alumina-DW and Copper Oxide –DW nanofluids at atmospheric and sub atmospheric pressure.

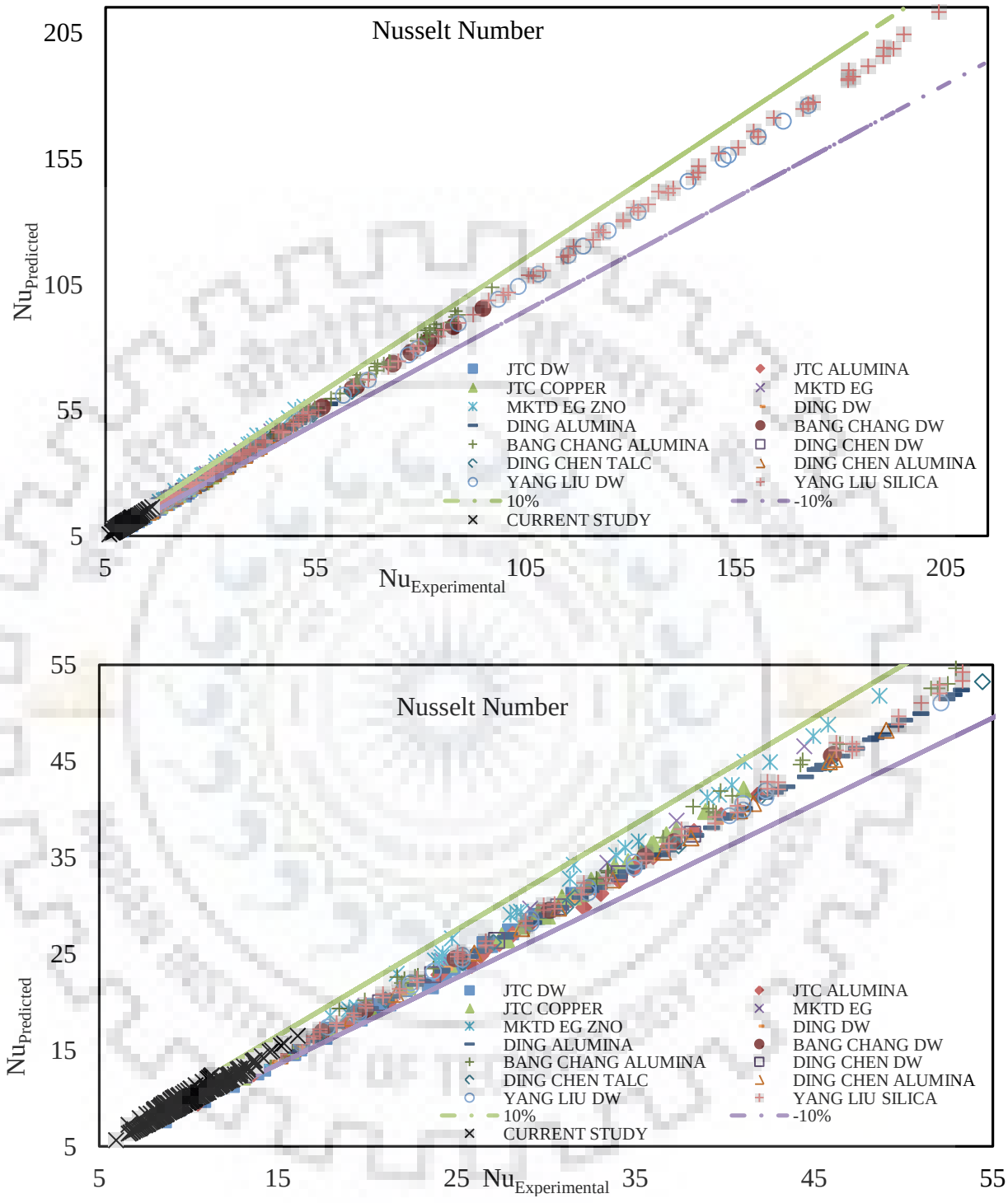

Figure 6.32(a) &(b) Comparison between Experimental and Predicted values of Nusselt number from Eq.(6.10) for present study with the work of other prominent researchers in nucleate pool boiling of various nanofluids at atmospheric and sub atmospheric pressure.

CHAPTER – 7

CONCLUSIONS AND RECOMMENDATIONS

7.1 Conclusions

From the work of current investigation following salient features have emerged out:

1. For generating the data for nucleate pool boiling of nanofluids namely alumina-distilled water and copper oxide-distilled water. Both the nanofluids are synthesized as per the procedure mentioned in section 3.2. Further, the thermophysical characteristics namely density, viscosity and thermal conductivity of alumina-distilled water and copper oxide-distilled water nanofluids have been studied. The experimental data of density of these two nanofluids have been generated for various concentrations of nanoparticles at atmospheric pressure. The value of density of nanofluid has been found to vary with temperature and concentration of nanoparticles according to the following equation:

$\rho_{eff} = C_1+C_2\varphi_p+C_3T$

The value of these constant depends upon the nanofluids. The experimental data predicted from the above equation matches excellently within an error of $\pm$ 2.5%.

2. The experimental data of thermal conductivity of both the nanofluids have been generated for various concentration of nanoparticles by using KD2 Pro Thermal Conductivity Analyzer. The experimental values of thermal conductivity of both the nanofluids have been compared with the Hamilton – Crosser Model. The comparison between the two shows that maximum deviation is 7 %. Further , the effect of temperature has been investigated for various concentration of nanoparticles. The value of thermal conductivity has been found to vary with temperature and concentration of nanoparticles according to power law relationship:

$$\frac{k_{eff}}{k_{bf}} \propto \varphi^a T^b$$

An equation relating the thermal conductivity with temperature and concentration has also been developed by regression analysis within an error of $\pm$ 6%.

3. The experimental data of viscosity have been generated for various concentration of nanoparticles and value of viscosity of nanofluids vary with the temperature according to the logarithmic relationship:

$$\ln(\mu_{nf}) = \frac{A}{T} - B$$

An equation relating the viscosity of nanofluid with temperature and concentration of nanoparticles has been developed by regression analysis within an error of $\pm$ 7%.

4. Experimental data for nucleate pool boiling of distilled water on stainless steel heating tube surface have been generated for different heat flux values at atmospheric and sub atmospheric pressure. Analysis of the data has shown that surface temperature, for a particular value of heat flux, increases from bottom to side to top positions and thus value of heat transfer coefficient increases from top to side to bottom position. The value of local heat transfer coefficient, at a given circumferential position, has been found to vary with heat flux according to power law relationship, $h_\psi \propto q^{0.7}$ for all the values of pressure taken in this investigation. In addition, an equation relating local heat transfer coefficient with heat flux and pressure has also been developed by regression analysis within an error of $\pm$ 4%.

5. Average heat transfer coefficient of distilled water boiling on stainless steel heating tube at atmospheric and sub atmospheric pressure has been found to vary according to the relationship $h \propto q^{0.7}$. Enhanced pressure improves the value of heat transfer coefficient. A power law expression for heat transfer coefficient has been developed as

$$h = C_1 q^{0.7} p^{0.32}$$

where C_1 is a constant representing the surface – liquid combination factor.

The predicted values of heat transfer coefficient match excellently with the experimentally determined values well within the maximum error limits of $\pm$ 7 %. It may be pointed that these observations corrobates with the findings of various researchers such as Benjamin & Balakrishnan [B3], Mihir [M1], Cryder and Finalborgo [C10], Liaw & Dhir [L7], T. Hinrichs et. al. [T4], Young & Hummel [Y4], Siraj et. al. [A10, A11]. Thus this investigation has corroborated the findings of

earlier investigators for saturated boiling of liquids on stainless steel heating surface at atmospheric and sub atmospheric pressures.

6. Experimental data of pool boiling of alumina-distilled water and copper oxide-distilled water nanofluids at atmospheric and sub atmospheric pressure has shown analogous boiling characteristics as that of distilled water. Hence, the variation of average heat transfer coefficient of nanofluids with respect to heat flux and pressure remains the same as that of distilled water. A functional relationship has been developed by regression analysis.

$$h = C_2 q^{0.7} p^{0.32}$$

within an error of $\pm$ 9% ; where C_2 is a constant whose value depends upon the concentration of nanoparticles and surface characteristics of heating tube. These observations also corrobates with the findings of various researchers such as Park & Jung [P2]; Kole and Dey [K14]; Kim et. al. [K11]; Johnathan and Kim [J4]; Sarfaraz and Peyghambarzadeh[S2] and Wen and Ding [W5,W6] over boiling of different concentration of nanoparticles.

7. A comparison of boiling characteristics of distilled water and the two nanofluids has been carried out. The pool boiling heat transfer coefficient enhances with increase in concentration of both alumina and copper oxide nanoparticles in distilled water. This behavior continues upto a certain optimum value of concentration of nanoparticles in distilled water. The maximum enhancement of 52.76% and 30.71% is obtained in heat transfer coefficient in case of alumina – distilled water and Copper Oxide – Distilled Water respectively, at 0.05% by concentration of both the nanoparticles in the distilled water. However, on further increasing the concentration of nanoparticles in base fluid i.e. distilled water yields deterioration in the boiling heat transfer coefficient.

8. A dimensionless correlation has been developed to estimate the heat transfer coefficient for pool boiling of nanofluids which is given as below:

$$Nu = 3.709 \times 10^{-4} \, Pr^{1.32} QP^{0.017} Ja^{-0.97}$$

This equation has been compared with the data of present investigation as well as other investigators namely Ceislinski [C7, C8]; Kole and Dey [K14]; Bang & Chang [B2]; Wen & Ding [W5,W6]; Ding & Chen [C2] and Yang & Liu [Y2]. The comparison between the

experimental values and predicted values due to correlation match excellently well within an error of $\pm$ 10%.

7.2 Recommendations

Following is recommended for the future research work:

1. The present investigation has been confined to saturated pool boiling of distilled water; alumina – distilled water and copper oxide – distilled water nanofluids on the stainless steel heating tube surface for various values of heat flux at atmospheric and sub atmospheric pressure. Therefore correlations developed in this investigation are valid only for the operating conditions of this investigation. It is desirable that experimental data at pressures higher than the atmospheric pressure be generated and thereby correlations be developed. Further, investigation should also include other industrially important nanofluids such as refrigerants, hydrocarbons, cryogenics and solvents etc.

2. In this investigation only three thermophysical characteristics of nanofluids namely density, thermal conductivity and viscosity have been investigated. However, it is desirable to investigate some more properties such as specific heat, surface wettability and surface tension of nanofluids.

3. Data for some factors such as change in the thermal conductivity and viscosity of nanofluids due to Brownian motion of the nanoparticles and large specific surface area can be obtained through experiments. There is a need of experimental research in this field specially for nanofluids containing spherical shaped nanoparticles.

4. To prepare stable nanoparticle based suspension remains a crucial issue for both scientific research and to bring the use of nanofluids in industrial applications. Thus the stability of nanofluids specifically for longer period of time remains a challenge and more attention should be paid towards this parameter and innovative techniques be explored for synthesis of nanofluid.

5. In depth research is required to investigate the mechanism of nanoparticle deposition onto the surface during pool boiling. Many researchers have observed the particle deposition phenomenon and establishing proper mechanism behind this phenomenon could help in preparing enhanced surfaces with optimum thickness of nanoparticle coating which could be a great potential in various refrigeration and cryogenic industrial applications.

Annexure - A

TABULATION OF EXPERIMENTAL DATA

Table A.1 : Boiling Heat Transfer Data of Distilled Water over Horizontal Stainless Steel Heating Tube

Run No.	HEAT INPUT Q(W)	HEAT FLUX ,q (W/m^2)	Wall Temp.; Tw_o(°C)				Liquid Pool Temperature, T_{lm} °C				WALL SUPERHEAT, ΔT_w °C	HEAT TRANSFER COEFFICIENT, h W/m^2 °C
			TOP	SIDE	BOTTOM	SIDE	TOP	SIDE	BOTTOM	SIDE		
	Pressure: 97.71 kN/m^2											
1	240	15957.45	113.31	113.09	113.08	113.18	100.29	100.16	100	100.19	8.95	1783.12
2	280	18617.02	115.19	115.03	114.48	115.08	100.32	100.18	100.02	100.24	10.32	1804.45
3	320	21276.6	116.09	115.95	115.21	116.01	100.34	100.26	100.08	100.28	10.49	2026.51
4	360	23936.17	117.05	116.81	116.42	116.89	100.46	100.32	100.14	100.31	10.78	2221.29
5	400	26595.75	117.97	117.82	117.29	117.86	100.4	100.33	100.17	100.35	11.09	2398.12
6	440	29255.32	118.81	118.71	118.38	118.74	100.49	100.38	100.24	100.41	11.31	2587.36
	Pressure:85.17 kN/m2											
7	240	15957.45	112.56	112.41	111.93	112.44	99.32	99.18	99.02	99.24	9.34	1709.14
8	280	18617.02	114.29	114.13	113.78	114.18	99.34	99.26	99.08	99.28	10.42	1787.59
9	320	21276.6	115.45	115.27	114.78	115.33	99.46	99.32	99.14	99.31	10.83	1965.28
10	360	23936.17	116.28	116.11	115.54	116.17	99.4	99.33	99.17	99.35	11.00	2175.56
11	400	26595.75	117.55	117.37	116.74	117.41	99.49	99.38	99.24	99.41	11.54	2304.27
12	440	29255.32	118.34	118.25	117.76	118.28	99.55	99.43	99.31	99.48	11.74	2492.78
	Pressure: 71.11 kN/m^2											
13	240	15957.45	111.28	111.14	110.51	111.17	97.78	97.69	97.58	97.69	9.54	1673.15
14	280	18617.02	113.09	112.91	112.41	112.95	97.81	97.71	97.61	97.73	10.68	1742.49
15	320	21276.6	114.13	114.01	113.51	114.08	97.86	97.75	97.67	97.78	11.09	1918.28
16	360	23936.17	115.21	115.07	114.19	115.14	97.93	97.78	97.72	97.84	11.37	2104.39
17	400	26595.75	116.17	115.98	115.58	116.05	97.96	97.84	97.77	97.89	11.74	2265.73
18	440	29255.32	117.18	117.02	116.79	117.06	98.02	97.87	97.81	97.92	12.13	2411.58

Table A1 (Contd.)

Run No.	HEAT INPUT Q(W)	HEAT FLUX ,q (W/m^2)	Wall Temp.; Tw_o(°C)				Liquid Pool Temperature, T_{lm} °C				WALL SUPERHEAT, ΔT_w °C	HEAT TRANSFER COEFFICIENT, h W/m^2 °C
			TOP	SIDE	BOTTOM	SIDE	TOP	SIDE	BOTTOM	SIDE		
	Pressure: 57.12 kN/m^2											
19	240	15957.45	108.63	108.46	107.94	108.55	93.68	93.65	93.51	93.68	10.95	1456.21
20	280	18617.02	109.98	109.85	109.15	109.89	93.81	93.65	93.54	93.69	11.61	1604.84
21	320	21276.6	111.29	111.14	110.45	111.21	93.84	93.68	93.58	93.73	12.24	1738.34
22	360	23936.17	112.45	112.26	111.67	112.33	93.91	93.72	93.62	93.77	12.71	1883.57
23	400	26595.75	113.32	113.14	112.94	113.21	93.94	93.79	93.68	93.81	13.01	2045.12
24	440	29255.32	114.35	114.21	113.71	114.26	93.97	93.81	93.73	93.84	13.32	2197.16
	Pressure:45.47 kN/m^2											
25	240	15957.45	106.44	106.32	105.78	106.37	90.48	90.42	90.31	90.45	12.01	1328.94
26	280	18617.02	107.64	107.47	106.91	107.52	90.48	90.43	90.34	90.45	12.52	1487.29
27	320	21276.6	110.59	110.35	109.17	110.44	90.51	90.47	90.37	90.48	14.61	1456.81
28	360	23936.17	111.25	111.08	110.36	111.14	90.56	90.5	90.42	90.53	14.75	1623.18
29	400	26595.75	112.17	112.03	111.18	112.09	90.62	90.54	90.45	90.57	14.98	1775.63
30	440	29255.32	112.49	112.35	112.05	112.41	90.67	90.59	90.51	90.62	14.75	1983.16

Table A.2 : Boiling Heat Transfer Data of 0.001% Alumina - Distilled Water Nanofluid over Horizontal Stainless Steel Heating Tube

Run No.	HEAT INPUT Q(W)	HEAT FLUX ,q (W/m^2)	Wall Temp.; Tw_o(°C)				Liquid Pool Temperature, T_{lm} °C				WALL SUPERHEAT, ΔT_w °C	HEAT TRANSFER COEFFICIENT, h W/m^2 °C
			TOP	SIDE	BOTTOM	SIDE	TOP	SIDE	BOTTOM	SIDE		
	Pressure: 97.71 kN/m^2											
1	240	15957.45	111.41	110.95	110.64	111.04	98.72	98.64	98.47	98.67	8.58	1860.33
2	280	18617.02	112.57	111.79	111.46	111.85	98.75	98.65	98.5	98.7	8.82	2109.99
3	320	21276.6	113.25	113.01	112.59	113.07	98.8	98.68	98.55	98.73	9.21	2309.59
4	360	23936.17	114.31	114.09	113.31	114.14	98.87	98.72	98.55	98.78	9.52	2513.84
5	400	26595.75	115.67	114.91	114.53	114.97	98.94	98.76	98.6	98.85	9.89	2689.84
6	440	29255.32	116.53	116.19	115.33	116.29	98.99	98.84	98.64	98.92	10.26	2851.95
	Pressure:85.17 kN/m2											
7	240	15957.45	108.41	108.17	107.31	108.2	95.68	95.55	95.32	95.58	8.68	1837.73
8	280	18617.02	109.45	109.24	108.56	109.27	95.69	95.58	95.33	95.61	9.14	2037.43
9	320	21276.6	110.65	110.35	109.37	110.37	95.72	95.62	95.36	95.66	9.52	2235.82
10	360	23936.17	111.85	111.43	110.89	111.48	95.78	95.65	95.42	95.69	10.07	2377.81
11	400	26595.75	112.59	112.21	111.69	112.27	95.82	95.71	95.49	95.73	10.16	2617.89
12	440	29255.32	113.64	113.27	112.41	113.31	95.88	95.79	95.58	95.8	10.42	2808.08
	Pressure: 71.11 kN/m^2											
13	240	15957.45	103.28	102.91	102.54	102.95	90.37	90.11	90.01	90.13	8.96	1781.21
14	280	18617.02	104.41	104.15	103.07	104.19	90.39	90.13	90.04	90.15	9.33	1994.59
15	320	21276.6	105.29	105.07	104.93	105.12	90.44	90.18	90.09	90.22	9.79	2172.36
16	360	23936.17	106.71	106.42	105.41	106.45	90.48	90.25	90.14	90.31	10.25	2336.43
17	400	26595.75	107.43	107.21	106.65	107.27	90.55	90.37	90.21	90.4	10.41	2553.91
18	440	29255.32	108.62	108.35	107.44	108.37	90.65	90.45	90.24	90.47	10.76	2717.95

Table A2 (Contd.)

Run No.	HEAT INPUT Q(W)	HEAT FLUX ,q (W/m^2)	Wall Temp.; Tw_o(°C)				Liquid Pool Temperature, T_{lm} °C				WALL SUPERHEAT, ΔT_w °C	HEAT TRANSFER COEFFICIENT, h W/m^2 °C
			TOP	SIDE	BOTTOM	SIDE	TOP	SIDE	BOTTOM	SIDE		
	Pressure: 57.12 kN/m^2											
19	240	15957.45	99.13	98.89	98.21	98.92	85.61	85.47	85.31	85.48	9.51	1677.26
20	280	18617.02	100.06	99.85	99.75	99.88	85.63	85.48	85.32	85.5	9.96	1868.8
21	320	21276.6	101.41	101.15	100.43	101.17	85.68	85.51	85.35	85.55	10.44	2037.55
22	360	23936.17	102.51	102.31	101.04	102.34	85.71	85.56	85.39	85.61	10.77	2221.87
23	400	26595.75	103.56	103.23	102.98	103.28	85.74	85.63	85.41	85.66	11.31	2352.51
24	440	29255.32	104.29	104.05	103.61	104.08	85.79	85.71	85.48	85.72	11.35	2576.65
	Pressure:45.47 kN/m^2											
25	240	15957.45	94.05	9.68	93.12	93.74	79.89	79.75	79.59	79.75	10.09	1580.45
26	280	18617.02	95.15	95.02	93.64	95.06	79.92	79.76	79.62	79.77	10.51	1771.24
27	320	21276.6	96.45	96.23	95.01	96.26	79.95	79.79	79.64	79.81	11.11	1914.87
28	360	23936.17	97.61	97.39	96.15	97.42	79.99	79.84	79.69	79.88	11.58	2066.4
29	400	26595.75	98.85	98.61	97.25	98.67	80.07	79.89	79.75	79.92	12.09	2199.95
30	440	29255.32	99.32	99.18	98.07	99.2	80.18	79.95	79.85	79.98	11.97	2443.24

Table A.3 : Boiling Heat Transfer Data of 0.005% Alumina - Distilled Water Nanofluid over Horizontal Stainless Steel Heating Tube

Run No.	HEAT INPUT Q(W)	HEAT FLUX ,q (W/m^2)	Wall Temp.; Tw_o(°C)				Liquid Pool Temperature, T_{lm} °C				WALL SUPERHEAT, ΔT_w °C	HEAT TRANSFER COEFFICIENT, h W/m^2 °C
			TOP	SIDE	BOTTOM	SIDE	TOP	SIDE	BOTTOM	SIDE		
	Pressure: 97.71 kN/m^2											
1	240	15957.45	110.25	110.05	109.74	110.09	98.12	98.08	98.05	98.08	8.14	1959.59
2	280	18617.02	111.18	111.01	110.79	111.06	98.14	98.08	98.06	98.1	8.47	2196.89
3	320	21276.6	112.61	112.27	111.45	112.29	98.32	98.22	98.14	98.24	8.85	2403.52
4	360	23936.17	113.48	113.19	112.84	113.24	98.41	98.31	98.28	98.34	9.14	2617.76
5	400	26595.75	114.58	114.41	113.89	114.45	98.53	98.5	98.35	98.49	9.52	2793.08
6	440	29255.32	115.38	115.19	115.03	115.21	98.57	98.51	98.38	98.51	9.73	3005.71
	Pressure:85.17 kN/m2											
7	240	15957.45	107.42	107.27	106.88	107.29	94.91	94.85	94.71	94.86	8.58	1860.12
8	280	18617.02	108.69	108.41	107.28	108.48	94.96	94.86	94.71	94.88	8.92	2086.88
9	320	21276.6	109.72	109.45	108.05	109.51	94.99	94.89	94.75	94.92	9.22	2308.47
10	360	23936.17	110.81	110.44	109.17	110.47	95.08	94.95	94.82	94.98	9.56	2505.09
11	400	26595.75	111.98	111.69	110.55	111.71	95.19	95.08	94.95	95.11	10.05	2645.31
12	440	29255.32	112.59	112.47	111.48	112.51	95.25	95.14	95.01	95.17	10.14	2885.18
	Pressure: 71.11 kN/m^2											
13	240	15957.45	102.76	102.52	101.98	102.54	89.78	89.71	89.65	89.73	8.93	1787.45
14	280	18617.02	103.83	103.51	102.74	103.53	89.81	89.72	89.65	89.74	9.24	2016.14
15	320	21276.6	104.98	104.65	103.48	104.67	89.87	89.75	89.68	89.76	9.61	2214.97
16	360	23936.17	106.12	105.92	104.56	105.99	89.95	89.83	89.76	89.84	10.09	2371.5
17	400	26595.75	106.91	106.74	105.94	106.77	90.08	89.94	89.89	89.96	10.28	2587.14
18	440	29255.32	107.94	107.72	107.14	107.77	90.24	90.05	89.95	90.08	10.58	2764.04

Table A3 (Contd.)

Run No.	HEAT INPUT Q(W)	HEAT FLUX ,q (W/m^2)	Wall Temp.; Tw_o(°C)				Liquid Pool Temperature, T_{lm} °C				WALL SUPERHEAT, ΔT_w °C	HEAT TRANSFER COEFFICIENT, h W/m^2 °C
			TOP	SIDE	BOTTOM	SIDE	TOP	SIDE	BOTTOM	SIDE		
	Pressure: 57.12 kN/m^2											
19	240	15957.45	98.62	98.38	97.92	98.4	85.09	85.01	84.88	85.01	9.53	1675.19
20	280	18617.02	99.58	99.39	98.65	99.43	85.11	85.03	84.89	85.02	9.81	1897.23
21	320	21276.6	100.85	100.46	99.72	100.48	85.17	85.06	84.94	85.07	10.24	2078.3
22	360	23936.17	101.98	101.7	100.56	101.75	85.25	85.14	85.03	85.14	10.65	2248.16
23	400	26595.75	103.07	102.84	101.99	102.89	85.37	85.22	85.14	85.21	11.12	2392.56
24	440	29255.32	103.63	103.45	102.65	103.48	85.42	85.25	85.17	85.26	11.05	2648.32
	Pressure:45.47 kN/m^2											
25	240	15957.45	93.71	93.48	92.71	93.49	79.47	79.39	79.25	79.42	10.16	1571.05
26	280	18617.02	94.32	94.18	93.59	94.21	79.51	79.4	79.26	79.43	10.23	1819.18
27	320	21276.6	95.86	95.62	94.45	95.68	79.58	79.43	79.3	79.45	10.89	1954.67
28	360	23936.17	96.79	96.56	95.63	96.59	79.65	79.45	79.35	79.49	11.19	2137.35
29	400	26595.75	97.98	97.77	96.83	97.84	79.77	79.51	79.42	79.54	11.70	2273.03
30	440	29255.32	98.56	98.34	97.55	98.37	79.83	79.55	79.48	79.59	11.62	2518.21

Table A.4 : Boiling Heat Transfer Data of 0.01% Alumina - Distilled Water Nanofluid over Horizontal Stainless Steel Heating Tube

Run No.	HEAT INPUT Q(W)	HEAT FLUX ,q (W/m^2)	Wall Temp.; Tw_o(°C)				Liquid Pool Temperature, T_{lm} °C				WALL SUPERHEAT, ΔT_w °C	HEAT TRANSFER COEFFICIENT, h W/m^2 °C
			TOP	SIDE	BOTTOM	SIDE	TOP	SIDE	BOTTOM	SIDE		
	Pressure: 97.71 kN/m^2											
1	240	15957.45	108.35	107.86	107.27	107.91	96.31	96.26	96.21	96.28	7.78	2052.34
2	280	18617.02	109.31	109.14	108.23	109.18	96.34	96.27	96.22	96.28	8.25	2257.08
3	320	21276.6	110.41	110.21	109.31	110.25	96.39	96.31	96.26	96.33	8.64	2462.93
4	360	23936.17	111.57	111.17	110.47	111.24	96.48	96.37	96.31	96.4	9.01	2656.03
5	400	26595.75	112.53	112.35	111.63	112.39	96.54	96.44	96.38	96.47	9.42	2821.98
6	440	29255.32	113.45	113.24	112.74	113.27	96.59	96.48	96.41	96.51	9.69	3016.56
	Pressure:85.17 kN/m^2											
7	240	15957.45	105.52	105.31	104.91	105.35	93.53	93.41	93.29	93.43	8.05	1982.12
8	280	18617.02	107.07	106.87	105.84	106.91	93.55	93.43	93.29	93.43	8.81	2114.49
9	320	21276.6	107.99	107.71	106.67	107.77	93.59	93.48	93.35	93.49	8.99	2367.75
10	360	23936.17	109.03	108.85	107.18	108.91	93.67	93.52	93.41	93.55	9.23	2593.65
11	400	26595.75	110.13	109.91	108.91	109.97	93.74	93.56	93.45	93.58	9.81	2711.71
12	440	29255.32	111.05	110.83	109.79	110.85	93.79	93.59	93.51	93.62	10.02	2918.96
	Pressure: 71.11 kN/m^2											
13	240	15957.45	101.32	101.15	100.43	101.19	88.78	88.65	88.51	88.68	8.56	1863.64
14	280	18617.02	102.56	102.37	101.64	102.41	88.81	88.68	88.53	88.71	9.12	2042.01
15	320	21276.6	103.49	103.29	102.53	103.32	88.86	88.74	88.57	88.74	9.35	2274.96
16	360	23936.17	104.71	104.51	103.65	104.54	88.93	88.79	88.64	88.77	9.86	2426.99
17	400	26595.75	105.59	105.42	104.27	105.49	88.99	88.87	88.73	88.88	9.98	2665.37
18	440	29255.32	106.58	106.35	105.83	106.41	89.04	88.92	88.77	88.95	10.39	2814.84

Table A4 (Contd.)

Run No.	HEAT INPUT Q(W)	HEAT FLUX ,q (W/m^2)	Wall Temp.; Tw_o(°C)				Liquid Pool Temperature, T_{lm} °C				WALL SUPERHEAT, ΔT_w °C	HEAT TRANSFER COEFFICIENT, h W/m^2 °C
			TOP	SIDE	BOTTOM	SIDE	TOP	SIDE	BOTTOM	SIDE		
	Pressure: 57.12 kN/m^2											
19	240	15957.45	96.65	96.42	95.71	96.49	83.65	83.57	83.51	83.59	8.93	1786.69
20	280	18617.02	97.83	97.66	96.85	97.69	83.67	83.58	83.52	83.61	9.47	1965.38
21	320	21276.6	99.15	98.83	98.23	98.88	83.71	83.62	83.56	83.63	10.06	2114.13
22	360	23936.17	99.95	99.71	99.12	99.77	83.78	83.68	83.63	83.67	10.24	2338.32
23	400	26595.75	101.04	100.83	99.97	100.85	83.87	83.75	83.69	83.72	10.57	2515.68
24	440	29255.32	101.98	101.74	100.93	101.79	83.96	83.79	83.74	83.76	10.82	2704.01
	Pressure:45.47 kN/m^2											
25	240	15957.45	91.53	91.41	90.55	91.44	78.05	78.01	77.92	78.04	9.42	1693.41
26	280	18617.02	92.69	92.39	91.61	92.44	78.08	78.03	77.96	78.07	9.81	1898.73
27	320	21276.6	93.89	93.71	92.56	93.75	78.14	78.07	78.01	78.11	10.32	2061.99
28	360	23936.17	95.14	94.97	93.87	94.99	78.21	78.1	78.06	78.14	10.89	2195.98
29	400	26595.75	96.15	96.03	94.54	96.09	78.31	78.18	78.11	78.22	11.15	2384.52
30	440	29255.32	96.89	96.71	95.25	96.74	78.38	78.25	78.17	78.27	11.15	2624.91

Table A.5 : Boiling Heat Transfer Data of 0.05% Alumina - Distilled Water Nanofluid over Horizontal Stainless Steel Heating Tube

Run No.	HEAT INPUT Q(W)	HEAT FLUX ,q (W/m^2)	Wall Temp.; Tw_o(°C)				Liquid Pool Temperature, T_{lm} °C				WALL SUPERHEAT, ΔT_w °C	HEAT TRANSFER COEFFICIENT, h W/m^2 °C
			TOP	SIDE	BOTTOM	SIDE	TOP	SIDE	BOTTOM	SIDE		
	Pressure: 97.71 kN/m^2											
1	240	15957.45	105.38	105.26	104.69	105.29	95.08	95.02	94.89	95.05	6.34	2518.14
2	280	18617.02	106.59	106.38	105.35	106.43	95.11	95.03	94.92	95.06	6.72	2772.45
3	320	21276.6	107.81	107.59	106.57	107.64	95.16	95.07	94.99	95.08	7.25	2935.04
4	360	23936.17	108.61	108.41	107.63	108.45	95.22	95.11	95.07	95.13	7.44	3218.74
5	400	26595.75	109.43	109.31	108.79	109.35	95.29	95.19	95.15	95.18	7.67	3465.69
6	440	29255.32	110.38	110.29	109.67	110.33	95.36	95.22	95.18	95.24	7.94	3685.47
	Pressure:85.17 kN/m2											
7	240	15957.45	102.95	102.74	102.03	102.77	92.23	92.15	92.03	92.18	6.67	2393.19
8	280	18617.02	104.06	103.81	102.97	103.85	92.26	92.15	92.06	92.19	7.06	2635.39
9	320	21276.6	105.19	105.03	104.11	105.07	92.31	92.19	92.13	92.21	7.56	2814.27
10	360	23936.17	106.03	105.84	105.04	105.91	92.39	92.25	92.23	92.28	7.710	3104.46
11	400	26595.75	106.98	106.79	106.17	106.85	92.46	92.34	92.29	92.35	7.99	3327.95
12	440	29255.32	107.94	107.77	107.35	107.83	92.51	92.41	92.36	92.4	8.32	3515.11
	Pressure: 71.11 kN/m^2											
13	240	15957.45	98.56	98.33	97.75	98.39	87.45	87.31	87.23	87.35	7.12	2242.87
14	280	18617.02	99.64	99.47	98.31	99.53	87.48	87.33	87.28	87.36	7.44	2503.72
15	320	21276.6	100.73	100.55	99.72	100.61	87.53	87.37	87.36	87.43	7.90	2692.38
16	360	23936.17	101.67	101.49	100.81	101.53	87.59	87.41	87.39	87.46	8.20	2918.87
17	400	26595.75	102.59	102.41	102.06	102.44	87.68	87.47	87.44	87.53	8.50	3128.71
18	440	29255.32	103.45	103.33	102.85	103.35	87.72	87.53	87.47	87.55	8.69	3365.18

Table A5(Contd.)

Run No.	HEAT INPUT Q(W)	HEAT FLUX ,q (W/m^2)	Wall Temp.; Tw_o(°C)				Liquid Pool Temperature, T_{lm} °C				WALL SUPERHEAT, ΔT_w °C	HEAT TRANSFER COEFFICIENT, h W/m^2 °C
			TOP	SIDE	BOTTOM	SIDE	TOP	SIDE	BOTTOM	SIDE		
	Pressure: 57.12 kN/m^2											
19	240	15957.45	93.64	93.49	92.93	93.51	82.12	82.04	81.93	82.06	7.55	2114.55
20	280	18617.02	94.89	94.69	93.85	94.72	82.14	82.05	81.96	82.06	8.04	2314.69
21	320	21276.6	96.03	95.77	94.77	95.81	82.18	82.08	82.01	82.09	8.43	2523.77
22	360	23936.17	96.91	96.45	95.47	96.56	82.25	82.13	82.06	82.15	8.49	2818.64
23	400	26595.75	97.82	97.51	96.84	97.56	82.34	82.21	82.15	82.25	8.85	3004.37
24	440	29255.32	98.94	98.79	97.65	98.85	82.39	82.26	82.19	82.28	9.29	3148.56
	Pressure:45.47 kN/m^2											
25	240	15957.45	88.85	88.69	87.93	88.72	76.72	76.64	76.54	76.65	8.10	1969.02
26	280	18617.02	90.36	90.04	89.13	90.08	76.75	76.65	76.57	76.66	8.81	2113.77
27	320	21276.6	91.14	90.97	90.29	91.03	76.81	76.68	76.63	76.71	9.07	2344.92
28	360	23936.17	91.98	91.83	90.95	91.89	76.89	76.73	76.67	76.75	9.19	2604.02
29	400	26595.75	92.93	92.78	91.93	92.87	76.97	76.78	76.74	76.79	9.46	2811.32
30	440	29255.32	94.21	94.08	92.65	94.14	77.05	76.81	76.77	76.84	9.93	2947.57

Table A.6 : Boiling Heat Transfer Data of 0.1% Alumina - Distilled Water Nanofluid over Horizontal Stainless Steel Heating Tube

Run No.	HEAT INPUT Q(W)	HEAT FLUX ,q (W/m^2)	Wall Temp.; Tw_o(°C)				Liquid Pool Temperature, T_{lm} °C				WALL SUPERHEAT, ΔT_w °C	HEAT TRANSFER COEFFICIENT, h W/m^2 °C
			TOP	SIDE	BOTTOM	SIDE	TOP	SIDE	BOTTOM	SIDE		
	Pressure: 97.71 kN/m^2											
1	240	15957.45	107.67	107.54	107.25	107.59	96.83	96.75	96.71	96.73	6.95	2296.15
2	280	18617.02	108.98	108.77	108.43	108.81	96.83	96.76	96.71	96.75	7.54	2467.83
3	320	21276.6	110.11	109.95	109.25	110.03	96.87	96.79	96.74	96.77	7.97	2671.19
4	360	23936.17	111.34	111.16	110.81	111.21	96.92	96.82	96.79	96.82	8.58	2788.38
5	400	26595.75	112.94	112.85	112.14	112.89	96.96	96.84	96.83	96.86	9.49	2802.31
6	440	29255.32	114.49	114.35	113.75	114.41	96.98	96.87	96.83	96.88	10.39	2815.65
	Pressure:85.17 kN/m2											
7	240	15957.45	105.41	105.24	104.94	105.27	94.19	94.11	94.02	94.12	7.29	2187.45
8	280	18617.02	106.59	106.43	105.81	106.49	94.2	94.13	94.05	94.13	7.76	2398.34
9	320	21276.6	107.94	107.83	107.16	107.88	94.23	94.16	94.09	94.18	8.46	2514.72
10	360	23936.17	108.87	108.75	108.13	108.79	94.27	94.21	94.14	94.22	8.714868255	2746.59
11	400	26595.75	110.47	110.35	109.52	110.39	94.31	94.24	94.17	94.25	9.59	2771.94
12	440	29255.32	111.98	111.83	110.98	111.89	94.32	94.26	94.19	94.28	10.43	2804.19
	Pressure: 71.11 kN/m^2											
13	240	15957.45	103.39	103.26	102.46	103.29	91.83	91.74	91.59	91.76	7.57	2108.17
14	280	18617.02	104.56	104.44	103.77	104.49	91.85	91.75	91.62	91.78	8.12	2291.56
15	320	21276.6	106.19	106.03	105.27	106.08	91.88	91.78	91.67	91.82	9.03	2356.17
16	360	23936.17	107.63	107.48	106.74	107.57	91.92	91.83	91.71	91.85	9.82	2437.89
17	400	26595.75	108.97	108.81	108.42	108.86	91.95	91.87	91.74	91.88	10.56	2518.43
18	440	29255.32	110.36	110.23	109.69	110.29	91.97	91.89	91.78	91.92	11.27	2595.14

Table A6 (Contd.)

Run No.	HEAT INPUT Q(W)	HEAT FLUX ,q (W/m^2)	Wall Temp.; Tw_o(°C)				Liquid Pool Temperature, T_{lm} °C				WALL SUPERHEAT, ΔT_w °C	HEAT TRANSFER COEFFICIENT, h W/m^2 °C
			TOP	SIDE	BOTTOM	SIDE	TOP	SIDE	BOTTOM	SIDE		
	Pressure: 57.12 kN/m^2											
19	240	15957.45	100.19	100.03	99.27	100.08	88.36	88.21	88.15	88.22	7.87	2028.13
20	280	18617.02	101.78	101.69	101.28	101.74	88.39	88.23	88.18	88.25	8.92	2087.48
21	320	21276.6	103.65	103.52	103.17	103.59	88.42	88.27	88.19	88.3	10.11	2104.56
22	360	23936.17	105.27	105.14	104.42	105.19	88.48	88.31	88.24	88.36	10.95	2185.61
23	400	26595.75	106.56	106.41	105.89	106.47	88.53	88.36	88.28	88.39	11.59	2293.27
24	440	29255.32	107.98	107.84	107.22	107.91	88.56	88.39	88.32	88.44	12.33	2372.47
	Pressure:45.47 kN/m^2											
25	240	15957.45	97.38	97.24	96.47	97.27	85.19	85.1	85.03	85.11	8.17	1952.14
26	280	18617.02	99.04	98.89	98.55	98.96	85.22	85.11	85.06	85.14	9.29	2004.57
27	320	21276.6	100.69	100.54	100.13	100.59	85.26	85.14	85.08	85.17	10.25	2075.85
28	360	23936.17	102.28	102.14	101.66	102.21	85.31	85.18	85.13	85.21	11.16	2145.17
29	400	26595.75	103.69	103.51	102.99	103.58	85.34	85.23	85.17	85.26	11.85	2245.17
30	440	29255.32	104.89	104.73	104.25	104.79	85.36	85.25	85.19	85.29	12.42	2356.18

Table A.7 : Boiling Heat Transfer Data of 0.001% Copper Oxide - Distilled Water Nanofluid over Horizontal Stainless Steel Heating Tube

Run No.	HEAT INPUT Q(W)	HEAT FLUX ,q (W/m^2)	Wall Temp.; Tw_o(°C)				Liquid Pool Temperature, T_{lm} °C				WALL SUPERHEAT, ΔT_w °C	HEAT TRANSFER COEFFICIENT, h W/m^2 °C
			TOP	SIDE	BOTTOM	SIDE	TOP	SIDE	BOTTOM	SIDE		
	Pressure: 97.71 kN/m^2											
1	240	15957.45	112.85	112.77	112.65	112.8	100.25	100.18	100.15	100.2	8.77	1820.0679
2	280	18617.02	113.87	113.73	113.64	113.78	100.28	100.2	100.16	100.21	9.10	2045.58
3	320	21276.6	115.21	115.09	114.89	115.16	100.33	100.22	100.18	100.24	9.77	2178.72
4	360	23936.17	116.09	115.95	115.57	115.98	100.38	100.26	100.22	100.29	9.90	2417.4518
5	400	26595.75	116.89	116.74	116.58	116.81	100.41	100.29	100.26	100.31	10.09	2635.38
6	440	29255.32	117.98	117.85	117.54	117.91	100.45	100.34	100.29	100.36	10.48	2791.14
	Pressure:85.17 kN/m2											
7	240	15957.45	111.65	111.56	111.37	111.59	98.62	98.54	98.43	98.57	9.19	1735.46
8	280	18617.02	112.67	112.43	112.23	112.47	98.67	98.58	98.45	98.6	9.44	1972.16
9	320	21276.6	113.95	113.81	113.61	113.85	98.73	98.61	98.48	98.65	10.11	2104.45
10	360	23936.17	114.75	114.61	114.35	114.67	98.79	98.65	98.52	98.68	10.22	2341.16
11	400	26595.75	115.81	115.62	115.24	115.65	98.82	98.67	98.55	98.72	10.54	2522.54
12	440	29255.32	116.93	116.73	116.13	116.77	98.87	98.73	98.58	98.77	10.92	2678.14
	Pressure: 71.11 kN/m^2											
13	240	15957.45	109.78	109.65	109.31	109.67	96.28	96.15	96.04	96.18	9.64	1656.12
14	280	18617.02	110.95	110.74	110.17	110.81	96.31	96.23	96.11	96.25	10.00	1861.41
15	320	21276.6	112.19	111.98	111.51	112.03	96.39	96.29	96.19	96.31	10.55	2016.45
16	360	23936.17	113.41	113.24	112.82	113.29	96.43	96.32	96.21	96.34	11.16	2145.78
17	400	26595.75	114.05	113.89	113.35	113.93	96.48	96.41	96.29	96.43	11.06	2405.16
18	440	29255.32	115.26	115.14	114.67	115.19	96.53	96.45	96.35	96.48	11.64	2514.18

Table A7 (Contd.)

Run No.	HEAT INPUT Q(W)	HEAT FLUX ,q (W/m^2)	Wall Temp.; Tw_o(°C)				Liquid Pool Temperature, T_{lm} °C				WALL SUPERHEAT, ΔT_w °C	HEAT TRANSFER COEFFICIENT, h W/m^2 °C
			TOP	SIDE	BOTTOM	SIDE	TOP	SIDE	BOTTOM	SIDE		
	Pressure: 57.12 kN/m^2											
19	240	15957.45	107.38	107.21	106.93	107.25	93.14	93.08	93.03	93.11	10.29	1550.12
20	280	18617.02	108.77	108.68	108.03	108.69	93.17	93.09	93.05	93.15	10.99	1694.35
21	320	21276.6	109.69	109.49	109.11	109.53	93.21	93.13	93.08	93.18	11.23	1895.16
22	360	23936.17	110.94	110.75	110.19	110.79	93.25	93.15	93.11	93.2	11.78	2032.15
23	400	26595.75	111.78	111.61	111.23	111.63	93.31	93.23	93.16	93.26	11.98	2219.45
24	440	29255.32	113.14	112.93	112.55	112.97	93.38	93.27	93.21	93.31	12.62	2318.19
	Pressure:45.47 kN/m^2											
25	240	15957.45	106.28	106.11	105.65	106.14	91.54	91.41	91.31	91.43	10.82	1475.12
26	280	18617.02	108.23	108.05	107.54	108.09	91.56	91.44	91.33	91.47	12.09	1540.38
27	320	21276.6	109.23	108.93	108.41	108.98	91.59	91.48	91.38	91.52	12.31	1728.16
28	360	23936.17	110.31	110.19	109.31	110.23	91.64	91.53	91.41	91.55	12.77	1875.14
29	400	26595.75	111.27	111.11	110.67	111.18	91.67	91.55	91.47	91.58	13.15	2022.56
30	440	29255.32	112.27	112.05	111.84	112.09	91.72	91.59	91.51	91.65	13.47	2172.55

Table A.8 : Boiling Heat Transfer Data of 0.005% Copper Oxide - Distilled Water Nanofluid over Horizontal Stainless Steel Heating Tube

Run No.	HEAT INPUT Q(W)	HEAT FLUX ,q (W/m^2)	Wall Temp.; Tw_o(°C)				Liquid Pool Temperature, T_{lm} °C				WALL SUPERHEAT, ΔT_w °C	HEAT TRANSFER COEFFICIENT, h W/m^2 °C
			TOP	SIDE	BOTTOM	SIDE	TOP	SIDE	BOTTOM	SIDE		
	Pressure: 97.71 kN/m^2											
1	240	15957.45	111.27	111.15	110.71	111.17	99.02	98.93	98.85	98.95	8.33	1915.45
2	280	18617.02	112.41	112.25	111.96	112.28	99.05	98.94	98.88	98.95	8.83	2108.97
3	320	21276.6	113.35	113.21	112.98	113.24	99.09	98.97	98.92	98.99	9.13	2331.45
4	360	23936.17	114.39	114.26	113.64	114.31	99.11	98.99	98.95	99.03	9.42	2540.12
5	400	26595.75	115.43	115.29	114.94	115.33	99.14	99.04	98.99	99.07	9.84	2702.18
6	440	29255.32	116.27	116.08	115.67	116.15	99.17	99.07	99.03	99.11	9.97	2935.45
	Pressure:85.17 kN/m^2											
7	240	15957.45	110.27	110.15	109.73	110.19	97.65	97.58	97.43	97.59	8.72	1831.11
8	280	18617.02	111.46	111.31	110.68	111.33	97.67	97.59	97.45	97.61	9.17	2029.78
9	320	21276.6	112.56	112.41	111.72	112.47	97.71	97.62	97.49	97.65	9.59	2218.49
10	360	23936.17	113.37	113.19	112.97	113.24	97.74	97.66	97.56	97.68	9.82	2436.92
11	400	26595.75	114.45	114.31	114.08	114.38	97.78	97.69	97.59	97.73	10.26	2591.45
12	440	29255.32	115.29	115.11	114.77	115.17	97.81	97.72	97.63	97.75	10.38	2818.43
	Pressure: 71.11 kN/m^2											
13	240	15957.45	108.04	107.92	107.66	107.96	95.02	94.97	94.83	94.97	9.14	1745.68
14	280	18617.02	109.51	109.34	108.89	109.41	95.05	94.99	94.85	95.01	9.87	1885.63
15	320	21276.6	110.27	110.17	109.91	110.22	95.09	95.03	94.89	95.03	10.06	2115.68
16	360	23936.17	111.43	111.25	111.03	111.27	95.11	95.05	94.93	95.08	10.49	2280.61
17	400	26595.75	112.25	112.14	111.93	112.18	95.15	95.07	94.95	95.09	10.72	2481.31
18	440	29255.32	113.49	113.29	113.03	113.37	95.18	95.13	94.98	95.13	11.21	2609.18

Table A8 (Contd.)

Run No.	HEAT INPUT Q(W)	HEAT FLUX ,q (W/m^2)	Wall Temp.; Tw_o(°C)				Liquid Pool Temperature, T_{lm} °C				WALL SUPERHEAT, ΔT_w °C	HEAT TRANSFER COEFFICIENT, h W/m^2 °C
			TOP	SIDE	BOTTOM	SIDE	TOP	SIDE	BOTTOM	SIDE		
	Pressure: 57.12 kN/m^2											
19	240	15957.45	106.48	106.39	105.68	106.43	92.71	92.63	92.51	92.64	9.82	1625.78
20	280	18617.02	107.79	107.61	107.23	107.65	92.72	92.65	92.54	92.68	10.48	1776.33
21	320	21276.6	108.85	108.69	108.13	108.71	92.75	92.68	92.58	92.69	10.85	1961.45
22	360	23936.17	109.65	109.54	109.31	109.59	92.78	92.71	92.61	92.73	11.11	2155.08
23	400	26595.75	110.98	110.83	110.48	110.87	92.83	92.75	92.67	92.77	11.69	2273.26
24	440	29255.32	111.94	111.79	111.32	111.83	92.86	92.77	92.69	92.81	11.96	2445.18
	Pressure:45.47 kN/m^2											
25	240	15957.45	104.87	104.73	104.15	104.75	90.45	90.31	90.22	90.35	10.49	1521.57
26	280	18617.02	106.34	106.09	105.73	106.13	90.48	90.34	90.25	90.38	11.27	1651.49
27	320	21276.6	107.47	107.31	106.53	107.38	90.53	90.39	90.31	90.41	11.68	1820.98
28	360	23936.17	108.27	108.09	107.79	108.15	90.58	90.42	90.35	90.43	11.92	2007.38
29	400	26595.75	109.58	109.43	109.07	109.49	90.61	90.48	90.41	90.51	12.55	2119.84
30	440	29255.32	110.49	110.38	109.93	110.41	90.67	90.56	90.46	90.59	12.76	2293.52

Table A.9 : Boiling Heat Transfer Data of 0.01% Copper Oxide - Distilled Water Nanofluid over Horizontal Stainless Steel Heating Tube

Run No.	HEAT INPUT Q(W)	HEAT FLUX ,q (W/m^2)	Wall Temp.; Tw_o(°C)				Liquid Pool Temperature, T_{lm} °C				WALL SUPERHEAT, ΔT_w °C	HEAT TRANSFER COEFFICIENT, h W/m^2 °C
			TOP	SIDE	BOTTOM	SIDE	TOP	SIDE	BOTTOM	SIDE		
	Pressure: 97.71 kN/m^2											
1	240	15957.45	109.89	109.69	109.45	109.75	98.31	98.19	98.14	98.22	8.07	1978.61
2	280	18617.02	110.96	110.81	110.47	110.86	98.34	98.23	98.19	98.27	8.47	2198.01
3	320	21276.6	112.14	112.01	111.4	112.07	98.38	98.28	98.25	98.3	8.92	2385.14
4	360	23936.17	112.91	112.71	112.52	112.77	98.41	98.31	98.28	98.34	9.07	2639.0516
5	400	26595.75	114.07	113.89	113.35	113.95	98.46	98.36	98.33	98.38	9.48	2805.67
6	440	29255.32	114.99	114.89	114.55	114.93	98.48	98.39	98.35	98.43	9.84	2972.68
	Pressure:85.17 kN/m2											
7	240	15957.45	109.04	108.91	108.51	108.95	96.74	96.65	96.54	96.68	8.39	1901.46
8	280	18617.02	110.43	110.29	109.81	110.35	96.76	96.67	96.58	96.69	9.10	2045.12
9	320	21276.6	111.31	111.11	110.65	111.18	96.81	96.72	96.66	96.75	9.25	2299.65
10	360	23936.17	112.43	112.25	111.75	112.31	96.84	96.75	96.69	96.78	9.71	2465.12
11	400	26595.75	113.31	113.11	112.87	113.16	96.89	96.78	96.73	96.82	9.96	2670.12
12	440	29255.32	114.19	114.04	113.61	114.09	96.91	96.84	96.78	96.87	10.15	2881.11
	Pressure: 71.11 kN/m^2											
13	240	15957.45	106.37	106.21	105.53	106.27	93.53	93.38	93.25	93.42	8.89	1794.7955
14	280	18617.02	107.79	107.55	106.81	107.61	93.55	93.41	93.29	93.46	9.57	1945.23
15	320	21276.6	108.71	108.49	108.09	108.57	93.58	93.45	93.35	93.49	9.92	2145.12
16	360	23936.17	109.61	109.41	108.91	109.46	93.63	93.48	93.38	93.51	10.14	2360.89
17	400	26595.75	110.59	110.36	109.77	110.42	93.68	93.56	93.42	93.57	10.38	2561.48
18	440	29255.32	111.73	111.55	111.18	111.61	93.71	93.59	93.45	93.63	10.95	2672.81

Table A9 (Contd.)

Run No.	HEAT INPUT Q(W)	HEAT FLUX ,q (W/m^2)	Wall Temp.; Tw_o(°C)				Liquid Pool Temperature, T_{lm} °C				WALL SUPERHEAT, ΔT_w °C	HEAT TRANSFER COEFFICIENT, h W/m^2 °C
			TOP	SIDE	BOTTOM	SIDE	TOP	SIDE	BOTTOM	SIDE		
	Pressure: 57.12 kN/m^2											
19	240	15957.45	104.37	104.23	103.49	104.29	90.89	90.75	90.61	90.76	9.54	1673.2829
20	280	18617.02	105.81	105.67	104.95	105.73	90.91	90.78	90.65	90.78	10.32	1804.15
21	320	21276.6	106.56	106.45	105.88	106.52	90.95	90.83	90.68	90.84	10.45	2035.93
22	360	23936.17	107.63	107.51	107.06	107.54	90.97	90.87	90.72	90.89	10.86	2204.09
23	400	26595.75	108.91	108.77	108.18	108.83	91.02	90.89	90.78	90.94	11.42	2329.27
24	440	29255.32	109.67	109.51	109.11	109.54	91.05	90.92	90.83	90.96	11.54	2535.14
	Pressure:45.47 kN/m^2											
25	240	15957.45	102.96	102.81	102.14	102.87	88.74	88.63	88.49	88.65	10.26	1555.4969
26	280	18617.02	104.49	104.29	103.38	104.37	88.76	88.64	88.53	88.65	11.05	1685.47
27	320	21276.6	105.56	105.42	104.59	105.45	88.81	88.69	88.58	88.69	11.49	1852.38
28	360	23936.17	106.31	106.11	105.63	106.17	88.85	88.73	88.65	88.75	11.60	2062.87
29	400	26595.75	107.47	107.29	106.91	107.34	88.87	88.78	88.69	88.81	12.12	2194.18
30	440	29255.32	108.37	108.25	108.07	108.28	88.92	88.84	88.71	88.89	12.42	2355.09

Table A.10: Boiling Heat Transfer Data of 0.05% Copper Oxide - Distilled Water Nanofluid over Horizontal Stainless Steel Heating Tube

Run No.	HEAT INPUT Q(W)	HEAT FLUX ,q (W/m^2)	Wall Temp.; Tw_o(°C)				Liquid Pool Temperature, T_{lm} °C				WALL SUPERHEAT, ΔT_w °C	HEAT TRANSFER COEFFICIENT, h W/m^2 °C
			TOP	SIDE	BOTTOM	SIDE	TOP	SIDE	BOTTOM	SIDE		
	Pressure: 97.71 kN/m^2											
1	240	15957.45	106.72	106.56	106.16	106.59	95.57	95.48	95.39	95.48	7.22	2209.51
2	280	18617.02	107.93	107.75	107.28	107.83	95.59	95.49	95.43	95.5	7.78	2392.36
3	320	21276.6	108.93	108.81	108.39	108.88	95.64	95.52	95.45	95.54	8.14	2614.56
4	360	23936.17	109.78	109.69	109.18	109.73	95.68	95.56	95.49	95.59	8.31	2881.14
5	400	26595.75	110.78	110.61	110.04	110.67	95.74	95.59	95.55	95.62	8.56	3108.45
6	440	29255.32	111.89	111.81	110.73	111.85	95.77	95.63	95.58	95.66	8.94	3275.42
	Pressure:85.17 kN/m^2											
7	240	15957.45	105.68	105.49	104.79	105.54	94.12	94.02	93.91	94.05	7.54	2115.41
8	280	18617.02	106.95	106.81	106.03	106.87	94.15	94.04	93.94	94.05	8.18	2276.52
9	320	21276.6	107.66	107.56	107.08	107.59	94.19	94.07	93.98	94.09	8.32	2558.92
10	360	23936.17	108.98	108.78	108.03	108.87	94.23	94.11	94.05	94.15	8.82	2714.31
11	400	26595.75	109.57	109.43	109.11	109.48	94.26	94.14	94.08	94.18	8.89	2991.87
12	440	29255.32	110.81	110.67	110.18	110.72	94.28	94.18	94.11	94.22	9.42	3106.23
	Pressure: 71.11 kN/m^2											
13	240	15957.45	103.79	103.61	103.26	103.65	91.81	91.74	91.65	91.74	8.04	1985.64
14	280	18617.02	105.09	104.89	104.56	104.95	91.83	91.75	91.69	91.75	8.68	2145.89
15	320	21276.6	105.98	105.85	105.31	105.89	91.86	91.79	91.75	91.8	8.88	2395.11
16	360	23936.17	107.08	106.94	106.47	106.99	91.91	91.84	91.79	91.87	9.31	2571.34
17	400	26595.75	107.89	107.71	107.15	107.76	91.94	91.88	91.82	91.89	9.40	2829.19
18	440	29255.32	109.07	108.74	108.28	108.81	91.96	91.92	91.85	91.92	9.83	2975.41

Table A10 (Contd.)

Run No.	HEAT INPUT Q(W)	HEAT FLUX ,q (W/m^2)	Wall Temp.; Tw_o(°C)				Liquid Pool Temperature, T_{lm} °C				WALL SUPERHEAT, ΔT_w °C	HEAT TRANSFER COEFFICIENT, h W/m^2 °C
			TOP	SIDE	BOTTOM	SIDE	TOP	SIDE	BOTTOM	SIDE		
	Pressure: 57.12 kN/m^2											
19	240	15957.45	101.73	101.59	101.14	101.65	88.94	88.82	88.71	88.85	8.89	1795
20	280	18617.02	102.87	102.68	101.96	102.73	88.97	88.83	88.74	88.86	9.27	2008.12
21	320	21276.6	103.54	103.41	103.04	103.45	89.02	88.87	88.78	88.91	9.39	2265.43
22	360	23936.17	104.81	104.65	103.75	104.69	89.07	88.93	88.81	88.95	9.83	2435.14
23	400	26595.75	105.64	105.49	104.81	105.56	89.12	88.96	88.86	88.98	10.05	2645.19
24	440	29255.32	106.97	106.79	106.18	106.85	89.15	88.99	88.89	89.02	10.70	2733.16
	Pressure:45.47 kN/m^2											
25	240	15957.45	99.49	99.31	98.47	99.37	85.78	85.66	85.51	85.67	9.70	1645.11
26	280	18617.02	100.18	100.04	99.51	100.09	85.81	85.68	85.54	85.71	9.83	1893.29
27	320	21276.6	101.29	101.14	100.04	101.17	85.86	85.71	85.59	85.74	10.11	2104.38
28	360	23936.17	102.45	102.22	101.31	102.29	85.92	85.75	85.64	85.79	10.58	2261.73
29	400	26595.75	103.19	103.05	102.63	103.11	85.95	85.79	85.7	85.86	10.83	2456.81
30	440	29255.32	104.49	104.31	103.68	104.39	85.97	85.84	85.74	85.89	11.38	2571.14

Table A.11 : Boiling Heat Transfer Data of 0.1% Copper Oxide - Distilled Water Nanofluid over Horizontal Stainless Steel Heating Tube

Run No.	HEAT INPUT Q(W)	HEAT FLUX ,q (W/m^2)	Wall Temp.; Tw_o(°C)				Liquid Pool Temperature, T_{lm} °C				WALL SUPERHEAT, ΔT_w °C	HEAT TRANSFER COEFFICIENT, h W/m^2 °C
			TOP	SIDE	BOTTOM	SIDE	TOP	SIDE	BOTTOM	SIDE		
	Pressure: 97.71 kN/m^2											
1	240	15957.45	107.38	107.25	106.63	107.32	96.08	95.93	95.81	95.94	7.40	2156.45
2	280	18617.02	108.83	108.71	107.79	108.73	96.11	95.94	95.83	95.94	8.12	2293.56
3	320	21276.6	110.53	110.45	109.51	110.48	96.15	95.97	95.86	95.98	9.18	2318.96
4	360	23936.17	111.78	111.59	110.94	111.64	96.21	95.99	95.91	96.04	9.75	2456.12
5	400	26595.75	112.87	112.71	112.19	112.76	96.24	96.05	95.95	96.07	10.21	2604.95
6	440	29255.32	113.69	113.51	112.93	113.58	96.26	96.07	95.97	96.11	10.35	2827.67
	Pressure:85.17 kN/m2											
7	240	15957.45	105.16	105.01	104.23	105.06	93.45	93.37	93.25	93.38	7.69	2073.28
8	280	18617.02	106.74	106.52	106.15	106.58	93.46	93.37	93.27	93.39	8.69	2143.59
9	320	21276.6	108.04	107.94	107.19	107.98	93.49	93.41	93.31	93.42	9.30	2287.15
10	360	23936.17	109.23	109.11	108.27	109.17	93.54	93.43	93.35	93.45	9.79	2444.29
11	400	26595.75	110.73	110.55	109.91	110.59	93.59	93.46	93.39	93.49	10.62	2504.31
12	440	29255.32	111.94	111.74	111.25	111.81	93.61	93.48	93.41	93.52	11.20	2611.23
	Pressure: 71.11 kN/m^2											
13	240	15957.45	102.45	102.29	101.64	102.37	90.27	90.18	90.06	90.19	8.20	1945.18
14	280	18617.02	104.24	104.11	103.01	104.18	90.29	90.18	90.08	90.21	9.25	2012.78
15	320	21276.6	105.38	105.24	104.42	105.29	90.32	90.23	90.12	90.25	9.78	2175.89
16	360	23936.17	106.51	106.29	105.89	106.35	90.36	90.26	90.16	90.29	10.28	2327.81
17	400	26595.75	107.68	107.49	107.09	107.56	90.41	90.31	90.21	90.36	10.79	2465.18
18	440	29255.32	108.82	108.71	108.45	108.75	90.43	90.33	90.24	90.38	11.36	2576.14

Table A11 (Contd.)

Run No.	HEAT INPUT Q(W)	HEAT FLUX ,q (W/m^2)	Wall Temp.; Tw_o(°C)				Liquid Pool Temperature, T_{lm} °C				WALL SUPERHEAT, ΔT_w °C	HEAT TRANSFER COEFFICIENT, h W/m^2 °C
			TOP	SIDE	BOTTOM	SIDE	TOP	SIDE	BOTTOM	SIDE		
	Pressure: 57.12 kN/m^2											
19	240	15957.45	100.59	100.51	99.94	100.54	87.56	87.41	87.32	87.45	9.15	1743.59
20	280	18617.02	102.29	102.14	101.51	102.18	87.59	87.42	87.34	87.48	10.14	1836.78
21	320	21276.6	103.56	103.37	102.58	103.42	87.63	87.45	87.37	87.51	10.67	1994.37
22	360	23936.17	104.73	104.56	103.65	104.63	87.67	87.49	87.41	87.54	11.15	2145.72
23	400	26595.75	105.68	105.53	105.08	105.58	87.72	87.54	87.46	87.58	11.54	2304.17
24	440	29255.32	107.03	106.94	106.38	106.98	87.74	87.57	87.49	87.6	12.26	2387.32
	Pressure:45.47 kN/m^2											
25	240	15957.45	98.93	98.79	98.24	98.86	85.12	85.03	84.92	85.03	9.88	1615.47
26	280	18617.02	100.71	100.51	99.89	100.58	85.14	85.04	84.95	85.05	10.93	1702.56
27	320	21276.6	101.87	101.64	100.93	101.68	85.19	85.07	84.99	85.09	11.37	1871.29
28	360	23936.17	102.99	102.79	102.04	102.87	85.25	85.12	85.06	85.14	11.82	2025.18
29	400	26595.75	104.23	104.05	103.48	104.13	85.29	85.18	85.11	85.2	12.43	2138.94
30	440	29255.32	105.31	105.17	104.78	105.24	85.33	85.21	85.14	85.25	12.91	2265.45

Annexure - B

SAMPLE CALCULATION

This annexure presents the experimental data of pool boiling carried over Stainless Steel heating tube, wall and liquid pool temperature recorded in milli volt by thermocouples has been converted to degree centigrade and is presented in tabular form in Annexure – B.

The wall superheat and heat transfer coefficient of surface are computed with the help of temperature recorded from thermocouples in the experimental run. The following section explains step by step the procedure followed to determine the surface area of the heating tube, the heat flux, the wall superheat, the local heat transfer coefficient and average heat transfer coefficient for a particular set of data for heating tube.

B.1 HEATING TUBE DETAILS

In the present investigation two stainless steel heating tubes; one for Alumina-DW nanofluid and another for Copper Oxide – DW nanofluids are taken to obtain boiling heat transfer data for DW and for various nanofluids. The heating tube are made up of AISI-304 Stainless steel. The details of heating tube dimensions are given in the following Table C- 1

Table B-1 Detail Dimensions of Heating Tube

Heating Tube	Diameter of tube d, (m)	Inner Diameter d_i, (m)	Pitch Circle Diameter d_h ,(m)	Effective Length L ,(m)
HT - 1	0.032010	0.01801	0.0250	0.1500
HT - 2	0.032011	0.01799	0.0250	0.1500

B.2 BOILING HEAT TRANSFER COEFFICIENT ON STAINLESS STEEL HEATING TUBE

The procedure involved in the calculation of local as well as average heat transfer coefficient are shown below by taking the data of Run no. 2 from Table A– 1 of Annexure – A, which

corresponds to the data of boiling of distilled water over SS heating tube. For convenience, the data corresponding to this run is reproduced below.

Power Input, Q = 280 W				Pressure, P = 97.71 kN/m^2			
Wall Temperature, T_{wm} ^{O}C				Liquid Temperature, T_{lm} ^{O}C			
Top	Side	Bottom	Side	Top	Side	Bottom	Side
115.19	115.03	114.48	115.08	100.32	100.18	100.02	100.24

B.2.1 Heat Transfer Surface Area of Heating Tube, A

$$A = \pi d_o l \qquad = \pi \times 0.03194 \times 0.150$$

$$= 0.01504 \text{ m}^2 \qquad \text{(B-1)}$$

B.2.2 Heat Flux, q

$$q = \frac{Q}{A} \qquad \text{(B-2)}$$

$$= \frac{280}{0.01504}$$

$$= 18617.02 \text{ W/m}^2$$

B.2.3 Outer Surface Temperature of Heating Tube, T_{wo}

The outer surface temperature of the heating tube is computed by subtracting the temperature drop in the tube wall, δT_w from the measured wall temperature, T_{wm} as follows,

$$T_{wo} = T_{wm} - \delta T_w \qquad \text{(B-3)}$$

Where temperature drop, δT_w is calculated by using Fourier one dimensional heat conduction equation for thin cylinder as follows,

$$\delta T_w = \frac{q d_0}{2k_w} \ln\left(\frac{d_0}{d_h}\right) \qquad \text{(B-4)}$$

$$= \left(\frac{21276.6 \times 0.031940}{2 \times 16.4}\right) ln\left(\frac{0.031940}{0.02500}\right)$$

$$= 5.08\,℃$$

Now, the surface temperature of heating tube at top, side and bottom is calculated using the equation (C.3). The calculated values are given below in tabular form,

Position	Temperature, ^{0}C		
	T_{wm}	δT_w	T_{wo}
Top	116.09	5.08	111.01
Side	115.95	5.08	110.87
Bottom	115.21	5.08	110.13
Side	116.01	5.08	110.93

B.2.4 Local Wall Superheat, $\Delta T_{w\psi}$

Liquid pool temperature is subtracted from the wall surface temperature and this difference in temperature is used to compute the local heat ttransfer coefficient at four circumferential positions of heating tube viz. two sides , top and bottom positions. The relation is given below:

$$\Delta T_{w\psi} = T_{wo} - T_{lm} \qquad \text{(B-5)}$$

The table below shows the computed values of local wall super heat using the above equation :

Position	Temperature, ^{0}C		
	T_{wo}	T_{lm}	$\Delta T_{w\psi}$
Top	111.01	100.34	10.67
Side	110.87	100.26	10.61
Bottom	110.13	100.08	10.05
Side	110.93	100.28	10.65

B.2.5 Local Heat Transfer Coefficient, h_ψ

Eq C-6 is used to compute the local heat transfer coefficient at top, bottom and both sides, around the circumference of the heating tube which is given below,

$$h_\psi = \frac{q}{\Delta T_{w\psi}} \qquad \text{(B-6)}$$

The values of Local heat transfer coefficient obtained using the above equation are given below in tabular form,

Position	q, W/m^2	$\Delta T_{w\psi}$, ^{0}C	h_ψ, W/m^2 ^{0}C
Top	21276.6	10.67	1994.06
Side	21276.6	10.61	2005.34
Bottom	21276.6	10.05	2117.08
Side	21276.6	10.65	1997.8

B.2.6 Average Outer Surface Temperature of Heating Tube, $\bar{T}_{wo}$

The average outer surface temperature is calculated by taking arithmetic mean of outer surface temperature measured respectively at top, side, bottom and side of the heating tube. It is expressed by the following equation;

$$\bar{T}_{wo} = \frac{1}{4}\left(T_{(wo)t} + T_{(wo)s} + T_{(wo)b} + T_{(wo)s}\right) \qquad \text{(B-7)}$$

where, subscripts t, s and b represents top, side and bottom position on heating tube, respectively. Hence,

$$\bar{T}_{wo} = \frac{1}{4}(111.01 + 110.87 + 110.13 + 110.93) = 110.74$$

B.2.7 Average Liquid Temperature, $\overline{T}_{lm}$

The average liquid temperature is calculated by taking arithmetic mean of liquid pool temperature measured at top, two sides and bottom of the heating tube. It is expressed by the following equation;

$$\overline{T}_{lm} = \frac{1}{4}\left(T_{(lm)t} + T_{(lm)s} + T_{(lm)b} + T_{(lm)s}\right) \quad \text{(B-8)}$$

hence,

$$\bar{T}_{lm} = \frac{1}{4}(100.34 + 100.26 + 100.08 + 100.28) = 100.29$$

B.2.8 Wall Superheat, ΔT_w

The wall superheat of the heating tube is calculated by subtracting the average liquid temperature from the average outer surface temperature as follows,

$$\Delta T_w = \overline{T}_{wo} - \overline{T}_{lm} \quad \text{(B-9)}$$

hence,

$$\Delta T_w = 110.78 - 100.29 = 10.49\ ℃$$

B.2.9 Average Boiling Heat Transfer Coefficient, h

The average boiling heat transfer coefficient is calculated using following equation;

$$h = \frac{q}{\Delta T_w} \quad \text{(B-10)}$$

$$= \frac{21276.6}{10.5} = 2026.34\ W/m^2℃$$

Annexure - C

UNCERTAINTY ANALYSIS

The current investigation deals with the determination of following basic parameters like power input, temperature of the heating tube across four circumferential positions viz. top, bottom, and two sides, the corresponding temperature of the liquid pool and nanofluids around the heating tube surface and surface area of the heating tube. The experimental heat transfer coefficient is computed using this data. The data is recorded by using various instruments such as digital wattmeter records the power input to the heater, a digital multi meter is employed to measure the temperatures of heating tube surface and test liquid and the dimensions of heating tube are measured using the Vernier calipers. Each instrument has its own least count which accounts for the uncertainity in the recorded data. Thus, while computing the heat transfer coefficient measurement of uncertainity associated with the experimental value determined from each instrument becomes necessary in order to determine the net uncertainity associated with the heat transfer coefficient.

By using Schultz & Cole [ ] the maximum and minimum possible uncertainty in calculation of heat transfer coefficient can be determined. As per the method, the dependent variable x, is expressed as a function of the independent measured quantities (y_1, y_2, y_3……y_n) in the following form:

$$x = f(y_1, y_2, y_3 \ldots\ldots\ldots\ldots y_n)$$

The uncertainty, U_x associated with the variable x, is defined as the absolute value of the maximum expected deviation from the reported experimental data and is expressed mathematically by the relation given below

$$U_X = \left[\sum_{i=1}^{n} \left\{\left(\frac{\partial x}{\partial y_i}\right) U_{y_i}\right\}^2\right]^{1/2} \qquad \text{(C-1)}$$

where, U_{y_i} is the uncertainty associated with quantity y_i.

In order to visualize the uncertainty associated with the calculated average heat transfer coefficient a demo calculation is shown below by taking data for the run no. 8 of Table A-2 of

Annexure-A for the boiling of Alumina – DW over plain heating tube. The set of data taken is given again below for ready reference.

Power input =280W				Pressure =85.17 kN/m^2			
Liquid Temperature, T_{lm}				Wall Temperature, T_{wm}			
Top	Side	Bottom	Side	Top	Side	Bottom	Side
95.69	95.58	95.33	95.61	109.45	109.24	108.56	109.27

C-1 Uncertainty in Power Input, U_Q

A digital wattmeter having least count 1 Watt is used in the present investigation to determine the power supplied to the heating tube. Thus, the maximum possible uncertainty associated in the measurement of power supply is 1 Watt.

Hence, $U_Q = [(Q)^2]^{1/2}$ = 1 W

C-2 Uncertainty in the Surface Area of the Heating Tube, U_A

The surface area of the plain heating tube is given by,

$$A = \pi d_o l \qquad = \pi \times 0.03194 \times 0.150$$

$$= 0.01504 \text{ m}^2$$

Therefore, the uncertainty associated with the heating tube surface area is given by the following expression,

$$U_A = \left[(\pi d_0 U_1)^2 + \left(\pi l U_{d_0}\right)^2\right]^{1/2} \qquad \text{(C-2)}$$

where, U_l and U_{d_0} are the uncertainties associated with the measurement of the effective length and the outside diameter of the heating tube respectively. The measurement of effective length and the outside diameter of the heating tube is done with the help of a vernier caliper having least count 0.01 mm.

So, $U_l = U_{d_0} = 1 \times 10^{-5}$ m

Putting the values of U_l and U_{d_0} in the above equation, we will get,

$$U_A = \left[(\pi \times 0.032010 \times 1 \times 10^{-5})^2 + (\pi \times 0.1504 \times 1 \times 10^{-5})^2{}^{1/2}\right]$$

$$U_A = 0.0000048290 \text{ m}^2$$

Thus the uncertainty in the measurement of surface area of the heating tube varies from 0.015005171 to 0.015014829 m2.

C-3 Uncertainty in Heat Flux, U_q

The heat flux is given by, $q = \frac{Q}{A}$

$$= \frac{280}{0.01504}$$

$$= 18617.02 \text{ W/m}^2$$

therefore, the uncertainty associated with the heat flux is given by the following expression,

$$U_q = \left[\left(\frac{U_Q}{A}\right)^2 + \left(-\frac{QU_A}{A}\right)^2\right]^{1/} \qquad \text{(C-3)}$$

Where, U_Q is the uncertainty associated with the measurement of input power and is equal to 1 W

$$U_q = \left[\left(\frac{1}{0.01504}\right)^2 + \left(-\frac{280 \times 0.0000048290}{A}\right)^2\right]^{1/}$$

$$U_q = \left[\left(\frac{1}{0.01504}\right)^2 + \left(-\frac{280 \times 0.0000048290}{0.01504}\right)^2\right]^{\frac{1}{2}}$$

So,

$$U_q = 92.5912 \text{ W/m}^2$$

Thus, the uncertainty in the measurement of heat flux varies from 18617.02 to 18709.61 W/m^2.

C-4 Uncertainty in Heating Tube Surface Temperature, $\mathbf{UT_{wm}}$

The heating tube wall and liquid temperature are measured by Copper constantan thermocouple probes. However, instead of direct temperature the e.m.f. of thermocouples are measured by a digital multimeter having least count of 0.001mV. From e.m.f-temperature chart, it is found that the value of 0.001 mV corresponds to 0.021^0C.

Thus, the uncertainty in the measurement of tube wall and liquid temperature is 0.021^0C.

Hence, $$U_{T_{wm}} = U_{T_{lm}} = 0.021^0C$$

Outer surface temperature = Measured wall temperature – Temperature drop

i.e. $$T_{wo} = T_{wm} - \delta T_w$$

where, temperature drop, δT_w, is given by,

$$\delta T_w = \frac{qd_0}{2k_w} \ln\left(\frac{d_0}{d_h}\right)$$

$$\delta T_w = \left(\frac{18617.02 \times 0.03201}{2 \times 108.75} ln\left(\frac{0.03201}{0.025}\right)\right)$$

$$= 0.727054764^0C$$

Hence, the Uncertainty associated with the temperature difference is given by the following expression:

$$U_{\delta T_w} = \left[\left\{\frac{d_0}{2k_w}\ln\left(\frac{d_0}{d_h}\right)U_q\right\}^2 + \left\{\left(\frac{q}{2k_w}\ln\left(\frac{d_0}{d_h}\right) + \frac{q}{2k_w}\right)U_{d_0}\right\}^2 + \left\{\frac{-qd_0}{2k_w^2}\ln\left(\frac{d_0}{d_h}\right)U_{k_w}\right\}^2 + \left\{\frac{qd_0}{2k_w}\left(\frac{-1}{d_h}\right)U_{d_h}\right\}^2\right]^{1/2} \quad \text{(C-4)}$$

Where,

U_{k_w} :is the uncertainty in the value of thermal conductivity of the heating tube material.

Assumption: U_{kw} is assumed to be equal to zero as the value of thermal conductivity of Stainless Steel material is taken from trusted PERRY'S HAND BOOK [121] and it is assumed that there is no uncertainty in the value of thermal conductivity.

Therefore,

$$U_{\delta T} = \left[\left\{\frac{0.0312010}{2\times108.75} ln\left(\frac{0.0312010}{0.025}\right)\times 92.5912\right\}^2 + \left\{\left(\frac{18617.02}{2\times108.75} ln\left(\frac{0.03185}{0.025}\right) + \frac{18617.02}{2\times389.34}\right)\times 1 \times \right.$$

$$10-52-18617.02\times.0312012\times108.752ln0.0312010.025\times0.012+18617.02\times.0312012\times108.75-10.0251\times10-5212$$

$$= 0.001119\ ^0C$$

Now, the surface temperature of the heating tube around its circumference at top, bottom and sides is calculated by subtracting δT_w from measured wall temperature. The details are given in a tabular form in the following table.

Position	Temperature, ^0C		
	T_{wm}	δT_w	T_{wo}
Top	109.45	0.72	108.73
Side	109.24	0.72	108.52
Bottom	108.56	0.72	107.84
Side	109.27	0.72	108.55

Hence, the uncertainty in outer surface temperature $U_{T_{wo}}$ is given by,

$$U_{T_{wo}} = \left[\left(U_{T_{wm}}\right)^2 + \left(-U_{\delta T_w}\right)^2\right]^{1/2} \qquad \text{(C-5)}$$

$$= [(0.072\ \ )^2 + (0.0011119)^2]^{1/2}$$

$$= 0.07210085\ ^0C$$

Thus, the uncertainty associated in the measurement of temperature of outer surface at top, sides or bottom of the heating tube is 0.021029 ^0C.

However, in the calculation of average heat transfer coefficient, we need to calculate average outer surface temperature and hence important to know the uncertainty associated in average outer surface temperature.

The average outer surface temperature is taken as arithmetic mean of the surface temperature of the heating tube at top, sides and bottom. Mathematically,

$$\overline{T}_{wo} = \frac{1}{4}\left(T_{wo,t} + T_{wo,s} + T_{wo,b} + T_{wo,s}\right)$$

where, subscripts t, s and b denotes the position on heating tube(t- top, s- side and b -bottom position) on heating tube respectively.

$T_{wo} = \frac{1}{4}((108.73+108.52+107.84+108.55)$

So, $= 108.41$

Now, the uncertainty associated with the average outer surface temperature is given by the following expression,

$$U_{\overline{T}_{wo}} = \left[\frac{1}{4}\left\{\left(U_{T_{wo.t}}\right)^2 + \left(U_{T_{wo.s}}\right)^2 + \left(U_{T_{wo.b}}\right)^2 + \left(U_{T_{wo.s}}\right)^2\right\}\right]^{1/2} \quad \text{(C-6)}$$

$$U_{\overline{T}_{wo}} = \left[\frac{1}{4}\{(0.001119)^2 + (0.001119)^2 + (0.001119)^2 + (0.001119)^2\}\right]^{1/2}$$

$U_{\overline{T}_{wo}} = 0.001119\ ^0C$

C-5 Uncertainty in Liquid Temperature, $U_{T_{lm}}$

As mentioned in section D-4 the uncertainty in the measurement of liquid temperature is 0.021^0C.

Hence, $U_{T_{lm}} = 0.021^0C$

Like average surface temperature, we need to determine the average liquid temperature and to find out the uncertainty associated with it. The average liquid temperature $\overline{T_l}$ is given by,

$$\overline{T}_l = \frac{1}{4}\left(T_{lm,t} + T_{lm,s} + T_{lm,b} + T_{lm,s}\right)$$

$$\overline{T_l} = \frac{1}{4}(95.69 + 95.58 + 95.33 + 95.61) = 95.55℃$$

Now, the uncertainty associated with the average liquid temperature is given by the following expression,

$$U_{\bar{T}_{lm}} = \left[\frac{1}{3}\left\{\left(U_{T_{lm,t}}\right)^2 + \left(U_{T_{lm,s}}\right)^2 + \left(U_{T_{lm,b}}\right)^2\right\}\right]^{\frac{1}{2}} \quad \text{(C-7)}$$

$$U_{\bar{T}_{lm}} = \left[\frac{1}{3}\left\{(0.072)^2 + (0.072)^2 + (0.072)^2\right\}\right]^{\frac{1}{2}}$$
$$= 0.0721^0 C$$

C-6 Uncertainty in Wall Superheat Temperature, $U_{\Delta Tw}$

The wall superheat i.e. the temperature difference between the average outer surface temperature of the heating tube and average liquid temperature is calculated using the expression as follows;

$$\Delta T_w = \bar{T}_{wo} - \bar{T}_l$$
$$= 108.41 - 95.55$$
$$= 12.86\ °C$$

So, the uncertainty associated with the wall super heat is given by the following expression,

$$U_{\Delta T_w} = \left[\left(U_{\bar{T}_{wo}}\right)^2 + \left(-U_{\bar{T}_l}\right)^2\right]^{\frac{1}{2}} \quad \text{(C-8)}$$

$$U_{\Delta T_w} = \left[(0.001119)^2 + (-0.0721)^2\right]^{\frac{1}{2}}$$
$$= 0.07210085^0 C$$

C-7 Uncertainty in Heat Transfer Coefficient, $U_{\bar{h}}$

The average heat transfer coefficient is determined by the following expression,

$$\bar{h} = \frac{q}{\Delta T_w} = \frac{18617.02}{9.14}$$

$=2037.12\ W/m^2\ °C$

So, the uncertainty associated with the average heat transfer coefficient is given by,

$$U_{\bar{h}} = \left[\left(\frac{U_q}{\Delta T_w}\right)^2 + \left(-\frac{qU_{\Delta T_w}}{\Delta T_w{}^2}\right)^2\right]^{\frac{1}{2}} \qquad \text{(C-9)}$$

$$= \left[\left(\frac{92.52}{9.14}\right)^2 + \left(\frac{18617.02 \times U_{\Delta T_w}}{(9.14)^2}\right)^2\right]^{\frac{1}{2}}$$

$$= 34.48\ W/m^2{}^{\circ}\mathrm{C}$$

Thus, the uncertainty associated with the average heat transfer coefficient varies from 2037.12 to 2071.6 W/m^2 ^{0}C i.e. 1.69% of the experimental value. Uncertainity associated with the measurement of average heat transfer coefficient for all experimental runs is determined by the similar procedure as explained and the maximum value of uncertainty is found to be 1.69% which is well within the acceptable limit. Therefore, the experimental data obtained in the present investigation may be considered to be reliable and consistent within the acceptable limit.

REFERENCES

A1. Agarwal S., Jayaraman G., Srivastava V.K. and Nigam K.D.P., **1994**, "Power-Law Fluids in a Circular Curved Tubes, Part III Numerical Simulation of Laminar Flow", Polymers-Plastics Technology and Engineering, 33(3), 357-379.

A2. Agrawal S., Jayaraman G., Srivastava V.K. and Nigam K.D.P., **1993**, "Power-Law Fluids in a Circular Curved Tubes, Part II Laminar Axial Dispersion", Polymers-Plastics Technology and Engineering, 32(6), 615-734.

A3. Agrawal S., Jayaraman G., Srivastava V.K. and Nigam K.D.P., **1993**, "Power-Law Fluids in a Circular Curved Tubes, Part I Laminar Flow", Polymers-Plastics Technology and Engineering, 32(6), 595-614.

A4. Aghaei A., Sheikhzadeh G.A., Dastmalchi M., Forozande H., **2015**, "Numerical Investigation of Turbulent Forced-Convective Heat Transfer of Al2O3–Water Nanofluid with Variable Properties in Tube", Ain Shams Engineering Journal, 6(2), 577–585.

A5. Ahuja A.S., **1975**, "Augmentation of Heat Transport in Laminar Flow of Polystyrene Suspensions. I. Experiments and Results", Journal of Applied Physics, 46(8), 3408–16.

A6. Akbari M. and Behzadmehr A., **2007**, "Developing Mixed Convection of a Nanofluid in a Horizontal Tube with Uniform Heat Flux", International Journal of Numerical Methods for Heat and Fluid Flow, 17(6), 566–586.

A7. Akhtar N., Alam S.S., Ali H. and Siddiqui M.A., **1992**, "An Experimental Study of Heat Transfer and Thermally Induced Flow Through a Uniformly Heated Inclined Tube", Proceedings of The International AMSE Conference "Application of Signals, Data, Systems Methodologies to Engineering Problems", Alexandria (Egypt), AMSE Press, 4, 21-32.

A8. Akoh, H., Tsukasaki, Y., S.Yatsuya, and Tasaki, A. Magnetic properties of ferromagnetic ultrafine particles prepared by vacuum evaporation on running oil substrate. Journal of Crystal Growth, 45, 495–500 (1978)

A9. Ali A., Vafai K. and Khaled A.R.A., **2004**, "Analysis of Heat and Mass Transfer Between Air and Falling Film in a Cross Flow Configuration", International Journal of Heat and Mass Transfer, 47(4), 743–755.

A10. Ali H. and Alam S.S., **1989**, "Heat Transfer to Boiling Liquids in a Thermosiphon Reboiler", Proceedings of the 10th National Heat Transfer, Srinagar, 129-134.

A11. Ali H. and Alam S.S., **1990**, "Boiling Heat Coefficient in a Vertical Tube Thermosiphon Reboiler", Chemical Engineering World, 10(25), 43-46.

B1. Bandyopadhyay K., Tan E., Ho L., Bundick S., Baker S.M. and Niemz A., **2006**, "Deposition of DNA-Functionalized Gold Nanospheres into Nanoporous Surfaces", Langmuir, 22(11), 4978-4984.

B2. Bang I.C. & Chang S.H., Boiling heat transfer performance and phenomena of Al2O3–water nanofluids from a plain surface in a pool, in: Proceedings of ICAPP, Pitterburgh, US, 2004.

B3. Benjamin, R.J. and Balakrishnan, A.R., 1999, Nucleate boiling heat transfer of binary mixtures at low to moderate heat fluxes, ASME J Heat Transfer, 121: 365–375.

B4. Bhagwat S.M. and **Ghajar A.J.**, **2017**, "Experimental Investigation of Non-Boiling Gas-Liquid Two Phase Flow in Downward Inclined Pipes", Experimental Thermal and Fluid Science, 89, 219-237.

B5. Bhattacharya P., Saha S.K., Yadav A., Phelan P.E. and Prasher R.S., **2004**, "Brownian Dynamics Simulation to Determine the Effect Thermal Conductivity of Nanofluids", Journal of Applied Physics, 95(11), 6492-6494

B6. Bhaumik S., Agarwal V.K. and Gupta S.C., **2004**, "A Generalized Correlation of Nucleate Boiling of Liquids", Indian Journal of Chemical Technology, 11(5), 719-725.

B7. Bonilla, C. F., and Perry, C. W., 1941, ''Heat Transmission to Boiling Binary Liquid Mixtures,'' Transactions of American Society of Chemical Engineers, 37, pp. 685–705.

B8. Boertz H., Baars A.J., Cieśliński J.T. and Smoleń S., **2018**, "Numerical Study of Turbulent Flow and Heat Transfer of Nanofluids in Pipes", Heat Transfer Engineering, 39(3), 241-251.

B9. Brinkman H.C., **1952**, "The Viscosity of Concentrated Suspensions and Solutions", Journal of Chemical Physics, 20(4), 571–581.

C1. Chandrasekar M., S. Suresh, and A. C. Bose, "Experimental investigations and theoretical determination of thermal conductivity and viscosity of Al_2O_3/water nanofluid," Experimental Thermal and Fluid Science, vol. 34, no. 2, pp. 210–216, 2010.

C2. Chen H., Yang W., He Y., Ding Y., Zhang L., Tan C., Lapkin A.A. and Bavykin D.V., **2008**, "Heat Transfer Behavior of Aqueous Suspensions of Titanate Nanofluids", Powder Technology, 183(1), 63–72.

C3. Choi S.U.S., Zhang Z.G., Yu W., Lockwood F.E. and Grulke E.A., **2001**, "Anomalous Thermal Conductivity Enhancement in Nanotube Suspensions", Applied Physics Letters, 79(14), 2252–2254.

C4. Choi S.U.S. and Eastmen J.A., **1995**, "Enhancing Thermal Conductivity of Fluids with Nanoparticles", Proceedings of the ASME International Mechanical Engineering Congress and Exposition, CA (USA), 99-105.

C5. Chopkar, M., Das, P. K., and Manna, I., "Synthesis and characterization of nanofluid for advanced heat transfer applications," Scripta Materialia, vol. 55, no. 6, pp. 549–552, 2006.

C6. Chougule S. S. and S. K. Sahu, "Thermal performance of automobile radiator using carbon nanotube-water nanofluid—experimental study," Journal of Thermal Science and Engineering Applications, vol. 6, no. 4, Article ID 041009, 2014.

C7. Cieśliński J.T., 2016, "Effect of Nanofluid Concentration On Two-Phase Thermosyphon Heat Exchanger Performance", Archives of Thermodynamics, 37(2), 23-40.

C8. Cieśliński J.T. and Kozak P., 2016, "Influence of Nanoparticle Concentration On Convective Heat Transfer of Water-Al2O3 Nanofluids Inside Horizontal Tubes", Applied Mechanics and Materials, 831, 208-215.

C9. Cieśliński J.T., Fiuk A., Miciak W. and Siemieńczuk B., 2016, "Performance of a Plate Heat Exchanger Operated with Water-Al2O3 Nanofluid", Applied Mechanics and Materials, 831, 188-197.

C10. Cryder, D. S., and Finalborgo, A. C., 'Heat Transmission From Metal Suf aces to Boiling Liquids: Effect of Temperature of the Liquid an Fila Coefficient,' As. Inst. Chem. Engrs. Vol. 33, 1937, p. 346.

D1. Das S.K., Putra N., Thiesen P. and Roetzel W., 2003, "Temperature Dependence of Thermal Conductivity Enhancement of Nanofluids", Journal of Heat Transfer, 125(4), 567–574.

D2. Das S.K., Putra N. and Roetzel W., 2003, "Pool Boiling Characteristics of Nano-Fluids", International Journal of Heat and Mass Transfer, 46(5), 851–862.

D3. Das S.K., Putra N. and Roetzel W., 2003, "Pool Boiling of Nano-Fluids On Horizontal Narrow Tubes", International Journal of Multiphase Flow, 29(8), 1237–1247.

D4. Das S., Saha B. and Bhaumik S., 2017, "Experimental Study of Nucleate Pool Boiling Heat Transfer of Water by Surface Functionalization With SiO2 Nanostructure", Experimental Thermal and Fluid Science, 81, 454-465.

D5. Das S., Saha B. and Bhaumik S., 2017, "Experimental Study of Nucleate Pool Boiling Heat Transfer of Water by Surface Functionalization With Crystalline TiO2 Nanostructure", Applied Thermal Engineering, 113, 1345-1357.

D6. Das M.K. and Kishor N., **2009**, "Adaptive Fuzzy Model Identification to Predict the Heat Transfer Coefficient in Pool Boiling of Distilled Water", Expert Systems with Applications, 36(2), 1142-1154.

D7. Daungthongsuk W. and Wongwises S., **2007**, "A Critical Review of Convective Heat Transfer of Nanofluids", Renewable and Sustainable Energy Reviews, 11(5), 797–817.

D8. Ding Y., Alias H., Wen D. and Williams R.A., **2006**, "Heat Transfer of Aqueous Suspensions of Carbon Nanotubes (CNT Nanofluids)", International Journal of Heat and Mass Transfer, 49(1-2), 240–250.

D9. Ding Y. and Wen D., **2005**, "Particle Migration in a Flow of Nanoparticle Suspensions", Powder Technology, 149(2-3), 84–92.

D10. D. Liu and Yu L., **2010**, "Single-Phase Thermal Transport of Nanofluids in a Minichannel", Journal of Heat Transfer, 133(3), 031009 (11 pages).

D11. Drew D.A. and Passman S.L., **1999**, "Theory of Multicomponent Fluids", Springer, Berlin.

D12. Duangthongsuk W. and Wongwises S., **2010**, "An Experimental Study On the Heat Transfer Performance and Pressure Drop of Tio2-Water Nanofluids Flowing Under a Turbulent Flow Regime", International Journal of Heat and Mass Transfer, 53(1-3), 334-344.

D13. Duangthongsuk W. and Wongwises S., **2012**, "A Dispersion Model for Predicting the Heat Transfer Performance of TiO2–Water Nanofluids Under a Laminar Flow Regime", International Journal of Heat and Mass Transfer, 55(11-12), 3138–3146.

E1. Eapen J., Li J. and Yip S., **2006**, "Probing Transport Mechanisms in Nanofluids by Molecular Dynamics Simulations", The Proceedings of the 18th National and 7th ISHMT – ASME Heat and Mass Transfer Conference, IIT Guwahati, India.

E2. Eastman J.A., Choi S.U.S., Li S., Thompson L. and Lee S., **1997**, "Enhanced Thermal Conductivity Through the Development of Nanofluids", Proceedings of the Fall Meeting of Materials Research Society (MRS), Boston, USA, 457, 3.

E3. Eastman J.A., Choi S.U.S., Li S., Yu W. and Thompson L.J., **2001**, "Anomalously Increased Effective Thermal Conductivity of Ethylene Glycol-Based Nanofluids Containing Copper Nanoparticles", Applied Physics Letters, 78(6), 718–720.

E4. Eastman J.A., Phillpot S.R., Choi S.U.S. and Keblinski P., **2004**, "Thermal Transport in Nanofluids", Annual Review on Materials Research, 34, 219–246.

E5. Ebrahimnia-Bajestan E., Niazmand H., Duangthongsuk W. and Wongwises S., **2011**, "Numerical Investigation of Effective Parameters in Convective Heat Transfer of Nanofluids

under a Laminar Flow Regime", International Journal of Heat and Mass Transfer, 54(19-20), 4376–4388.

E6. Evans W., Fish J. and Keblinski P., **2006**, "Role of Brownian Motion Hydrodynamics on Nanofluid Thermal Conductivity", Applied Physics Letters, 88(9), 093116.

F1. Faulkner DJ, Rector DR, Davidson JJ, Shekarriz R (2004) Enhanced heat transfer through the use of nanofluids in forced convection. In: ASME 2004 international mechanical engineering congress and exposition. American Society of Mechanical Engineers, pp 219–224.

F2. Ferrouillat S., Bontemps A., Poncelet O., Soriano O. and Gruss J.A., **2013**, "Influence of Nanoparticle Shape Factor On Convective Heat Transfer and Energetic Performance of Water based SiO2 and ZnO Nanofluids", Applied Thermal Engineering, 51(1-2), 839-851.

F3. H. K. Forster and N. Zuber, "Dynamics of Vapor Bubbles and Boiling Heat Transfer," AIChE Journal, Vol. 1, No. 4, 1955, p. 531.Convective Heat Transfer of Dilute γ-Al2O3/Water Nanofluid inside a Circular Tube", International Journal of Heat and Fluid Flow, 31(4), 606–612.

G1. Gianluca P., **2012**, "Properties of Au–H2O Nanofluids Using Molecular Dynamics", Ph.D. Thesis, Department of Aerospace and Mechanical Engineering, University of Notre Dame.

G2. Gosselin L. and Da Silva A.K., **2004**, "Combined Heat Transfer and Power Dissipation Optimization of Nanofluid Flows", Applied Physics Letters, 85(18), 4160–4162.

G3. Granqvist C.G. and Buhrman R.A., **1976**, "Ultrafine Metal Particles", Journal of Applied Physics, 47(5), 2200–2219.

G4. Garg P., J. L. Alvarado, C. Marsh, T. A. Carlson, D. A. Kessler, and K. Annamalai, "An experimental study on the effect of ultrasonication on viscosity and heat transfer performance of multi-wall carbon nanotube-based aqueous nanofluids," International Journal of Heat and Mass Transfer, vol. 52, no. 21-22, pp. 5090–5101, 2009.

G6. Gupta S.C. and Varsheney, B.S. , " Boiling heat transfer from a horizontal cylinder to a liquid pool", Instt. Of Engineers (CH), volume 61, Occt. 1980.

H1. Hamilton R.L. and Crosser O.K., **1962**, "Thermal Conductivity of Heterogeneous Two-Component Systems", Industrial and Engineering Chemistry Fundamentals, 1(3), 187–191.

H2. Harish G. , V. Emlin, V. Sajith, Effect of surface particle interactions during pool boiling of nanofluids, Int. J. Therm. Sci. 50 (2011) 2318 - 2327.

H3. Heris S.Z., Esfahany M.N. and Etemad G., **2007**, "Numerical Investigation of Nanofluid Laminar Convection Heat Transfer Through a Circular Tube", Numerical Heat Transfer Part A: Applications, 52(11), 1043–1058.

H4. Heris S.Z., Etemad S.Gh. and Esfahany M.N., **2006**, "Experimental Investigation of Oxide Nanofluids Laminar Flow Convection Heat Transfer", International Communications in Heat and Mass Transfer, 33(4), 529-535.

H5. H. M. Kurihara and J. E. Myers, The effect of superheat and surface roughness on boiling coefficients, AIChEJ. 6, 82 (1960).

H6. Hojjat M., Etemad S.Gh., Bagheri R. and Thibault J., **2011**, "Convective Heat Transfer of Non-Newtonian Nanofluids through a Uniformly Heated Circular Tube", International Journal of Thermal Sciences, 50(4), 525-531.

H7. Hong, K., Hong, T.-K., and Yang, H.-S. Thermal conductivity of Fe nanofluids depending on the cluster size of nanoparticles. Applied Physics Letters, 88, no. 3, 31,901–1–3 (2006).

H8. Hussein M. Adnan, K. V. Sharma, R. A. Bakar, and K. Kadirgama.'The Effect of Nanofluid Volume Concentration on Heat Transfer and Friction Factor inside a Horizontal Tube' Hindawi Publishing Corporation 'Journal of Nanomaterials' Volume 2013, Article ID 859563, 12 pages.

H9. Hwang K.S., Jang S.P. and Choi S.U.S., **2009**, "Flow and Convective Heat Transfer Characteristics of Water-Based Al2O3 Nanofluids in Fully Developed Laminar Flow Regime", International Journal of Heat and Mass Transfer, 52(1-2), 193–199.

H10. Hwang, Y. J., Ahn, Y. C., Shin, H. S., Lee, C. G., Kim, G. T., Park, H. S., and Lee, J. K. Investigation on characteristics of thermal conductivity enhancement of nanofluids. Current Applied Physics, 6, no. 6, 1068–1071 (2005).

J1. Jana S.K. and Bhaskarwar A.N., **2011**, "Measurement of Surface-Transfer Coefficient Values for CO2 Absorption in Lime Solutions in Presence of Surfactants", The Canadian Journal of Chemical Engineering, 90(1), 196-204.

J2. Jana S.K. and Bhaskarwar A.N., **2011**, "Gas Absorption Accompanied by Chemical Reaction in a System of Three-Phase Slurry-Foam Reactors in Series", Chemical Engineering Research and Design, 89(6), 793-810.

J3. Jana S.K. and Bhaskarwar A.N., **2010**, "Modeling Gas Absorption Accompanied by Chemical Reaction in Bubble Column and Foam-Bed Slurry Reactors", Chemical Engineering Science, 65(11), 3649-3659.

J4. Johnathan S. Coursey, J. Kim, Nanofluid boiling: The effect of surface wettability, Int. J. Heat Fluid Flow, 29(6) (2008) 1577-1585.

J5. Jung A., Natter H., Hempelmann R. and Lach E., **2009**, "Nanocrystalline Alumina Dispersed in Nanocrystalline Nickel: Enhanced Mechanical Properties", Journal of Materials Science, 44(11), 2725-2735.

K1. Kakaç S. and Yener Y., **1995**, "Convective Heat Transfer", Second Edition, CRC Press, Boca Raton.

K2. Kalapatapu S., Bhagwat S.M., Oyewole A. and **Ghajar A.J., 2014**, "Non-Boiling Heat Transfer in Horizontal and Near Horizontal Upward Inclined Gas-Liquid Two Phase Flow", Proceedings of the 10th International Conference on Heat Transfer, Fluid Mechanics and Thermodynamics (HEFAT 2014), Orlando, Florida, 2283-2291.

K3. Kang M.G., "Effect of surface roughness on pool boiling heat transfer", Int. J. of Heat and Mass transfer, 2000, 43: 4073.

K4. Kathiravan R., Kumar R., Gupta A., and Chandra R., "Preparation and pool boiling characteristics of copper nanofluids over a flat plate heater," International Journal of Heat and Mass Transfer, vol. 53, no. 9-10, pp. 1673–1681, 2010.

K5. Kayhani M.H., Nazari M., Soltanzadeh H., Heyhat M.M. and Kowsary F., **2012**, "Experimental Analysis of Turbulent Convective Heat Transfer and Pressure Drop of Al2O3/Water Nanofluid in Horizontal Tube", Micro and Nano Letters, 7(3), 223–227.

K6. Keblinski P. and Thomin J., **2006**, "Hydrodynamic Field around a Brownian Particle", Physical Review E, 73, 010502.

K7. Khaled A.R.A. and Vafai K., **2005**, "Heat Transfer Enhancement through Control of Thermal Dispersion Effects", International Journal of Heat and Mass Transfer, 48(11), 2172–2185.

K8. Khanafer K., Vafai K. and Lightstone M., **2003**, "Buoyancy-Driven Heat Transfer Enhancement in a Two-Dimensional Enclosure Utilizing Nanofluids", International Journal of Heat and Mass Transfer, 46(19), 3639–3653.

K9. Khedkar R.S., Sonawane S.S. and Wasewar K.L., **2012**, "Influence of CuO Nanoparticles in Enhancing the Thermal Conductivity of Water and Monoethylene Glycol Based Nanofluids", International Communications in Heat and Mass Transfer, 39(5), 665-669.

K10. Kim J., Kang Y.T. and Choi C.K., **2004**, "Analysis of Convective Instability and Heat Transfer Characteristics of Nanofluids", Physics of Fluids, 16(7), 2395–2401.

K11. Kim J., Choi C.K., Kang Y.T. and Kim M.G., **2006**, "Effect of Thermodiffusion Nanoparticles On Convective Instability in Binary Nanofluids", Nanoscale and Microscale Thermophysical Engineering, 10(1), 29–39.

K12. Kishor N. and Das M.K., **2010**, "Soft Computing Techniques for Prediction of Boiling Heat Transfer Coefficient of Liquids On Copper Coated Tubes", Applied Artificial Intelligence: An International Journal, 24(3), 210-232.

K13. Koo J. and Kleinstreuer C., **2005**, "Laminar Nanofluid Flow in Microheat-Sinks", International Journal of Heat and Mass Transfer, 48(13), 2652–2661.

K14. Kole M., T.K. Dey, Investigations on the pool boiling heat transfer and critical heat flux of ZnO-ethylene glycol nanofluids, Appl. Therm. Eng. 37 (2012) 112 - 119.

K15. Kulkarni D.P., Namburu P.K., Ed Bargar H. and Das D.K., **2008**, "Convective Heat Transfer and Fluid Dynamic Characteristics of Sio2 Ethylene Glycol/Water Nanofluid", Heat Transfer Engineering, 29(12), 1027-1035.

K16. Kumar S. and Murthy J.Y., **2005**, "A Numerical Technique for Computing Effective Thermal Conductivity of Fluid–Particle Mixtures", Numerical Heat Transfer, Part B: Fundamentals, 47(6), 555–572.

K17. Kwark S.M, Kumar R., Moreno G., Yoo J., You S.M., Pool boiling characteristics of low concentration nanofluids, Int. J. Heat. Mass Transf. 53 (2010) 972 - 981.

K18. Kurihara, H.M. and Myers, J.E. , The effects of superheat and surface roughness on boiling coefficients, AIChE J., Vol. 6 , pp 83 – 91, 1960.

L1. Lai W.Y., Vinod S., Phelan P.E. and Prasher R., **2009**, "Convective Heat Transfer for Water Based Alumina Nanofluids in a Single 1.02-mm Tube", Journal of Heat Transfer, 131(11), 112401 (9 pages).

L2. Lakshmi B.V., Subrahmanyam T., Dharma Rao V. and Sharma K.V., **2012**, "Turbulent Film Condensation of Pure Vapors Flowing Normal to a Horizontal Condenser Tube - Constant Heat Flux at The Tube Wall", International Journal of Automotive and Mechanical Engineering, 4, 455-470.

L3. Layth W. Ismael, Dr. Khalid Faisal. Sultan" A comparative Study on the Thermal Conductivity of Micro and Nano fluids by Using Silver and Zirconium Oxide" Al-Qadisiya Journal For Engineering Sciences, Vol. 7, No. 2, 2014.

L4. Lee S. and Choi S.U.S., **1996**, "Application of Metallic Nanoparticle Suspensions in Advanced Cooling Systems", Argonne National Lab, IL (USA), 630, 252- 6439.

L5. Lee S., Choi S.U.S., Li S. and Eastman J.A., **1999**, "Measuring Thermal Conductivity of Fluids Containing Oxide Nanoparticles", Journal of Heat Transfer, 121(2), 280-289.

L6. Li C.H. and Peterson G.P., **2006**, "Experimental Investigation of Temperature and Volume Fraction Variations on the Effective Thermal Conductivity of Nanoparticle Suspensions (Nanofluids)", Journal of Applied Physics, 99(8), 084314.

L7. Liaw, S., and Dhir, V. K., 1993, "Void Fraction Measurements During Saturated Pool Boiling of Water on Partially Wetted Vertical Surfaces", Journal of Heat Transfer, Vol. 111, pp.731-738.

L8. Li Y., Zhou J., Tung S., Schneider E. and Xi S., **2009**, "A Review on Development of Nanofluid Preparation and Characterization", Powder Technology, 196(2), 89–101.

L9. Liu C.H., Yella A., Li B.Q. and Bandyopadhyay K., **2013**, "Measurement of Light Attenuation in Phantom Tissue Embedded with Gold Nanoshells", Advanced Materials Research, 647, 232-238.

L10 Lo C.H., Tsung T.T. and Chen L.C., **2005**, "Shape-Controlled Synthesis of Cu Based Nanofluid Using Submerged Arc Nanoparticle Synthesis System (SANSS)", Journal of Crystal Growth, 277(1-4), 636-642.

M1. Madhesh D., Parameshwaran R., Kalaiselvam S., Experimental investigation on convective heat transfer and rheological characteristics of Cu–TiO2 hybrid nanofluids, Exp Thermal Fluid Sci, 52 (2014) 104–115.

M2. Maiga H.B., Wilson C., Borgmeyer B., Park K., Yu Q., Choi S.U.S. and Tirumala M., **2006**, "Effect of Nanofluid on the Heat Transport Capability in an Oscillatory Heat Pipe", Applied Physics Letters, 88(14), 143116.

M3. Maiga S.E.B., Nguyen C.T., Galanis N. and Roy G., **2004**, "Heat Transfer Behaviors of Nanofluids in a Uniformly Heated Tube", Superlattices Microstructures, 35(3-6), 543–557.

M4. Maiga S.E.B., Palm S.J., Nguyen C.T., Roy G. and Galanis N., **2005**, "Heat Transfer Enhancement by Using Nanofluids in Forced Convection Flows", International Journal of Heat and Fluid Flow, 26(4), 530-546.

M5. Maiga S.E.B., Nguyen C.T., Galanis N., Roy G., Maré T. and Coqueux M., **2006**, "Heat Transfer Enhancement in Turbulent Tube Flow using Al2O3 Nanoparticle Suspension", International Journal of Numerical Methods of Heat and Fluid Flow, 16(3), 275–292.

M6. Mago P.J. and Sherif S.A., **2003**, "Heat and Mass Transfer on a Cylinder Surface in Cross Flow under Supersaturated Frosting Conditions", International Journal of Refrigeration, 26(8), 889-899.

M7. Manna A., Kulkarni B.D., Vijayamohanan K. and Bandyopadhyay K., **1997**, "Synthesis and Characterization of Hydrophobic, Approtically Dispersible Silver Nanoparticles in Windsor II Type Microemulsions", Chemistry of Materials, 9(12), 3032-3036.

M8. Mansour R.B., Galanis N. and Nguyen C.T., **2007**, "Effect of Uncertainties in Physical Properties On Forced Convection Heat Transfer with Nanofluids", Applied Thermal Engineering, 27(1), 240–249.

M9. Masuda H., Ebata A., Teramae K. and Hishinuma N., **1993**, "Alteration of Thermal Conductivity and Viscosity of Liquid by Dispersing Ultra-Fine Particles (Dispersion of Al2O3, SiO2 and TiO2 Ultra-Fine Particles)", Netsu Bussei, 7(4), 227–233.

M10 Maxwell J. C., A Treatise on Electricity and Magnetism, Clarendon, Oxford, UK, 1873.

M11. Mihir K. Das, Kishor, N., (2010) "Determination of Heat Transfer Coefficient in Pool Boiling of Organic Liquids Using Fuzzy Modeling Approach" Heat Transfer Engineering, 31 : 1, 45 – 58.

N1. Namburu P.K., Kulkarni D.P., Misra D. and Das D.K., **2007**, "Viscosity of Copper Oxide Nanoparticles Dispersed in Ethylene Glycol and Water Mixture", Experimental Thermal and Fluid Science, 32(2), 397-402.

N2. Nguyen C.T., Desgranges F., Galanis N., Roy G., Mare T., Boucher S. and Mintsa H.A., **2008**, "Viscosity Data for Al2O3-Water Nanofluid-Hysteresis: Is Heat Transfer Enhancement Using Nanofluids Reliable?", International Journal of Thermal Sciences, 47(2), 103-111.

N3. Narayan, K.B. Anoop, S.K. Das, Mechanism of enhancement/deterioration of boiling heat transfer using stable nanoparticle suspensions over vertical tubes, J. Appl. Phys. 102 (7) (2007) 074317.

N4. Nukiyama S., Maximum and minimum values of heat q transmitted from metal to boiling water under atmospheric pressure. J. Soc. Mech. Eng. Jpn. 37 (1934) 53-54, 367-374.

P1. Pak B.C. and Cho Y.I., **1998**, "Hydrodynamic and Heat Transfer Study of Dispersed Fluids with Submicron Metallic Oxide Particles", Experimental Heat Transfer, 11(2), 151-170.

P2. Park, K., Jung, D., 2007, Boiling heat transfer enhancement with carbon nanotubes for refrigerants used in building air-conditioning, Energy and Buildings, vol. 39, p. 1061–1064.

P3. Pantzali M. N., Kanaris A. G., Antoniadis K. D., Mouza A. A., and Paras S. V., “Effect of nanofluids on the performance of a miniature plate heat exchanger with modulated surface,” International Journal of Heat and Fluid Flow, vol. 30, no. 4, pp. 691–699, 2009.

P4. Plawsky J.L., Fedorov A.G., Garimella S.V., Ma H.B., Maroo S.C., Chen L. and Nam Y., **2014**, “Nano- and Micro-Structures for Thin Film Evaporation - A Review”, Nanoscale and Microscale Thermophysical Engineering, 18(3), 251-269.

P5. Prakash M, Giannelis EP. Mechanism of heat transport in nano- fluids. J Comput Aided Mater Des. 2007;14:109–117

P6. Prasher R., Evans W., Meakin P., Fish J., Phelan P. and Keblinski P., **2006**, “Effect of Aggregation on Thermal Conduction in Colloidal Nanofluids”, Applied Physics Letters, 89, 143119.

P7. Prasher R., Song D., Wang J. and Phelan P., **2006**, “Measurements of Nanofluid Viscosity and its Implications for Thermal Applications”, Applied Physics Letters, 89(13), 133108.

R1. Ramakrishna N. Hegde, Dr. Shrikantha S. Rao, R. P. Reddy,” Investigations on Heat Transfer Enhancement in Pool Boiling with Water-CuO Nano-Fluids”, Journal of Thermal Science Vol.21, No.2 , pp.179-183, 2012.

R2. Rohsenow, W.M., "A Method of Correlating Heat Transfer Data for Surface Boiling Liquids," Trans. ASME, Vol. 74, p. 969, 1952

R3. Young R.K. and Hummel R.L, Improved nucleate boiling heat transfer, Chem. Engg. Prog., 60(7) (1964) 53-58.

R4. Roy G., Nguyen C.T. and Lajoie P.R., **2004**, “Numerical Investigation of Laminar Flow and Heat Transfer in a Radial Flow Cooling System with the use of Nanofluids”, Superlattices Microstructures, 35(3-6), 497–511.

S1. Saha G. and Paul M.C., **2014**, “Numerical Analysis of the Heat Transfer Behaviour of Water Based Al_2O_3 and TiO2 Nanofluids in a Circular Pipe under the Turbulent Flow Condition”, International Communications in Heat and Mass Transfer, 56, 96-108.

S2. Sarafraz M.M., Hormozi F., “Nucleate pool boiling heat transfer characteristics of dilute Al_2O_3-ethyleneglycol nanofluids”; Int. Commun. Heat. Mass Transf. 58 (2014) 96 - 104.

S3. Salem A.M. and Paul M.C., **2018**, “An Integrated Kinetic Model for Downdraft Gasifier Based On a Novel Approach That Optimises The Reduction Zone of Gasifier”, Biomass and Bioenergy, 109, 172-181.

S4. Sato Y., Deutsch E. and Simonin O., **1998**, "Direct Numerical Simulations of Heat Transfer by Solid Particles Suspended in Homogeneous Isotropic Turbulence", International Journal Heat and Fluid Flow, 19(2), 187–192.

S5. Schiller L. and Naumann A., **1935**, "A Drag Coefficient Correlation", Z. Ver. Deutsch. Ing., 77, 318–320.

S6. Schwartz L.M., Bentz D.P. and Garboczi E.J., **1995**, "Interfacial Transport in Porous Media: Application to DC Electrical Conductivity of Mortars", Journal of Applied Physics, 78(10), 5898–5908.

S7. Sepe A.M., Li J. and Paul M.C., **2016**, "Assessing Biomass Steam Gasification Technologies Using a Multi-Purpose Model", Energy Conversion and Management, 129, 216-226.

S8. Shamim J.A., Bhowmik P.K., Xiangyi C. and Suh K.Y., **2016**, "A New Correlation for Convective Heat Transfer Coefficient of Water–Alumina Nanofluid in a Square Array Subchannel under PWR Condition", Nuclear Engineering and Design, 308, 194–204.

S9. Shokohmand H., Kazemi M. and Sajadi A.R., **2011**, "Investigation of Turbulent Convective Heat Transfer of TiO2/Water Nanofluid in Circular Tube", Proceedings of the IEEE 3rd International Conference on Communication Software and Networks (ICCSN 2011), Xi'an, China, 254-258.

S10. S.M. Peyghambarzadeh, S.H. Hashemabadi, M.S. Jamnani, S.M. HoseiniImproving the cooling performance of automobile radiator with Al_2O_3/water nanofluid Appl Therm Eng, 31 (2011), pp. 1833-1838.

S11. Sherif S.A., Lear W.E. and Winowich N.S., **1999**, "Effect of Slip Velocity and Heat Transfer on the Condensed Phase Momentum Flux of Supersonic Nozzle Flows", Journal of Fluids Engineering, 122(1), 14-19.

S12. Shi, L., Kim, P., Majumdar, A. and McEuen, P. L. 2001. Thermal Transport Measurements of Individual Multiwalled Nanotubes. Physical Review Letters, vol. 87(no. 21): 215502–1–4.

S13. Singh P.K., Anoop K.B., Patel H.E., Sundararajan T., Pradeep T. and Das S.K., **2010**, "Anomalous Size Dependent Rheological Behavior of Alumina Based Nanofluids", International Journal of Micro-Nano Scale Transport, 1(2), 179-188.

S14. Singh V. and Gupta M., **2016**, "Heat Transfer Augmentation in a Tube Using Nanofluids Under Constant Heat Flux Boundary Condition: A Review", Energy Conversion and Management, 123, 290–307.

S15. Sonawane S.S., Khedkar R.S. and Wasewar K.L., **2013**, "Study On Concentric Tube Heat Exchanger Heat Transfer Performance Using Al2O3–Water Based Nanofluids", International Communications in Heat and Mass Transfer, 49, 60-68.

S16. Sonawane S.S., Khedkar R.S. and Wasewar K.L., **2015**, "Effect of Sonication Time on Enhancement of Effective Thermal Conductivity of Nano TiO2–Water, Ethylene Glycol, and Paraffin Oil Nanofluids and Models Comparisons", Journal of Experimental Nanoscience, 10(4), 310-322.

S17. Sundar L.S. and Sharma K.V., **2011**, "An Experimental Study on Heat Transfer and Friction Factor of Al2O3 Nanofluid", Journal of Mechanical Engineering and Sciences, 1, 99-112.

S18. Suresh S., Venkitaraj K.P., Selvakumar P. and Chandrasekar M., **2012**, "Effect of Al2O3–Cu/Water Hybrid Nanofluid in Heat Transfer", Experimental Thermal and Fluid Science, 38, 54-60.

T1. Tam H.K., Tam L.M., **Ghajar A.J.** and Chen I.P., **2017**, "Experimental Study of the Ultrasonic Effect on Heat Transfer Inside a Horizontal Mini-Tube in the Laminar Region", Applied Thermal Engineering, 114, 1300-1308.

T2. Tang C.C. and **Ghajar A.J.**, **2007**, "Validation of a General Heat Transfer Correlation for Non-Boling Two-Phase Flow with Different Flow Patterns and Pipe Inclination Angles", Proceedings of the ASME-JSME 2007 Thermal Engineering Heat Transfer Summer Conference, Vancouver, British Columbia, Canada, 2, 205-218.

T3. Taylor RA, Phelan PE, Otanicar TP, Walker CA, Nguyen M, Trimble S, Prasher R. Applicability of nanofluids in high flux solar collectors. Journal of Renewable and Sustain Energy.2011; 3: 023104.

T4. T. Hinrichs, E. Hennecke and H. Yasuda, The effect of plasma-deposited polymers on the nucleate boiling behavior of copper heat transfer surfaces, International Journal of Heat and Mass Transfer, **24**, 8, (1359), (1981).

T5. Tiwari Dhiraj 2015 Experimental Study on Heat Transfer Enhancement by using Water-Alumina Nano fluid in Heat Exchanger International Journal of Advance Research in Science and Engineering **4** 92-200

T6. Trisaksri S. and Wongwises V., **2007**, "Critical Review of Heat Transfer Characteristics of Nanofluids", Renewable and Sustainable Energy Reviews, 11(3), 512–523.

U1. Utomo A.T., Poth H., Robbins P.T. and Pacek A.W., **2012**, "Experimental and Theoretical Studies of Thermal Conductivity, Viscosity and Heat Transfer Coefficient of Titania and

Alumina Nanofluid", International Journal of Heat and Mass Transfer, 55(25-26), 7772–7781.

V1. Vajjha R.S., Das D.K. and Kulkarni D.P., **2010**, "Development of New Correlations for Convective Heat Transfer and Friction Factor in Turbulent Regime for Nanofluids", International Journal of Heat and Mass Transfer, 53(21-22), 4607–4618.

V2. Vassallo P., R. Kumar, S.D. Amico, Pool boiling heat transfer experiments in silica–water nano-fluids, International Journal of Heat and Mass Transfer 47 (2004) 407–411

W1. Wagener, M., Murty, B. S., and Gunther, B. Preparation of metal nanosuspensions by highpressure DC-sputtering on running liquids. In Komarnenl, S., Parker, J. C., and Wollenberger, H. J. (Editors), Nanocrystalline and Nanocomposite Materials II, volume 457, 149– 154. Materials Research Society, Pittsburgh PA (1997).

W2. Wang X., Xu X. and Choi S.U.S., **1999**, "Thermal Conductivity of Nanoparticle-Fluid Mixture", Journal of Thermophysics and Heat Transfer, 13(4), 474–480.

W3. Wang X.Q. and Mujumdar A.S., **2007**, "Heat Transfer Characteristics of Nanofluids: A Review", International Journal of Thermal Sciences, 46(1), 1–19.

W4. Wang Z., **2009**, "Thermal Wave in Thermal Properties Measurements and Flow Diagnostics: With Applications of Nanofluids Thermal Conductivity and Wall Shear Stress Measurements", Ph.D. Thesis, Mechanical, Industrial and Manufacturing Engineering, Oregon State University.

W5. Wen D. and Ding Y., **2004**, "Experimental Investigation into Convective Heat Transfer of Nanofluids at The Entrance Region Under Laminar Flow Conditions", International Journal of Heat and Mass Transfer, 47(24), 5181-5188.

W6. Wen D. and Ding Y., **2004**, "Effective Thermal Conductivity of Aqueous Suspensions of Carbon Nanotubes (Carbon Nanotube Nanofluids)", Journal of Thermophysics and Heat Transfer, 18(4), 481–485.

W7. Wen D. and Ding Y., **2005**, "Effect of Particle Migration On Heat Transfer in Suspensions of Nanoparticles Flowing Through Minichannels", Microfluids and Nanofluids, 1(2), 183–189.

W8. Wen D. and Ding Y., **2005**, "Experimental Investigation into Pool Boiling Heat Transfer of Aqueous Based C-Alumina Nanofluids", Journal of Nanoparticle Research, 7, 265–274.

W9. Wen D. and Ding Y., **2005**, "Formulation of Nanofluids for Natural Convective Heat Transfer Applications", International Journal of Heat and Fluid Flow, 26(6), 855–864.

W10. White SB, Shih AJ-M, Pipe KP (2011) Investigation of the electrical conductivity of propylene glycol-based ZnO nanofluids. Nanoscale Res Lett 6:1–5.

W11. Witharana, S., Chen, H., and Ding, Y. (2010). Shear stability and thermophysical properties of nanofluids. In IEEE-International conference on Information and Automation for Sustainability (Colombo, Sri Lanka)

X1. Xie H., Wang J., Xi T. and Liu Y., **2002**, "Thermal Conductivity of Suspensions Containing Nanosized SiC Particles", International Journal of Thermophysics, 23(2), 571–580.

X2. Xie H., Wang J., Xi T. Liu Y. and Ai F., **2002**, "Thermal Conductivity Enhancement of Suspensions Containing Nanosized Alumina Particles", Journal of Applied Physics, 91(7), 4568–4572.

X3. Xie H., Wang J., Xi T., Liu Y. and Ai F., **2002**, "Dependence of the Thermal Conductivity of Nanoparticles-Fluid Mixture on the Base Fluid", Journal of Material Science Letters, 21, 1469–1471.

X4. Xuan Y. and Li Q., **2002**, "Investigation on Convective Heat Transfer and Flow Features of Nanofluids", Journal of Heat Transfer, 125(1), 151-155.

X5. Xuan Y. and Li Q., **2000**, "Heat Transfer Enhancement of Nanofluids", International Journal of Heat and Fluid Flow, 21(1), 58-64.

X6. Xuan Y. and Roetzel W., **2000**, "Conceptions for Heat Transfer Correlation of Nanofluids", International Journal of Heat and Mass Transfer, 43(19), 3701-3707.

X7. Xue L., Keblinski P., Phillpot S.R., Choi S.U.S. and Eastman J.A., **2004**, "Effect of Liquid Layering at the Liquid–Solid Interface on Thermal Transport", International Journal of Heat and Mass Transfer, 47(19-20), 4277–4284.

Y1. Yang Y., Zhang Z.G., Grulke E.A., Anderson W.B. and Wu G., **2005**, "Heat Transfer Properties of Nanoparticle-in-Fluid Dispersions (Nanofluids) in Laminar Flow", International Journal of Heat and Mass Transfer, 48(6), 1107–1116.

Y2. Yang X.F. and Liu Z.-H., "Pool boiling heat transfer of functionalized nanofluid under sub-atmospheric pressures," International Journal of Thermal Sciences, vol. 50, no. 12, pp. 2402–2412, 2011.

Y3. Yang Y. M. and. Maa J. R, "Boiling of suspension of solid particles in water," Int. J. Heat Mass Transfer, vol. 27, 1984, pp. 145–147.

Y4. Young R.K. and Hummel R.L, Improved nucleate boiling heat transfer, Chem. Engg. Prog., 60(7) (1964) 53-58.

Y5. Yu W., France D.M., Choi S.U.S. and Routbort J.L., **2007**, "Review and Assessment of Nanofluid Technology for Transportation and Other Applications", Argonne National Laboratory, Argonne, IL (USA).

Y6. Yu W. and Choi S.U.S., **2003**, "The Role of Interfacial Layers in The Enhanced Thermal Conductivity of Nanofluids: A Renovated Maxwell Model", Journal of Nanoparticle Research, 5(1-2), 167–171.

Y7. Yu W. and Xie H., **2012**, "A Review on Nanofluids: Preparation, Stability Mechanisms and Applications", Journal of Nanomaterials, 2012, 435873 (17 pages).

Z1. Zarringhalam M., Karimipour A. and Toghraie D., **2016**, "Experimental Study of the Effect of Solid Volume Fraction and Reynolds Number on Heat Transfer Coefficient and Pressure Drop of CuO–Water Nanofluid", Experimental Thermal and Fluid Science, 76, 342–351.

Z2. Zhang J., Diao Y., Zhao Y. and Zhang Y., **2014**, "Experimental Study of TiO2–Water Nanofluid Flow and Heat Transfer Characteristics in a Multiport Minichannel Flat Tube", International Journal of Heat and Mass Transfer, 79, 628–638.

Z3. Zhang J., Li W. and Sherif S.A., **2016**, "A Numerical Study of Condensation Heat Transfer and Pressure Drop in Horizontal Round and Flattened Minichannels", International Journal of Thermal Sciences, 106, 80-93.

Z4. Zhu, H., Lin, Y., and Yin, Y. A novel one-step chemical method for preparation of copper nanofluids. Journal of Colloid and Interface Science, 227, 100–103 (2004).